BULGARIAN CHEMICAL COMMUNICATIONS

2009 Volume 41 / Number 2

Journal of the Chemical Institutes
of the Bulgarian Academy of Sciences
and of the Union of Chemists in Bulgaria

EDITORIAL

The Bulgarian Peptide Society organized the Fifth Bulgarian Peptide Symposium under the auspices of the European Peptide Society. This event took place at Bachinovo, Rila mountain resort, on 28–30 May 2008. The symposium was aimed at bringing together peptide researchers and young investigators to present and discuss results of common interest. There were 70 registered participants from different Bulgarian universities, laboratories, hospitals, and organizations. The Organizing Committee highly appreciated the attendance of Prof. Jean Martinez, Prof. Ettore Benedetti, Prof. Anna-Maria Papini, Prof. Beatriu Escuder, Prof. Rudolph Willem, and Dr. Tzvetana Lazarova. Also, young foreign participants were present.

The scientific program within three days included 15 lectures and 38 posters. The lectures and posters covered topics such as structure-activity studies on bioactive peptides, peptidomimetics, physiological studies on bioactive peptides, synthesis and physiological studies of modified amino acids and structural and conformational analysis of peptides, isolation and biological activity of natural peptides, kinetic investigation and theoretical studies on peptide mimetics, and proteomic and neuropeptides investigations. Two memorial lectures in tribute to Prof. Dimitar Petkov, D.Sc., were dedicated to its life and scientific achievements. Prof. Jean Martinez and Prof. Ettore Benedetti delivered a welcoming speech. The lectures were delivered by Prof. J. Martinez, Prof. E. Benedetti, Prof. A. Papini, Prof. L. Vezenkov, Prof. B. Escuder, Prof. B. Tchorbanov, Dr. Tz. Lazarova, Dr. D. Danalev, Dr. S. Vezenkov, Dr. D. Tzekova, Dr. Camelia Mihai, and Dr. O. Apostolov. L. Van Lokeren and B. Benkova, both Ph.D. students, gave interesting talks on the same problems. The best three scientific works presented by young researchers were awarded.

Financial support from the European Peptide Society, MakMetal Co., Aquachim Co. Ltd., University of Chemical Technology and Metallurgy, Sofia, Med Co., South-Western University of Blagoevgrad, and FOT Co., enabled the Organizing Committee to invite several distinguished scientists, to support the participation of more than 15 young researchers and students, and to organize the publishing of part of presented scientific communications.

Prof. Lyubomir Vezenkov, D.Sc.
University of Chemical Technology and Metallurgy

Assoc. Prof. Tamara Pajpanova, Ph.D.
Institute of Molecular Biology,
Bulgarian Academy of Sciences

In Memoriam

Professor Dimitar Petkov

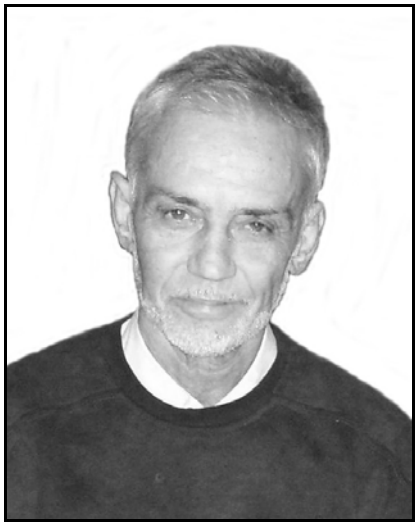

Professor Dimitar D. Petkov, D.Sci., Ph.D., died on March 8, 2008 at the age of 66 after a short and bitter fight with cancer. By sheer strong will, he supervised his Ph.D. students to the last.

Born in 1941 in the village of Sushica, VelikoTarnovo District, Petkov graduated chemistry at Sofia University in 1967. His Master's Thesis with N. Tyutyulkov was in the field of quantum chemistry. Petkov joined the Institute of Organic Chemistry, Bulgarian Academy of Sciences (1967–2007), first in D. Shopov's Laboratory of Organic Catalysis doing theoretical work, soon after went over (1969) to the Laboratory "Proteins" headed by M. Karadjova, where his main interest was enzyme catalysis by proteinases. He spent six months (1976) in Cornell University with Hames. He became Head of the Spin-off Laboratory BIOCATALYSIS (1988). The last decade of his life was dedicated to the intriguing field of ribosome catalysis.

Being Docent (1984) in Sofia University he taught there Bioorganic Chemistry and related courses in the Chemical and the Biological Faculties.

The scientific legacy of Dimitar Petkov comprises 85 papers cited more than 400 times, a text book "Biorganic Chemistry" (1996), several patents on peptide synthesis. He was a Member of the American Peptide Society and the European Peptide Society and co-founding Member of the Bulgarian Peptide Society.

Even the first studies of D. Petkov (coauthored with A. Andreev and D. Shopov) provoked already keen interest. One of the papers (J. Catalysis, 1969) treating the quantum chemical estimation of the modes of hydrogen adsorption on nickel was cited 55 times.

Moving to the Protein Laboratory headed by Maria Karadjova, Petkov's research work focused on the chemistry of serine proteinases: urokinase, trypsin, chymotrypsin covering a wide range of problems: from enzyme-catalysed synthesis of peptides, methods of assay of activity to the mechanism of enzymatic action. Highlights issues from a practical point of view are his papers "Nucleophilic specificity in chymotrypsin peptide synthesis" (Biochem. Biophys. Res. Commun. 1984, most cited paper 82 times), "Enzyme peptide synthesis and semisynthesis – kinetic and thermodynamic aspects" defining the best conditions for *in vitro* synthesis nicely demonstrated by the development of an iterative procedure of peptide synthesis in a nucleophile pool. Structure-activity relationships helped to elucidate the transition state in urokinase aided peptide hydrolysis. Most of the peptide work was carried out in collaboration with Senior Research Fellow Dr. Ivanka Stoineva. The recognition of these achievements is materialized in the foundation of a commercial laboratory for conversion of swine into human insulin, the activity of which was unfortunately discontinued because of market considerations.

As it was already mentioned, the last decade of the research efforts of Petkov and his numerous associates were dedicated to the fascinating field of the catalytic action of ribosomes during protein biosynthesis. Using model substrates complex enough to mimic credibly the nucleoside structure and aprotic solvents, imitating the anhydrous environment of the active site of the ribosome, the catalytic role of neighbouring sugar hydroxyl and the modes of proton transfer were established using the experimental methods of physical

organic and computational chemistry. The publication of these results in JACS and Angewandte Chemie proves convincingly the quality of these results.

Science dominated his life and his emotions. He would come early in the morning on his bicycle and work the whole day. Dominating in his research work and teaching was his keen interest in modern science, which drew the best young scientists to work or do Ph.D. with him. Many of them are now scattered in renowned labs in the world. Over the years, he corresponded and collaborated with top scientists in the field.

The way Petkov treated science reminds of a story told about the Nobel Prize-winner biochemist Albert Szent-Gyorgi, discoverer of vitamin C. He was fishing in the lake of Balaton when a fellow fisherman noticed: Why are you using such large hooks – there are no such large fish in the lake?! Szent-Gyorgi answered: I have no time for small fish.

The memory of Professor D. D. Petkov will be revered by the traces he left in the world of science, by his many former students whom he introduced to the frontiers of scientific endeavour and by his friends for his stimulating personality.

Ivan Pojarlieff
Corresponding Member of the Bulgarian Academy of Sciences

Bulgarian Chemical Communications, Volume 41, Number 2 (pp. 99–103) 2009

Design, synthesis and anticoagulant studies of new antistasin isoform 2 and 3 amide analogues

D. L. Danalev*, L. T. Vezenkov

Department of Organic Chemistry, University of Chemical Technology and Metallurgy, 8 Kliment Ohridski Blvd., 1756 Sofia, Bulgaria

Received July 6, 2008; Revised September 18, 2008

One of the most important enzymes in blood coagulation cascade is Factor Xa. That is why its inhibitors are promising alternative against thrombotic disorders. In our previous work, we reported the synthesis of hybrid structure between isoform 2 and 3 of antistasin and the active sequences D-Phe-Pro-Arg; D-Arg-Gly-Arg; Phe-Ile-Arg and Tyr-Ile-Arg. Besides the analogues with C-terminal COOH group, the peptide D-Phe-Pro-Arg-Pro-Lys-Arg-NH_2 was synthesized. The biological activity of the last one was 60 times bigger than that of the natural isoform 3 of ATS and some times more active than that of the all other synthesized analogues. In the current work, we described synthesis and biological activity of C-terminal amide analogues of all early synthesized peptides in order to deduce the structure-activity relationship. The anticoagulant activity according to the APTT and IC_{50} was determined.

Key words*:* anticoagulant activity, Factor Xa, thrombin, antistasin, peptide mimetics.

INTRODUCTION

During the last years the number of deaths due to hemostatic impairments such as coronary angioplasts, coronary thromboembolisms, myocard heart attack, pulmonary embolism, etc. has become equal to those caused by cancer formations. Haemostasis is a key process whose correct functioning is an important defence mechanism of the human organism. It is a blood coagulation process activated in case of injury of the blood system. If it is functioning correctly, vascular-motor and cell reactions are triggered and the blood coagulation cascade is activated. Coagulation is a defence function of the organism that has to be strictly regulated. After the bleeding is stopped, a number of limiting self-regulatory mechanisms are initiated. They act competitively and their role is to:

- stop further coagulation;
- prevent the thrombus formation in the organism;
- restrict the coagulation to the injured are.

Besides the mechanisms limiting the formation of thrombocytes, the availability of plasma proteins is also important in this respect as they deactivate the serine proteinase of the coagulation, i.e. they act as inhibitors. The main function of blood coagulation is the conversion of the soluble fibrinogen into insoluble fibrin clot. This process is accompanied by a series of enzyme reactions described in 1964 as an enzyme cascade (Fig. 1) [1]

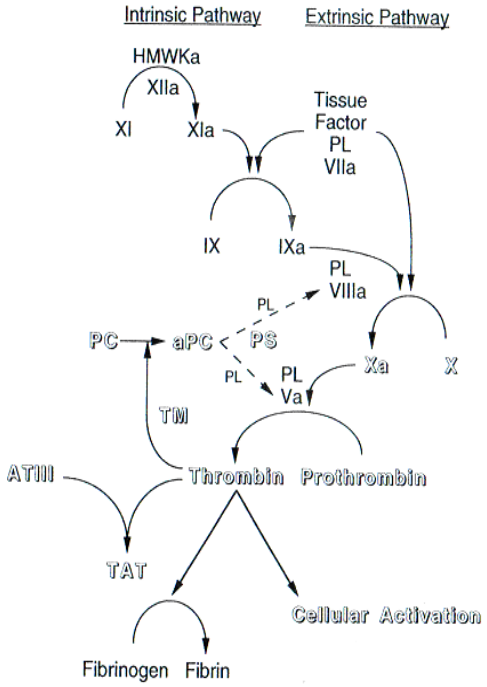

Fig. 1. Scheme of the blood coagulation cascade.

A major role in them plays a number of serine proteinases, which are known as:

- Blood clotting factors
  - extrinsic system: Factor III, Factor VII;
  - intrinsic system: Factor XII, high molecule kininogen, prekalikrein, Factor XI, Factor IX, Factor VIII;
  - common pathway: Factor XI, Factor V, Phospholipids, Factor II, Factor I, Factor XIII
- Factors of the fibrinolysis;
- Factors of the control mechanisms (inhibitors).

* To whom all correspondence should be sent:
E-mail: dancho_danalev@yahoo.com

According to the avalanche theory, coagulation can be considered as an auto-bioenhancing process. As a result, the inhibition of proteinases located in the centre of the process would prevent the avalanche formation of strong enzyme substrates down the chain. This thesis is proved by the fact that the inhibition of Factor Xa prevents the activation of 138 thrombin molecules [2]. That is why the main target in the creation of anticoagulants is the inactivation of Factor Xa.

In the last 20 years, a number of proteins and peptides with different molecule mass and well-established anticoagulation activity have been isolated from the salivary glands of several bloodsucking animals. Many of the strongest anticoagulants isolated from bloodsucking animals are found in the saliva of different types of leeches (Table 1).

In 1987 Tuszynski *et al*. reported for 119 amino acids protein isolated form the salivery glands of Mexican leech *Haementeria officinalis* with strong anticoagulant properties, which they named antistasin [64] (Fig. 2).

One year later kinetic investigations of Nutt *et al*. revealed that antistasin is a potent, slow, tight-binding Factor Xa inhibitor [45, 65]. A large part of the natural anticoagulant peptides and proteins isolated later show partial or complete similarity between their active centres and other parts of their molecules and those of antistasin. Thus, it becomes the founder of the largest group of natural anticoagulants – antistasin type inhibitors.

Two years later Condra *et al*. reported that they have isolated three isoforms of antistasin corresponding to its C-terminus which saved good anticoagulant activity [66]:

- isoform 1 /Arg-Pro-Lys-Arg-Lys-Leu-Ile-Pro-Arg/IC_{50} = 5 nM;
- isoform 2 /Arg-Pro-Lys-Arg-Lys/IC_{50} = 500 nM;
- isoform 3 /Arg-Pro-Lys-Arg/IC_{50} = 740 nM.

Recently, the data in literature for short peptides with strong anticoagulant activity increased. A lot of authors publish data for tripeptide sequences as D-Phe-Arg-Pro, D-Arg-Gly-Arg, Tyr-Ile-Arg, Phe-Ile-Arg, which show anticoagulant activity in nanomolar range [51, 57, 58].

EXPERIMENTAL

All compounds were synthesized by standard SPPS by means of Rink amide resin/Fmoc-strategy. The structures were proved by ES/MS.

Table 1. Sources, molecular mass and attacked enzymes of natural inhibitors of the series proteinases published in literature [3–63].

Name of inhibitor	Inhibition activity against different series proteases								Molecular weight, Da	Source
	thrombin	plasmin	trypsin	Chimo-trypsin	Plasma calicrein	Tissuae calicrein	elastase	Factor Xa		
AT III	+	ND	ND	ND	ND	ND	ND	+	65000	Blood plasma
haemadin	+	-	-	-	-	-	-	-	5000	*Haemadipsa sylvestris*
draculliND	-	-	-	-	-	-	-	+	83000	*Desmodus rotundus*
TAP	-	-	-	-	-	-	-	+	6977	*Ornithodorus moubata*
savignin	+	-	-	-	-	-	-	-	12430	*Ornithodorus savignyi*
AcAP	ND	ND	ND	ND	ND	ND	ND	+	8697	*Ancylostoma caninum*
anophelin	+	ND	ND	ND	ND	ND	ND	ND	6500	*Anopheles abimanus*
Hirudin	+	ND	ND	ND	ND	ND	ND	ND	ND	*Hirudo medicinalis*
bdellastasin	-	+	+	-	-	-	-	-	6333	*Hirudo medicinalis*
hirostasin	-	-	-	-	-	+	-	-	ND	*Hirudo medicinalis*
madanins	+	ND	ND	ND	ND	ND	ND	ND	7000	*Haemaphysalis longicornis*
therostasin	-	-	+	-	-	-	-	+	8990	*Theromyzon tessulatum*
theromin	+	-	-	-	-	-	-	-	7215	*Theromyzon tessulatum*
therin	-	-	+	-	-	-	-	-	5376	*Theromyzon tessulatum*
rhodniin	+	ND	ND	ND	ND	ND	ND	ND	ND	*Rhodnius prolixus*
lefaxin	ND	ND	ND	ND	ND	ND	ND	+	30000	*Haementeria depressa*
ixolaris	ND	-	-	-	ND	ND	ND	-	ND	*Ixodes scapularis*
guamerin	ND	ND	ND	ND	ND	ND	+	-	6110	*Hirudo nipponia*
pyguamerin	-	+	+	+	+	+	-	-	5090	*Hirudo nipponia*
ekotin	-	-	+	+	-	-	+	+	36000	*Escherichia coli*
ATS	-	-	+	-	-	-	-	+	15000	*Haementeria officinalis*
ghilantens	-	-	+	-	-	-	-	+	15000	*Haementeria ghilianii*

* 2.6 μM plasma concentration is enough to NDutralized reserve of proteins of factor Xa and thrombin.
ND – not determined.

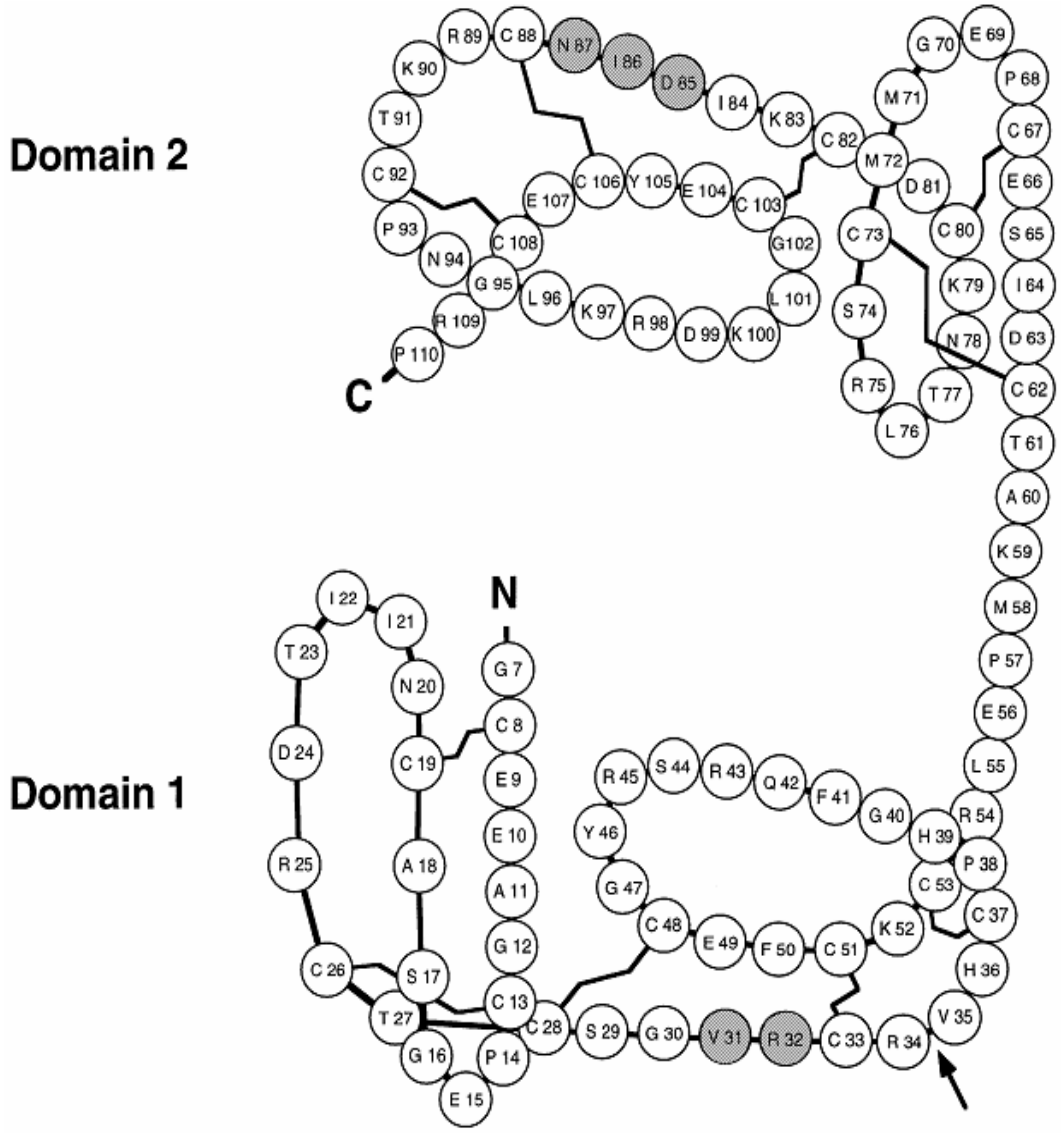

Fig. 2. Primary structure of antistasin.

RESULTS AND DISCUSSION

In 2004 we synthesized and characterized a series of hybrid structures between isoform 2 and 3 of antistasin and the above mentioned tripeptides [59]. The aim of these compounds creation was to obtain new structures with better anticoagulant activity and good selectivity towards different enzymes included in the blood coagulation cascade as well as to reveal the role of some amino acids in the different positions of the molecule. We have established interesting structure-activity relationships. In the same work, we reported for the synthesis of one hexapeptide replacing its C-terminal COOH function with $CONH_2$: D-Phe-Pro-Arg-Pro-Lys-Arg-NH_2. The latter showed 12 times better activity than its analogues with C-terminal COOH group and 40 times higher activity than the natural isoform 3 of antistasin (IC_{50} = 60.6 nmoles).

Based on the fact mentioned above, herein we reported the synthesis of all previously obtained hybride structures but replacing their C-terminal COOH function with amide:

Tyr-Ile-Arg-Pro-Lys-Arg-NH_2
Tyr-Ile-Arg-Pro-Lys-Arg-Lys-NH_2
Phe-Ile-Arg-Pro-Lys-Arg-NH_2
Phe-Ile-Arg-Pro-Lys-Arg-Lys-NH_2
D-Arg-Gly-Arg-Pro-Lys-Arg-NH_2
D-Arg-Gly-Arg-Pro-Lys-Arg-Lys-NH_2.

The anticoagulant activity according to APTT and IC_{50} values were determined. All newly synthesized peptides have manyfold higher activity than the natural isoforms of antistasin. Their IC_{50} are in nanomolar range. The kinetic investigations on the enzymes from blood coagulation cascades are in progress in order to determine the specificity of new hybride structures. The toxicity studies are in progress, too.

CONCLUSIONS

1) Lys^{113} is very important for the substrate-enzyme interaction.

2) The replacement of C-terminal COOH with $CONH_2$ results in manifold increasing of anti-coagulant activity.

3) The replacement of L- with D-amino acid in P_3 position is not a key factor for increasing the anticoagulant activity.

REFERENCES

1. R. Gould, J. Shafer, *Perspect. Drug Discovery Des.*, **1**, 419 (1993).
2. C. Richard, M. D. Becker, A. Frederick, M. D. Spencer, *Curr. Intervent. Cardiol. Rep*., **3**, 251 (2001).
3. J. Travis, J. Salvesen, *Annu. Rev. Biochem*., **52,** 655 (1983).
4. S. I. Rapaport, *Blood*, **73,** 359 (1989).
5. L. Waxmann, D. E. Smith, K. E. Arcuri, G. P. Vlasuk, *Science*, **48,** 593 (1990).
6. M. P. Neeper, L. Waxmann, D. E. Smith, C. A. Schulman, M. Sardana, R. W. Ellis, L. W. Schaffer, P. K. Siegl, G. P. Vlasuk, *J. Biol. Chem*., **265,** 17746 (1990).
7. E. D. Lexman, T. F. Shaefer, C. T. Przysiecki, J. G. Jouse, F. J. Bailey, C. A. Schulman, C. J. Burke, W. J. Miller, *Chromatographia*, **574,** 225 (1992).
8. W. F. Novotny, S. G. Broun, J. P. Mileyich, D. J. Rader, G. J. Broze, *Blood*, **78,** 387 (1991).
9. F. Faria, E. M. Kelen, C. A. Sampaio, C. Bon, N. Duval, A. M. Chudzinski-Tavassi, *Thromb. Haemostasis*, **82**(5), 1469 (1999).
10. J. Hofsteenge, H. Taguchi, S. R. Stone, *Biochem. J*., **237**, 234 (1986).
11. S. R. Stone, J. Hofsteenge, *Biochemistry*, **25**, 4622 (1986).
12. K. H. Strube, B. Kroger, S. Bialojan, M. Otte, J. Dodt, *J. Biol. Chem.*, **268**, 8590 (1993).
13. A. Z. Fernandez, A. Tablante, S. Beguin, H. C. Hemker, R. Apitz-Castro, *Biochim. Biophys. Acta*, **1434**, 135 (1999).
14. R. Apitz-Castro, S. Beguin, A. Tablante, F. Bartoli, J. C. Holt, H. C. Hemker; *Thromb. Haemostasis*, **73**, 94 (1995).
15. A. V. Basnova, I. P. Baskova, L. L. Zavalova; *Biochemistry (Moscow)*, **67**, 143 (2002).
16. A. Edward, *Biochemistry*, **43**, 3368 (2004).
17. J. Nienaber, A.R. Gaspar, A.W. Neitz, *Exp. Parasitol.*, **93**, 82 (1999).
18. M. Capello, G. P. Vlasuk, P. W. Bergum, S. Huang, P. J. Hotez, *Proc. Natl. Acad. Sci. USA*, **92**, 6152 (1995).
19. X. Zang, R. M. Maizels; *Trends Biochem. Sci.*, **26**, 191 (2001).
20. I. M. Francischetti, J. G. Valenzuela, J. M. Ribeiro; *Biochemistry*, **38**, 16678 (1999).
21. H. D. Menssen, K. Melber, N. Brandt, E. Thiel; *Clin. Chem. Lab. Med.*, **39**, 1267 (2001).
22. M. Moser, E. Auerswald, R. Mentele, C. Eckerskorn, H. Fritz, E. Fink, *Eur. J. Biochem*. **253**, 212 (1998).
23. S. Di Marco, G. Fendrich, R. Knecht, G. Pohlig, J. Heim, J. P. Priestle, C. P. Sommernof, M. G. Grutter, *Protein Sci.*, **6**, 109, (1997).
24. I. Usón, G. M. Sheldrick, E. de la Fortelle, G. Bricogne, S. Di Marco, J. P. Priestle, M. G. Grütter, P. Mittl, *Structure*, **7,** 55 (1999).
25. S. Iwanaga, M. Okada, H. Isawa, A. Morita, M. Yuda, Y. Chinzei, *Eur. J. Biochem.,* **270**, 1926 (2003).
26. V. Chopin, M. Salzet, J. Baerti, F. Vandenbulcke, *J. Biol. Chem.*, **275**, 32701 (2000).
27. M. Salzet, V. Chopin, J. Baerti, I. Matias, J. Malecha, *J. Biol. Chem.*, **275**, 30774 (2000).
28. V. Chopin, I. Matias, G. B. Sefano, M. Salzet; *Eur. J. Biochem.,* **254**, 565 (1998).
29. H. Isawa, M. Yuda‡, K. Yoneda, Y. Chinzei, *J. Biol. Chem.*, **275**, 6636 (2000).
30. P. Ascenzi, M. Nardini, M. Bolognesi, W. R. Montfort, *Biochem. Mol. Biol. Educ.*, **30**, 68 (2002).
31. D. E. Champagne, R. H. Nussenzveig, J. M. Ribeiro, *J. Biol. Chem.*, **270**, 8691 (1995).
32. J. F. Andersen, W. R. Montfort, *J. Biol. Chem.*, **275**, 30496 (2000).
33. V. de Locht, D. Lamba, M. Bauer, R. Huber, T. Friedrich, B. Kroger, W. Hoffken, W. Bode, *EMBO J.*, **14**, 5149 (1995).
34. K. Mende, O. Petoukhova, V. Koulitchkova, G. A. Schaub, U. Lange, R. Kaufmann, G. Nowak, *Eur. J. Biochem*., **266**, 583 (1999).
35. M. B. Francischetti, J. G. Valenzuela, J. F. Andersen, T. N. Mather, J. M. C. Ribeiro; *Blood*, **99**, 3602 (2002).
36. H. I. Jung, S. A. Kim, K. C. Ha, C. O. Joe, K. W. Kang, *J. Biol. Chem.*, **270**, 13879 (1995).
37. S. J. Hong, K. C. Ha, C. O. Joe, K. W. Kang, *J. Enzime Inhib.*, **10**, 81 (1996).
38. D. R. Kim, K. W. Kang, *Eur. J. Biochem.*, **254**, 6922 (1998).
39. C. H. Chung, H. E. Ives, S. Almeda, A. L. Goldberg, *J. Biol. Chem.*, **258**, 11032 (1983).
40. J. L. Seymour, R. N. Lindquist, M. S. Dennis, B. Moffat, D. Yansura, D. Reilly, M. E. Wessinger, R. A. Lazarus, *Biochemistry*, **33**, 3949 (1994).
41. N. Fusetani, S. Matsunga, *J. Am. Chem. Soc*., **112**, 7053 (1990).
42. B. J. Mans, A. I. Louw, A. W. H. Neitz, *Mol. Biol. Evol*. **19**, 1695 (2002).
43. S.-S. Mao, *Perspect. Drug Discovery Des.,* **1**, 423 (1994).
44. N. Ohta, M. Brush, J. W. Jacobs, *Thromb. Haemostasis*, **72**, 825 (1994).
45. E. Nutt, T. Gasic, J. Rodkey, G. J. Gasic, J. W. Jacobs, P. A. Friedman, E. Simpson*, J. Biol. Chem.*, **263**, 10162 (1988).
46. D. T. Blankenship, R. G. Brankamp, G. D. Manley, A. D. Cardin, *Biochem. Biophys. Res. Commun.*, **166**, 1384 (1990).

47. S. S. Mao, C. T. Przysiecki, J. A. Krueger, C. M. Cooper, S. D. Lewis, J. Joyce, C. Lellis, V. M. Garskyi, M. Sardana, J. A. Shafer, *J. Biol. Chem.*, **273**, 30086 (1998).
48. K. Kamata, H. Kawamoto, T. Honma, T. Iwama, S.H. Kim, *Biochemistry*, **95**, 6630 (1998).
49. T. Steinmetzer, M. Renatus, S. Kunzel, A. Eichinger, J. Sturzebecher, *Eur. J. Biochem.,* **265**, 598 (1999).
50. T. Steinmetzer, M. Batdordshjin, F. Pineda, L. Seyfarth, A. Vogel, S. Reißmann, J. Hauptmann, J. Stürzebecher, *Biol. Chem.*, **381**, 603 (2000).
51. J. A. Ostrem, F. Al-Obeidi, *Biochemistry*, **37**, 1053 (1998).
52. M. T. Fox, B. Greer, G. J. Allen, J. Lawson, A. Healy, P. Harriot, J. Sturzebecher, F. Markwardt, P. Walsmann, *Thromb. Res.*, **9,** 637 (1976).
53. C. W. Pratt, F. C. Church, *Semin. Hematol*., **28,** 3 (1991).
54. W. Kiesel, W. M. Canfield, L. H. Ericsson, E. W. Davie, *Biochemistry*, **16**, 5824 (1997).
55. J. Wityak, R. A. Earl, M. M. Abelman, Y. B. Bethel, B. N. Fisher, G. F. Kaufmann, C. A. Kettner, P. Ma, J. L. McMillan, P. N. Confalone, *J. Org. Chem*., **60**, 3717 (1995).
56. L. Cheng, C. A. Goodwin, M. F. Scully, V. V. Kakkar, G. Glaeson, *Tetrahedron Lett.*, **32**, 7333 (1991).
57. S. Bajusz, E. Szell, D. Bagdy, E. Barabas, G. Horvath, M. Dioszegi, Z. Fittler, G. Szabo, A. Juhasz, E. Tomori, G. Szilagyi, *J. Med. Chem*.**, 33,** 1729 (1990).
58. C. K. Marlowe, U. Sinha, A. C. Gunn, R. M. Scarborough, *Bioorg. Med. Chem. Lett*., **10**, 13 (2000).
59. D. Danalev, L. Vezenkov, B. Grigorova, *J. Pept. Sci*., **10**, 27 (2004).
60. H. Angliker, S. Stone, E. Shaw, *Peptides*, **4**, 35 (1990).
61. F. Markwardt, H. Landmann, P. Walsmann, *Eur. J. Biochem*., **6,** 502 (1968).
62. J. Loscalzo, A. I. Schafer (eds), Thrombosis and Hemorrhage, 2nd ed., Williams and Wilkins, Baltimore, 1998.
63. D. R. Light, W. J. Guilford, *Curr. Top. Med. Chem.*, **1**, 121 (2001).
64. G. P. Tuszynski, T. B. Gasic, G. J. Gasik, *J. Biol. Chem.,* **262**, 9718 (1987).
65. E. M. Nutt, D. Jain, A. B. Lenney, L. Schaffer, P. K. Siegl, C. T. Dunwiddie, *Arch. Biochem. Biophys.*, **285**, 37 (1991).
66. C. Condra, E. M. Nutt, C. J. Petroski, *Thromb. Haemostasis*, **61**, 437 (1989).

ДИЗАЙН, СИНТЕЗ И АНТИКОАГУЛАНТНИ ИЗСЛЕДВАНИЯ НА НОВИ АМИДНИ АНАЛОЗИ НА ИЗОФОРМИ 2 И 3 НА АНТИСТАЗИН

Д. Л. Даналев*, Л. Т. Везенков

Катедра „Органична химия“, Химикотехнологичен и металургичен университет, бул. „Климент Охридски“ № 8, 1756 София

Постъпила на 6 юли 2008 г.; Преработена на 18 септември 2008 г.

(Резюме)

Един от най-важните ензими в каскадата на кръвната коагулация е Фактор Ха. Ето защо неговите инхибитори са една обещаваща алтернатива срещу тромботични заболявания. В предишна наша работа ние докладвахме синезата на хибридни структури между изоформи 2 и 3 на антистазина и активните последователности D-Phe-Pro-Arg; D-Arg-Gly-Arg; Phe-Ile-Arg и Tyr-Ile-Arg. Освен аналозите с С-крайна COOH група, беше синтезиран и хексапептид амида D-Phe-Pro-Arg-Pro-Lys-Arg-NH_2. Той показа 60 пъти по-висока биологична активност от природната изоформа 3 на антистазина и няколко пъти по-висока активност от всички останали новосинтезирани аналози. В настоящата работа ние описваме синтеза и биологичната активност на С-крайните амидни аналози на всички по-рано синтезирани пептиди с цел да изведем зависимости структура-биологична активност. Антикоагулантната активност беше измерена по отношение на APTT и бяха определени IC_{50} стойностите за всички новосинтезирани съединения.

Bulgarian Chemical Communications, Volume 41, Number 2 (pp. 104–109) 2009

From molecule to sexual behaviour – the role of brain neuropentapeptide proctolin in acoustic communication of the grasshopper *Chorthippus biguttulus* (L. 1758)

St. R. Vezenkov[1]*, H. Ralf[2], N. Elsner[2]

[1] *Department of Speech Pathology, Neofit Rilski South-West University, 66 Ivan Mihailov St., 2700 Blagoevgrad, Bulgaria*
[2] *Department of Neurobiology, Institute of Zoology, Anthropology and Developmental Biology, 28 Berliner St., 37073 Göttingen, Germany*

Received July 20, 2008; Revised September 30, 2008

The acoustic communication of *Chorthippus biguttulus* (*Ch.b.*) is a suitable behavioural model system to explore the physiological effects and underlying molecular mechanisms of identified neuropeptides. Neuropentapeptide proctolin was shown to play a modulatory role in a brain neuronal circuit that controls the acoustic, respectively sexual behaviour of males *Ch.b.* Proctolin receptors activation triggered courtship singing, the second level of excitation in the sexual behaviour preceded by calling singing, triggered by mAChRs activation. Pharmacological studies showed that PLC pathway is involved in courtship singing since neomycine and Li^+ showed strong inhibitory effect on the proctolin-stimulated singing. In addition, the phorbol ester, injected in proctolin sensitive sites in the brain, elicited stridulation alone. The latter showed that PKC could mediate the effects of PLC activation. The observed results suggest possible molecular mechanisms that are involved in the decision-making brain center controlling the sexual behaviour – what (by altering the context), when (by controlling the initiation) and how long (by increasing the basal excitation) should the male sing.

Key words: neuropeptide, proctolin, PKC, acoustic communication, courtship, *Chorthippus biguttulus.*

INTRODUCTION

Acoustic communication in orthopteran insects has become one of the favourite subjects for investigations on the neuronal basis of invertebrate behaviour. The stereotyped stridulation patterns, the relative ease of their elicitation, and the simplicity of the neuromuscular organization, which permits electrophysiological and pharmacological work in freely-moving animals, favour both an ethological and a neurophysiological approach [1]. Proctolin (RYLPT) was the first neuropeptide to be isolated and sequenced from insects [2] and was subsequently found to have wide distribution throughout the arthropods [3]. First proctolin has been reported [4] as a "gut factor", which caused slow graded contractions of proctodeum longitudinal muscles in the cockroach *Periplaneta americana*. On the other side, a G-protein coupled receptor (encoded by CG6986) for proctolin in *Drosophila melanogaster* has been identified and characterized [5]. Proctolin receptor immunosignals have been found in the hindgut, heart and in distinct neuronal populations of the CNS.

Previous studies have demonstrated a role for acetylcholine (ACh) and both nicotinic acetylcholine receptors (nAChRs) and muscarinic acetylcholine receptors (mAChRs) in the cephalic control of the singing behaviour of various grasshopper species [6, 7]. Injections of proctolin into the protocerebrum can elicit species-specific stridulation in both male and female grasshoppers of the species *Ch.b.* The stimulated behaviour is similar to the natural stridulation with respect both to the temporal structure and patterns of stridulatory movements of the hindlegs [8]. This study presents the role of intracellular signal transduction coupled to proctolin-stimulated singing behaviour.

EXPERIMENTAL

Animals

Adult specimen of the gomphocerine grasshopper *Chorthippus biguttulus* (L. 1758) *(Ch.b.*) were caught in the vicinity of Göttingen, Germany, and kept in the laboratory for up to several weeks. Additional *Ch. biguttulus* were reared from eggs that were collected in the previous summer and kept at 4°C for > 4 months. The nymphs hatched after ~ 1 week at 26°C and were raised on wheat and supplemental food for crickets (Nekton, Pforzheim) at a 16/8 h light-dark-cycle. All pharmacological experiments were conducted with male and female

* To whom all correspondence should be sent:
E-mail: vezenkov_neuro@abv.bg

adults at room temperatures of 20–25°C. Virgin females were separated as third or fourth stage nymphs kept in separation and used as adult for acoustic stimulation experiments.

Basic scheme

Small amounts (< 10 nl) of neuroactive substances were pressure-injected *via* microcapillaries inserted dorsally into the brain. By the use of double-barrel electrodes two different substances were administered to the same location within the brain. Therefore, sequential injections of identical volumes of the same or of two different substances (excitatory, inhibitory or modulatory) could in principle influence the same set of neurons. To monitor the stridulatory behaviour, the hind leg movements and the produced sound were recorded with two opto-electronic cameras and a microphone. The animal is attached to a holder. The head is opened and the brain is exposed. The micro-capillary is attached to the mechanic micromanipulator and is connected to the pressure-injection device through pressure resistant tubes. A three-way stopcock allows the pressed air to flow in two directions, respectively into one of the two barrels of the micro-capillary. The pump is connected to a system that continuously supplies compressed air. Two optic-electronic devices according to von Helversen [7] record the stridulatory movements of the hind legs and transform them into a voltage signal. The latter is amplified and visualized on the computer screen. The signal is stored in data format (*.dat) by the program Turbo Lab 4.2 or 4.3 for DOS.

Drugs used for injection

The neuroactive substances were usually dissolved in grasshopper saline [9] to give concentrations of 1 mM. Muscarine, proctolin, neomycin obtained from Sigma-Aldrich; SQ 22536 obtained from Calbiochem; phorbol-12-myristate-13-acetate (PhE, porbol ester), thapsigargin, TMB-8, ryanodine, LiCl, purchased from Sigma-Aldrich were studied using the upper-described basic scheme. Stock solutions of proctolin (10 mM concentration in d H_2O) were preserved at –20°C. Water-soluble substances were dissolved in grasshopper saline to give concentrations of 1 to 0.1 mM. Different ions (Ba^{2+}, Ni^{2+}) were added to the saline to give 1 to 5 mM. Substances soluble in DMSO (thapsigargin, TMB-8, ryanodyne, obtained from Sigma-Aldrich) were dissolved in saline to give a 5% final content of DMSO. All solutions were preserved at –4°C, not longer than 1 day.

Data processing

The recorded signals were digitized on-line by means of an A/D-converter card (Real Time Devices AD3300) with the software Turbolab 4.2 (Bressner Technology, Germany) and stored as data files. The sampling rate for recording the stridulatory movements, the sound and the injection pulses was 5 kHz per recorded channel. The software NEUROLAB (8.2, Hedwig and Knepper) was used for visual examination and filtering of the original data. One injection of a stimulating drug usually released several song sequences separated by short pauses. The time between stimulation pulse and the beginning of the first stridulatory sequence was determined as Latency. The sum of the durations of all individual song sequences released by one stimulation was calculated as the total sequence duration (S Duration) of stridulation. The duration from the beginning of the first sequence to the end of the last sequence was taken as the complete duration (C Duration) of stridulation. Latency and the durations of stridulation were normalized to the longest latency and the duration in that particular experiment (same volume of drug injected to the same site within the brain). The values were calculated and given in percent (%). Normalization was necessary to enable comparison between different experiments with variable efficacy of proctolin stimulations, depending on the exact site of injection and the condition of the grasshopper. Potential changes in the latency and duration of proctolin-induced stridulation following the injection of a test-substance were evaluated by the nonparametric Friedman test (ANOVA). “Raw” diagrams were generated with Excel 2000 and subsequently imported into graphics program CorelDraw 9 (Corel Corporation) for assembly into composite figures and labelling. Original data (hind leg movements, pressure pulse) were exported from Neurolab 8.2. and subsequently re-assembled and labelled with CorelDraw 9. All figures were stored as graphics files (*.jpg) and imported into Word 2000.

RESULTS AND DISCUSSION

Proctolin alone elicits courtship singing behaviour in males Ch.b.

Injections of proctolin into the frontal part of the central complex and an adjacent neuropil anterior and dorsal to it elicited a species-specific singing behaviour in males of *Ch.b* (Fig. 1). Both proctolin and muscarine stimulated stridulation in a region that includes the anterior portion of the central body and the area between the central body and Proto-

cerebral Bridge. However, the responses to both drugs differed in latency, duration (Fig. 2), also in internal time courses of the hind legs movements. The temporal structure of muscarine- and proctolin-stimulated stridulation were likely to respectively calling song and courtship song which correlate to two different excitation levels [8]. The proctolin-elicited singing might be the second level of excitation because the courtship singing in the natural sexual behaviour appears after the calling singing. The male produces courtship song when duets together with the responding female that shows copulatory readiness. Thus, proctolin might trigger the courtship singing of the male, respectively the higher, behavioural different, level of excitation in comparison to muscarine-stimulated calling singing.

PLC pathway and the proctolin-stimulated singing

Typically, the actions of proctolin are slow in onset and prolonged, suggesting the involvement of a second messenger activated by a metabotropic receptor or G-protein coupled receptor. An ubiquitous cascade that is mediated through G proteins and evokes many responses is the phosphoinositide cascade or simply PLC pathway. Likewise the other cascades, it converts extracellular signals into intracellular ones. It has previously been reported that the PLC/IP_3/DAG signal transduction cascade mediates the performance of calling singing behaviour in *Ch.b.* following activation of mAChRs. Inhibition of PLC activity by U-73122 and neomycin, which act by different mechanisms, can completely suppressed muscarine-stimulated stridulation [10]. It was shown also that scopolamine, an inhibitor of mAChR, did not affect the proctolin-stimulated singing injected together with proctolin [8]. To investigate a possible involvement of phosphoinositides in mediating the proctolinergic excitation, neomycin, a substance that reduces PLC activity by binding to the enzyme's substrate PIP_2 was injected to site where proctolin stimulates singing. Injection of this inhibitor produced a gradual reversing reduction of proctolin-stimulated stridulation. The average duration of singing in all experiments decreased significantly ($P < 0.05$, $n = 10$) in the period of 12–16 min (Fig. 3A). In 3 other experiments, the proctolin-initiated stridulation was suppressed irreversibly and were not put into analysis. Li^+, also known as a PLC inhibitor, was tested. In all experiments ($n = 9$, $P < 0.05$) a reversible decrease of both sequential (SD) and complete (CD) duration of proctolin-stimulated singing occurred (Fig. 3B).

The robust appearance of the inhibitory effect of neomycin and Li^+ on proctolin-stimulated singing behaviour suggested a main role for the PLC pathway mediating proctolinergic excitation in the brain of *Ch.b*.

PKA might mediate the proctolin-stimulated singing

Diacylglycerol (DAG) is a second messenger generated through PLC signaling and activates the proteinkinase C which phosphorilates proteins, ion channels, receptors, *etc*. and alters the neuronal activity. In various insect preparations, DAG has been shown to contribute to proctolin receptor-triggered excitation [11, 12].

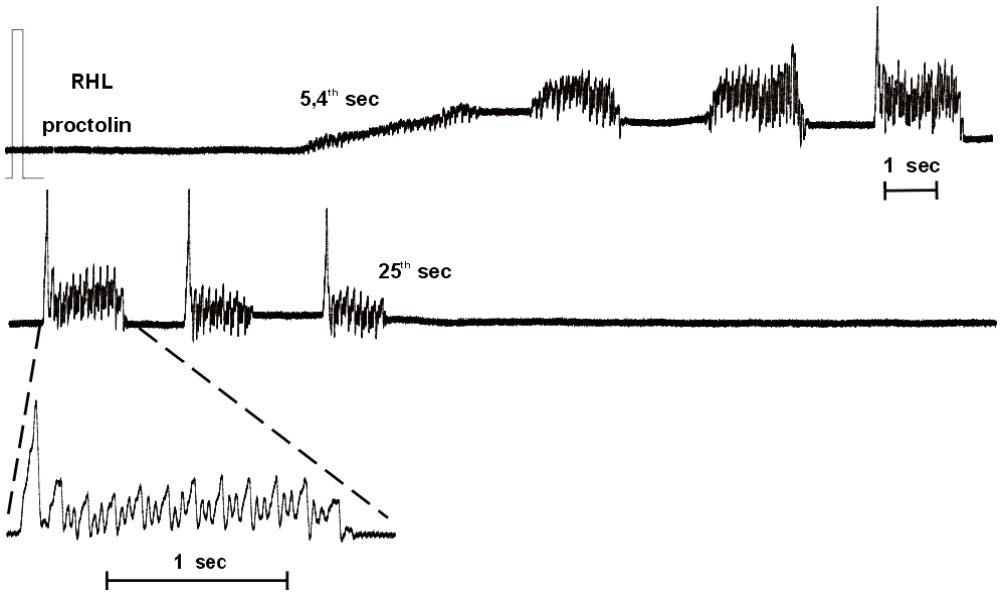

Fig. 1. Proctolin, injected inbetween the central body and Protocerebral Bridge of the brain, alone elicits courtship singing in male *Ch.b.* (RHL – right hindleg).

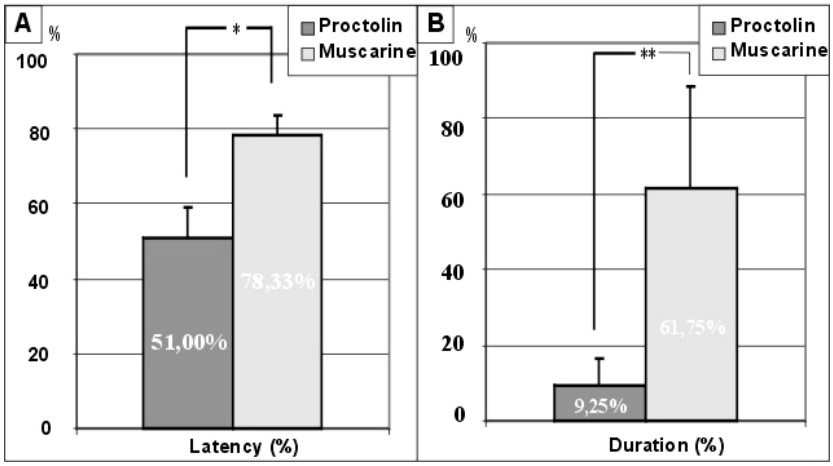

Fig. 2. Comparison between proctolin- and muscarine-stimulated stridulation induced at the same spots in the protocerebrum of males *Ch.b.* A. The latency of proctolin-induced stridulation was shorter ($P < 0.05$); B. The duration of the proctolin produced singing was much shorter than muscarinic ($P < 0.01$).

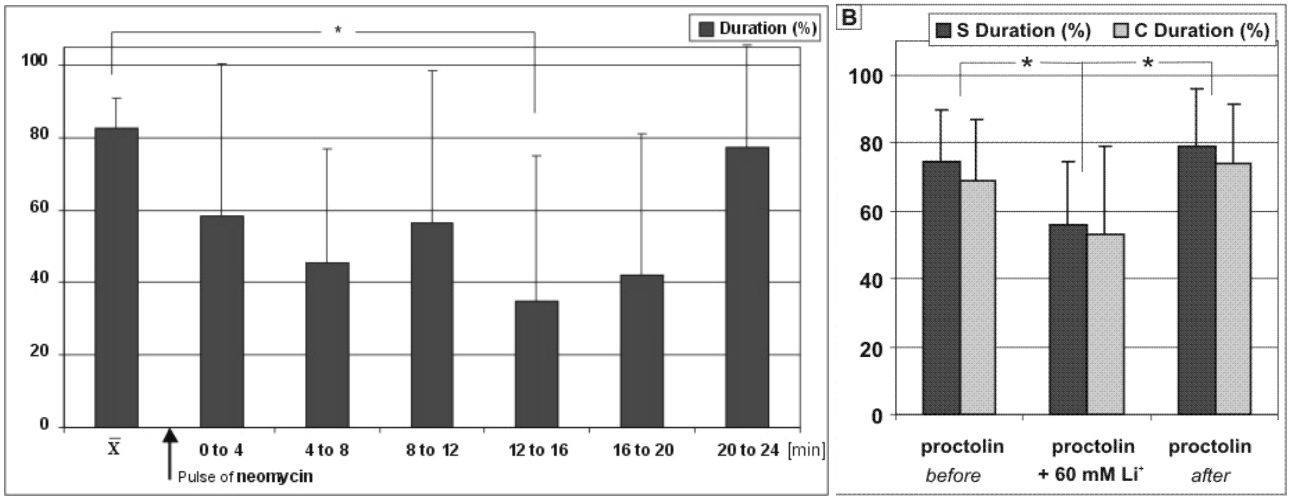

Fig. 3. Effects of the PLC inhibitors neomycin (A) and Li^+ (B) on proctolin-stimulated singing (males, Ch.b.). A. Two phases of reversible inhibition were observed: the first one from 4^{th} to 8^{th} min and the second – 12^{th} to 20^{th} min ($n = 10$, $P < 0.05$); B. Li^+ co-injected with proctolin reduced both S and C Duration of proctolin-induced singing ($n = 9$, $P<0.05$).

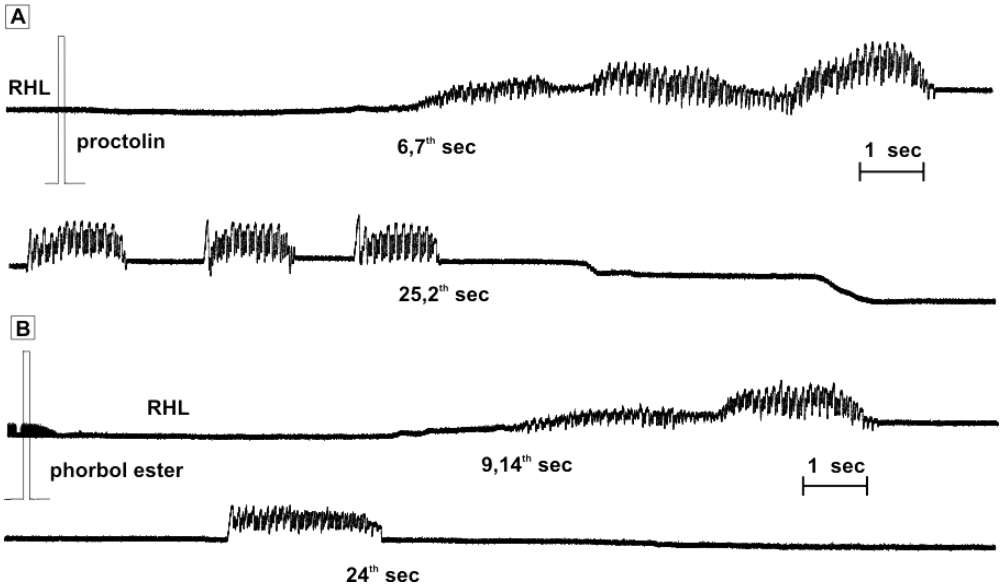

Fig. 4. Male singing (*Ch.b.*) induced through proctolin (A) and phorbol-12,13-dibutirate (phorbol ester, PhE) (B), injected at the same spot in the brain.

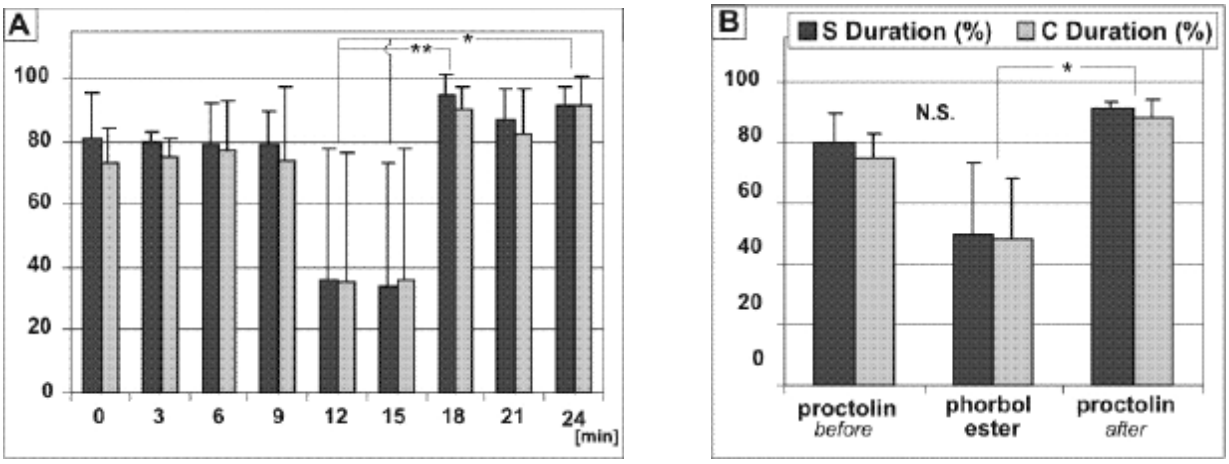

Fig. 5. S and D durations of proctolin- and phorbol ester-induced singing (males, *Ch.b.*, n = 4).
A. 0, 3, 6 min and 18, 21, 24 min – responses to proctolin; 9, 12, 15 min – responses to PhE;
B. Average values of the S and D durations ($P < 0.05$).

A possible role of DAG in proctolin-stimulated singing was examined through injections of phorbol-12,13-dibutirate (phorbol ester, PhE) at the same brain areas of *Ch.b.*, where proctolin stimulated singing. In the first series of experiments PhE was injected alone from the second chamber of the capillary following and preceding 3 proctolin pulses all injected with the same interval between individual stimulations. Injections of PhE into the *Ch.b.* brain elicited coordinated singing movements that were indistinguishable from proctolin-stimulated singing induced at the same site within the brain (Fig. 4A, B). However, the time course of the released singing differed in that the average relative duration of singing behaviour after injection of PhE was significantly shorter (from 80%, SD = 9.77% down to 50%, SD = 23.88%; $P < 0.05$; n = 4) than the preceding and following injections of proctolin (Fig. 5A, B), while the latency was significantly longer (data not shown). After 3 pulses PhE the durations of proctolin-elicited singing increased up to slightly higher levels than before (Fig. 5A, B), indicating a weak after-effect on the excitation due to PhE stimulation. Thus, the PKC might mediate the PLC activity triggered by proctolin and the relevant G-protein coupled receptors.

CONCLUSIONS

The proctolin-stimulated singing differed significantly from muscarine-stimulated one due to its time course and context, respectively courtship and calling singing. Additionally, the blockade of PLC through neomycine and Li^+ showed strong inhibitory effect on the proctolin-stimulated singing in males (*Ch.b.*), since complete inhibition was common in most of the experiments. On the other hand, proctolin effects have been not altered by scopolamine, a mAChRs inhibitor. This suggests that the proctolin receptors, coupled to PLC pathway, play a main role in the brain control of courtship singing, triggered by proctolin in comparison to the controlled by mAChRs activation calling singing.

PKC activation (through phorbol ester) potentiated proctolin-stimulated responses, indicating additional level of excitation to this induced by proctolin. This may suggest a potential side entry for additional synergistic effects on singing related arousal from other receptors coupled to PLC signalling pathway. Moreover, phorbol ester injected alone to sites, where proctolin was induced singing, mimicked partly the proctolin response.

The latter suggests that proctolin receptors, activated by proctolin that stimulate courtship singing behaviour in males (*Ch.b.),* are coupled to intracellular PLC signalling pathway and most likely uses DAG as a second messenger.

The observed results suggested possible molecular mechanisms that are involved in the decision-making brain centre controlling the sexual behaviour – what (by altering the context), when (by controlling the initiation) and how long (by increasing the basal excitation) should the male sing in presence (courtship) or absence (calling) of a female.

REFERENCES

1. N. Elsner, *J. Comp. Physiol.*, **88**, 67 (1974).
2. B. E. Brown, *Life Sci.*, **17**, 1241 (1975).
3. D. Konopinska , G. Rosinski, *J. Pept. Sci.*, **5**, 533 (1999).
4. B. E. Brown, *Science*, **155**, 595 (1967).
5. E. C. Johnson, S. F. Garczynski, D. Park, J. W. Crim, D. R. Nässel, P. H. Taghert, *Proc. Nat. Acad. Sci., USA*, **100**, 6198 (2003).
6. R. Heinrich, B. Wenzel, N. Elsner, *J. Comp. Physiol., A*, **187**, 155 (2001).

7. O. von Helversen, N. Elsner, *J. Comp. Physiol.*, **122**, 53 (1977).
8. S. R. Vezenkov, PhD Thesis, GAU, Goettingen, 2004.
9. A. N. Clements, T. E. May *J. Exp. Biol.*, **61**, 421 (1974).
10. B. Wenzel, N. Elsner, R. Heinrich, *J. Neurophysiol.*, **87**, 876 (2001).
11. J. M. Hinton, M. Nejad, J. P. Issberner, J. T. Hancock, R. H. Osborne, *Insect. Biochem. Mol. Biol.*, **28**, 331 (1998).
12. C. Wegener, D. R. Nässel, *J. Neurophysiol.*, **84**, 3056 (2000).

ОТ МОЛЕКУЛАТА ДО СЕКСУАЛНОТО ПОВЕДЕНИЕ – РОЛЯТА НА МОЗЪЧНИЯ НЕВРОПЕНТАПЕПТИД ПРОКТОЛИН В АКУСТИЧНАТА КОМУНИКАЦИЯ НА СКАКАЛЕЦА *Chorthippus Biguttulus* (L.1758)

Ст. Р. Везенков[1]*, Р. Хайнрих[2], Н. Елснер[2]

[1] Катедра „Логопедия“, Югозападен университет „Неофит Рилски“, ул. „Иван Михайлов“ № 66, 2700 Благоевград,
[2] Департамент „Невробиология“, Институт по зоология, антропология и биология на развитието, ул. „Берлинер“ № 28, 37073 Гьотинген, ФР Германия

Постъпила на 20 юли 2008 г.; Преработена на 30 септември 2008 г.

(Резюме)

Звуковата комуникация на скакалеца *Chorthippus biguttulus* (*Ch.b.*) е удобен поведенчески модел за изследване на неврофизиологичните ефекти на идентифицирани невропептиди и стоящите зад тях молекулярни механизми. Невропентапептидът проктолин играе модулираща роля в мозъчната невронална мрежа, която контролира звуковата комуникация (стридулация), респективно сексуалното поведение на мъжките от вида *Ch.b.* Активирането на проктолиновите рецептори инициира изпълнението на любовна песен (courtship song), второ ниво на сексуално поведение, предхождано от серенада (calling song), контролирано от активирането на мускариновите ацетилхолинови рецептори (mAChRs). Фармакологичните изследвания показаха, че вътреклетъчната сигнална каскада на фосфолипаза Ц (PLC) е свързана с любовното пеене, тъй като неомицинът и литиевите йони имаха силен инхибиторен ефект върху стимулираното от проктолина пеене. Нещо повече, форболовият естер (аналог на вторичния посредник диацилглицерол), инжектиран в чувствителните към проктолин места в мозъка, предизвиква стридулация самостоятелно. Това показва, че протеинкиназа Ц медиира ефектите на активираната фосфолипаза Ц. Получените резултати показват възможните молекулярни механизми, които участват при взимането на решение в мозъчен център, контролиращ сексуалното поведение – какво (чрез промяна на контекста на изпълняваната песен), кога (чрез контрол на инициацията на продуциране на звуци) и колко продължително (чрез повишаване нивото на възбудния процес) мъжкия скакалец да произвежда видово и полово специфични звуци.

Bulgarian Chemical Communications, Volume 41, Number 2 (pp. 110–115) 2009

Solvent-free self-assembly of small organic molecules into fibrilar microstructures

D. S. Tsekova[1]*, B. Escuder[2], J. Miravet[2]

[1] *Department of Organic Chemistry, University of Chemical Technology and Metallurgy, 8 Kliment Ohridski Blvd., 1756 Sofia, Bulgaria*
[2] *Department of Inorganic and Organic Chemistry, Universitat Jaume I, 12071-Castellon, Spain*

Received July 17, 2008; Revised September 25, 2008

Self-assembly is an efficient approach for the preparation of supramolecular structures with sizes ranging from nanometers to micrometers. Investigation of self-assembled fibres and fibrils is in the focus of very active research as these materials have potential applications in tissue engineering, template for inorganic nanofibres, electrooptical materials, etc. Here we report that recently synthesized L-valine and pyridine containing low-molecular compounds, self-assemble under solvent-free conditions into fibril structures in solid state. Heating of a dry powdered sample caused formation of rod-like particles. The initially formed nanofibres evolved to microscale needles upon further heating. The habitus of the fibres grown remains stable upon cooling. Results obtained represent an interesting alternative for the preparation of organic crystalline nanoobjects and microfibres in solvent-free conditions.

Key words: low-molecular gelators, supramolecular complexes, organic nano- and microfibres.

INTRODUCTION

The interest in new designs for self-assembly approaches in producing microscopically small objects continuously increases in the last decades [1–3]. An attractive morphology of such nano- and micro-items is the fibrous one as many properties (mechanical, electrical, optical, transport, *etc*.) can be controlled along the fibre sizes. Conventional methods used up to now in the preparation of supramolecular nano- and micro fibres from small molecular organic compounds involve work in solution. Here, we are describing organic compounds that are capable of self-assembling into fibres with nano- and micro-dimensions in the absence of solvent. Some examples for solvent-free processes like chemical reactions [4, 5], synthesis of nano-capsules [6], *etc*. are presented in literature and although they are still limited in number, obviously it is more economic and pure approach, definitely preferred, when it is applicable. It is also in a good agreement with the principles of green chemistry.

Recently we reported [7] that compound **1** (Fig. 1), which belongs to the family of the so-called low-molecular gelators (LMWG), forms gels or other precipitates in organic solvents and in water. All the solids obtained from its solutions (xerogels, spherulites, *etc*.) were found to be constructed by thin fibres which X-ray powder diffraction (XRPD) data showed the crystalline structure called **1α**. We found that when heating a powdered solid material from **1α** above 225°C, a solid state polymorphic transition took place leading to a fiber-like polymorph **1β**. Polymorph **1β** was obtained also after melting of the product and cooling down to room temperature. XRPD, differential scanning calorimetry (DSC), infrared spectroscopy (IRS) and circular dichroism spectroscopy (CD) measurements gave an evidence of the solid-solid transformation [7].

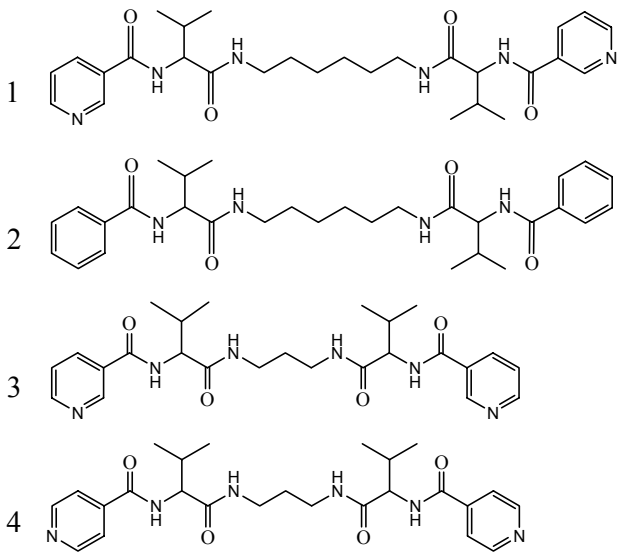

Fig. 1. Compounds used in the experiments.

Here we report that compounds related to **1** (Fig. 1) during the heating in the absence of solvents exchange their morphology and the particles, shapeless at the micro scale (Fig. 2a), self-organize into filament formations (Fig. 2b). The fibres formed belong to two types: the first one corresponds to

* To whom all correspondence should be sent:
E-mail: d_tsekova@abv.bg

straight fibres which are isolated and with no branching and the second one – to twisted pronged fibres that can even be wrapped as rope. Their habitus depends on the chemical structure and conditions of obtaining (Fig. 2, 3). Polymorphic exchange noticed for compound **1** during the heating [7] (Fig. 4.1) is not always observable with the other compounds. Noticeably, the fibres obtained from compounds **3** and **4** under the same conditions posses helical structure (Fig. 3a, b, d, e,), which is a very good example for amplification of molecular chirality in supramolecular aggregates. One of the active research fields nowadays concerns translation of chirality from molecular level to micro- and macro scale. It was pointed by other authors summarising the results obtained over the past decade that the predicting of amplification of chirality is challenging but still impossible [8].

EXPERIMENTAL

Compounds used in this work are presented in Fig. 1. They were synthesized according to previously described protocols for compound **1** [7], **2** [9], **3** and **4** [10]. All they belong to the group of LMWG and form gels or other solid precipitates in different solvents. In order to check their self-assembly ability in the absent of solvent, demonstrated from compound **1**, as well as correlated with this process phenomena, e.g. solid state phase transition, a series of experiments was realised.

Thermal treatment and preparation of samples for scanning electron microscopy (SEM). Thermal treatment of the substances was done in two ways. First one was similar to that explained for compound **1** [7]. Briefly: Sample of well-crushed material obtained as a product of the synthesis, or after recrystallization (xerogel, spherulites, etc.), was put on a cover glass slide, placed over a heating plate and observed with the loupe while heating. Along the heating, at temperatures individual for each compound, the powdered material (Fig. 2a) starts to rearrange into fibril objects. Keeping the temperature higher than this one and lower than the melting point leads to exchanges of the fibril sizes. Temperature intervals and time of heating are individual. The observed habitus remained stable upon cooling the samples to room temperature. A number of samples were prepared and for each one the heating was stopped at a different level of shape exchange, left for cooling and used for SEM studies (Fig. 2b, c, Fig. 3a, b, d, e). Second way for preparation of patterns for SEM studies was in DSC apparatus. We tried to relate conditions of the open system with those in a closed system in DSC pans, where all parameters were strictly defined. In DSC pans, the powdered material was enclosed, sealed very well and thermal conditions were set before starting the experiments. After cooling, the pans were opened and transformations were recorded by SEM observations (Fig. 3c, f).

DSC measurements also were done to follow the thermal behaviour of the compounds, in order to have precise data for melting points and polymorph transitions, in case they take place. XRPD, IR and CD measurements of solids obtained from solutions as well as after thermal treatment at specific temperature were performed in order to determine the characteristics of these materials and any relation between them.

RESULTS AND DISCUSSION

First of all, we should notice again that all compounds from Fig. 1 belong to LMWG. Results, concerning the behaviour of these compounds in solutions, show that all they always make gels or solid precipitates, constructed from thin fibrils and their structure was studied by electron microscopy [7, 9, 10]. Xerogels and other solid precipitates that were formed in the supersaturated solutions of compound **1** showed no brunched adhered each to other fibers with diameter about a micron [7]. The morphology of solids obtained from compound **2** solutions is similar to that found for compound **1** [9]. Detailed studies of xerogels from each of the four compounds revealed elongated objects of different size (in nano- and microscale) [9], as well as entangled network of fibres [10].

Thermally-induced self-assembly in the absence of solvent

As it is mentioned above, during the heating of ground material the morphology of the powdered substance exchanges and compound reorders into fibrils. Depending on the substance and conditions of thermal treatment two main types of fibrils have been obtained. Compounds **1** and **2** (Fig. 4) have very close melting points (270 and 276°C), both reveal solid-state self-assembly in the same temperature range (~ 220–270°C) and the obtained crystalline needles look straight and very well shaped rods. Needles obtained from both compounds have similar morphology; nevertheless they have been prepared on the heating plate in the hood, or in DSC pans. Fig. 2 presents fibres obtained from **1** and **2**, the sizes and number of the needles for any of these two compounds depend on amount of the used material and thermal regime (temperature, time and rate of heating).

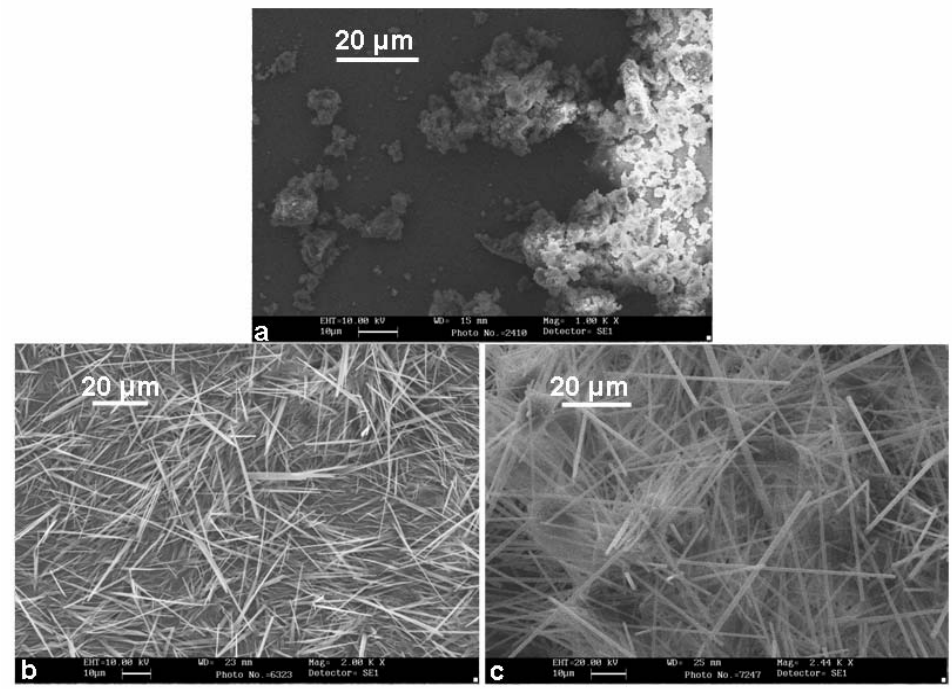

Fig. 2. Crystalline microfibres obtained from **1** and **2**: a – Sample of the starting grounded material; b, c – Straight needles formed during the thermal treatment from **1** (b) and **2** (c).

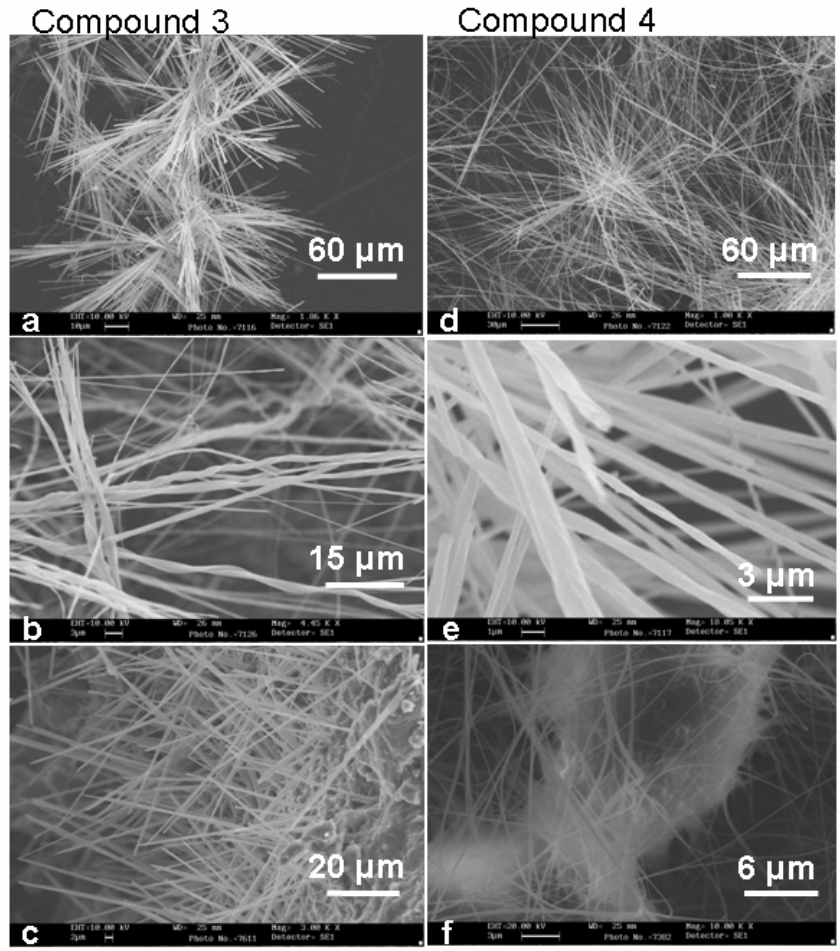

Fig. 3. Fibrils obtained from compounds **3** and **4** on the heating plate and in the DSC pans: a-c – Compound **3**; d-f – Compound **4**; a, b, d and e – Samples obtained on a heating plate; c and f – Samples obtained in the DSC pans.

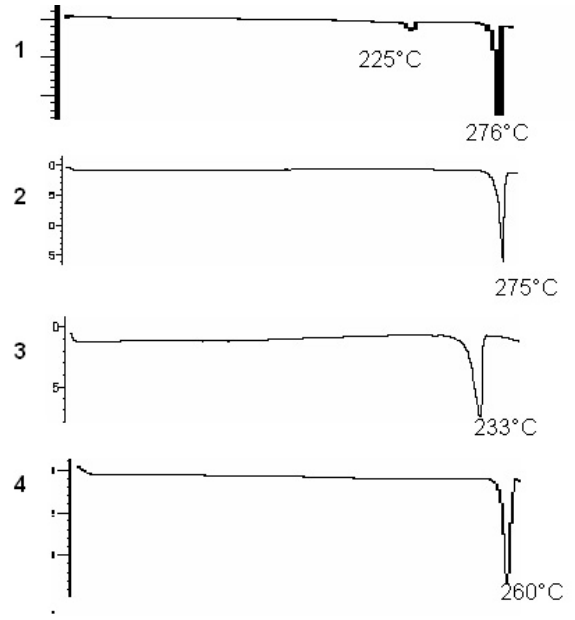

Fig. 4. DSC data for compounds **1**, **2**, **3** and **4**, prepared according to the protocols described in [7, 9, 10].

Compounds **3** and **4** also self-organize into fibril shapes. The type of the fibrils obtained for these two compounds depend on the conditions of thermal treatment, too. The most important difference for these two compounds in comparison with the first two, is the fact that they self-assembly into helicoidal structures in case of thermal treatment on the heating plate (in the hood) (Fig. 3a, b, d, e). When the heating was performed in DSC apparatus again straight fibres (at the highest possible magnifications) were observed (Figs. 3c and 3f).

Thermally induced self-assembly in the presence of solvent

As it was reported before, compound **1** in all solids obtained from different solvents has one and the same crystalline structure, denoted as **1α**, which structure during the heating undergoes polymorphic transition at ~ 225°C to **1β** (Fig. 4) Then, at up of 225°C starts rearrangement of **1β** in the crystalline nano- and microfibres [7] (Fig. 2b). Compound **2** does not reveal such transition no matter how the solid was obtained (Fig. 4.2). Compounds **3** and **4** do not show such solid-solid transition in the forms obtained as products of synthetic reaction (Fig. 4.3 and 4.4). In some cases, depending on the solvent and conditions of preparations, **3** and **4** also undergo such transitions, but, obviously, it is not influential for the crystals shape exchanging. DSC studies show also that the exact place of peak(s) denoting phase transitions depends on the solvent used for the solution prepared before gelation or precipitation.

The four compounds make gels, spherulites and other formations from supersaturated solute but single crystal was impossible to obtain from any of these compounds.

All solids formed from solutions or after thermal treatment are represented by very thin 1D formations (Figs. 2 and 3), which cannot be used for routine XRD analysis. That is why XRPD have been done only to the starting materials and those obtained after prolonged heating at temperatures, at which morphology transformation took place. XRPD spectra for the four compounds are represented in the Fig. 5 and its four subfigures (5.1–5.4). Two spectra for each compound are given – before and after thermal treatment. All XRPD spectra contain very sharp peaks, which means that all used samples are crystalline, but spectra, obtained after the heating, show low amount (not more than 10%) of amorphous phase. As it is seen from Fig. 5.1, only compound **1** has entirely different diffractograms, which testifies to two different polymorphic phases. Completely identical diffractograms were registered for compound **2**, no matter the spectra are taken before or after thermal treatment, which is in accordance with DSC data that this compound changes its morphology during the heating, but does not change its polymorphic state. Compound **3** has the same behaviour like compound **2**. In case of compound **4** (Fig. 5.4) all peaks characteristic for the thermally treated form (e.g. 2θ = 6, 9.8, 18.5) were observed in the pattern of solution obtained solid. Probably, compound **4** crystallizes from the solution in a mixture of two or more polymorphs.

CD signals confirm that thermal treatment of compound **1** leads to rearrangement of the molecules into different mode, while for all other compounds any significant difference has not been noticed. In Fig. 6 the CD spectra of the compounds are presented and all they have negative absorbance at about 230–235 nm, which corresponds to the aromatic π-π^* transition, and many of them have well-defined absorbance at about 280 nm, which, most probably, is associated with carbonyl/aromatic transitions.

IRS data for compounds **2**, **3** and **4** are also in accordance with the other results. The IR spectra [9, 10] are absolutely identical for both materials (before and after thermal treatment) and, because of that, they are not presented here.

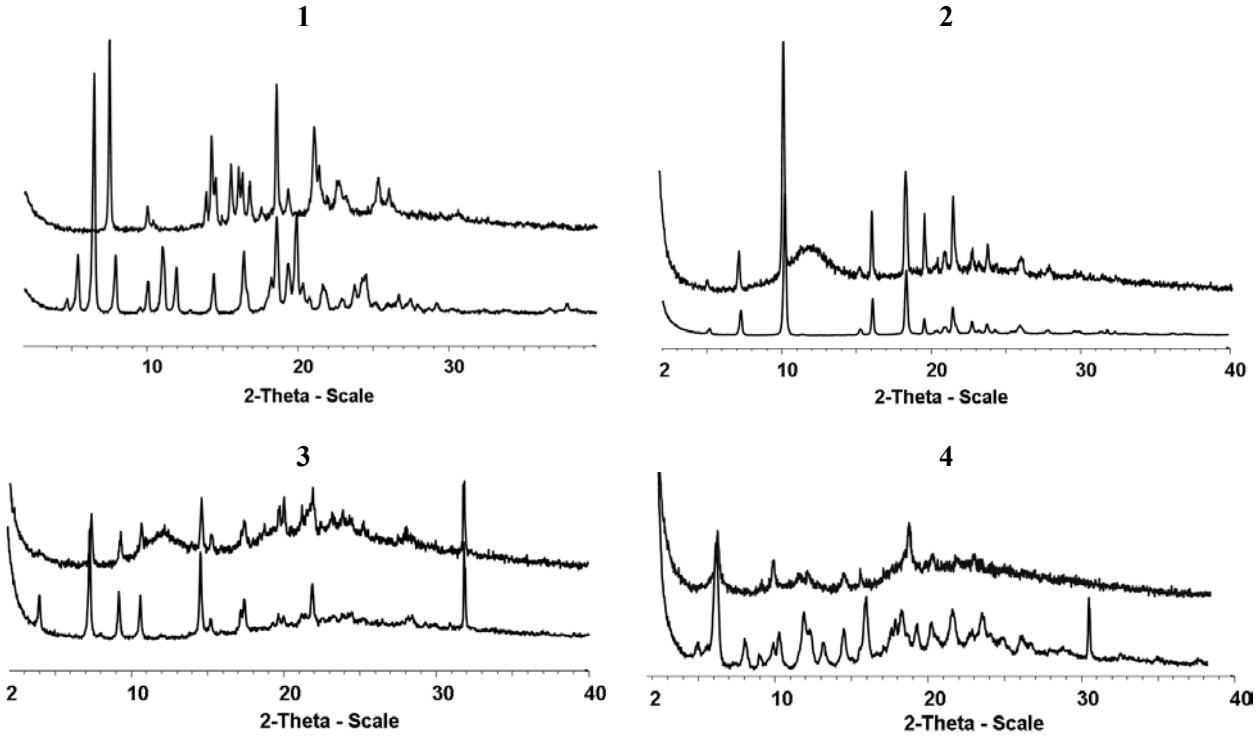

Fig. 5. XRPD spectra of the four compounds before (bottom line) and after (top line) thermal treatment.

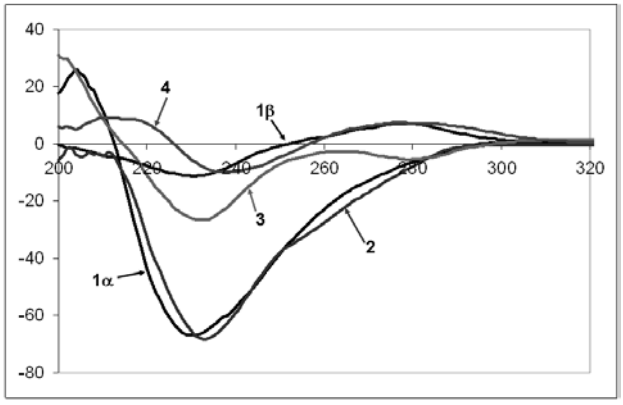

Fig. 6. CD spectra of of compounds **1α**, **1β**, **2**, **3** and **4** (KBr pellets 0.25% w/w).

On the basis of the results for solid-state polymorphic transition and solvent-free self-assembly of compound **1**, recently reported by us [7], we amplified this study on more compounds with similar structures and found that all they are capable of solvent-free self-assembly during heating. It turned out that the solid-state polymorphic transition is not a main condition for fibril formation, as for more compounds it does not take part. One of the possible reasons for the solid-state self-assembly observed in the described experiments is sublimation and deposition in new crystalline fibril formations

CONCLUSIONS

As a conclusion, we present a new approach for nano- and microfibres formation at solvent-free conditions that can substitute commonly applied work in solution aiming fibre formation. All used compounds tend to form fibril networks in solutions and we have shown that this property is manifested without using solvents. This self-assembly procedures are advantageous from technical and environmental points of view and they are related to active research in solvent-free procedures for organic and organometallic synthesis [4, 5]. Fibres, formed at some conditions, are an interesting example of amplification of molecule's chirality to supramolecular complexes that could be used in appropriate fields as asymmetric catalysis, molecular recognition, optoelectronics, *etc*.

Acknowledgments: *Dr. Daniela Tsekova thanks Generalitat Valenciana for a postdoctoral fellowship. We thank for the funding provided by Universitat Jaume I (P1 1B2007-11).*

REFERENCES

1. L. Isaacs, D. Witt, J. C. Fettinger, *Chem. Commun.*, 2549 (1999).
2. A. Brizard, R. Oda, I. Huc, in: Low Molecular Mass Gelators: Design, Self-assembly, Function (Topics in Current Chemistry), F. Fages (ed.), Springer-Verlag GmbH & Co., Berlin and Heidelberg, 2005, p. 167.
3. C. N. R. Rao, W. Jones (eds.), Supramolecular Organization and Materials Design, Cambridge University Press, Cambridge, 2002.
4. K. Tanaka, F. Koda, *Chem. Rev.*, **100**, 1025 (2000).
5. A. L. Garay, A. Pichon, S. L. James, *Chem. Soc. Rev.*, **36**, 846 (2007).

6. J. Antesberger, G. W. V. Cave, M. C. Ferrarelli, M. W. Heaven, C. L. Raston, J. L. Atwood, *Chem. Commun*., 892 (2005).
7. D. S. Tsekova, B. Escuder, J. F. Miravet, *Cryst. Growth Des.,* **8**, 11 (2007).
8. A. R. A. Palmans, E. W. Meijer, *Angew. Chem. Int. Ed.*, **46**, 8948 (2007).
9. B. Escuder, S. Martı, J. F. Miravet, *Langmuir*, **21**, 6776 (2005).
10. J. F. Miravet, B. Escuder, *Chem. Commun*., 5796 (2005).

САМОПОДРЕЖДАНЕ НА МАЛКИ ОРГАНИЧНИ МОЛЕКУЛИ В НИШКОВИДНИ МИКРОСТРУКТУРИ В ОТСЪСЪТВИЕ НА РАЗТВОРИТЕЛ

Д. С. Цекова[1]*, Б. Ескюдер[2], Х. Миравет[2]

[1] Катедра „Органична химия“, Химикотехнологичен и металургичен университет, бул. „Климент Охридски“ № 8, 1756 София
[2] Департамент по неорганична и органична химия, Университет „Хайме I“, 12071 Кастелон, Испания

Постъпила на 17юли 2008 г., Преработена на 25 септември 2008. г.

(Резюме)

Самоорганизацията е един ефикасен подход за получаването на надмолекулни комплекси с размери от порядъка на нано- до микрометри. Изучаването на този процес в случай на образуване на нишки и влакнести структури е обект на активни научни изследвания, тъй като получените с такава морфология материали имат потенциално приложение в тъканното инженерство, като шаблони за неорганични нанонишки, материали в електрооптиката и др. Тук съобщаваме за наскоро синтезирани нискомолекулни производни на L-валина и пиридина, които се самоорганизират в нишкови структури в твърда фаза, т.е. в отсъствие на какъвто и да е разтворител. Нагряването на сухото разпрашено вещество води до образуването на игловидни частички с наноразмери, които се развиват в микро-пръчици при продължаващо нагряване. Хабитусът на нарастнатите нишки се запазва и след охлаждане. Получените резултати представят интересна алтернатива за получаването на кристалинни органични нанообекти и микронишки в условие на отсъствие на разтворител.

Bulgarian Chemical Communications, Volume 41, Number 2 (pp. 116–121) 2009

Involvement of endogenous nitric oxide in the effects of kyotorphin and its synthetic analogue on immobilization and cold stress-induced analgesia

E. B. Dzambazova[1]*, A. I. Bocheva[1], V. P. Nikolova[2]

[1] *Department of Pathophysiology, Faculty of Medicine, Medical University, 2 Zdrave Str., 1431 Sofia, Bulgaria*
[2] *Department of Biology, Faculty of Medicine, Medical University, 2 Zdrave Str., 1431 Sofia, Bulgaria*

Received July 16, 2008

The aim of the present study was to investigate the involvement of endogenous nitric oxide (NO) in the effects of neuropeptide kyotorphin (Kyo) and its synthetic analogue D-kyotorphin (D-Kyo) on immobilization and cold stress-induced analgesia (SIA). In scientific literature, Kyo is considered as neuromodulator. D-Kyo is more stable enzimatically. Some studies demonstrate that Kyo is a possible substrate for neuronal and inducible NO synthase, also the NO system is stress-limiting and plays an important role in initiation and maintenance of pain.

Kyo and D-kyo were synthesized by the Group of Antimetabolites at the Institute of Molecular Biology, Bulgarian Academy of Sciences. The proposed synthetic route was based on well-established liquid-phase methods of peptide synthesis – active esters, using *tert*-butyloxycarbonyl (Boc) group for protection of the Nα-amino group according to the protocol previously described in the literature. Male *Wistar* rats were used in acute immobilization and cold stress models. The evaluation of nociceptive effects was carried out using the paw pressure (PP) and hot plate (HP) tests. Kyo and D-Kyo (both in dose 5 mg/kg), L-NAME (10 mg/kg), and L-Arginine (1 mg/kg) were dissolved in saline and were injected intraperitoneally.

The result showed that endogenous NO is differently involved in the effects of peptides, which may be due to different implication of opioid and non-opioid components of SIA. Probably, L- or D-form of the peptide is also important, as well as the type of the stressor and its neurochemical signature.

Key words: kyotorphin, D-kyotorphin, nitric oxide, stress-induced analgesia.

INTRODUCTION

Kyotorphin (Kyo) is a dipeptide (L-Tyr-L-Arg) (Fig. 1A) synthesized in specific brain regions [1]. The highest levels were found in the lower brain stem and dorsal spinal cord, areas closely associated with the pain regulatory system [2, 3]. D-Kyotorphin (D-Kyo or L-Tyr-D-Arg) (Fig. 1B) is a synthetic analogue of Kyo. Both peptides bind to a specific Kyo-receptor and induced Met-enkephalin release at rates of approximately 4 times basal release [4]. Literature data showed that Kyo-receptor is identified in the membrane-preparations of the brain, which suggests that it plays a physiological significance in the neurotransmission as a neurotransmitter/neuromodulator [5]. However, D-Kyo shows enhanced analgesic activity, i.e. 5.6-fold higher than that observed with Kyo. Takagi and co-workers [1] suggested that this effect is a result of protease resistance conferred by the substitution of L-arginine (L-Arg) with a D-arginine residue [6].

It is also known that acute and chronic stress induces biochemical changes affecting both pain threshold and behaviour [7]. Stressors such as immobilization and cold exposure can cause stress-induced analgesia (SIA) [8]. It can be resolved into an opioid, when it is antagonized by naloxone, but also a non-opioid component [9].

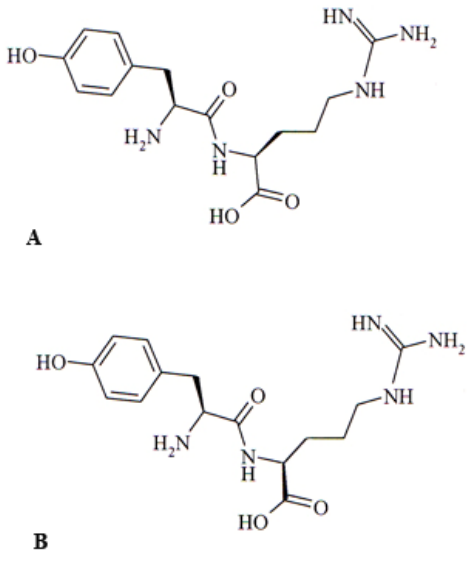

Fig. 1. Structural formula of: A. kyotorphin (L-Tyr-L-Arg); B. D-kyotorphin (L-Tyr-D-Arg).

* To whom all correspondence should be sent:
E-mail: el_dji@abv.bg

Rat experiments have demonstrated that the nitric oxide (NO) system fulfils the main criteria of a stress-limiting system [10]. Earlier it was reported that the mechanism of NO-induced antinociception involved opioid components and was also dependent on brain NO [11]. NO is an unique neurotransmitter was synthesized by the enzyme nitric oxide synthase (NOS) and plays an important role in initiation and maintenance of pain [12]. Also, it is known that Kyo, as well as L-Arg, are possible substrates for neuronal and inducible NOS [13, 14]. The aim of the present study was to investigate the involvement of endogenous NO in the effects of kyotorphin and D-kyotorphin on immobilization and cold stress-induced analgesia.

EXPERIMENTAL

Chemistry. All reagents and solvents were of reagent grade and used without further purification. Amino acid derivative Boc-Tyr-OH was prepared according to the general procedure of Pozdnev [15] and Boc-Tyr-OSu – according to [16].

Active ester procedure (AE). Nα-protected tyrosine succinimide ester (1 mmol) was dissolved in l ml dimethylformamide (DMF), and 1.2 mmol arginine (L- or D- form) in 1 ml DMF was added to it. The pH was adjusted to 8–9 with 5% $NaHCO_3$, and the mixture was stirred at room temperature overnight. After reduced pressure evaporation, the residue was partitioned between 0.5 M $NaHSO_4$ and *n*-BuOH. The acidic aqueous layer was extracted twice with *n*-BuOH (2 × 30 ml) and the combined organic extracts were washed with 10% $NaHCO_3$ and brine. The organic phase was dried over Na_2SO_4 and evaporated *in vaccuo* to a smaller volume;

Trifluoroacetic acid (TFA) deprotection. The fully protected peptides were treated with TFA (1/10 molar ratio) in the presence of anisole for 30 min at room temperature to remove the Boc-protecting groups. The crude peptides were purified by suitable crystallization. The pure TFA salt obtained in this way was converted to the target product by treatment with ion-exchange resin Amberlite IR-45, dissolved in water and lyophilized.

Analyses. The purity of the peptides and structural identity was established by TLC, analytical HPLC and electrospray mass spectometry. TLC was carried out on silicagel 6OF254 pre-coated (Merck) aluminum plates, with the use of the following solvent systems: A = *n*-butanol:acetic acid:water (4:1:5); B = chloroform:methanol:water (80:30:5). Visualization was done with either UV, or ninhydrin. For the analytical gradient RP-HPLC, a Merck-Hitachi liquid chromatograph, was used. A water/0.1% TFA buffer, pH 2.25, and a linear acetonitrile gradient were used for elution on a 100-5 Nucleosil Ci8 column. To check the purity of compounds, a 5–100% acetonitrile gradient in 30 min was performed. Optical rotation was measured with a Perkin-Elmer Model 141 polarimeter.

Animals. Male *Wistar* rats (180–200 g) were used. The animals were housed in groups of 6 per cage and kept under a normal 12 h light/dark cycle and 22 ± 2°C temperature. Rats had free access to food and water.

Acute models of stress: Immobilization stress (IS). The animals were placed for 1 hour in a plastic tube with adjustable plaster tape on the outside so that the animals were unable to move. There were holes for breathing.

Cold stress (CS). The animals were placed in a refrigerating chamber at 4°C for 1 hour.

Nociceptive tests. The evaluation of antinociceptive effects was carried out using the paw pressure (PP) test of Randall and Selitto [17] and hot plate (HP) test.

Paw-pressure test. The changes in the mechanical nociceptive threshold of the rats were measured by using an analgesimeter (Ugo Basile). The pressure was applied to the hind-paw and the pressure (*g*) required to elicited nociceptive responses such as squeak and struggle was taken as the mechanical nociceptive threshold. A cut-off value of 500 g was used to prevent damage of the paw.

Hot plate test. The latency of response to pain was measured from the moment of placing an animal on a metal plate (heated to 55 ± 0.5ºC) to the first signs of pain (paw licking, jumping). The cut-off time was 30.

Drugs and treatment. Kyotorphin and D-kyotorphin (both in dose 5 mg/kg) were synthesized by the Group of Antimetabolites at the Institute of Molecular Biology, Bulgarian Academy of Sciences. NOS inhibitor L-N^G-nitroarginine ester (L-NAME) (10 mg/kg) and L-Arginine (L-Arg, 1 mg/kg) were obtained from Sigma. All drugs were dissolved in sterile saline (0.9% NaCl) solution and were injected intraperitoneally (i.p.). The control group was not submitted to stress procedure and was injected with saline 1 ml/kg, i.p. The nociceptive tests were performed 15 min after peptide injection.

The experiments were approved by the Animal Care and Use Committee of the Medical University, Sofia.

Data analysis. The results were statistically assessed by analysis of variance (ANOVA) followed by Dunnetts's multiple comparison test. Values are mean ± S.E.M. Values of $p < 0.05$ were considered to indicate statistical significance.

RESULTS AND DISCUSSION

The proposed synthetic route was based on well-established liquid-phase methods of peptide synthesis – active esters, using *tert*-butyloxycarbonyl (Boc) group for protection of the Nα-amino group (Fig. 2) according to the protocol previously described in literature [18]. The strategy of the minimal side-chain protection was adopted. Thus, the phenolic group of tyrosine and δ-guanidino group of arginine were unprotected.

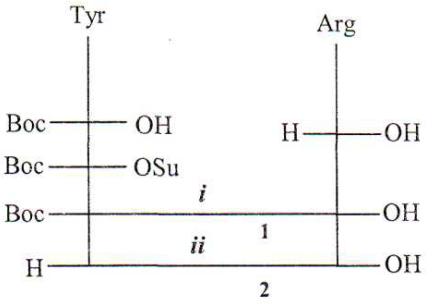

Fig. 2. Scheme for the synthesis of kyothorphin and D-kyotorphin. *i)* 5% $NaHCO_3$, DMF; *ii)* 3 N HCl/EtOAc (TFA).

The Kyo and D-Kyo were synthesized by condensation of the preliminary prepared Boc-Tyr-OSu with L-Arg or D-Arg, respectively. The reaction carried out for 16–24 hours at room temperature resulted in high yields.

After isolation and purification, the peptides were identified and characterized by optical rotation, TLC, analytical HPLC, mass-spectra and elemental analysis.

The investigations started 15 min after intraperitoneal injection of each of the peptides. Our results showed that in PP test Kyo ($p < 0.01$) and D-Kyo ($p < 0.01$) (both at a dose of 5 mg/kg, i.p.) administered immediately after stress procedure significantly inhibited 1 hour immobilization stress-induced analgesia (ISIA) at the beginning of the experiment. On the 30th min only Kyo had kept this effect, while D-Kyo significantly potentated pain threshold ($p < 0.05$) (Fig. 3).

L-NAME (10 mg/kg, i.p.) and L-Arg (1 mg/kg, i.p.) were injected 20 min before investigated peptides and their interactions have been studied after each stress model. Co-administration of Kyo and D-Kyo with L-NAME or L-Arg significantly decreased analgesia induced by IS and CS and measured by PP and HP tests (Figs. 3, 4, 5 and 6).

In PP test L-NAME or L-Arg significantly decreased inhibiting effect of Kyo on ISIA. Their effect on D-Kyo was the same only on the 15th min, while on the 30th min they significantly decreased its increasing pain threshold (Fig. 3).

Injected immediately after 1 hour CS, Kyo ($p < 0.01$) significantly inhibited cold stress-induced analgesia (CSIA) during the whole investigated period, while D-Kyo injected after 1 hour CS procedure decreased significantly the analgesic effect of CS on the 45th min ($p < 0.01$) from the beginning of the experiment (Fig. 4).

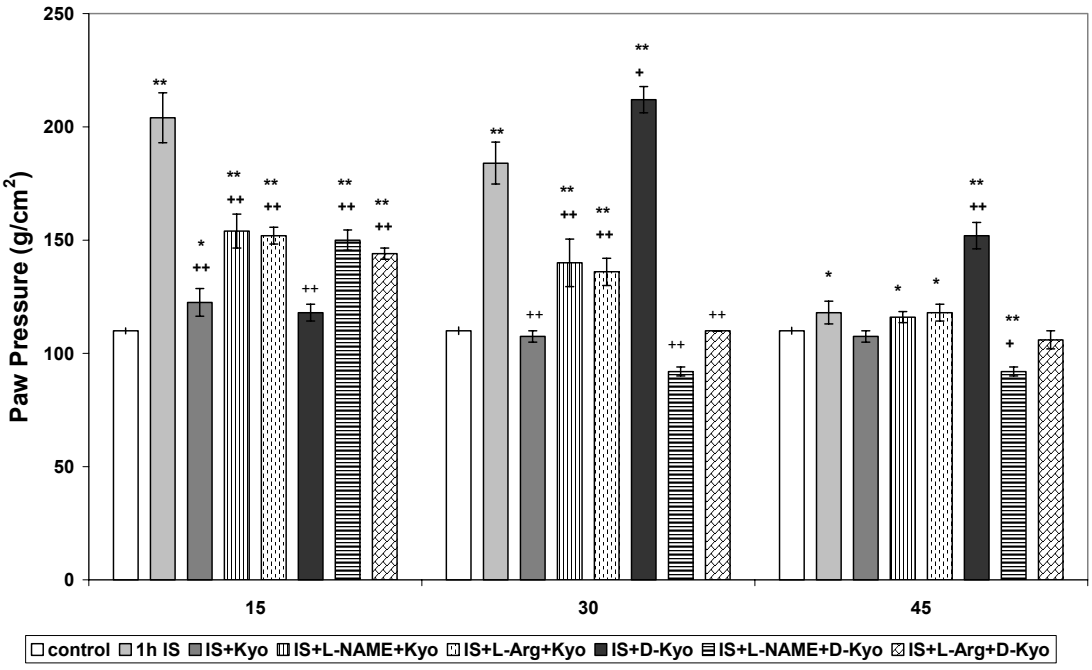

Fig. 3. Effects of Kyo and D-Kyo (both in 5 mg/kg, i.p.) and their combination with L-NAME (10 mg/kg, i.p.) and L-Arg (1 mg/kg, i.p.) on nociception measured with paw pressure test after 1 hour immobilisation stress (IS) in male *Wistar* rats ($n = 5$). Mean values ± S.E.M. are presented. *$p < 0.05$, **$p < 0.01$ vs. control; $^{+}p < 0.05$, $^{++}p < 0.01$ vs. IS.

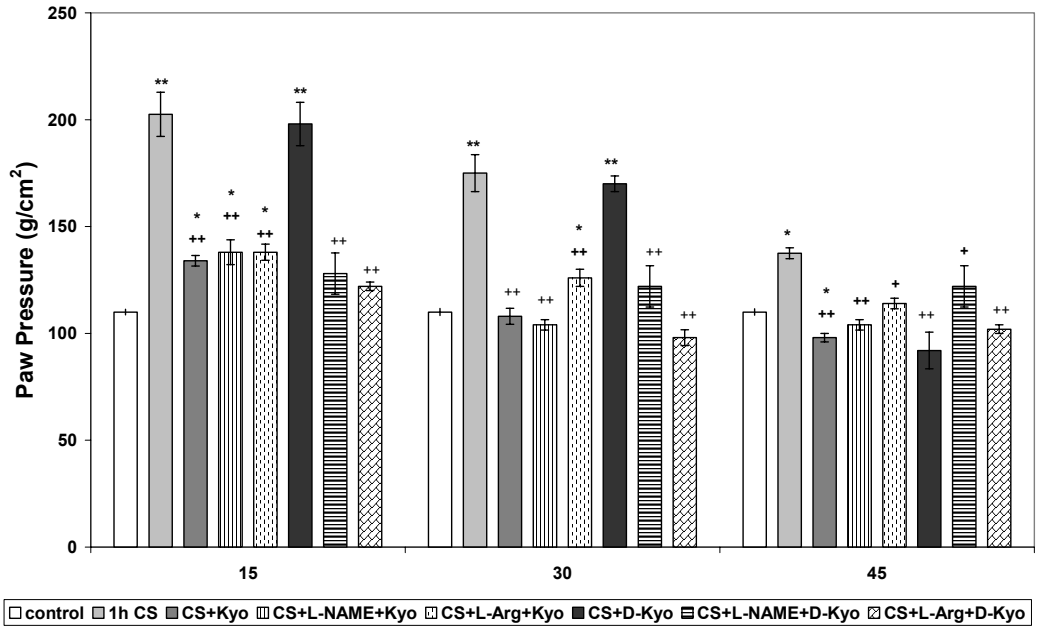

Fig. 4. Effects of Kyo and D-Kyo (both in 5 mg/kg, i.p.) and their combination with L-NAME (10 mg/kg, i.p.) and L-Arg (1 mg/kg, i.p.) on nociception measured with paw pressure test after 1 hour cold stress (CS) in male *Wistar* rats ($n = 5$). Mean values ± S.E.M. are presented. *$p < 0.05$, **$p < 0.01$ vs. control; $^{+}p < 0.05$, $^{++}p < 0.01$ vs. CS.

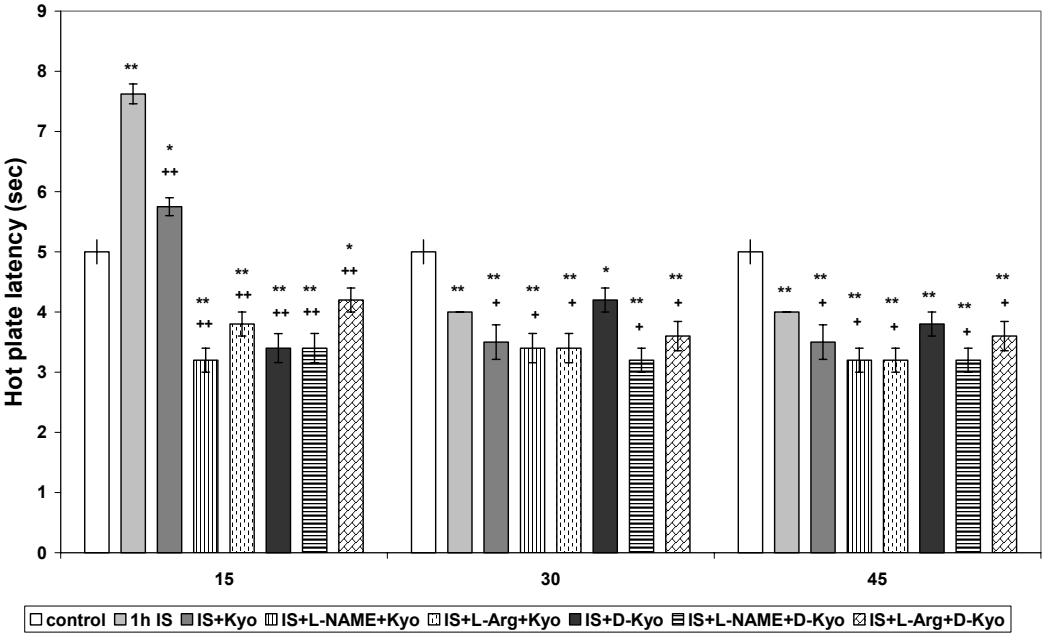

Fig. 5. Effects of Kyo and D-Kyo (both in 5 mg/kg, i.p.) and their combination with L-NAME (10 mg/kg, i.p.) and L-Arg (1 mg/kg, i.p.) on nociception measured with hot plate test after 1 hour immobilisation stress (IS) in male *Wistar* rats (n = 5). Mean values ± S.E.M. are presented. *$p < 0.05$, **$p < 0.01$ vs. control; $^{+}p < 0.05$, $^{++}p < 0.01$ vs. IS.

L-NAME and L-Arg significantly decreased inhibiting effect of D-Kyo on CSIA on the 45th min. Co-administrations L-NAME+Kyo and L-Arg+Kyo showed pain thresholds commensurable to that of Kyo administered after CS (Fig. 5).

In HP test IS significantly increased HP latency only on the 15th min compared to control group ($p < 0.01$). This enlargement on analgesic activity was significantly decreased by Kyo ($p < 0.01$) and D-Kyo ($p < 0.01$) (Fig. 5).

In Fig. 6 CS increased HP latency on the 15th min ($p < 0.01$) and 30th min ($p < 0.05$) compared to control. Kyo significantly inhibited CSIA ($p < 0.05$). D-Kyo showed the same effect, where HP latency was more pronounced on the 30th min ($p < 0.01$) and was shorter than control.

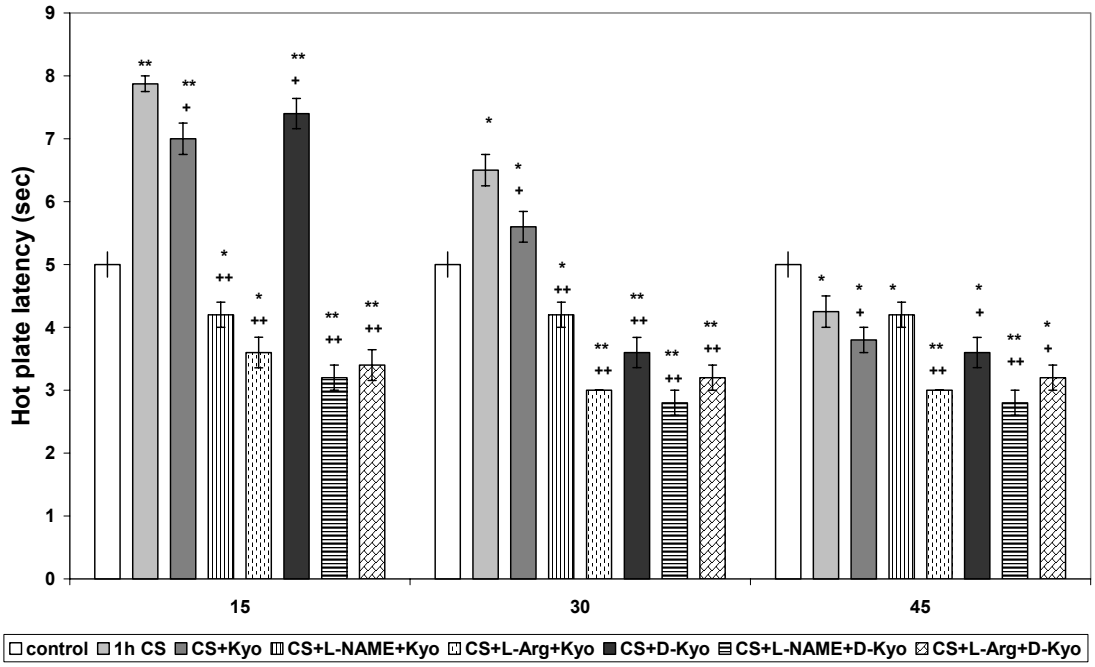

Fig. 6. Effects of Kyo and D-Kyo (both in 5 mg/kg, i.p.) and their combination with L-NAME (10 mg/kg, i.p.) and L-Arg (1 mg/kg, i.p.) on nociception measured with hot plate test after 1 hour cold stress (CS) in male *Wistar* rats ($n = 5$). Mean values ± S.E.M. are presented. *$p < 0.05$, **$p < 0.01$ vs. control; $^{+}p < 0.05$, $^{++}p < 0.01$ vs. CS.

Co-administration of Kyo and D-Kyo with L-NAME or L-Arg significantly increased inhibiting effects of peptides on ISIA and CSIA measured by HP test (Figs. 5 and 6).

NO is an exclusively important and many-sided regulator of a number of physiological functions in animals. It also acts as a neurotransmitter itself and/or as a neuromodulator, influences plastic properties of the neurons, in particular the phenomenon of long-lasting potentiation. NO production occurs in the spinal cord after activation of NMDA receptors and gives rise to acute pain [19].

It is known that stress activates the hypothalamic-pituitary-adrenal (HPA) axis by stimulating neuronal activity within the paraventricular nucleus of the hypothalamus [20]. Some workers have reported that HPA axis responses to neural stimuli, which are not dependent on immune factors, can be modulated by NO and also NO plays an important role in regulating the response of the HPA axis to various stresses. Data in literature showed that endogenous NO influenced nociceptive effects induced by IS and thermogenesis [21].

Our previous data showed that Kyo and D-Kyo applied alone exerted well marked and time dependent analgesic effects, reduced by naloxone. Also, they modulated ISIA and CSIA [22, 23]. Injection of L-NAME or L-Arg before Kyo or D-Kyo showed different effects on ISIA and CSIA in two nociceptive tests. These findings indicate that endogenous NO is differently involved in the effects of peptides, which may be due to different implication of opioid and non-opioid components in two types of SIA – immobilization and cold.

Our unpublished observation and literature data showed that the non-opioid system is mostly involved in cold stress, while both systems – opioid and non-opioid are equally presented in immobilization stress [8]. On the other hand, Kyo, as well as L-Arg, are possible substrates for neuronal and inducible NOS [13, 14]. Literature data revealed that endogenous opioid peptides and NO mediated a wide variety of physiological processes including pain transmission and SIA [7]. The morphological studies present evidence for the existence of a signaling pathway between an opioidergic and the NO systems in the hypothalamus of the rat brain [24]. Also, L- or D-form of the peptide is important for possible NO production.

In conclusion, we suggest that there is a different kind of involvement of endogenous nitric oxide in the mechanisms of nociception of Kyo and D-Kyo after immobilization and cold stress, which may be due to different implication of opioid and non-opioid components of SIA. Probably L- or D-form of the peptide is also important, as well as type of the stressor and its neurochemical signature.

REFERENCES

1. H. Takagi, H. Shiomi, H. Ueda, H. Amano, *Nature*, **282**, 410 (1979).

2. S. C. Lopes, C. M. Soares, A. M. Baptista, E. Goormaghtigh, B. J. Cabral, M. A. Castanho, *J. Phys. Chem. B.,* **110**, 3385 (2006).
3. J. Y. Summy-Long, V. Bui, S. Gestl, E. Koehler-Stec, H. Liu, M. L. Terrell, M. Kadekaro, *Brain Res. Bull.*, **45**, 395 (1998).
4. S. C. Lopes, A. Fedorov, M. A. Castanho, *Chem. Med.Chem.*, **1**, 723 (2006).
5. M. Inoue, T. Yamada, H. Ueda, *Brain Res. Mol. Brain Res*., 69, 302 (1999).
6. H. Takagi, H. Shiomi, Y. Kuraishi, H. Ueda, *Experientia*, **38**, 1344 (1982).
7. A. Costa, A. Smeraldi, C. Tassorelli, R. Greco, G. Nappi, *Neurosci. Lett.*, **383**, 7 (2005).
8. K. Pacák, M. Palkovits, *Endocr. Rev.*, **22**, 502 (2001).
9. I. B. Lapo, M. Konarzewski, B. Sadowski, *Physiol. Behav.*, **78**, 345 (2003).
10. M. A. Gilinskii, G. M. Petrakova, T. G. Amstislavskaya, L. N. Maslova, V. V. Bulygina, *Neurosci. Behav. Physiol.*, **35**, 171 (2005).
11. E. Chung, B. Burke, A. J. Bieber, J. C. Doss, Y. Ohgami, R. M. Quock, *Brain Res. Bull.*, **70**, 245 (2006).
12. L. Givalois, S. Li, G. Pelletier, *Brain Res. Mol. Brain Res.*, **102**, 1 (2002).
13. T. Arima, Y. Kitamura, T. Nishiya, H. Takagi, Y. Nomura, *Neurosci. Lett.*, **212**, 1 (1996).
14. T. Arima, Y. Kitamura, T. Nishiya, T. Taniguchi, H. Takagi, Y. Nomura, *Neurochem. Int.*, **30**, 605 (1997).
15. V. F. Pozdnev, *Chem. Nat. Prod*., **6**, 764 (1974).
16. T. Pajpanova, *Compt. Rend. Acad. Bulg. Sci*., **53**, 53 (2000).
17. L. O. Randall, J. J. Selitto, *Arch. Int. Pharmacodyn.*, **111**, 409 (1957).
18. M. Spasova, E. Popgeorgieva, Ts. Milkova, T. Pajpanova, *Compt. Rend. Acad. Bulg. Sci*., **57**, 53 (2004).
19. A. H. Dickenson, *Ann. Med.*, **27**, 223 (1995).
20. M. G. Swain, M. Maric, *Hepatology*, **24**, 914 (1996).
21. S. Pu, T. L. Horvath, S. Diano, F. Naftolin, P. S. Kalra, S. P. Kalra, *Endocrinology*, **138**, 1537 (1997).
22. E. Dzambazova-Maximova, A. Bocheva, Hr. Nocheva, *Bulg. Chem. Commun.*, **38**, 36 (2006).
23. E. B. Djambazova, H. H. Nocheva, A. I. Bocheva, *Coll. Symp. Ser.*, **9**, 37 (2007).
24. V. Gupta, A. Gupta, S. Saggu, H. M. Divekar, S. K. Grover, R. Kumar, *Evid. Based Complement. Alternat. Med*., **2**, 93 (2005).

УЧАСТИЕ НА ЕНДОГЕННИЯ АЗОТЕН ОКСИД В ЕФЕКТИТЕ НА КИОТОРФИН И НЕГОВ СИНТЕТИЧЕН АНАЛОГ ВЪРХУ ИМОБИЛИЗАЦИОННА И СТУДОВА СТРЕС-ИНДУЦИРАНА АНАЛГЕЗИЯ

Е. Б. Джамбазова[1]*, А. И. Бочева[1], В. П. Николова[2]

[1] Катедра по патофизиология, Медицински факултет, Медицински университет, ул. „Здраве“ № 2, 1431 София
[2] Катедра по биология, Медицински факултет, Медицински университет, ул. „Здраве“ № 2, 1431 София

Постъпила на 16 юли 2008 г.

(Резюме)

Целта на настоящата работа е да се изследва участието на ендогенния азотен оксид (NO) в ефектите на невропептида киоторфин (Kyo) и неговия синтетичен аналог D-киоторфин (D-Kyo) върху имобилизационна и студова стрес-индуцирана аналгезия (SIA). В научната литература Kyo е известен като невромодулатор, а D-Kyo е по-стабилен на ензимно разграждане. Някои изследвания показват, че Kyo е възможен субстрат за невронална и индуцибилна NO синтаза, а NO система е стрес-лимитираща и играе важна роля в инициирането и поддържането на болката.

Синтезата на Kyo и D-Kyo бе извършена в института по молекулярна биология при БАН, и бе основана на добре известната методика за пептиден синтез в разтвор – метод на активираните естери, при който се използва третична-бутилоксикарбонилна (Boc) група за защита на Nα-амино групата. За острите модели на имобилизационен и студов стрес бяха използвани мъжки плъхове линия *Wistar*. Оценяването на ноцицептивните ефекти беше извършвано с paw pressure (PP) и hot plate (HP) тестове. Kyo и D-Kyo (5 mg/kg), L-NAME (10 mg/kg), и L-аргинин (1 mg/kg) бяха разтворени във физиологичен разтвор и инжектирани интраперитонеално.

Резултатите показаха, че ендогенният NO по различен начин участва в ефектите на пептидите, което може би е свързано с различното участие на опиоидната и неопиоидна компонента на SIA. Вероятно L- и D-формата на пептидите е също важна, както типа стресор и неговият неврохимичен „подпис“.

Bulgarian Chemical Communications, Volume 41, Number 2 (pp. 122–126) 2009

Synthesis of model peptide substrates and investigation of the reaction of their phenylacetyl protecting group enzyme transformation by means of penicillin G acylase

D. L. Danalev[1]*, L. K. Yotova[2]

[1] *Department of Organic Chemistry, University of Chemical Technology and Metallurgy, 8 Kliment Ohridski Blvd., 1756 Sofia, Bulgaria*
[2] *Department of Biotechnology, University of Chemical Technology and Metallurgy, 8 Kliment Ohridski Blvd., 1756 Sofia, Bulgaria*

Received July 4, 2008; Revised September 18, 2008

The development of new protective groups by means of stereospecific and selective reactions is very important for the practice especially in the synthesis of semi-synthetic antibiotics and biologically active peptides. The aim of the present investigation is to study the kinetics of enzyme hydrolysis of the Phenylacetyl (Phac) group in synthetic peptide substrates. Two model compounds with two and three Phac, respectively, were studied. The enzymatic hydrolysis by means of penicillin G acylase in pH range 6–9 was studied. The substrate concentration was between 0.4–40 mM. Maximum degree of substrate conversion 75.5% (pH 9), which is closed to the degree of conversion to pH 7.8 (74.5%), was obtained for 3 to 10 min. At pH 6.5 and 7 the degree of hydrolysis was 62.5 and 37.5%, respectively. The possibilities for the reaction of hydrolysis in the presence of salts of different complex agents $CuSO_4.5H_2O$, $NiCl_2$, $Ni(NO_3)_2$ and $MnCl_2$ were investigated, too. There was 100% degree of Phac group hydrolysis in the presence of 10% $Ni(NO_3)_2$ for 9 min and full shift of equilibrium to the direction of hydrolysis was monitored in the presence of 25% $Ni(NO_3)_2$.

Key words: enzyme kinetic; penicillin G acylase; peptide mimetics; phenylacetyl protecting group.

INTRODUCTION

Peptides and α-amino acids are widely used in the medical practice. The development of new protective groups by means of stereo specific and selective reactions is very important for the practice especially in the synthesis of semi-synthetic antibiotics and biologically active peptides. Penicillin G acylase (PGA) is an enzyme that demonstrated high specificity on the phenyl acetyl residue. The enzyme's hydrolase activity is of a great importance for the new substrates modifications [1–5].

The aim of the present investigation is to study the kinetics of enzyme hydrolysis of the amide function between Phenylacetyl (Phac) group and amino acid residue.

EXPERIMENTAL

Materials and Methods

PGA [E.C 3.5.1.11] from *E. Coli* was supplied by Fluka (Switzerland). The enzyme activity of 980 E/ml was determined according to [6]. In the reaction solution, the product was diluted to 98 E/ml. The solution with concentration 0.15 mg/ml was used. KOH, KCl, NaOH, HCl; NH_4OH, KH_2PO4; K_2HPO_4 and CH_3CN - gradient grade for HPLC were received from MERCK (Darmstadt, Germany); $NiCl_2$; $Ni(NO_3)_2$; $CuSO_4.5H_2O$; $MnCl_2$ were purchased from Reanal (Budapest , Hungary)

The IR spectra were recorded on a Perkin-Elmer Model 1600 Series FTIR instrument. The purity of the products and kinetics of the hydrolysis reactions of phenylacetyl group were checked by RP-HPLC on a Perkin-Elmer apparatus, C_{18} column 4.6×250 mm ODS-A, S-5 micron 120 A. 50% 0.02 M KH_2PO_4:K_2HPO_4 pH = 7: 50% CH_3CN were used as eluents, rate 0.8 ml/min, λ = 220 nm and diode array detector.

The needed substrates Boc-Lys(Phac)-Val-OMe and Boc-Lys(Phac)-Lys(Phac)-Lys(Phac)-OH were obtained by conventional peptide synthesis in solution.

Boc-Lys(Phac)-Lys(Phac)-Lys(Phac)-OH was synthesized by drop-wise addition of Boc-Lys(Phac)-OH to C-terminal H-Lys(Phac)-OH by using of MA (mixed anhydrides) method:

1.00 mmol of Boc (or Z) amino acid (or peptide obtained from Boc-peptide by treatment with 10-fold excess of TFA) was dissolved in THF (10 ml) and after cooling to –10 ÷ –15°C and good stirring

* To whom all correspondence should be sent:
E-mail: dancho_danalev@yahoo.com

1.00 mmol Et_3N and 0.98 mmol isobutyl chloroformate were added. After 15 min 1.00 mmol of amino component without protecting groups dissolved in 1.1 mmol 2 N NaOH was added dropwise. The reaction mixture was stirred for 1 h at –10 ÷ –15°C and 24 h at room temperature. After that it was concentrated *in vacuo* and 2 N HCl was added to pH 2–3. The product was extracted with EtOAc (3×10 ml) and the organic layer was washed with 10% citric acid (3×10 ml) and H_2O to pH 7. The solvent was dried with Na_2SO_4 and removed *in vacuo*. The obtained products Boc-Lys(Phac)-Lys(Phac)-OH and Boc-Lys(Phac)-Lys(Phac)-Lys(Phac)-OH were oils.

Boc-Lys(Phac)-Val-OMe was obtained by the DCC/1-HOBt method:

1.00 mmol of HCl.H-Val-OMe was dissolved in DMF (10 ml) and after cooling to –5°C, neutralized to pH 7–7.5 with Et_3N. 1.2 mmoles of Boc-Lys(Phac)-OH; 1.20 mmol of DCC and 1.4 mmol of 1-HOBt were added. The reaction mixture was stirred for 24 h at room temperature. The obtained DC-urea was removed by filtration and then 30 ml of water were added. The product was extracted with EtOAc (3×10 ml) and the organic layer was washed with 5% $NaHCO_3$ (3×10 ml), H_2O (3×10 ml), 10% citric acid (3×10 ml) and H_2O to pH 7. The solvent was dried with Na_2SO_4 and removed *in vacuo* followed by recristalization in EtOAc/petroleum ether.

The obtained product has the following IR spectral characteristics: [cm^{-1}] 3328 ν_{N-H}; 3067 ν_{C-H} (aromatic system); 2930 ν_{C-H} (CH_3); 2853 ν_{C-H} (CH_2); 1740 $\nu_{C=O}$ (ester); 1700 $\nu_{C=O}$ (uretan); 1680 $\nu_{C=O}$ (amide I); 1661 $\nu_{C=O}$ (amide II); 1574 δ_{N-H} (amide I); 1545 δ_{N-H} (amide II); 1390 and 1367 δ_{C-H} (isopropyl and *tert*-butyl groups); 1247 ν_{C-O-C} (uretan); 743 $\delta_{C=C}$ and 696 $\delta_{C=C}$ (monosubstituted aromatic system).

General procedure for the reaction of hydrolysis of Phac by means of PGA

20 ml of substrate with the needed concentration in 10% DMF/0.1 M KCl were alkalized till pH 9 with 4 M K_2HPO_4. The solution of PGA with needed concentration was added. The hydrolysis of substrate was monitored on HPLC at 0, 1, 2, 3, 5, 9, 15, 30 and 60 min after acidification. During the reaction pH of the reaction mixture was hold up by titration with solution with pH 11–12 of complex agent's salt with needed concentration or NH_4OH.

RESULTS AND DISCUSSION

Two model reactions of hydrolysis of Phac were studied in the presence of substrates containing one and three Phac groups, respectively. The principal scheme of the reaction is presented in Figs. 1 and 2.

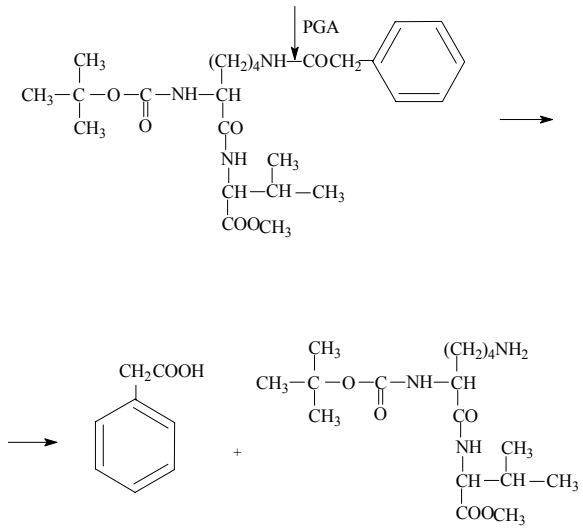

Fig. 1. Reaction of hydrolysis of Phac group in dipeptide ester Boc-Lys(Phac)-Val-OMe with PGA.

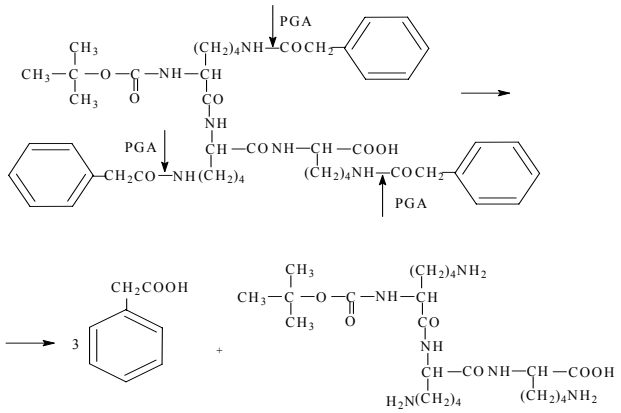

Fig. 2. Reaction of hydrolysis of Phac group in tripeptide Boc-Lys(Phac)-Lys(Phac)-Lys(Phac)-OH with PGA.

It is well known that pH optimum of PGA according to its natural substrate benzylpenicillin sodium or potassium salt is 7.8–8.0 [7–9]. In our investigation the used substrates are two peptides which are not specific substrates for PGA, thus the reaction of hydrolysis was monitored at pH range 6 ÷ 9. Series of reactions were carried out with 0.4 mM substrate at different pH (Fig. 3).

Maximum degree of substrate conversion 75.5% (pH 9), which is closed to the degree of conversion at pH 7.8 (74.5%), was obtained for 3 and 10 min, respectively. At pH 6.5 and 7, the degree of hydrolysis was 62.5 and 37.5%, respectively. By that reason, our next investigations on the reactions were carried out at the optimum value of pH 9 and at 37°C. Kinetic studies of the Phac group's hydrolysis were done with different enzyme concentrations in the synthetic substrate Boc-Lys(Phac)-Lys(Phac)-

Lys(Phac)-OH. The results are shown in Fig. 4. Maximum degree of substrate conversion 73.75% was obtained in the presence of 0.04 ml PGA for 8 min, which is closed to that obtained with 0.4 ml of PGA for 15 min (72.5%).

The obtained curves in the Figs. 3 and 4 clearly show that the reaction of Phac group hydrolysis is reversible. In order to attempt to shift the equilibrium of the reaction to the direction of full hydrolysis of the protecting group in the model peptide substrates and to make this reaction non-reversible, the same reaction was carried out in the presence of metal ions, which are good complexing agents. Their addition to the system might lead to the formation of complex with released ε-amino function of Lys residues (Fig. 5). The obtained complex might precipitate the forming product and to shift the reaction to the right direction. The possibility of similar complex formation was discussed previously by Schröder and Lubke [10].

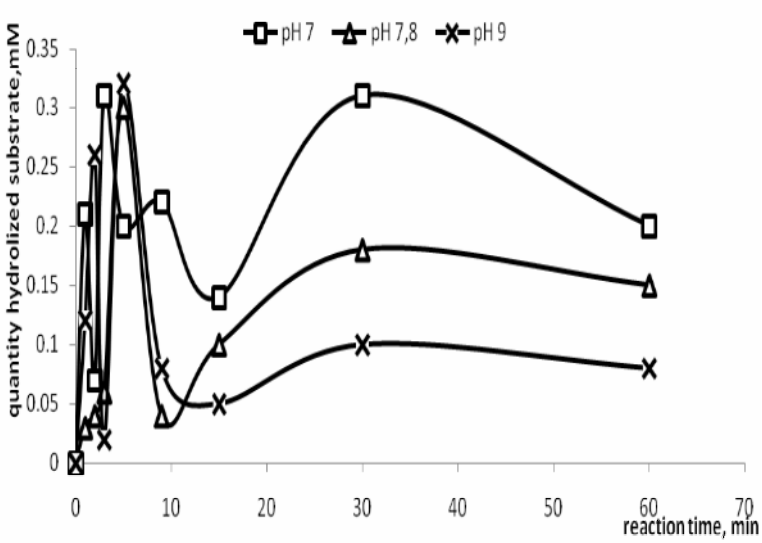

Fig. 3. Kinetics of hydrolysis of 0.4 mM synthetic substrate with 0.4 ml PGA at different pH.

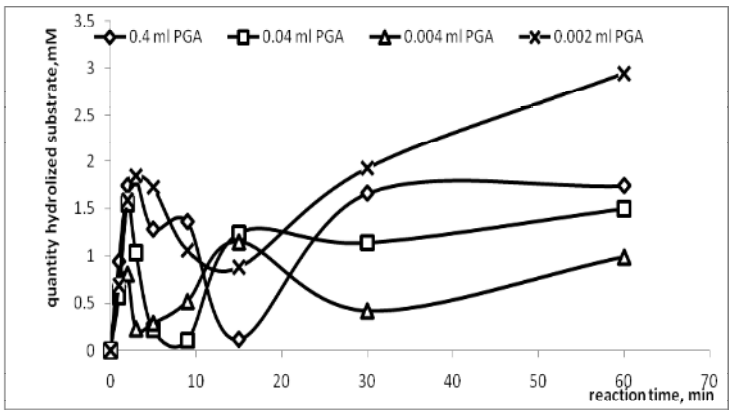

Fig. 4. Kinetics of hydrolysis of 5.0 mM synthetic substrate with different concentrations of PGA.

The kinetic results depending on the $Ni(NO_3)_2$ concentration, as a complex agent, are shown in Fig. 6. The figure clearly shows that the reaction equilibrium of hydrolysis of Phac group with stepwise addition of 10% $Ni(NO_3)_2$ was shifted to the direction of full hydrolysis of the protecting group for 9 min. In this case the substrate was 40 mM and the final concentration of $Ni(NO_3)_2$ – 1 M.

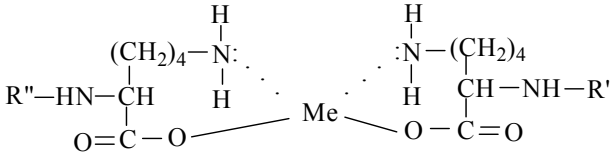

Fig. 5. Structure of the complex of ε-amino function of Lys residues with different metals.

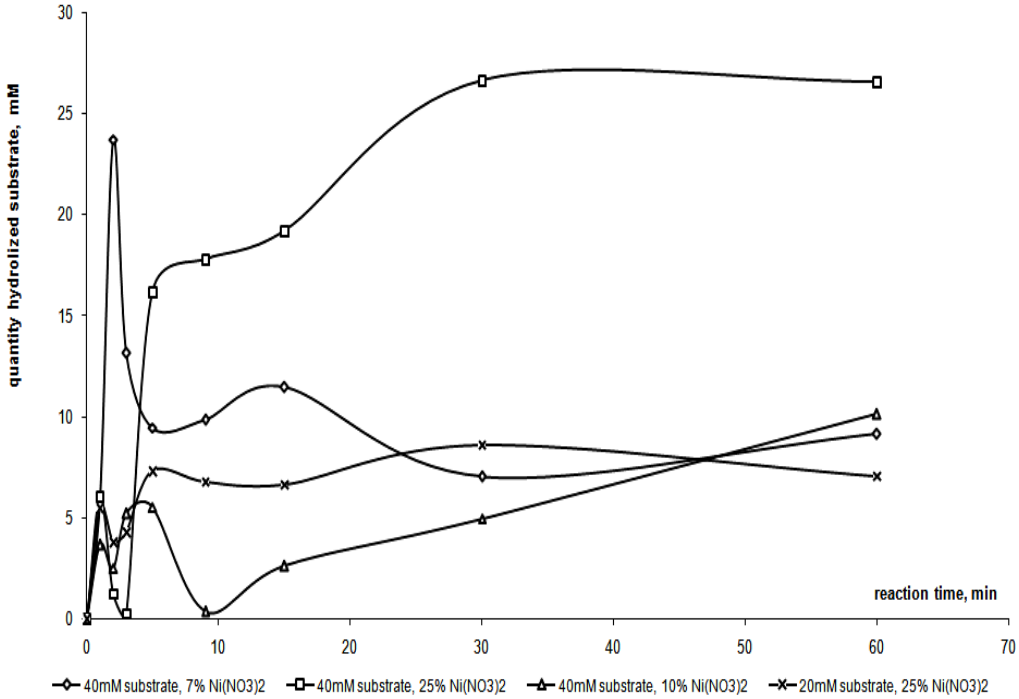

Fig. 6. Kinetics of hydrolysis of different amounts of synthetic substrate Boc-Lys(Phac)-Lys(Phac)- Lys(Phac)-OH with 0.002 ml PGA at pH = 9.0 and 37°C by stepwise addition of $Ni(NO_3)_2$ at different concentrations.

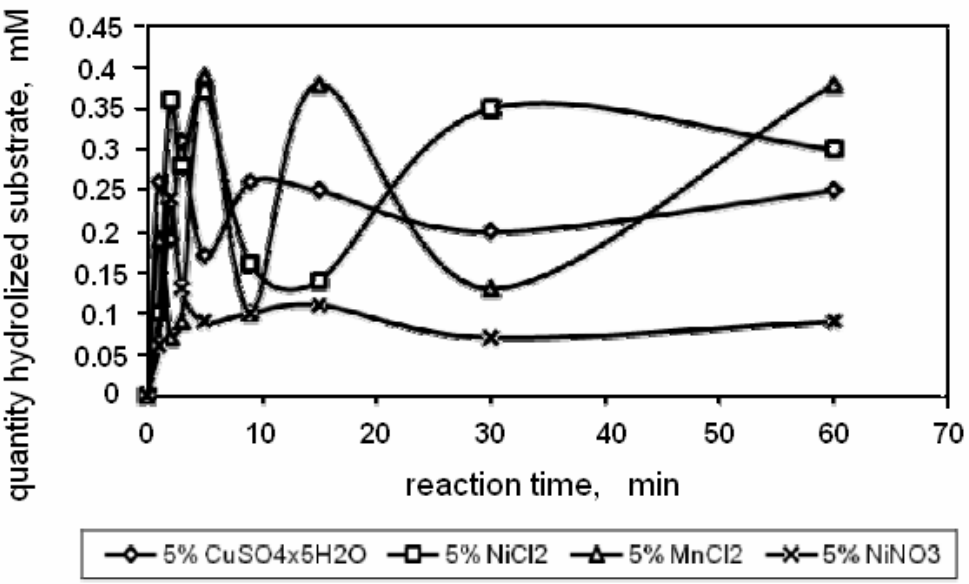

Fig. 7. Kinetics of hydrolysis of 0.4 mM synthetic substrate Boc-Lys(Phac)-Val-OH with 0.4 ml PGA in the reaction mixture at pH = 9.0 and 37°C by partial addition of different complex agents' salts.

The possibilities for the reaction of hydrolysis in the presence of salts of different complexing agents like $CuSO_4.5H_2O$, $NiCl_2$, and $MnCl_2$ were investigated, too (Fig. 7). As it can be clearly seen from the figure, the maximum degree of conversion was achieved in the presence of Ni^{2+} in the reaction mixture. The equilibrium of the reaction is shifted to the direction of full hydrolysis of the protecting group only in the case with stepwise addition of Ni^{2+}. It was revealed that the concentration of Ni^{2+} and the type of its salts are important, too. There was 100% degree of Phac group hydrolysis in the presence of 10% $Ni(NO_3)_2$ for 9 min and a full shift of the equilibrium to the direction of hydrolysis was monitored in the presence of 25% $Ni(NO_3)_2$.

CONCLUSIONS

The obtained results showed that the reaction of Phac group's hydrolysis was reversible at defined

conditions of pH, temperature range and reaction time.

Kinetic modelling studies of model peptide substrates reveal that:

- The use of metal ions as complexing agents of amino acid residues is a promising alternative for the studied enzymatic reaction.

- An acceptable approach is found to draw out the reaction of hydrolysis of phenylacetyl group with PGA in model peptide substrates to a desired direction.

- The best complex agents are Ni^{2+}.

- Maximum degree of substrate conversion (100%) was obtained at pH 9 and 37°C in the presence of 10% $Ni(NO_3)_2$.

REFERENCES

1. D. Rossi, A. Calcagni, *Experientia*, 35, (1985).
2. R. J. Didizapetris, V. K. Svedas*, Biomed. Biochem. Acta*, **50**, 5237 (1991).
3. V. K. Svedas, A. I. Beltser, *Ann. N.Y.Acad. Sci.*, **864**, 524 (1998).
4. R. Didziapetris, B. Drabnig, V. Schellenberger, H. D. Jakubke, V. Svedas, *FEBS Lett.*, **287**, 31 (1991).
5. H. Waldmann, P. Braun, H. Kunz, *Biomed. Biochim. Acta,* **50**, 243 (1991).
6. L. Yotova., I. Dobrev, I. Ivanov, Practical Course in Biochemistry*,* Diagnosis Press, Sofia, 2001, p. 191 (in Bulgarian).
7. K. Lummer, A. Rieks, B. Galunski, V. Kasche, *Biochim. Biophys. Acta*, **143,** 327 (1999).
8. M. Gololobov, U. Schellenberger, F. Schellenberger, H. D. Jakubke, V. K. Svedas, *Biokhimiia*, **55**, 338 (1990).
9. D. T. Guranda, T. S. Volovik, V. K. Svedas, *Biochemistry (Moscow)*, **69,** 1386 (2004).
10. E. Schröder, K. Lubke, Methods of Peptide Synthesis I, Academic Press, New York, 1965, p. 172.

СИНТЕЗ НА МОДЕЛНИ ПЕПТИДНИ СУБСТРАТИ И ИЗСЛЕДВАНЕ НА РЕАКЦИЯТА НА ЕНЗИМНА ТРАНСФОРМАЦИЯ НА ФЕНИЛАЦЕТИЛНА ГРУПА С ПОМОЩТА НА ПЕНИЦИЛИН G АЦИЛАЗА

Д. Л. Даналев[1]*, Л. К. Йотова[2]

[1] Катедра „Органична химия“, Химикотехнологичен и металургичен университет, бул. „Климент Охридски“ № 8, 1756 София

[1] Катедра „Биотехнология“, Химикотехнологичен и Металургичен Университет, бул. „Климент Охридски“ № 8, 1756 София

Постъпила на 4 юли 2008 г.; Преработена на 18 септември 2008 г.

(Резюме)

Откриването на нови защитни групи за органичния синтез, основани на стереоспецифични и стереоселективни реакции, е важно за практиката, особено при синтеза на полусинтетични антибиотици и биологично активни пептиди. Целта на настоящата работа е да изследваме кинетиката на ензимна хидролиза на фенилацетилна група в синтетични пептидни субстрати. Бяха използвани два моделни пептиди, съдържащи съответно една и три фенилацетилни защитни групи. Ензимната хидролиза беше направена с помощта на Пеницилин G ацилаза в широк pH диапазон 6–9. Използваните субстратни концентрации бяха 0.4–40 mM. Максимална степен на конверсия 75.5% (pH 9), близка до тази при pH 7.8 (74.5%) беше наблюдавана за 3 до 10 минути. При pH 6.5 и 7 степента на хидролиза беше съответно 62.5 и 37.5%. Беше изследвана възможността за провеждане на реакцията в присъствие на соли на различни метални комплексообразуватели $CuSO_4.5H_2O$, $NiCl_2$, $Ni(NO_3)_2$ и $MnCl_2$. Беше постигната 100% степен на конверсия на фенилацетилната група в присъствие на 10% $Ni(NO_3)_2$ за 9 минути и пълно изтегляне на химичното равновесие в посока на процеса на хидролиза в присъствие на 25% $Ni(NO_3)_2$.

Bulgarian Chemical Communications, Volume 41, Number 2 (pp. 127–132) 2009

Fast oscillations of arterial blood pressure during nociceptin analogues application in *Wistar* rats

R. A. Girchev[1]*, P. P. Markova[1], E. D. Naydenova[2], L. T. Vezenkov[2]

[1] *Department of Physiology, Medical University, 1 G. Sofiiski Blvd, 1431 Sofia, Bulgaria*
[2] *Department of Organic Chemistry, University of Chemical Technology and Metallurgy, 8 Kliment Ohridski Blvd., 1756 Sofia, Bulgaria*

Received July 16, 2008; Revised September 27, 2008

The effects of nociceptin analogues N/OFQ(1–13)-NH_2 or [Orn^9]/OFQ(1–13)-NH_2 on the blood pressure variability were studied in conscious *Wistar* rats. Arterial blood pressure (ABP) wave was registered directly through a femoral artery catheter by Gould Statham transducer connected to Biopac MP100WS. After a control period the effects of N/OFQ(1–13)-NH_2 or [Orn^9]/OFQ(1–13)-NH_2 applied in equal dose of 100 nmol/kg b.w., *i.v.* were investigated within nine consecutive 10-min intervals. The spectrograms for systolic (SAP), diastolic (DAP) and mean (MAP) arterial blood pressure were derived through Lab View 3.1.1 by Fast Fourier Transform (FFT) algorithm. Spectral power (P) in the low- (LF), mid- (MF) and high- (HF) frequency band in $mmHg^2$ for SAP, DAP and MAP spectrograms were determined. The administration of N/OFQ(1–13)-NH_2 or [Orn^9]/OFQ(1–13)-NH_2 did not change the mean value of ABP during the whole experiment. N/OFQ(1–13)-NH_2 application led to a decrease in P_{LF} in the spectrograms of SAP: from 2.37 ± 0.31 to 1.46 ± 0.34, 1.38 ± 0.33 and 1.55 ± 0.23 $mmHg^2$; DAP: from 2.17 ± 0.39 to 1.29 ± 0.24, 1.01 ± 0.20 and 1.31 ± 0.19 $mmHg^2$ and MAP: from 2.24 ± 0.35 to 1.42 ± 0.25, 1.14 ± 0.10 and 1.42 ± 0.15 $mmHg^2$ in the first three investigated periods, ($p < 0.05$). It also reduced P_{MF} in the spectrograms of SAP by 34.5%, 47.9%, 43.7%; DAP by 46.9%, 41%, 43% and MAP by 42.3%, 44.3%, 36.8%, ($p < 0.05$) in the same investigated intervals. The application of [Orn^9]/OFQ(1–13)-NH_2 did not change the fast oscillation of ABP. The replacement of lysine with ornitine in the 9th position abolished the effects of nociceptin analogue N/OFQ(1–13)-NH_2 on blood pressure variability in *Wistar* rats.

Key words: *Wistar* rats, nociceptin analogues, blood pressure variability.

INTRODUCTION

The autonomic nervous system plays an important role in the regulation of cardiovascular function. Methods to quantify heart rate and arterial pressure variability have emerged as useful tools for evaluating sympathetic and parasympathetic modulation of the cardiovascular system in humans [1] and experimental animals [2]. Blood pressure variability has received considerable attention, not only because enhanced blood pressure variability has been an independent cardiovascular risk factor [3, 4], but also because the patterns of blood pressure variability may provide important information about cardiovascular regulation [5–7].

Nociceptin is the endogenous ligand of a seven-transmembrane domain G protein-coupled receptor referred to as OP_4. Via OP_4 receptor activation nociceptin modulates several biological actions [8]. It has been established that both nociceptin and OP_4 receptors are present in neuronal tissues involved in the regulation of cardiovascular function [9]. An intravenous injection of nociceptin as well as its smallest analogue nociceptin (1–13)NH_2 produced a dose-dependent fall of systemic arterial blood pressure in both anesthetized and conscious rats [10–12]. It has been established that nociceptin inhibits in a concentration-dependent manner noradrenalin release evoked by chemical or electrical stimulation [13, 14]. The modulator action of nociceptin on the peripheral activity of the parasympathetic fibres is also described [15]. Potent and selective ligands are required for investigating the functions regulated by the N/OFQ-OP_4 receptor system in detail and ultimately, for identifying the therapeutic indications of OP_4 receptor agonists and antagonists.

Despite the established facts about the modulator role of nociceptin and its analogues on the autonomic nervous system, there are no reports addressing the participation of nociceptin or its analogues in the regulation of fast oscillation of blood pressure.

The aim of the present study was to determine the effects of nociceptin analogues N/OFQ(1–13)-NH_2 or [Orn^9]/OFQ(1–13)-NH_2 on blood pressure variability in conscious *Wistar* rats.

* To whom all correspondence should be sent:
E-mail: girchev@medfac.acad.bg

EXPERIMENTAL

Synthesis of nociceptin analogues

The solid-phase peptide synthesis by Fmoc (9-fluorenylmethoxycarbonyl) chemistry was used to obtain N/OFQ(1–13)-NH_2 and [Orn^9]N/OFQ(1–13)-NH_2. Rink-amide resin was used as a solid-phase carrier, and 2-(1-OH-benzotriazole-1-yl)-1,1,3,3-tetramethyl-carbamide tetrafluoroborat (TBTU) – as a coupling reagent. The 3-functional amino acids were embedded as follows: Arg-as N^{α}-Fmoc-Arg(Pbf)-OH, Lys-as N^{α}-Fmoc-Lys(Boc)-OH, Orn-as N^{α}-Fmoc Orn(Boc)-OH, Ser-as N^{α}-Fmoc-Ser(tBu)-OH and Thr-as N^{α}-Fmoc-Thr(tBu)-OH. All coupling reactions were performed, at a molar ratio of 3/2.9/3/6/1 for amino acid/TBTU/HOBt/DIEA/resin. The Fmoc-group was deprotected by a 20% piperidine solution in dimethylformamide. The coupling and deprotection reactions were checked by the Kaiser test. The cleavage of the synthesized peptide from the resin was done using a mixture of 95% trifluoroacetic acid (TFA), 2.5% triisopropyl-silan (TIS) and 2.5% water. The protected amino acids were purchased from IrisBiotech (Germany). All other reagents and solvents were analytical or HPLC grade and were supplied by Merck (Germany).

The crude peptides were purified on a reversed-phase high performance liquid chromatography (HPLC) C18 column, using gradient elution with the following solvents: A – H_2O/0.1% TFA and B – CH_3CN/0.1% TFA. The peptide purity was checked by electrospray ionization massspectrometry. The analytical data for the new compound [Orn^9]N/OFQ(1–13)-NH_2 are as follows: tR 7.91 min, > 99% pure, 1368.6 calculated (MH+), 1368.5 observed (MH+).

Experimental design

Experiments were carried out on male, normotensive *Wistar* rats at the age of 12–14 weeks. The experiments were conducted in accordance with guidelines for the care and use of laboratory animals of the ethical commission at the Medical University, Sofia based on the Convention on Animal Protection. The animals were housed under standard conditions: 12/12 hours light/dark cycle; 22°C room temperature; free access to tap water and standard rat chow. The effects of nociceptin analogues N/OFQ(1–13)-NH_2 or [Orn^9]/OFQ(1–13)-NH_2 were investigated in two different experimental groups each consisting of 10 animals. For surgical preparation, one day before the experiments the animals were anesthetized with Pentobarbital Sodium (Nembutal, Sigma) 35 mg/kg b.w. given intraperitoneally. The femoral artery for a continuous blood pressure measurement and the femoral vein for drug application were catheterized. To avoid clotting the femoral catheters were flushed with 20 IU/ml heparin in 0.9% sterile saline. The catheters were tunnelled subcutaneously and exteriorized at the back of the neck. Rats were allowed 24 hours to recover from the surgical intervention and the experiments were performed on conscious, freely moving animals. In both experimental groups, blood pressure wave was monitored during 40-min control period, 5-min equilibration and 40-min experimental period. Arterial blood pressure wave was registered by a Gould Statham transducer P23ID connected to computerized data acquisition system Biopac MP100WS through an arterial catheter. The analogue to digital converted signal was received and monitored by AcqKnowledge 3.8 software. The nociceptin analogues N/OFQ(1–13)NH_2 or [Orn^9]/OFQ(1–13)-NH_2 were applied in the first and second experimental groups by *i.v.* bolus injection in a dose of 100 nmol/kg dissolved in 100 µl 0.9% NaCl. The effects were studied five minutes after the bolus injection of nociceptin analogues for nine consecutive 10-min long intervals. The values of systolic (SAP), diastolic (DAP) and mean (MAP) arterial blood pressure were determined by peak and rate detectors of the AcqKnowledge 3.8 software and thereafter the mean values of SAP, DAP and MAP were calculated. The obtained row data of investigated parameter were resampled for 10 Hz. The spectrograms for SAP, DAP and MAP were derived from 512 successive values through a virtual instrument developed in graphical programming environment Lab VIEW 3.1.1., by using Fast Fourier Transform algorithm. In the spectrograms, the spectral power (P) in the low- (LF), mid- (MF) and high- (HF) frequency band typical for rats (20–195; 195–605; 605–3000 mHz, respectively) in $mmHg^2$ was studied [1].

Statistical analysis was performed by Student's t-test. The results are presented as mean ± SEM. Differences at a level $p < 0.05$ were considered statistically significant.

RESULTS AND DISCUSSION

The application of nociceptin analogues N/OFQ(1–13)-NH_2 or [Orn^9]/OFQ(1–13)-NH_2 in a dose of 100 nmol/kg did not provoke changes of the mean values of SAP, DAP and MAP during the whole experimental period in *Wistar* rats (Table. 1).

In the spectral characteristics N/OFQ(1–13)-NH_2 application led to a decrease of P_{LF} in the spectrograms of SAP by 38.2% (from 2.37 ± 0.31 to

1.46 ± 0.34 $mmHg^2$), by 41.7% (to 1.38 ± 0.33 $mmHg^2$), by 34.4% (to1.55 ± 0.23 $mmHg^2$); DAP by 40.4% (from 2.17 ± 0.39 to 1.29 ± 0.24 $mmHg^2$), by 53.1% (to 1.01 ± 0.20 $mmHg^2$), by 39.5% (to 1.31 ± 0.19 $mmHg^2$) and MAP by 36.6% (from 2.24 ± 0.35 to 1.42 ± 0.25 $mmHg^2$), by 49.2% (to1.14 ± 0.10 $mmHg^2$) by 36.9% (to1.42 ± 0.15 $mmHg^2$) in the first three investigated 10-min long periods, ($p < 0.05$), (Fig. 1A). It also reduced P_{MF} in the spectrograms of SAP by 34.5%, (from 1.21 ± 0.14 to 0.79 ± 0.07 $mmHg^2$), 47.9% (to 0.63 ± 0.23 $mmHg^2$), 43.7% (to 0.68 ± 0.12 $mmHg^2$); DAP by 46.9% (from 1.11 ± 0.13 to 0.79 ± 0.07 $mmHg^2$), 41% (to 0.65 ± 0.07 $mmHg^2$), 43% (to 0.63 ± 0.09 $mmHg^2$) and MAP by 42.3% (from 1.26 ± 0.13 to 0.73 ± 0.08 $mmHg^2$), 44.3% (to 0.75 ± 0.07 $mmHg^2$), 36.8% (to 0.75 ± 0.07 $mmHg^2$), ($p < 0.05$) during one and the same investigated periods. In the course of the fourth investigated period after application of N/OFQ(1–13)-NH_2 the spectral power in the low- and mid- frequency bands returned to their control level. The fast oscillations in the high-frequency band were not affected. The application of [Orn^9]/OFQ(1–13)-NH_2 did not change the fast oscillation of arterial blood pressure (Fig. 1B).

The experimental data summarized in the present study demonstrate that intravenous application of N/OFQ(1–13)-NH_2 as well as of [Orn^9]/OFQ(1–13)-NH_2 does not lead to changes in the mean values of arterial blood pressure in conscious *Wistar* rats five minutes after its applications. Previously, it was reported that a transient depressor effect of nociceptin on the cardiovascular system in conscious rats develops within 30–90 s [16]. In our experiments we investigated the effects of N/OFQ(1–13)-NH_2 or [Orn9]/OFQ(1–13)-NH_2 5 minutes after its application. Thus, we excluded the non-stationary interval, caused by bolus injection on blood pressure signal, unsuitable for spectral analysis. In the absence of changes of the mean value of arterial blood pressure in our work we established a reduction in the spectral power in mid- and low-frequency bands as a result of N/OFQ(1–13)-NH_2 application. Mid-frequency blood pressure fluctuations (0.2–0.6 Hz in rats), the so-called Mayer waves, were associated mostly with the sympathetic modulation of vascular tone [17–19]. It has been established that nociceptin inhibits noradrenalin release evoked by chemical or electrical stimulation [20]. The experimental data suggest that nociceptin inhibits transmitter release from sympathetic neurons by a selective blockade of N-type Ca^{2+} channels, which may be of importance for its depressive effect on the cardiovascular system [21]. Evidence has been provided that nociceptin besides neurogenic properties has a direct effect on blood vessels [22]. The experimental data for involvement of prostaglandins and histamine in the effects of nociceptin have been available [23]. It is known that direct vasodilatation produced by nociceptin on the isolated vessels is endothelium independent [24]. Several experimental data have clearly indicated that the action of nociceptin is not involved in the NO-cGMP-dependent pathway [25]. It has been established that muscarinic and alfa-adrenergic receptors are not involved in the vasodilatation evoked by nociceptin in the rat mesenteric vascular bed [24]. The decrease in P_{LF} during N/OFQ(1–13)-NH_2 infusion may be a result of its interaction with a variety of factors associated with LF blood pressure variability (0.02–0.2 Hz in rats) at frequencies below the frequency of the Mayer waves

Table 1. Mean values of systolic (SAP), diastolic (DAP) and mean (MAP) arterial blood pressure in control period and in nine consecutive 10-min long intervals after bolus injection of N/OFQ(1–13)-NH_2 (left panel) or [Orn^9]/OFQ(1–13)-NH_2 (right panel) both applied in a dose of 100 nmol/kg.

	N/OFQ(1–13)-NH_2			[Orn^9]/OFQ(1–13)-NH_2		
	SAP ($mmHg^2$)	DAP ($mmHg^2$)	MAP ($mmHg^2$)	SAP ($mmHg^2$)	DAP ($mmHg^2$)	MAP ($mmHg^2$)
Control	131.40 ± 3.45	85.61 ± 3.69	104.34 ± 3.30	134.02 ± 2.33	86.02 ± 2.62	105.34 ± 2.28
I	130.40 ± 4.91	82.83 ± 4.43	102.10 ± 5.16	137.53 ± 3.59	85.31 ± 5.05	104.76 ± 3.44
II	134.93 ± 4.99	83.83 ± 4.11	104.30 ± 5.14	134.90 ± 3.20	84.62 ± 4.14	105.80 ± 3.99
III	132.73 ± 3.99	84.01 ± 2.64	104.62 ± 4.76	135.93 ± 2.52	86.36 ± 3.17	106.91 ± 3.91
IV	131.80 ± 4.51	84.35 ± 3.45	104.76 ± 4.77	136.56 ± 1.65	88.41 ± 5.56	106.86 ± 3.55
V	132.00 ± 3.31	82.42 ± 4.90	102.14 ± 4.88	137.77 ± 1.22	89.70 ± 4.58	104.06 ± 4.27
VI	133.54 ± 3.12	84.00 ± 3.50	104.56 ± 4.52	137.00 ± 1.31	85.55 ± 5.07	106.00 ± 4.90
VII	130.77 ± 2.93	82.27 ± 4.99	103.22 ± 4.46	133.93 ± 3.60	88.02 ± 5.02	107.06 ± 4.00
VIII	132.62 ± 3.75	83.47 ± 4.58	101.28 ± 4.12	137.42 ± 1.55	83.79 ± 5.71	104.35 ± 4.05
IX	133.01 ± 3.23	85.42 ± 5.27	104.99 ± 4.45	133.13 ± 1.67	82.99 ± 5.21	103.10 ± 3.78

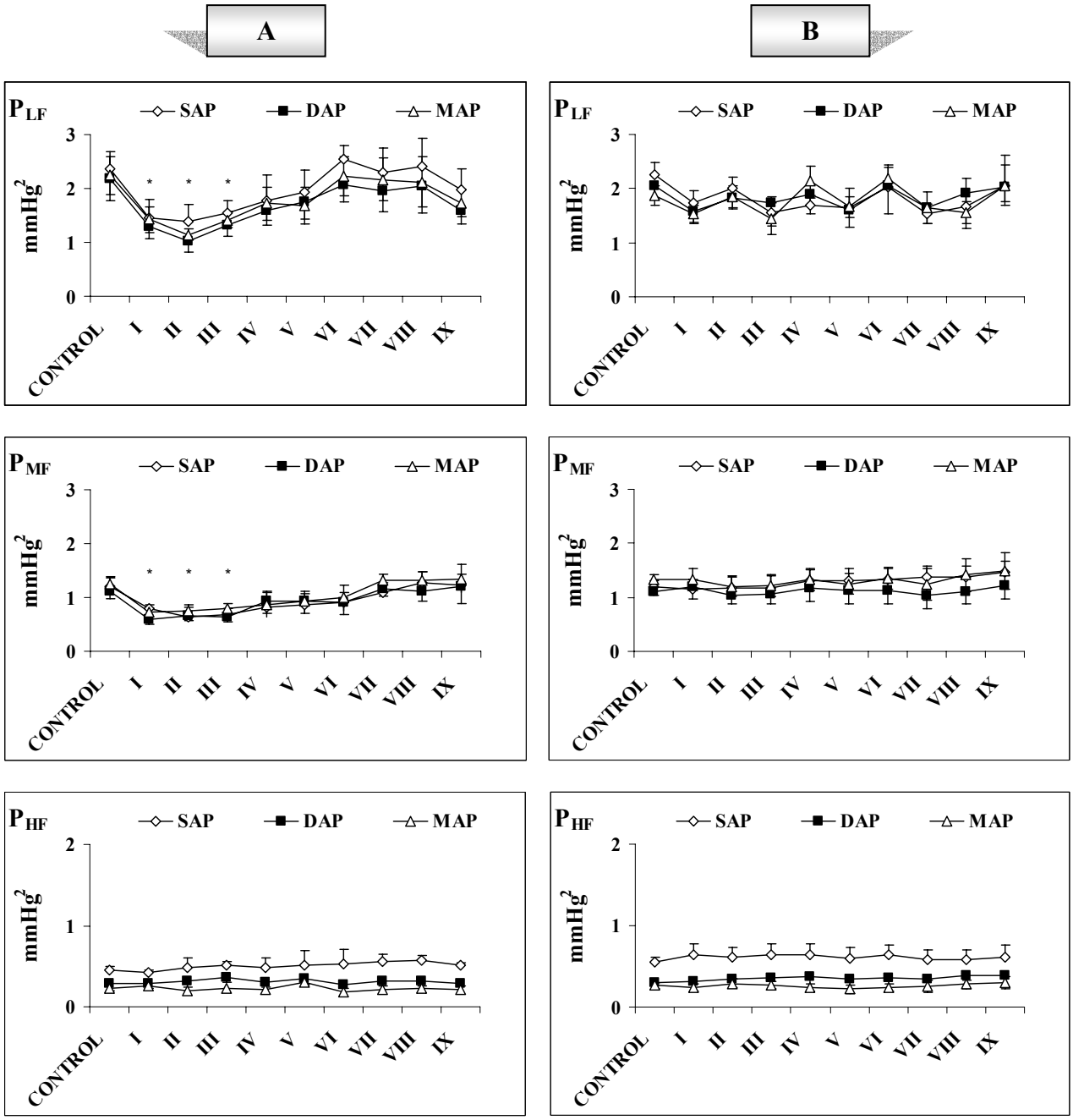

Fig. 1. Power distribution in spectrograms of systolic (SAP), diastolic (DAP) and mean arterial blood pressure (MAP) in low- (P_{LF}), mid- (P_{MF}) and high- (P_{HF}) frequency bands in normotensive *Wistar* rats during the control period and after N/OFQ(1–13)-NH_2 (A) or [Orn^9]/OFQ(1–13)-NH_2 (B), application in a dose of 100 nmol/kg in nine consecutive 10-min intervals. * ($p < 0.05$) shows statistically significant effects as a result of intravenous application (100 nmol/kg b.w.) of nociceptin analogue N/OFQ(1–13)-NH_2 compared to control value.

It is known that spectral power in the low-frequency band is modified by bradykinin [26] and the activity of the renin angiotensin system [26, 27] or catecholamines [28]. The established decrease in P_{LF} and P_{MF} after N/OFQ(1–13)-NH_2 application may be due to its interaction with different factors involved in the modulation of low fluctuations as well as in the direct inhibitor effect on the sympathetic nerve activity. High-frequency (HF) blood pressure variability linked to respiration [1] was not affected neither by N/OFQ(1–13)-NH_2 nor [Orn^9]/OFQ(1–13)-NH_2 applications.

The replacement of lysine with ornitine in the 9th position abolished the effects of nociceptin analog N/OFQ(1–13)-NH_2 on the blood pressure variability in *Wistar* rats.

Acknowledgements*: This work was supported by the National Science Fund through Grant No VU-L-205/2006.*

REFERENCES

1. M. A. Cohen, J. A. Taylor, *J. Physiol.,* **542,** 669 (2002).
2. S. C. Malpas, *Am. J. Physiol.*, **282,** H6 (2002).
3. G. Mancia, A. Frattola, G. Parati, C. Santucciu, L. Ulian, *J. Cardiovasc. Pharmacol.,* **24,** S6 (1994).
4. P. Martinka, J. Fielitz, A. Patzak, V. Regitz-Zagrosek, P. Persson, H. Stauss, *Am. J. Physiol*., **288**, R767 (2005).
5. S. Akselrod, D. Gordon, J. B. Madwed, N. C. Snidman, D. C. Shannon, R. J. Cohen. *Am. J. Physiol.,* **249,** H867 (1985).
6. C. Julien, Z. Q. Zhang, C. Cerutti, C. Barres, *J. Auton. Nerv. Syst.,* **50**, 239 (1995).
7. A. Malliani, M. Pagani, F. Lombardi, S. Cerutti, *Circulation,* **84**, 482 (1991).
8. G. Calò, R. Guerrini, A. Rizzi, S. Salvadori, D. Regoli, *Br. J. Pharmacol*., **129**, 1261 (2000).
9. C. Mollereau, L. Mouledous, *Peptides*., **21**, 907 (2000).
10. C. H. Champion, J. P. Kadowitz, *Life Sci*., **60**, 241 (1997).
11. S. Giuliani, M. Tramontana, A. Lecci, C. A. Maggi, *Eur. J. Pharmacol*., **333**, 177 (1997).
12. R. Bigoni, S. Giuliani, G. Calò, A. Rizzi, R. Guerrini, S. Salvadori, D. Regoli, C. A. Maggi, *Naunyn Schmiedebergs Arch. Pharmacol*., **359**, 160 (1999).
13. B. Bucher, *Naunyn Schmiedebergs Arch. Pharmacol*., **358**, 682 (1998).
14. A. U. Trendelenburg, S. L. Cox, V. Schelb, W. Klebroff, L. Khairallah, K. Starke, *Br. J. Pharmacol*. **130**, 321 (2000).
15. S. Giuliani, C. A. Maggi, *Eur. J. Pharmacol*., **332**, 231 (1997).
16. B. Malinowska, G. Godlewski, E. Schlicker, *J. Physiol. Pharmacol.,* **53**, 301 (2002).
17. C. Julien, S. C. Malpas, H. M. Stauss, *J. Hypertens.,* **19**, 1707 (2001).
18. H. M. Stauss, K. C. Kregel, *Am. J. Physiol.,* **271,** H1416 (1996).
19. H. M. Stauss, P. B. Persson, A. K. Johnson, K. C. Kregel, *Am. J. Physiol*., **273**, H786 (1997).
20. B. Malinowska, J. Piszcz, B. Koneczny, A. Hryniewicz, E. Schlicker, *Naunyn Schmiedebergs Arch. Pharmacol.*, **364**, 233 (2001).
21. K. P. Larsson, U. B. Olsen, A. J. Hansen, *Neurosci. Lett.,* **296,** 121 (2000).
22. M. A. Czapla, H. C. Champion, P. J. Kadowitz, *Peptides*, **18,** 1197 (1997).
23. T. Kimura, K. Kitaichi, K. Hiramatsu, M. Yoshida, Y. Ito, H. Kume, K. Yamaki, R. Suzuki, K. Takagi, *Eur. J. Pharmacol*., **407**, 327 (2000).
24. H. C. Champion, R. L. Pierce, P. J. Kadowitz, *Regul. Pept.,* **78,** 69 (1998).
25. W. M. Armstead, *Brain Res*., **835**, 315 (1999).
26. P. Ponchon, J. L. Elghozi, *Eur. J. Pharmacol.*, **297**, 61 (1996).
27. J. Blanc, G. Lambert, J. L.. Elghozi, *Eur. J. Pharmacol.,* **394**, 311 (2000).
28. A. Radaelli, P. Castiglioni, M. Centola, F. Cesana, G. Balestri, A. Ferrari, M. Di Rienzo, *Am. J. Physiol.*, **290**, H357 (2006).

БЪРЗИ ОСЦИЛАЦИИ НА АРТЕРИАЛНОТО НАЛЯГАНЕ У ПЛЪХОВЕ *Wistar* ПО ВРЕМЕ НА ПРИЛОЖЕНИЕТО НА НОЦИЦЕПТИНОВИ АНАЛОЗИ

Р. А. Гърчев[1]*, П. П. Маркова[1], Е. Д. Найденова[2], Л. Т. Везенков[2]

[1] *Катедра „Физиология", Медицински университет, бул. „Георги Софийски" № 1, 1431 София*
[2] *Катедра „Органична химия", Химикотехнологичен и металургичен университет, бул. „Климент Охридски" № 8, 1756 София*

Постъпила на 16 юли 2008 г.; Преработена на 27 септември 2008 г.

(Резюме)

Ефектите на ноцицептиновите аналози N/OFQ(1–13)-NH_2 и [Orn^9]/OFQ(1–13)-NH_2 върху бързите колебания на артериалното налягане бяха изследвани на будни нормотензивни плъхове *Wistar*. Артериалното кръвно налягане (ABP) беше регистрирано директно през катетър имплантиран във феморалната артерия, чрез трансдюсер за налягане Gould Statham, свързан към Biopac MP100WS. След контролен период ефектите на N/OFQ(1–13)-NH_2 и [Orn^9]/OFQ(1–13)-NH_2 прилагани съответно в еднакви дози 100 nmol/kg т.м., *i.v.* бяха изследвани в 9 последователни 10-минутни интервала. Спектрограмите за систолното (SAP), диастолното (DAP) и средното (MAP) артериално кръвно налягане бяха получени чрез Бърза Фурие трансформация в Lab View 3.1.1. В спектрограмите на SAP, DAP и MAP бяха изследвани спектралните мощности (P) в зоните на ниски (LF), средни (MF), и високи (HF) честоти. Приложението както на N/OFQ(1–13)-NH_2 така и на [Orn^9]/OFQ(1–13)-NH_2 не промени средните стойности на ABP по време на целия експеримент. Приложението на N/OFQ(1–13)-NH_2 предизвика понижаване на P_{LF} в спектрограмите на SAP: от 2.37 ± 0.31 на 1.46 ± 0.34, 1.38 ± 0.33 и на 1.55 ± 0.23 mm Hg2; DAP: от 2.17 ± 0.39 на 1.29 ± 0.24, 1.02 ± 0.20 и на 1.31 ± 0.19 mm Hg2 и MAP: от 2.24 ± 0.35 на 1.42 ± 0.25, 1.14 ± 0.10 и на 1.42 ± 0.15 mm Hg2 в първите три изследвани интервала, ($p < 0.05$). Намалена беше също P_{MF} в спектрограмите на SAP с 34.5%, 47.9%, 43.7%; DAP с 46.9%, 41.6%, 43.1% и MAP с 42.3%, 40.4%, 36.8%, ($p < 0.05$) в същите изследвани периоди. Приложението на [Orn^9]/OFQ(1–13)-NH_2 не предизвика промени в бързите осцилации на артериалното налягане. Заместването на лизин с орнитин в 9^{та} позиция премахва ефекта на ноцицептиновия аналог N/OFQ(1–13)-NH_2 върху вариабилността на артериалното кръвно налягане у плъхове *Wistar*.

Bulgarian Chemical Communications, Volume 41, Number 2 (pp. 133–137) 2009

Structure-activity relationships of new L-Valine derivatives with neuropharmacological effects

D. S. Tsekova[1]*, E. Ts. Makakova[2], P. S. Alov[3], G. A. Gorneva[4], I. K. Pajeva[3], L. P. Tancheva[5], V. V. Petkov[5], A. R. Surleva[6], B. Escuder[7], J. F. Miravet[7], E. Katz[8]

[1] *Department of Organic Chemistry, University of Chemical Technology and Metallurgy, 8 Kliment Ohridski Blvd., 1756 Sofia, Bulgaria*
[2] *Faculty of Chemistry, Kliment Ohridski University of Sofia, 1 J. Bouchier Blvd., 1164 Sofia, Bulgaria*
[3] *Center of Biomedical Engineering, Bulgarian Academy of Sciences, Acad. G. Bonchev St., Block 105, 1113 Sofia, Bulgaria*
[4] *Institute of Molecular Biology, Bulgarian Academy of Sciences, Acad. G. Bonchev St., Block 21, 1113 Sofia, Bulgaria*
[5] *Institute of Neurobiolog,y, Bulgarian Academy of Sciences, Acad. G. Bonchev St., Block 23, 1113 Sofia, Bulgaria*
[6] *Department of Analytical Chemistry, University of Chemical Technology and Metallurgy, 8 Kliment Ohridski Blvd., 1756 Sofia, Bulgaria*
[7] *Department of Inorganic and Organic Chemistry, Universitat Jaume I, 12071 Castellon, Spain*
[8] *Hebrew University, Jerusalem, Israel*

Received July 17, 2008; Revised September 27, 2008

Four derivatives of L-Valine were studied as potential pharmacological agents. L-Valine is bound to either nicotinic (*m*-pyridinic) acid (M) or isonicotinic (*p*-pyridinic) acid (P) from N-side and to an alkyl fragment (or species) consisting of 3 or 6 methylene groups from C-side. In experiments *in vivo* (in albino mice) and *in vitro* (on cell cultures F4N) the compounds showed very low toxicity (intraperitoneal and oral toxicity over 2000 mg/kg and citotoxicity lower than vitamin C). At the same time, they demonstrated significant neuropharmacological activity. The experimental data obtained for their solubility in water and octanol, as well as with calculated log*P* correlate well with the results for their Central Nervous System effects.

Key words: L-Valine derivatives, neuropharmacological effect, pKa, logP, toxicity, *in vivo*, *in vitro.*

INTRODUCTION

Four compounds, derivatives of L-Valine, nicotinic (*m*-pyridinic) acid (M) or isonicotinic (*p*-pyridinic) acid (P) were studied as potential pharmacological agents. The codes M3, M6, P3 and P6, are used depending on the position and the length of the alkyl fragment (or species) consisting of 3 or 6 methylene groups. The compounds belong to the group of low-molecular gelators (LMWG) and have very high ability to form intermolecular H-bonds, involving also solvent molecules in their supramolecular complexes formation [1, 2]. The four compounds are constructed by the natural L-α-aminoacid – Valine, connected by amide (peptide) bonds with neighbouring groups in a way different from the natural L-α-aminoacids. In this meaning, these compounds are representatives of the class of peptidomimetics. The other ingredient of the molecule is either nicotinic or isonicotinic acid, which are expected to determine their specific biological activities.

There are number of reports in literature for pronounced biological activities of compounds – derivatives of nicotinic and isonicotinic acids. Nicotinic acid and nicotinamide in the form of NAD+ and NADP+ participate in many enzymatic reactions [3]. Nicotinamide, known as vitamin B3 or PP is essential for normal function of the nervous system, gastrointestinal tract, normal tissue metabolism, it has also shown anti-anxiety anxiolytic properties similar to benzodiazepines [4] and has demonstrated anti-inflammatory actions [5]. Some isonicotinic acid derivatives are antituberculosis medications [6, 7] and others possess antidepressant activities [8, 9].

Recently we reported that two of these compounds (M6 and P6) had neuropharmacological activities [10]. Up to this report, similar analogs have not been used as major structures for drug synthesis. Here we present additional results for M6 and P6 and two new structurally-related compounds (M3 and P3). Physicochemical properties obtained

* To whom all correspondence should be sent:
E-mail: d_tsekova@abv.bg

experimentally and by model calculations, *in vitro* and *in vivo* toxicity and pharmacological activities are summarized and compared.

The directions of this study include:

Defining the physicochemical characteristics of the target compounds:

- Solubility in different solvents.
- pKa .
- Partition coefficients.

Toxicity:

- *In vitro* toxicity (citotoxicity).
- Acute toxicity, effective doses, therapeutic index.

Analysis of structure-activity relationships.

EXPERIMENTAL

Materials and methods

Physicochemical properties were defined by:

- UV spectrophotometry - for determining of pKa and solubility concentrations. VARIAN CARY 100 Scan UV-VIS Spectrophotometre was used.
- ACD Labs.

Experimental biological activities:

Materials. 1. Male Albino mice ICR with initial body weight of 18–20g (10 in groups).

2. F4N-mouse erythro-leukimic cells, obtained by erythroidal cells, transformed by the Friend virus.

Methods. *Toxicological studies*. *In vitro*: The method is based on the ability of the live cells to extrude the blue dye (Methylene blue) which penetrates through membranes and remains uncoloured, while the dead cells are stained blue.

In vivo: For toxicology activities estimation the following effects in the living body were defined:

1. Parameters of acute toxicity:
   - Limit of acute activity (Limac).
   - No observed effect level (NOEL).
   - Lethal dose 50% (LD50) – according to Bulgarian standards 15380-81.
2. Prolonged toxicity – after 5, 7 and 14 days.
3. Reversibility of the toxic damages – till the 14th day after acute administration of the compounds.

RESULTS AND DISCUSSION

Data for pKa of M3, P3, M6 and P6

Applying ACD Labs data for *pKa* were calculated and they are presented in Table 1.

The experimental values of pKa_1 and pKa_2 of P3 compound, related to both pyridine N atoms (1st and 2nd N) were determined using a well-known spectrophotometric method [11]. The analytical wavelengths were chosen from the UV-absorption spectra of P3 (at constant concentration of 1×10^{-4} mol/l (48.3 μg/ml)) at different pH. In Fig. 1a three spectra are presented: of the neutral molecule – R that exists at pH 7, the double ionized form RH_2^{2+} existing at pH 1 and the mixture of forms that exist at pH ~ 4, namely R, RH^+ and RH_2^{2+}.

Table 1. Calculated pKa data for the four compounds.

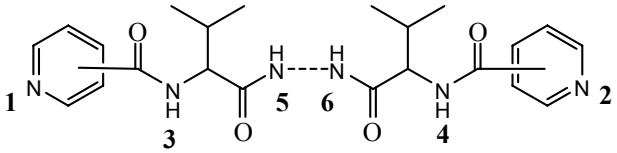

	Compound			
	P3	P6	M3	M6
pKa_1	3.19	3.08	3.14	2.93
pKa_2	3.8	3.71	3.74	3.62
pKa_3	11.33	11.35	11.76	11.78
pKa_4	11.94	11.95	12.37	12.38
pKa_5	15.73	15.96	15.75	15.97
pKa_6	16.64	16.58	16.65	16.59

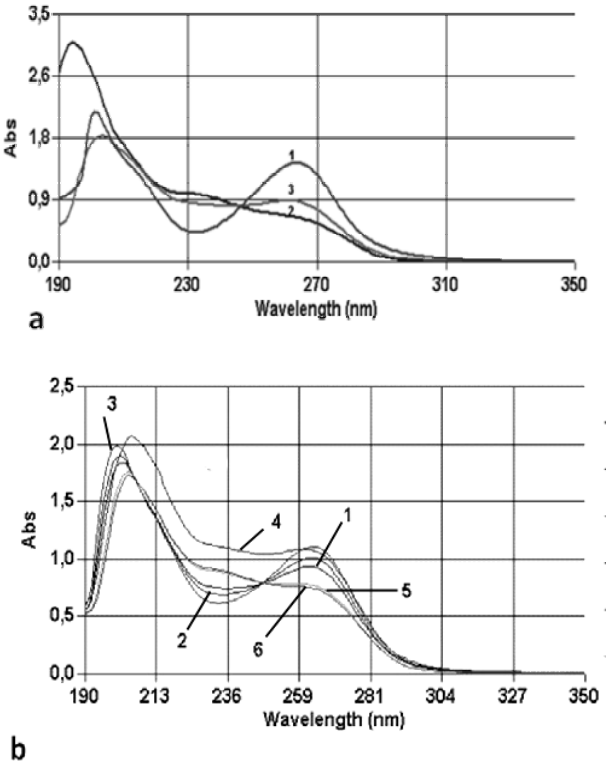

Fig. 1. Absorption of compound P3 in the UV range at different pH: a) 1– pH = 7; 2 – pH = 1; 3 – pH=3,8; b) 1 – pH = 3.64; 2 – pH = 3.47; 3 – pH = 3.16; 4 – pH = 4.02; 5 – pH = 4.19; 6 – pH = 4.33.

As it is seen from the figure, the differences in the absorption (*A*) of both states R and RH_2^{2+} at λ = 231 and 264 nm have analytical values. Using the data for the absorption at these wavelengths and

applying equation (1) approximated *pKa* were calculated:

$$pKa = pH + \log \frac{A - A_R}{A_{RH_2^{2+}} - A}$$

or

$$pKa = pH + \log \frac{A_R - A}{A - A_{RH_2^{2+}}} \qquad (1)$$

where A_R is the absorption of unionized molecule (at pH 7), $A_{RH_2^{2+}}$ – the absorption of the double ionized molecule (at pH = 1) and A is the absorption at pH, which is between 1 and 7.

Results obtained show that:

- at pH 7, solution contains 99.99% R and 0.01% of the mixture $RH^+ + RH_2^{2+}$:
- at pH 1, 99.99% of the compound P3 exist in the fully ionized form RH_2^{2+};
- pKa_1 is higher than 3.2;
- pKa_2 is lower than 4.3.

Both values of *pKa* are very close. The conditions where only the monoionized form RH^+ exists in a solution at concentrations higher than 99% can not be created experimentally and thus its absorption can not be measured. In such cases, the absorption of RH^+ can be calculated by an extrapolation of the absorption values of the other two forms (R and RH_2^{2+}) at different pH. The absorption of P3 has been measured in the pH range between 3.16 and 4.33 and the resulting UV-spectra are presented in Fig. 1b. The values of pKa_1 and pKa_2 were calculated using the method of consecutive approximations: pKa_1 = 3.23 ± 0.15 and pKa_2 = 4.16 ± 0.10 (n = 3, p = 95%) at 20°C.

As the experimentally established values of *pKa* were close enough to the theoretically calculated ones, we accepted theoretically the found data as applicable for all four substances.

Data for logP

One of the very important physicochemical characteristic of the drugs is their partition coefficient log*P* that characterizes their distribution between water and lipid phase in the body. In the experimental model systems lipids are usually presented by octanol and log*P* is defined by the following equation:

$$\log P = \log\left(\frac{C_{octanol}}{C_{water}}\right) \qquad (2)$$

where C is concentration of the unionized solute in both solvents, octanol and water. The *pKa* data of the four compounds, (Table 1), show that all they exist in unionized form at the physiologically active pH 7.4 (the physiological pH of blood serum), which means that log*P* and log*D* (the apparent log*P*) do not differ.

In order to define log*P* experimentally, we needed information for solubility of the compounds in both solvents. Experiments were performed to define the standard calibration lines for absorption in both solvents. The absorption bands in the region 190–310 nm for compound P3 are presented in Fig. 2. Concentrations used for water solutions were between 0.1 and 0.0025 mg/ml, and those used for octanol solutions – between 0.15 and 0.02 mg/ml.

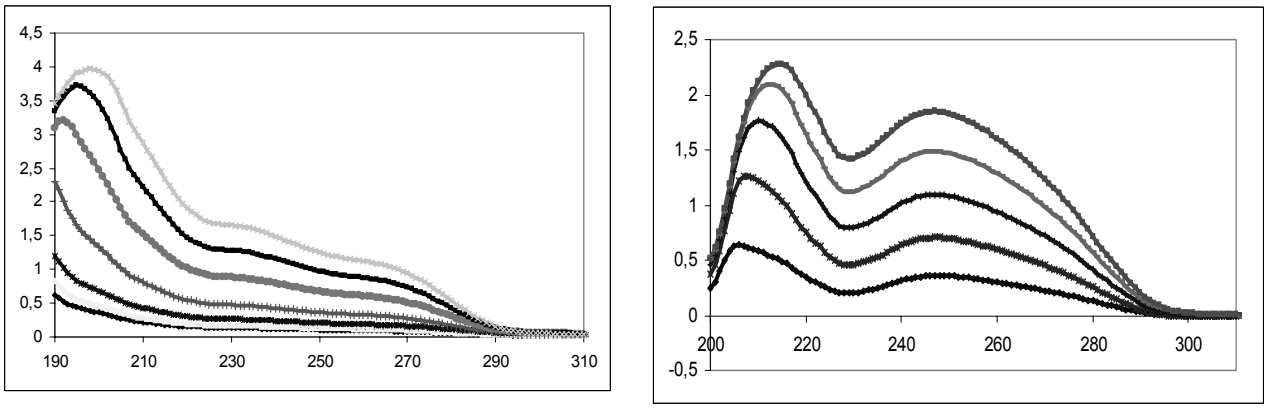

a b

Fig. 2. a. Bands of absorbance in the UV range for compound P3 in water. Used concentrations of P3 in water (mg/ml) were: 0.1; 0.075; 0.05; 0.025; 0.01; 0.0075; 0.005; b. Bands of absorbance in the UV range for compound P3 in octanol. Used concentrations of P3 in octanol (mg/ml) were: 0.15; 0.12; 0.09 0.06 0.003.
On the abscissas is the wavelength, λ nm, and on the ordinates is the absorbance, *A*.

The spectra presented in Fig. 2 display two main bands. It turned out that the lower one is more sensitive to variation in concentrations and its maximum appears at constant wavelength (λ), while the maximum of the higher one appears at different wavelengths with exchanging of concentrations, namely upon increase in concentration this taller maximum shifts to higher values of λ. Using data for the absorptions of the compounds in water solutions at 261 nm, and in octanol at 248 nm, standard lines concentration/absorption were drawn. In the course of the experiment an interesting fact was detected: in water solutions the same substance shows different molar absorptions depending on the starting concentration. Figure 3 illustrates one of the sets of calibration lines obtained for compound P3. This result shows that after dissolving at high temperatures and subsequent cooling each compound forms stable supramolecular complexes of different size depending on the initial concentration obtained in hot solution. That finding restricted the exact experimental log P measurement. On the other hand, comparison of the solubility of four compounds in water and in octanol shows that the solubilities in octanol are in orders higher than those in water, namely for M6 and P6 about 80–100 times, for M3 and P3 – 30–50 times, which results agree with data obtained by theoretical calculations (Table 2).

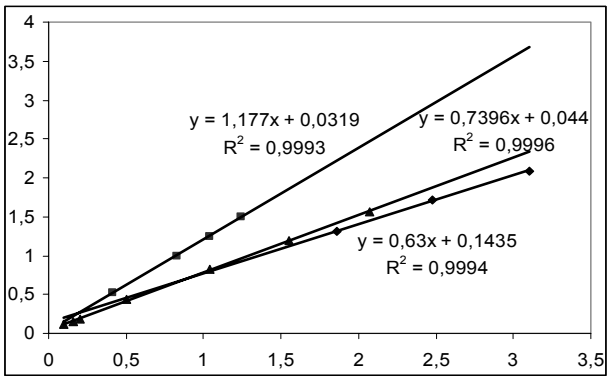

Fig. 3. Calibrating lines obtained for P3 in water with starting concentrations of 3.1, 2.07 and 1.24×10^{-4} M P3. On the abscissas is the molar concentration and on the ordinates is *A* at λ = 261 nm.

Table 2. Data calculated for log*P* for the four compounds.

Substance	Log*P* (Theoretical data)
M3	1.14 ± 0.76
P3	0.33 ± 0.67
M6	2.20 ± 0.68
P6	1.4 ± 0.67

Biological activities

Toxicity in vitro (citotoxicity): The four peptidomimetics were found as nontoxic at concentrations equal or lower than 250 μM. For purpose of comparison we tested Vitamin C at the same experimental conditions and established that it revealed toxicity at 200 μM, *i.e.* our compounds were less toxic than Vit. C.

Toxicity in vivo: As a result of the experiments performed, a low acute effect and lack of prolonged toxicity were observed. At doses over 2000 mg/kg each of the tested compounds (applied in both modes: intraperitoneal (i.p.) and oral (p.os)) did not provoke any symptoms of intoxication, *i.e.* LD50 is over 2000 mg/kg (p.os and i.p.).

No observed effect level (NOEL) was estimated as 40 mg/kg i.p. and limit of acute toxicity (Limac) was found at 80 mg/kg i.p.

Dissection of the animals at the 5, 7 and 14 day of the treatment did not show any changes or irreversible toxic damages in the organs which points to the lack of prolonged toxicity.

In most of the experiments the effective doses (ED50) of the compounds were about 250 mg/kg b.w. i.p. Bearing in mind that LD50 is over 2000 mg/kg, a therapeutic index (LD50/ED50) higher than 8 could be expected.

Preliminary data showed that some of the compounds (M6 and P6) had pronounced analgesic effect as well as good dose-dependent effect on learning and memory [10].

CONCLUSIONS

The four compounds are nontoxic at concentrations ≤ 250 μM. They show citotoxicity even lower than that of Vit C.

High therapeutic index > 8 can be expected.

At physiological pH 7.4 the four compounds exist mainly in their unionized form.

Their solubility in octanol is much higher than in water (for M6 and P6 about 80–100 times, for M3 and P3 – 30–50 times), which could be related to the differences in the observed neuropharmacological effects.

In water solutions each compound shows different molar absorptions that points to formations of stable supramolecular complexes with sizes depending on the concentration of the compound.

The above data will be further used for purposeful synthesis and molecular modelling studies of structure-activity relationships of this new class of peptidomimetics.

***Acknowledgements**: We thank for the funding provided by the University of Chemical Technology and Metallurgy (Research Contract 10508).*

REFERENCES

1. D. S. Tsekova, B. Escuder, J. F. Miravet, *Cryst. Growth Des.*, **8**, 11 (2008).
2. J. F. Miravet, B. Escuder, *Chem. Commun*., 5796 (2005).
3. P. Belenky, K. L. Bogan, C. Brenner, *Trends Biochem. Sci.,* **32,** 12 (2007).
4. J. F. Tallman, S. M. Paul, P. Skolnick, D. W. Gallager, *Science,* **207**, 274 (1980).
5. N. M. Niren, *Cutis,* **77** (1 Suppl), 11 (2006).
6. A. Dömling, S. Achatz, B. Beck, *Bioorg. Med. Chem. Lett*., **17**, 5483 (2007).
7. G. S. Timmins, V. Deretic, *Mol. Microbiol.,* **62**, 1220 (2006).
8. M. Kobayashi, E. Arai, *Psychopharmacology*, **46**, 317 (1976).
9. P. O. Ganrot, E. Rosengren, C. G. Gottfries, *Cell. Mol. Life Sci.***, 18**, 260 (1962).
10. L. Tantcheva, V. V. Petkov, G. Karamukova, S. Abarova, Y. Chekalarova, D. Tsekova, B. Escuder, J. Miravet, K. Lyubomirova, *Bulg. Chem. Comm.,* **38***,* 54 (2006).
11. A. Albert, E. Sergeant, Ionization Constants of Acids and Bases, Khimiya,. Moscow-Leningrad, 1964, p. 64 (in Russian).

ВРЪЗКА СТРУКТУРА-АКТИВНОСТ ПРИ НОВИ ПРОИЗВОДНИ НА L-ВАЛИНА ПРОЯВЯВАЩИ НЕВРОФИЗИОЛОГИЧНИ ЕФЕКТИ

Д. С. Цекова[1]*, Е. Ц. Макакова[2], П. С. Алов[3], Г. А. Горнева[4], И. К. Пъжева[3], Л. П. Танчева[5], В. В. Петков[5], А. Р. Сурлева[6], Б. Ескюдер[7], Х. Ф. Миравет[7], Е. Катц[8]

[1] Катедра „Органична химия“, Химикотехнологичен и металургичен университет, бул. „Климент Охридски“ № 8, 1756 София
[2] Химически факултет, Софийски университет „Климент Охридски“, бул. „Дж. Баучър“ № 1, 1164 София
[3] Център по биомедицинско инженерство, Българска академия на науките, ул. „Акад. Г. Бончев“, бл. 105, 1113 София
[4] Институт по молекулярна биология, Българска академия на науките, ул. „Акад. Г. Бончев“, бл. 21, 1113 София
[5] Институт по невробиология, Българска академия на науките, ул. „Акад. Г. Бончев“, бл. 23, 1113 София
[6] Катедра „Аналитична химия“, Химикотехнологичен и металургичен университет, бул. „Климент Охридски“ № 8, 1756 София
[7] Департамент по неорганична и органична химия, Университет „Хайме I“, 12071 Кастелон, Испания
[8] Еврейски университет, Йерусалим, Израел

Постъпила на 17 юли 2008 г., Преработена на 27 септември 2008. г.

(Резюме)

Изследвани бяха четири производни на L-валина като потенциални фармакологични агенти. От N-края си α-аминокиселината е свързана с никотинова (*m*-пиридинова) киселина или с изоникотинова (*p*-пиридинова) киселина и от С-края си – с алкилов остатък съдържащ 3 или 6 метиленови групи. В *in vivo* (бели мишки) и *in vitro* (клетъчни култури F4N) експерименти и четирите съединения показаха много ниска токсичност (интраперитонеално и орално въведени веществата проявяваха токсичност над 2000 мг/кг, а при клетъчните култури токсичността бе по-ниска от тази на витамин С). Същевременно бе отчетена значима неврофармакологична активност при доста по-ниски дози на изследваните вещества. Експериментално получените данни, отнасящи се до тяхната разтворимост във вода и октанол (log*P*), както и изчислените данни за log*P*, са в добра корелация с резултатите свързани с техните ефекти върху цетралната нервна система.

Bulgarian Chemical Communications, Volume 41, Number2 (pp. 138–142) 2009

Antinociceptive effects of des-octapeptide-insulin connected with enkephalins

N. St. Pencheva[1]*, A. I. Bocheva[2], K. Zh. Grancharska[1], T. Barth[3]

[1] *Department of Kinesitherapy, South-West University, 66 Iv. Mihailov St., 2700 Blagoevgrad, Bulgaria*
[2] *Department of Pathophysiology, Medical Faculty, Medical University, 2 Zdrave St., 1431 Sofia, Bulgaria*
[3] *Institute of Organic Chemistry and Biochemistry, Academy of Sciences of the Czech Republic, 2 Flemingovo nam., 166 10 Praha 6, The Czech Republic*

Received July 17, 2008; Revised September 30, 2008

Three insulin analogues with modifications of the B-chain were synthesized by trypsin-catalyzed coupling of des-octapeptide (B^{23}-B^{30})-insulin (DOI) with Met^5-enkephalin (Met^5-enk) or Leu^5-enkephalin (Leu^5-enk). The derivatives DOI-Met^5-enk and DOI-Leu^5-enk were prepared by a condensation between the amino group of the enkephalins and the carboxyl group of arginine in position B^{22}. To test the properties of DOI as a navigating molecule of active opioid peptides, we examined DOI, DOI-Met^5-enk and DOI-Leu^5-enk following three types of *in vivo* nociceptive methods: writhing test in mice, paw-pressure test and hot plate test in rats. The peptides were administered both intracerebroventricularly (icv) and subcutaneously (sc). The ability of the peptides to inhibit the electrically-evoked contraction in guinea-pig ileum and mouse vas deferens was also tested. To prove the opioid nature of the responses we used naloxone (1 mg/kg intraperitoneally). Using paw-pressure and hot-plate test, all compounds exerted well-pronounced antinociceptive effects (DOI < DOI-Met^5-enk < DOI-Leu^5-enk), with duration at least 40 min after icv application. The differences in order of potency were established after sc application and the effects of all compounds were developed for 20 min. The results obtained with writhing test in mice showed that all compounds did not influence the visceral pain. *In vitro* effects were poor and were observed at concentration higher than 20 μM for DOI-Met^5-enk and higher than 100 nM for DOI-Leu^5-enk. The present results suggested that the derivatives of DOI: DOI-Met^5-enk and DOI-Leu^5-enk achieved prolonged antinociceptive action, while DOI at some extent could be used as a transport molecule across the blood-brain barrier.

Keywords: des-octapeptide insulin; DOI; Met^5-enkephalin; Leu^5-enkephalin; pain; antinociception.

INTRODUCTION

The endogenous opioid pentapeptides Leu^5-enkephalin (Leu^5-enk) and Met^5-enkephalin (Met^5-enk) and their selective analogues participate in pain control, have analgetic potency and decrease electrically-evoked contractions during *in vitro* assays [1–3]. Leu^5-enk and Met^5-enk are released from the polypeptide precursor proenkephalin (267 amino acids), but can not be used as therapeutic drugs, because: (i) the endogenous peptidases degrade them rapidly; and (ii) the so-called peptide transport system 1 [4], which transports enkephalins out of the central nervous system or in both directions, is disputable. However, an artificial precursor of these short opioid peptides was constructed in a previous study of Barth *et al*. [5] by condensing desoctapeptide-insulin (DOI), which molecule is much larger, with Leu^5-enk or Met^5-enk. We suggested that the resulting peptides of this condensation could be distributed in the organism and enkephalins would be released from them gradually with prolonged analgetic action. Moreover, the analgetic potency of DOI, as a part of insulin molecule, was also presumed because the antinociceptive effects of insulin are well-documented [6–7] and the painful neuropathy is common in human diabetes [8]. So, the aims of the present study were: (1) to investigate the analgesic properties of DOI, DOI-Leu^5-enk and DOI-Met^5-enk, using different *in vivo* tests for antinociception and *in vitro* assays; and (2) to elucidate further if the DOI could be used as a transport molecule across the blood-brain barrier using both – intracerebroventricularly (icv) and subcutaneously (sc) application of the peptides before testing procedures.

EXPERIMENTAL

Animals

The experiments were carried out on male *Wistar* rats (180–200 g), male albino mice ICR strain bred (18–20 g) and male guinea-pigs housed in groups under an artificial 12 h light/dark cycle in air-conditioned room at a temperature of 24 ± 1°C with food and water available *ad libitum* except during

* To whom all correspondence should be sent:
E-mail: nevena_pencheva@yahoo.com

the experiments. Each group included 6–8 animals. All tests were conducted between 09:00–12:00 h.

The following treatment groups were tested for a given peptide: (1) control groups (rats) for NaCl (i.p. 0.9%) after icv or sc application; (2) group (rats) for peptide tested after icv application in volume of 50 μl and activity of 1 IU/kg b.wt.; (3) group (rats) for peptide tested after icv application with naloxone (i.p., 0.5 mg/kg b.wt.) injected 10 min before the test compound; (4) group (rats) for peptide tested after sc application in volume of 50 μl and activity of 1 IU/kg b.wt.; (5) group (rats) for peptide tested after sc application with naloxone (i.p., 0.5 mg/kg b.wt.) injected 10 min before the test compound; (6) group (mice) for acetic acid administered i.p. in the volume of 0.1 ml/10 g b.wt.; and (7) groups for *in vitro* (guinea-pig ileum or mouse vas deferens).

All experimental procedures were carried out in accordance with the institutional guidance and the general recommendations on the use of animals for scientific purposes.

Peptides, drugs, solutions, application

DOI was prepared by trypsin-catalyzed cleavage of porcine insulin as previously described [5]. It was isolated and characterized by mass spectrometry (MS), capillary electrophoresis, amino acid analysis and analytic RP HPLC.

Leu^5-enk and Met^5-enk were commercial preparations. DOI-enkephalins (DOI-Leu^5-enk and DOI-Met^5-enk) were prepared at the Institute of Organic Chemistry and Biochemistry (Academy of Sciences of the Czech Republic) according to the procedure described previously [5]. The monitoring of the condensation between DOI and enkephalins and the isolation of the products was undertaken by RP-HPLC. The derivatives of DOI were characterized by RP HPLC, capillary electrophoresis, MS-FAB and amino acid analysis.

For *in vivo* and *in vitro* experiments DOI, DOI-Leu^5-enk and DOI-Met^5-enk were dissolved in HCl and saline (with a correction of pH) and administered icv or sc. For icv application rats were anaesthetized by i.p. injection of ketamine (80 mg/kg b.wt.) solution for surgical manipulation before application of peptides or NaCl. After sectioning along sagital sature a small hole into the skull was made with the following coordinates from brigma: AP 0.8 mm, ML 1.5 mm and DV 3.5 mm. Rats were allowed 24 h to recover from surgery.

To prove the opioid nature of the responses we used the blocker of the opioid receptors naloxone.

Nociceptive methods (in vivo)

Chemical stimulus - writhing test (or acetic acid-induced abdominal constriction test). Acetic acid (diluted with distilled water to a concentration of 1%) was administered i.p. in the volume of 0.1 ml/10 g b.wt. The mice were placed in individual cages and the number of abdominal constrictions (writhes) of each mouse was counted at 5-min intervals for 30 min. Counting of abdominal constrictions started immediately after injection of acetic acid. The mice with decreased number of writhes were considered protected by the test agent.

Mechanical stimulus - paw-pressure test (or Randall-Selitto test). The changes in the mechanical nociceptive threshold of the rats were measured using an Ugo Basil analgesimeter (probe tip diameter 1 mm). The pressure was applied to the left hind-paw and the pressure (*g*) required to elicited nociceptive responses such as squeak and struggle was taken as the mechanical nociceptive threshold. A cut-off value of 500 g was used to prevent damage of the paw.

Thermal stimulus - the hot plate test. This test consists of introducing a rat into an open-ended, cylindrical space with a floor consisting of a metallic plate that is heated by a thermode. Hot plate temperature was set at 55 ± 0.5°C. Rats were removed from the hot plate in the absence of nociceptive response within 60 s to avoid the tissue damage. We measure the reaction time or the latency (s) of the first evoked behaviour events such as paw-licking followed by jumping.

In vitro

Male guinea-pigs (200–300 g) or mice were stunned by a blow on the head. The terminal ileum from guinea-pig or vas deferens from mice were removed and placed in the modified Krebs solution containing (mM): NaCl 112.5; KCl 4.75; $NaHCO_3$ 25.00; KH_2PO_4 1.19; $MgCl_2$ 1.2; $CaCl_2$ 2.4; glucose 11.5. The segments, 1.5-cm long were dissected out from the ileum, while the length of vas deferens preparations was about 12 mm.

Organ bath experiments. Each ileal segment was set up in an organ bath containing 10 ml of modified Krebs solution aerated with 95% O_2 and 5% CO_2 and maintained at 37°C. The segments were suspended under 5 mN tension. There was a 60 min equilibration period before any measurements were made. Contractile activity was recorded under isometric conditions. Electrical field stimulation (EFS) (0.5 ms, 0.1 Hz, supramaximal voltage intensity) was applied. Vas deferens preparations were set up

in 3 or 5 ml organ bath with 1 mN tension and the same EFS.

RESULTS AND DISCUSSION

In vivo

Paw-pressure test and hot-plate test – icv application. All compounds DOI, DOI-Leu^5-enk and DOI-Met^5-enk exerted well-pronounced antinociceptive effects using paw-pressure test and hot-plate test (Fig. 1). During the paw-pressure assay the pain threshold at the 10-min test interval, which was 120 ± 25 g/cm^2 for the control group, was increased as follows: DOI – to 240 ± 30 g/cm^2, DOI-Leu^5-enk – to 370 ± 20 g/cm^2 and DOI-Met^5-enk – to 250 ± 30 g/cm^2. DOI-Leu^5-enk exerted a maximal antinociceptive potency in the hot-plate assay also, because the maximal latency of the response was 31 ± 5 s at the 20-min interval, while that of DOI and DOI-Met^5-enk were 20 ± 4 s (at the 20-min and at the 30-min interval) and 20 ± 5 s (at the 30-min interval), respectively.

In the presence of the opioid antagonist naloxone (in a dose of 1 mg/kg; i.p.) the antinociceptive effects of all compounds tested were antagonized (data not shown), which proved their opioid character. Moreover, in the presence of naloxone, the application of the DOI-Leu^5-enk and DOI-Met^5-enk, but not of DOI, hyperalgesia was observed.

Paw-pressure test and hot-plate test - sc application. Using this type of injection of the DOI and derivatives we obtain similar antinociceptive effects, but with the following differences (Fig. 2):

– the antinociceptive effect of DOI and DOI-Leu^5-enk was less revealed than that after icv application;

– the effects of all compounds were developed for 20 min time course, while those after icv – for at least 40 min;

– in the presence of naloxone we did not observed hyperalgesia (data not shown).

It is well known that opioid receptors in the brain modulate descending pain pathways and consequently increase nociceptive response thresholds [9]. Although attenuated at a big extent as compared with icv application, the antinociceptive responses of the DOI and derivatives after sc application suggest that they probably penetrate the blood-brain barrier. However, based on the results with these two tests we need additional experiments to precise the mechanisms of action as far as penetration of blood-brain barrier is concerned.

Writhing test in mice (acetic acid-induced abdominal constriction test). The results obtained with writhing test in mice, which is informative for visceral pain, showed that all compounds did not change the number of the abdominal constrictions after either icv or sc injection. Thus, they did not influence the visceral pain probably because the endogenous enkephalins are rather delta- than mu-selective, while according to Riviere [10] the peripheral kappa-opioid agonists are specific for visceral pain.

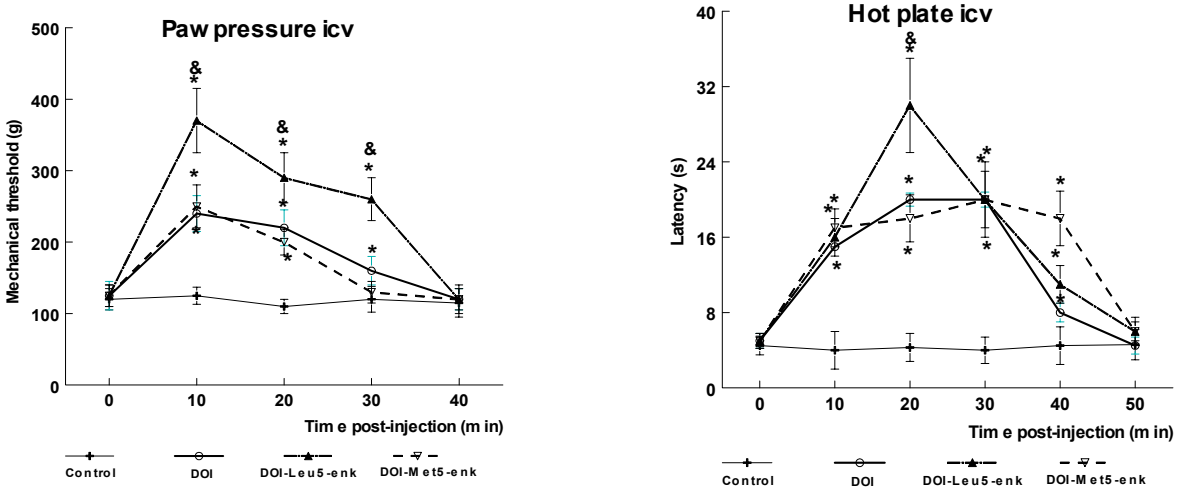

Fig. 1. Antinociceptive effect of icv administrated desoctapeptide-insulin (DOI), DOI-Leu^5-enkephalin (DOI-Leu^5-enk) and DOI-Met^5-enkephalin (DOI-Met^5-enk) in the paw-pressure and hot-plate test, expressed as mechanical thresholds (*g*) and latencies (s) respectively. Each data point represents the means ± s.e.m. response of 6–8 rats. *$p \leq 0.05$ compared to control by using Mann-Whitney U test; $^{\&}p \leq 0.05$ compared to DOI and DOI-Met^5-enk by using Mann-Whitney U test.

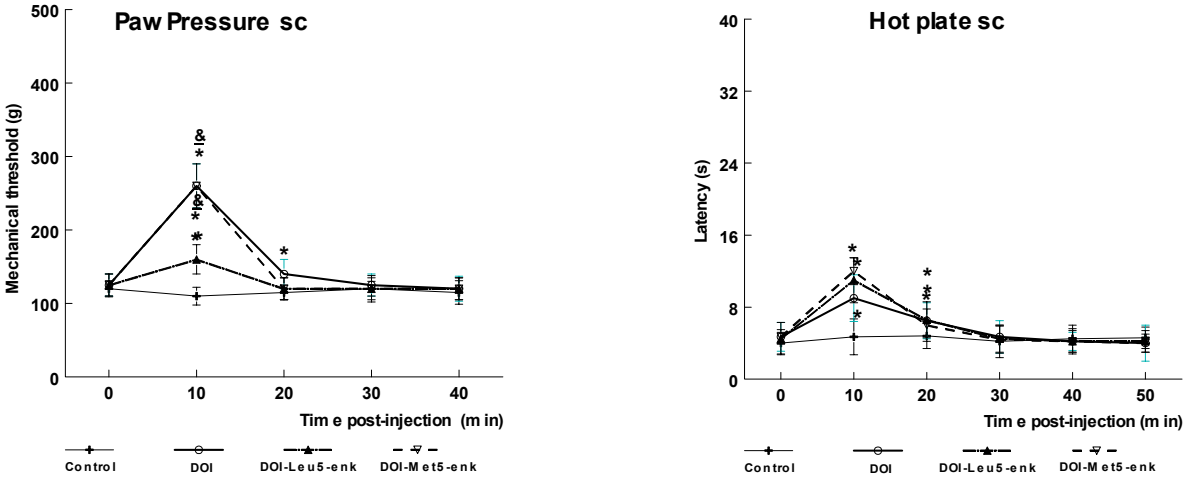

Fig. 2**.** Antinociceptive effect of sc administrated desoctapeptide-insulin (DOI), DOI-Leu^5-enkephalin (DOI-Leu^5-enk) and DOI-Met^5-enkephalin (DOI-Met^5-enk) in paw-pressure and hot-plate test expressed as mechanical thresholds (*g*) and latencies (s) respectively. Each data point represents the means ± s.e.m. response of 6–8 rats. *$p \leq 0.05$ compared to control by using Mann-Whitney U test; $^{\&}p \leq 0.05$ compared to DOI-Leu^5-enk by using Mann-Whitney U test.

In vitro

All three compounds did not affect the electrically-evoked contractions of guinea-pig ileum (mu- and delta-opioid receptors). However, at concentrations higher than 20 μM DOI-Met^5-enk had naloxone-reversible opioid inhibitory effect, which was about 20% inhibition of the control contractile response.

In the mouse vas deferens (mu-, delta- and kappa-opioid receptors, but predominantly model system for delta-opioid receptors) only DOI-Met^5-enk showed naloxone-reversible opioid inhibitory effect at concentrations higher than 100 nM. The extent of the effect was about 65% inhibition of the evoked electrical contractions. Since, the inhibitory effects of endogenous enkephalins on electrically-evoked contractions in different smooth-muscle preparations are well documented [1–2], the poor effects of DOI-Leu^5-enk and DOI-Met^5-enk could be due to changes in enzyme degradation and in release of the opioid pentapeptides from the condensation peptide in these tissues.

CONCLUSIONS

The present results show that: (i) After mechanical or thermal stimuli DOI, DOI-Leu^5-enk and DOI-Met^5-enk exert antinociceptive effects with opioid nature; (ii) The DOI and derivatives do not influence the visceral pain and their *in vitro* effects are also poor; (iii) The antinociceptive effects of the peptides investigated after sc application in both paw pressure test and hot-plate test suggest that they probably have crossed the blood-brain barrier due to DOI, which at some extent could be used as a transport molecule; (iv) The antinociceptive effects of the peptides investigated after icv application in both paw pressure test and hot-plate test suggest that analogues of DOI probably achieved prolonged antinociceptive action, due to gradual release.

Acknowledgments: *This study was supported by Grant of Neofit Rilski South-West University on Pain assessment, session: "Collective projects 2008" of the Faculty of Education.*

REFERENCES

1. N. Pencheva, J. Pospišek, L. Hauzerova, T. Barth, P. Milanov, *Br. J. Pharmacol*., **128**, 569 (1999).
2. N. Pencheva, P. Milanov, L. Vezenkov, T. Pajpanova, E. Naydenova, *Eur. J. Pharmacol*., **498,** 249 (2004).
3. N. Pencheva, I. Topouzov, J. Barthova, T. Barth, *Compt. Rend. Acad. Bulg. Sci.*, **55,** 65 (2002).
4. W. A. Banks, A. J. Kastin, *Am. J. Physiol.*, **259**, E1 (1990).
5. T. Barth., L. Klasova, A. Ciencialova., J. Strakova, J. Barthova, V. Kašička, K. Ubik, *Compt. Rend. Acad. Bulg. Sci.*, **55**, 45 (2002).
6. N. Takeshita, S. Yamaguchi, *J. Pharmacol. Exp. Ther*., **281**, 315 (1997).
7. T. Sasaki, H. Yasuda, K. Maeda, R. Kikkawa, *Neuroreport*, **9**, 243 (1998).
8. Ch. Courteix, M. Bardin, J. Massol, J. Fialip, J. Lavarenne, A. Eschalier, *Neuroreport*, **7**, 1922 (1996).
9. A. I. Basbaum, H. L. Fields, *Annu. Rev. Neurosci.*, **7**, 309 (1984).
10. P. J. Riviere, *Br. J. Pharmacol*., **141**, 1331 (2004).

АНТИНОЦИЦЕПТИВНИ ЕФЕКТИ НА DES-ОКТАПЕПТИД-ИНСУЛИН СВЪРЗАН С ЕНКЕФАЛИНИ

Н. Ст. Пенчева[1]*, А. И. Бочева[2], К. Ж. Грънчарска[1], Т. Барт[3]

[1] Катедра „Кинезитерапия", Югозападен университет, ул. „Иван Михаилов" № 66, Благоевград 2700,
[2] Катедра „Патофизиология", Медицински факултет, Медицински университетет, ул. „Здраве" № 2, София 1431,
[3] Институт по Органична химия и биохимия, Аакадемия на науките на Чешката република, Флемингово 2, 166 10 Прага 6, Чешка република

Постъпила на 17 юли 2008 г.; Преработена на 30 септември 2008 г.

(Резюме)

Три инсулинови аналога с модификации на B-веригата бяха синтезирани чрез трипсин-катализирано куплиране на des-октапапептид (B^{23}-B^{30})-инсулин (DOI) с Met^5-енкефалин (Met^5-enk) или Leu^5-енкефалин (Leu^5-enk). Аналозите DOI-Met^5-enk и DOI-Leu^5-enk бяха получени чрез кондензация между амино групите на енкефалините и карбоксилната група на аргинина в позиция B^{22}. За да тестваме свойствата на DOI като транспортна молекула за активни опиоидни пептиди, ние изследвахме DOI, DOI-Met^5-enk and DOI-Leu^5-enk, чрез три типа *in vivo* ноцицептивни методи: writhing тест на мишки, paw-pressure тест и hot plate тест на плъхове. Пептидите бяха приложени по два начина: интрацереброventрикуларно (icv) и подкожно (sc). Способността на пептидите да инхибират електрически-предизвикани контракции на илеум от морско свинче и vas deferens от мишка, също беше изследвана. За верификация на опиодината природа на отговорите използвахме налксон (1 mg/kg, интраперитонеално). Приложението на paw-pressure и hot-plate теста показа, че всички съединения упражняваха добре изразени антиноцицептивни ефекти (DOI < DOI-Met^5-enk < DOI-Leu^5-enk) с продължителност от минимум 40 min след icv приложение. Бяха установени различия в потентността на пептидите при sc приложение и ефектите се развиваха за 20 min. Резултатите от writhing теста на мишки показаха, че всички изследвани пептиди не повлияват висцералната болка. Ефектите in vitro бяха твърде слаби и се наблюдаваха при концентрации над 20 μM за DOI-Met^5-enk и над 100 nM за DOI-Leu^5-enk. Въз основа на представените експериментални резултати може да се направи предположението, че аналозите на DOI: DOI-Met^5-enk and DOI-Leu^5-enk проявяват пролонгирано антиноцицептивно действие, а DOI в някаква степен може да играе роля на транспортна молекула през кръвно-мозъчната бариера.

Bulgarian Chemical Communications, Volume 41, Number 2 (pp. 143–148) 2009

New peptide mimetics with potential β-secretase inhibition activity

I. T. Ivanov, D. L. Danalev, L. T. Vezenkov*

Department of Organic Chemistry, University of Chemical Technology and Metallurgy, 8 Kliment Ohridski Blvd., 1756 Sofia, Bulgaria

Received July 10, 2008; Revised September 25, 2008

Alzheimer's disease (AD) is affecting about 20 millions people worldwide. The last forecast shows that during the next 20–30 years their number will double because of the human life-span increasing. The transformation of amyloid β (Aβ) soluble from the insoluble β-fibers is a critical stage in the AD progression. Aβ resulted from the precursor protein cleavage which is catalyzed by different proteinases named α, β and γ-secretases. That is why the inhibition of some of these enzymes is a promising alternative for AD treatment. The shortest peptide structure found with β-secretase inhibition activity is Glu-Val-Asp-Leu-Ala. A lot of investigations show the role of various amino acids in different positions for the inhibition activity and reveal important structure-activity relationships. Based on these investigations, we synthesized ten peptide mimetics with potential β-secretase inhibition activity by means of conventional peptide synthesis in solution. All newly synthesized compounds were characterized by TLC, m.p. and $[\alpha]_{546}^{22}$. The biological trials are in progress.

Key words: Alzheimer's disease; β-secretase inhibitors, peptide mimetics.

INTRODUCTION

Alzheimer's disease (AD) is affecting about 20 millions people worldwide. The last forecast shows that during the next 20–30 years their number will double because of the human life-span-increasing. The transformation of amyloid β (Aβ) soluble from the insoluble β-fibers is a critical stage in the AD progression. Aβ resulted from the precursor protein containing 695 to 770 amino acid residues. This process starts with four cleavages of this protein catalyzed by different proteinases, named α, β and γ-secretases. The tearing in $A\beta_1$ and $A\beta_{11}$ is catalyzed by the enzyme β-secretase. There is no data in literature whether this enzyme is a part of the other life process in the organism.

Last ten years provide a number of different investigations on the β-secretase inhibition process. Tung et al. revealed that the shortest peptide structure with β-secretase inhibition activity is Glu-Val-Asp-Leu-Ala [1]. Their experiments show that Leu or Phe at P_1 position, Val or Leu at P_3 position and Asp or Asn at P_2 position is compulsory for inhibition activity availability. Additional investigations reveal that the minimal substrate with passable β-secretase inhibition activity is Boc-Val-Asp-Leu-Ala-OH. Based on that structure, we investigate the influence of different amino acid residues at P_4, P_3 and P_2 positions on the inhibition activity. At some structures the residues at P_4 and P_3 position were removed. It is well-known that the enzyme β-secretase includes high hydrophobic S_1 and S_3-pockets [2]. That is why the availability of hydrophobic amino acids at these positions is obligatory for inhibition activity. In our new structure, we choose Leu residue for these two positions. S_2 and S_4-pockets are hydrophilic [3]. Tung *et al*. investigated the residues Asn and Met for P_2 position. Their X-ray analysis revealed that P_2 Asn residue in the substrate made a hydrogen bond with Arg^{235} in the enzyme binding site [1]. In our structure, Asp in this position was used because we suppose that its hydrogen bond formation potential is better than Asn. For P_4 position Tung *et al*. choose Glu or Boc residue and they proved that –C=O function participates in the strong hydrogen bond obtaining. There is no data whether the bonds made by Boc group are stronger than those obtained by the δ-COOH function of Glu [1]. We decided to investigate the length of the chain of the amino acid in this position and choose Asp.

The additional investigations on the high-potent β-secretase inhibitors conformation show that at P_2' position the chain of the compounds is turned off and the side chains of the residues at P_3' and P_4' positions do not participate in the enzyme-substrate interaction [4]. Based on the latter conclusion, Ghosh *et al*. removed and replaced the residues at P_3' and P_4' positions by different C-terminal residues [2]. They investigated the activity of derivatives based on the sequence Boc-Val-Asp-Leu-

* To whom all correspondence should be sent:
E-mail: lvezenkov@yahoo.com

Ala-Val-Glu(P_3')-Phe(P_4')-OH. They succeeded to increase β-secretase inhibition activity replacing C-terminal amino acids at P_3' and P_4' positions by benzylamine. The latter results to fourfold inhibition activity increasing (IC_{50} = 28 nM, K_i = 2.5 nM). The other potential residue they determined was piridinylmethylamine (IC_{50} = 70 nM) [1]. Because of the better activity of the compounds with benzylamine C-terminus in our new structure the same fragment as C-terminal moiety was used. On the other hand, it is well-known that high hydrophobic moieties play a key role in the molecule for blood brain barrier passing. Based on this fact, a series of analogues with C-terminal 3,4-dimethoxybenzylamine residue was synthesized.

The X-ray investigations on the crystal structure of the enzyme-substrate complex revealed that COOH group of the residue at P_2' position made a strong hydrogen bond with OH group of Tyr^{198} which plays key role in the enzyme-substrate interaction. That is why even in the shortest peptide structure with β-secretase inhibition activity Glu-Val-Asp-Leu-Ala(P_1') the availability of P_2' residue is obligatory. The question is: which is the best choice for amino acid residue in this position? In 2005 Hanessian *et al*. synthesized three peptides differing only by their residue at P_2' position – NH-Butyl (IC_{50} = 1.82 μM), Ala (IC_{50} = 0.6 μM) and Val (IC_{50} = 0.19 μM) [5]. The obtained results show that the most powerful is the analogue with Val at P_2' position. That is why our design with Val in this position was done.

EXPERIMENTAL

All newly synthesized compounds were characterized by TLC, m.p. and $[\alpha]_{546}^{22}$. Their structures were proved by ES/MS. The purity of the products was checked by TLC on precoated plates of Silica gel 60 F_{254} (MERCK) with the following solvent systems: $CHCl_3$:AcOH 9:1 (v/v); *n*-BuOH:AcOH:H_2O 3:1:1 (v/v/v) and *n*-BuOH:AcOH:pyridine:H_2O 60:6:24:20. Spots on TLC chromatograms were detected by chlorine/*o*-tolidine reaction. The melting points were deter-mined on a Kofler apparatus and were uncorrected. The optical rotation was measured on a Quick Russel-Jouan Type SL1D polarimeter.

General procedure for preparation by the N,N'-dicyclohexylcarbodiimid (DCC)/1-hydroxybenzotriazol (HOBt) method

1.00 mmol of the peptide (obtained from Boc-peptide ester by treatment with 10-fold excess of TFA) was dissolved in minimal amount of DMF and after cooling to –5ºC neutralized to pH 7–7.5 with Et_3N. 1.20 mmoles of Z- or Boc-amino acid, 1.20 mmoles of DCC and 1.40 mmoles of 1-HOBt were added. The reaction mixture was stirred for 24 h at 0ºC and for another 24 h at room temperature. The obtained DC-urea was removed by filtration and then 30 ml of water were added. The product was extracted into EtOAc (3×10 ml) and the organic layer was washed with 5% $NaHCO_3$ (3×10ml), H_2O (3×10ml), 10% citric acid (3×10ml) and H_2O to pH = 7. The solvent was dried with Na_2SO_4 and removed in *vacuo* followed by recristallization.

General procedure for preparation by the TBTU or TCTU method

1.00 mmol of the peptide (obtained from Boc-peptide ester by treatment with 10-fold excess of TFA) was dissolved in minimal amount of DMF and after cooling to –5ºC neutralized to pH 7–7.5 with diisopropylethylamine (DIEA). 1.20 mmoles of Z- or Boc-amino acid, 1.20 mmoles of 2-(1H-benzotriazole-1-yl)-1,1,3,3-tetramethyluronium tetrafluoroborate (TBTU) or O-(6-chloro-1-hydroxybenzotriazol-1-yl)-1,1,3,3-tetramethyluronium tetrafluoroborate (TCTU) and 1.20 mmoles of DIEA were added. The reaction mixture was stirred for 24 h at room temperature. Finally, 30 ml of water were added. The product was extracted into EtOAc (3×10 ml) and the organic layer was washed with 5% $NaHCO_3$ (3×10ml), H_2O (3×10ml), 10% citric acid (3×10ml) and H_2O to pH = 7. The solvent was dried with Na_2SO_4 and removed in *vacuo* followed by recristallization.

Deblocking of Z- and OBzl groups by catalytic hydrogenation in the presence of Pd/C

1.00 mmol of protected peptide was dissolved in MeOH and then Pd/C and 1.00 mmol (or catalytic amount) of HCl was added. Hydrogen was passed through the reaction mixture at room temperature. The deblocking of the protecting groups was controlled by TLC and after finishing the reaction, Pd/C was filtered out and MeOH was evaporated in *vacuo*. The formed oil was subjected to the next deblocking.

RESULTS AND DISCUSSION

Based on the information above, a design of peptide mimetics including minimal substrate subunits with C-terminal benzylamine and 3,4-dimethoxybenzylamine functions was done. Ten peptide mimetics with potential β-secretase inhibition activity were synthesized by peptide synthesis in solution according to Scheme 1–5: H-Asp-Leu-Ala-Val-NH-Bzl; H-Asp-Leu-β-Ala-Val-NH-Bzl; Boc-Leu-Asp-Leu-Ala-Val-NH-Bzl; Boc-Leu-Asp-Leu-

β-Ala-Val-NH-Bzl; H-Asp-Leu-Asp-Leu-Ala-Val-NH-Bzl; H-Asp-Leu-Asp-Leu-β-Ala-Val-NH-Bzl; Boc-Leu-Asp-Leu-Ala-Val-NH-3,4-dimethoxybenzyl; Boc-Leu-Asp-Leu-β-Ala-Val-NH-3,4-dimethoxybenzyl; H-Asp-Leu-Asp-Leu-Ala-Val-NH-3,4-dimethoxybenzyl; H-Asp-Leu-Asp-Leu-β-Ala-Val-NH-3,4-dimethoxybenzyl.

The first series of compounds include benzylamine moiety as C-terminal residue. Initially, a fragment condensation for all peptides was tried. Because of a lot of secondary products obtained during these reactions all newly compounds were synthesized by stepwise addition of amino acids starting from C- to N-terminus. The condensation reactions in the presence of variety of coupling reagent like TBTU, TCTU and DCC/1-HOBt were done. The best methods according to the purity and yields of the products were chosen. They are presented in the reaction schemes.

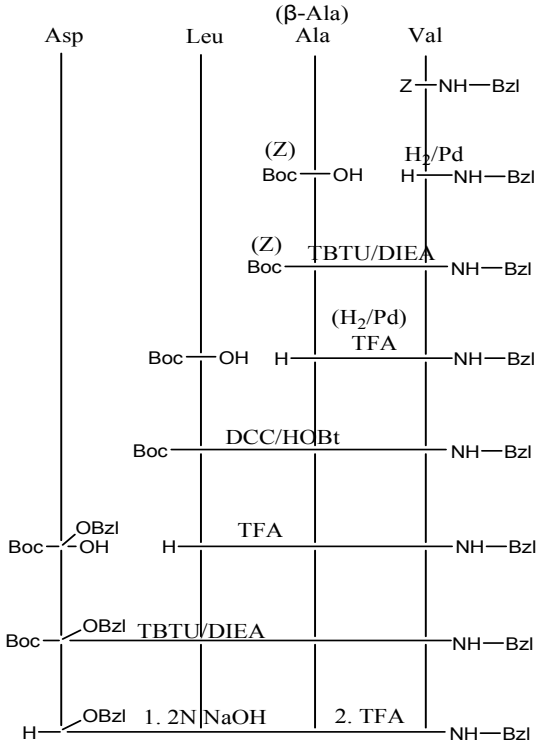

Scheme 1. Synthesis of tetrapeptides H-Asp-Leu-Ala(β-Ala)-Val-NH-Bzl.

The shortest needed fragments H-Asp-Leu-Ala-Val-NH-Bzl and H-Asp-Leu-β-Ala-Val-NH-Bzl were synthesized by stepwise attachment of Boc-Ala-OH or Z- β-Ala-OH, Boc-Leu-OH, Boc-Asp(OBzl)-OH and Boc-Leu-OH to the C-terminal H-Val-NH-Bzl residue according to Scheme 1. Most of the reactions ran with high yields and good purity. Some difficulties with Leu residue attachment were met. DCC/1-HOBt method finally was chosen as the most effective according to the yield of the target product (78%). Asp and Ala residues were subjected condensation in the presence of TBTU with quantitative yields.

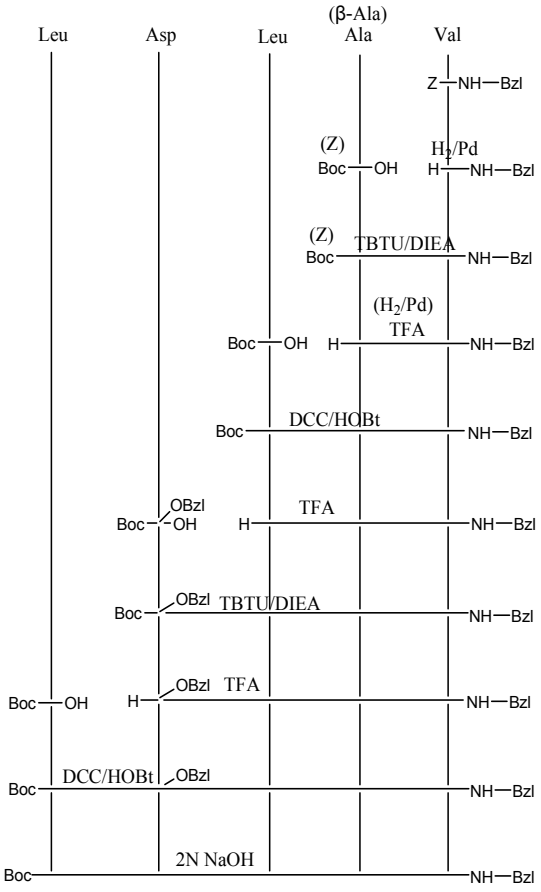

Scheme 2. Synthesis of pentapeptides Boc-Leu-Asp-Leu-Ala (β-Ala)-Val-NH-Bzl.

According to Scheme 2, N-terminal Boc-Leu-OH was linked to H-Asp-Leu-Ala-Val-NH-Bzl and H-Asp-Leu-β-Ala-Val-NH-Bzl obtained by Scheme 1. The same difficulties as with condensation of first Leu residue were met. The same methods were carried out and finally TCTU was chosen leading to quantitative yield of 96% for the reaction with H-Asp(OBzl)-Leu-Ala-Val-NH-Bzl (67% for the same reaction with DCC/1-HOBt method) and 45% for the reaction with H-Asp(OBzle)-Leu-β-Ala-Val-NH-Bzl (37% for the same reaction with DCC/1-HOBt method) and better purity of the target compounds.

The protected hexapeptides Boc-Asp(OBzl)-Leu-Asp(OBzl)-Leu-Ala-Val-NH-Bzl and Boc-Asp(OBzl)-Leu-Asp(OBzl)-Leu-β-Ala-Val-NH-Bzl were obtained by consecutive attachment of Asp residue to the products synthesized by Scheme 2 in quantitative yields (Scheme 3). The final products were obtained by deblocking the protecting groups by treatment with 2 N NaOH and TFA, subsequently.

The second series of compounds include 3,4-dimethoxyphenylamine as C-terminal residue and were synthesized according to Schemes 4 and 5

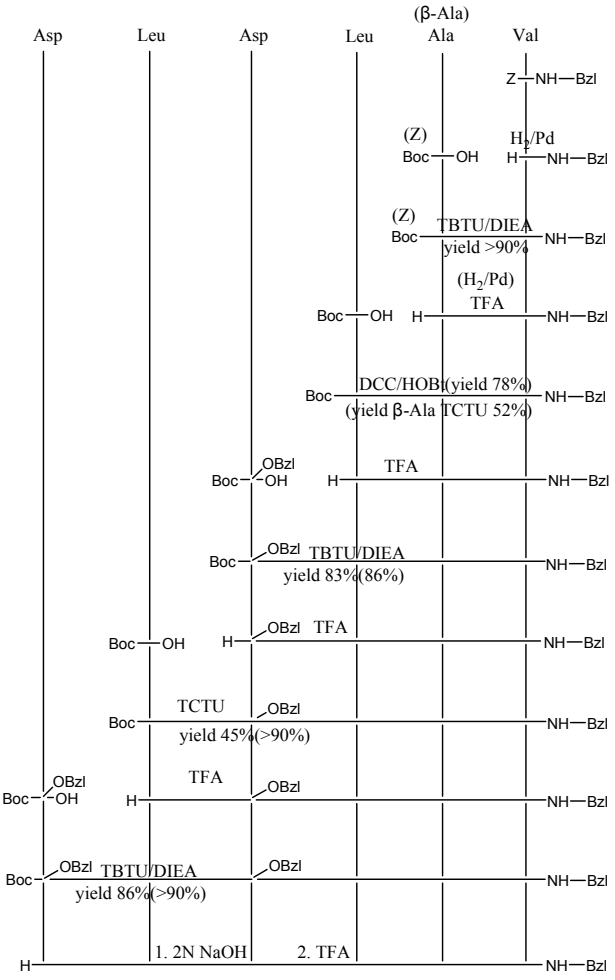

Scheme 3. Synthesis of hexapeptides H-Asp-Leu-Asp-Leu-Ala(β-Ala)-Val-NH-Bzl.

The same problems as with the first series of compounds, concerning the reactions of condensation of Leu residues were met. The reactions of condensation were carried out again at different conditions and in the presence of condensation agents with a view to get the best results with respect to yields and purity of products. Similar problems in this series of compounds were met with the reaction of condensation with participation of Boc-Asp(OBzl)-OH. The best results according to the condensation agent and yields are shown in the reaction schemes.

Boc-protecting group in all compounds was removed by treatment with 10-fold excess of TFA. Z- and –OBzl protecting groups were removed by catalytic hydrogenation in the presence of HCl (molar or catalytic amount) and Pd/C. The melting points and $[\alpha]_{546}^{22}$ are presented in Table 1:

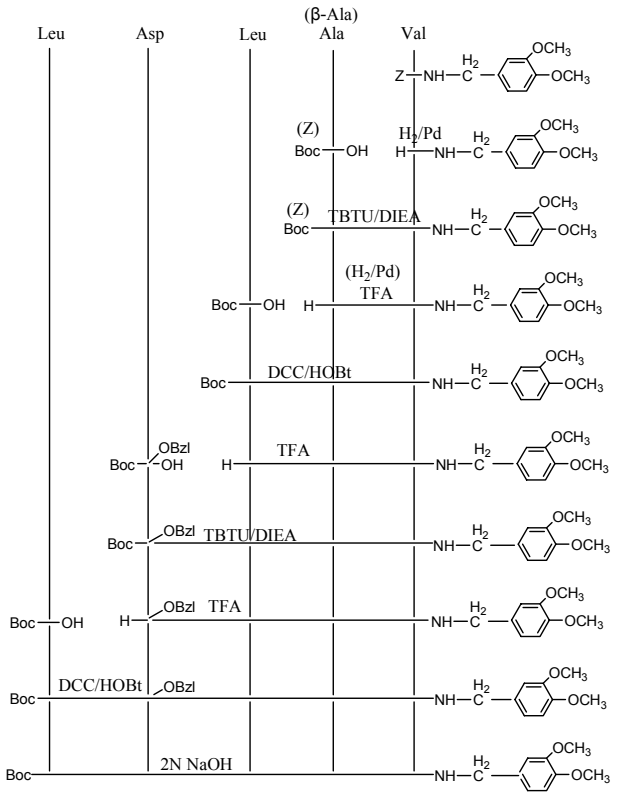

Scheme 4. Synthesis of pentapeptides Boc-Leu-Asp-Leu-Ala(β-Ala)-Val-3,4-dimethoxybenzylamide.

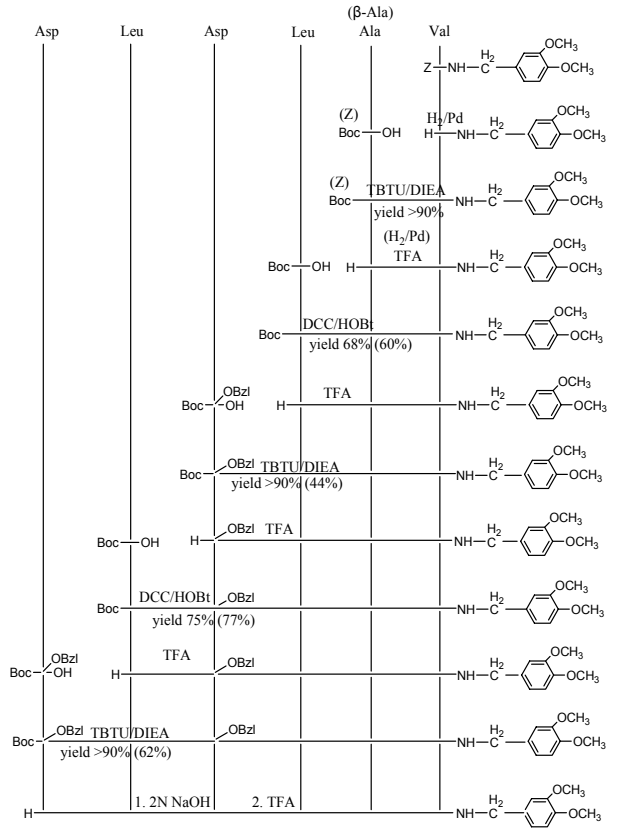

Scheme 5. Synthesis of hexapeptides H-Asp-Leu-Asp-Leu-Ala(β-Ala)-Val-3,4-dimethoxybenzylamide.

Table 1. Melting points and $[\alpha]^{22}_{546}$ of the newly synthesized products.

No	Product	M.p., °C	$[\alpha]^{22}_{546}$, °
1	Z-Val-NH-Bzl	167–169	–40
2	Boc-Ala-Val-NH-Bzl	164–166	–120
3	Z-β-Ala-Val-NH-Bzl	184–186	-
4	Boc-Leu-Ala-Val-NH-Bzl	139–141	–130
5	Boc-Leu-β-Ala-Val-NH-Bzl	169–171	–40
6	Boc-Asp(OBzl)-Leu-Ala-Val-NH-Bzl	121–123	–0.2*
7	Boc-Asp(OBzl)-Leu-β-Ala-Val-NH-Bzl	124–126	+40
8	Boc-Leu-Asp(OBzl)-Leu-Ala-Val-NH-Bzl	197–199	-
9	Boc-Leu-Asp(OBzl)-Leu-β-Ala-Val-NH-Bzl	200–201	-
10	Boc-Asp(OBzl)-Leu-Asp(OBzl)-Leu-Ala-Val-NH-Bzl	193–195	-
11	Boc-Asp(OBzl)-Leu-Asp(OBzl)-Leu-β-Ala-Val-NH-Bzl	191–193	–10
12	Asp-Leu-Ala-Val-NH-Bzl	119–121	–50
13	Asp-Leu-β-Ala-Val-NH-Bzl	152–154	+30
14	Boc-Leu-Asp-Leu-Ala-Val-NH-Bzl	125–127	+30
15	Boc-Leu-Asp-Leu-β-Ala-Val-NH-Bzl	123–125	+20
16	Asp-Leu-Asp-Leu-Ala-Val-NH-Bzl	117–119	+40
17	Asp-Leu-Asp-Leu-β-Ala-Val-NH-Bzl	114–116	+60
18	Z-Val-3,4-dimethoxybenzylamide	144–146	-
19	Boc-Ala-Val-3,4-dimethoxybenzylamide	151–153	–90
20	Z-β-Ala-Val-3,4-dimethoxybenzylamide	187–189	-
21	Boc-Leu-Ala-Val-3,4-dimethoxybenzylamide	183–185	–60
22	Boc-Leu-β-Ala-Val-3,4-dimethoxybenzylamide	169–171	–20
23	Boc-Asp(OBzl)-Leu-Ala-Val-3,4-dimethoxybenzylamide	178–180	–10
24	Boc-Asp(OBzl)-Leu-β-Ala-Val-3,4-dimethoxybenzylamide	191–193	+36
25	Boc-Leu-Asp-Leu-Ala-Val-3,4-dimethoxybenzylamide	136–138	-
26	Boc-Leu-Asp-Leu-β-Ala-Val-3,4-dimethoxybenzylamide	210–212	-
27	Asp-Leu-Asp-Leu-Ala-Val-3,4-dimethoxybenzylamide	amorphus	-
28	Asp-Leu-Asp-Leu-β-Ala-Val-3,4-dimethoxybenzylamide	217–219	-

For all compounds $[\alpha]^{22}_{546}$ [°] is for C 1 MeOH except *C 0.5 MeOH.

Biological trials of all newly synthesized compounds are in progress.

***Acknowledgements**: This work is supported by the Ministry of Education and Science grant BY-16.*

REFERENCES

1. J. S. Tung, D. L. Davis, J. P. Anderson, D. E. Walker, S. Mato, N. Jewett, R. K. Hom, S. Sinha, E. D. Thorsett, V. John, *J. Med. Chem.*, **45**, 259 (2002).
2. A. K. Ghosh, T. Devasamudram, L. Hong, C. De Zutter, X. Xu, V. Weerasena, G. Koelsch, G. Bilcer, J. Tang, *Bioorg. Med. Chem. Lett.*, **15**, 15 (2005).
3. S. J. Stachel, C. A. Coburn, T. G. Steele, M. C. Crouthamel, B. L. Pietrak, M. T. Lai, M. K. Holloway, S. K. Munishi, S. L. Graham, J. P. Vacca, *Bioorg. Med. Chem. Lett.*, **16**, 641 (2006).
4. A. K. Ghosh, G. Bilcer, C. Harwood, R. Kawahama, D. Shin, K. Hussain, L. Hong, J. Loy, C. Nguyen, G. Koelsch, J. Ermolieff, J. Tang, *J. Med. Chem.*, **44**, 2865 (2001).
5. S. Hanessian, H. Yun, Y. Hou, G. Yang, M. Bayrakdarian, E. Therrien, N. Moitessier, S. Roggo, R. Veenstra, M. Blomley, J. Rondeau, C. Ostermeier, A. Strauss, P. Ramage, P. Paganetti, U. Neumann, C. Betschart, *J. Med. Chem.*, **48**, 5175 (2005).

НОВИ ПЕПТИДНИ МИМЕТИЗИ С ПОТЕНЦИАЛНА β-СЕКРЕТАЗНА ИНХИБИТОРНА АКТИВНОСТ

И. Т. Иванов, Д. Л. Даналев, Л. Т. Везенков*

Катедра „Органична химия“, Химикотехнологичен и металургичен университет, бул. „Климент Охридски“ № 8, 1756 София

Постъпила на 10 юли 2008 г.; Преработена на 25 септември 2008 г.

(Резюме)

Болестта на Алцхаймер (БА) е засегнала около 20 милиона души по целия свят. Последните проучвания показват, че през следващите 20–30 години броят им ще се удвои поради нарастващата продължителност на човешкия живот. Превръщането на разтворимия β амилоиден пептид (Aβ) в неговата неразтворима форма е ключов стадий в прогресията на БА. Aβ се получава като резултат от разкъсване на прекурсорния β амилоиден пептид, което е катализирано от различни протеази, известни като α-, β- и γ-секретази. Ето защо инхибирането на някой от тези ензими е обещаваща алтернатива при лечението на БА. Най-късата пептидна структура с установена инхибиторна активност срещу β-секретазата е Glu-Val-Asp-Leu-Ala. В литературата са публикувани множество изследвания, показващи ролята на различните аминокиселини в този пептид за инхибиторната му активност и са изведени някои зависимости структура–активност. Основавайки се на тези литературни данни ние направихме дизайн и синтезирахме 10 пептидни миметици с потенциална β-секретазна инхибираща активност, с помощта на стандартен пептиден синтез в разтвор. Всички новосинтезирани съединения бяха охарактеризирани чрез TLC, т.т. и $[\alpha]_{546}^{22}$. Биологичните изследвания са в ход.

Bulgarian Chemical Communications, Volume 41, Number 2 (pp. 149–152) 2009

Microstructure of new metal-organic gels obtained by low-molecular gelators

D. S. Tsekova[1]*, V. B. Stoyanova[2]

[1] *Department of Organic Chemistry, University of Chemical Technology and Metallurgy, 8 Kliment Ohridski Blvd., 1756 Sofia, Bulgaria*
[2] *Rostislav Kaischev Institute of Physical Chemistry, Bulgarian Academy of Sciences, Acad. G. Bonchev St., Block 11, 1113 Sofia, Bulgaria*

Received July 17, 2008; Revised September 27, 2008

We have studied self-assembly properties of recently synthesized L-Valine and pyridine containing low-molecular compounds, in the presence of some metal ions. It turned out that availability of $CuCl_2$ in ethanol solution of these compounds leads to metal-organic framework (MOF) gel formation. Hydrogels including Na^+ and K^+ ions are also concerned. Here we present some topological features of such gels including Na^+, K^+ and Cu^{2+} ions in their structures.

Key words: Metal-organic polymers, xerogel, porous structure, pH responsive gels.

INTRODUCTION

Investigations of gels based on low-molecular organic molecules have received increased attention in the recent years [1–7]. Physical and chemical properties of such gels are useful for the development of functional materials that have potential applications in fields including tissue engineering, catalysts, photonic materials, pharmaceutical diagnosis, *etc*. [8–11]. Gels structure consists of nano- and micro-shaped objects. That is why their study is also of great interest for application as templates for preparation of nanotubular materials [12–15]. A few cases of low-molecular gelators containing pyridine units have been reported until now [16–20]. The presence of a pyridine moiety in this type of molecules provides the basis for the formation of pH-responsive gels and for the incorporation of catalytic metals onto the fibres. Here we report on the formation of physical gels of two pyridine and L-Valine containing compounds (Fig. 1) in the presence of some metal ions. In some cases of metal-organic compounds, the metal ions are able to serve as centres linked into one-, two- or three-dimensional structures by directional bonding with small organic molecules. This type of hybrid materials is known in literature as metal-organic frameworks (MOFs). Although MOF research is still in its very beginning, this concept has been developed extremely rapidly in the recent years [21–23]. Like other gels, these ones obtained by MOF, consist of nano- and micro-sized particles and after removing (evaporating) the solvent they convert into porous materials with unique properties that found applications as catalytic, absorbents, sensors and other responsive materials [24–26], endowed with complex behaviours by the presence of metal centres. On the other hand, their porous structure was found very useful, moreover they can be used as templates for other porous materials [27], as microporous materials have properties with exploitable industrial applications (e.g. as molecular sieves or supports), as well as every day use, e.g. laundry detergent [28]. Perhaps the most fundamental and important aspect of the syntheses of microporous materials is the control over pore topology (i.e. pore dimensions and shape). The experimental data obtained reveal topology of two types of metal-organic gels. The first one is obtained in water solutions by adjusting pH in the presence of Na^+ or K^+ ions. The second type – where a simple mix between two clear solutions of the organic compound and the cupro salt in a short time led to coloured gel formation, although in the absence of this salt, the used organic compounds (substances) never made gels in methanol, ethanol or propanol.

EXPERIMENTAL

Organic compounds used for the experiments (Fig. 1) were synthesized by applying previously reported procedures [19–20].

As it was mentioned above, two main types of metal containing gels were prepared. The first one was hydrogel containing alkali metals Na or K.The second one was organogel obtained in ethanol by reacting of organic molecule (**1** or **2**) with $CuCl_2$. Preparation was done following next recipes:

* To whom all correspondence should be sent:
E-mail: d_tsekova@abv.bg

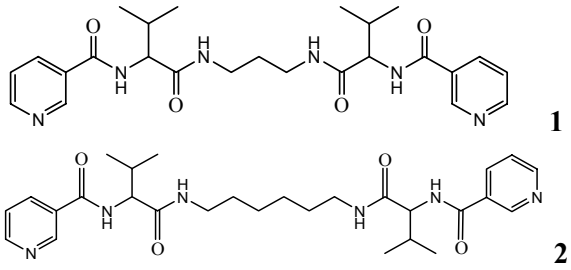

Fig. 1. Organic compounds used in the described experiments with codes **1** and **2**.

I. 5 mg of the organic compound (**1** or **2**) were dissolved in 500 µl of 0.1 M HCl. Adequate amount of water solution of NaOH, $NaHCO_3$ or K_2CO_3, prepared in the range from 0.2 to 1 M, was added to the above described acidic solution. The obtained mixture turned into gel. The time for gelation depended on the concentration of the substance and varied from seconds, for the most concentrated, to days for the most diluted. At these conditions, compound **2** gave opaque to white gels, while compound **1** gelated in opaque to transparent formations in dependence on the concentration.

II. 5 mg of the organic compound (**1** or **2**) were dissolved in 500 µl hot ethanol. Solutions of 20 mM $CuCl_2$ in ethanol in equivalent amount were added to the hot solution of organic compound and the mixture obtained immediately turned into gel coloured in blue and green nuances.

Scanning electron micrographs were taken in a JEOL JSM 6390, as well as LEO 440I microscopes equipped with digital cameras. The accelerating voltage was 10 keV in all cases. Before electron microscope observations the xerogel samples were covered by thin (nano-size) layer of amorphous carbon or Au/Pd for their better conductivity.

RESULTS AND DISCUSSION

Bearing in mind that the molecules of the studied compounds possess two pyridine rings and the calculated and measured for both compounds protonation constants Ka_1 and Ka_2 are between 3 and 4 [10], it is obvious that they are soluble in water at pH < 3 as both pyridine groups are protonated. After dissolving of any of the compounds in acidic water (HCl, higher than 0.1 M), gels were easyly obtained (immediately or in a few minutes to hours) after addition of solutions of NaOH, $NaHCO_3$ or K_2CO_3 in relevant concentrations and amount. The stability of the obtained gels increased with increasing the ionic strength of the solution (NaCl, 0.1 M).

The second type of gel was obtained as a result of the reaction between organic compound and $CuCl_2$ in hot ethanol and most probably, the resulting coloured gels are coordination polymers, the so-called MOFs. The fast gelation of the metal and ligand suggests that there is a rapid cross-linking polymerisation between Cu^{2+} and organic molecule (**1** and **2**), leading to the growth of coordination polymer particles, which themselves subsequently cross-link to leave macroscopic solvent-filled cavities. In fact, compounds **1** and **2** are able to make gels in some organic solvents (e.g. toluene, dioxane) but having high solubility in lower alcohols, they never made any kind of gels in methanol, ethanol or propanol.

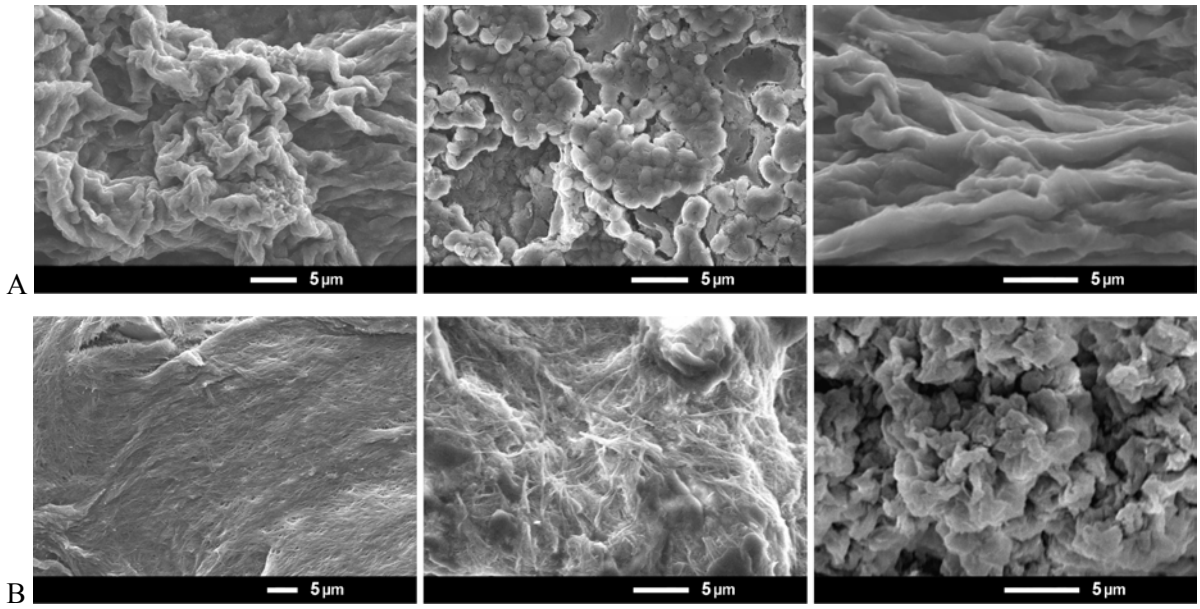

Fig. 2. A. SEM microphotographs of xerogels obtained from compound **1**: a) only organic compound in CH_2Cl_2; b) from hydrogel containing NaCl; c) **1**:$CuCl_2$ = 1:1 in ethanol**;** B. SEM microphotographs of xerogels obtained from compound **2**: a) only organic compound in dioxane; b) from hydrogel containing KCl; c) **2**:$CuCl_2$ = 1:1 in ethanol.

SEM study of the microstructures of dried gels (xerogels) obtained only by organic compound, hydrogels containing Na^+ or K^+ ions and these obtained as organogels in the presence of $CuCl_2$ show pronounced differences in the topology of materials, some of them are shown in Fig. 2. The observations of gels obtained reveal that both organic compounds can make gels with different microstructure: fibril (Fig. 2Ba) and laminar (Fig. 2Aa). Most probably, the gel structure depends also on the solvent used, as previously published data show that gels of compound **1** in some solvents are constructed by very thin fibres [19]. That is why we do not exclude that this laminar structure, presented in Figure. 2Aa, consists of fibers, which diameter is in the range of several nm (bellow the resolution of the used microscope technique). Nevertheless, from the photo (Fig. 2Aa) it is obvious that the gel obtained from compound **1** has very large pores due to undulation of the lamellas, while this formed by compound **2** (Fig. 2Ba) could be regarded as meso-porous.

Comparison of hydrogels, containing alkali metals (Na, K) presented in Figs 2Ab and 2Bb, displays that both gels have fibril structures with 10 to 30 nm diameter of a fibre and in case of 2Ab, fibrils are additionally organized in spheres, which diameter is lower than 2 μm. Again the material obtained from compound **1** possesses higher pores than **2** (Fig. 2Bb) because of the space included among the micro-spheres (Fig. 2Ab).

Figures 2Ac and 2Bc present xerogels, obtained after reaction between organic compounds and $CuCl_2$, and most probably they belong to MOFs. Fibrilar structure was not observed in gels obtained and obviously, these materials are macroporous, as their pores are in the range of microns.

CONCLUSIONS

In summary, we report the formation of novel metal-organic hydro- and organogels with different porous structures. Further studies into their porosity, magnetic property and other characteristics of these materials as well as the molecular structure defining are in progress.

Acknowledgements: *We are grateful to the University of Chemical Technology and Metallurgy for funding this work under the project 10508.*

REFERENCES

1. P. Terech, R. G. Weiss, *Chem. Rev*., **97,** 3133 (1997).
2. D. J. Abdallah, R. G. Weiss, *Adv. Mater*., **12**, 1237 (2000).
3. J. van Esch, B. L. Feringa, *Angew. Chem., Int. Ed*., **39,** 2263 (2000).
4. O. Gronwald, E. Snip, S. Shinkai, *Curr. Opin. Colloid Interface Sci*., **7,** 148 (2002).
5. L. A. Estroff, A. D. Hamilton, *Chem. Rev*., **104,** 1201 (2004).
6. W. H. Binder, O. W. Smrzka, *Angew. Chem. Int. Ed.,* **45,** 7324 (2006).
7. R. G. Weiss, P. Terech, (eds.), Molecular Gels: Materials with Self-Assembled Fibrillar Networks, Kluwer Academic Publishers, Dordrecht, 2005.
8. A. Ajayaghosh, S. J. George, V. K. Praveen, *Angew. Chem., Int. Ed.,* **42,** 332 (2003).
9. Z. Yang, H. Gu, D. Fu, P. Gao, J. K. Lam, B. Xu, *Adv. Mater*.,**16,** 1440 (2004).
10. K. Sugiyasu, N. Fujita, S. Shinkai, *Angew. Chem., Int. Ed*., **43,** 1229 (2004).
11. S. Yao, U. Beginn, T. Gress, M. Lysetska, F. Wurthner, *J. Am. Chem. Soc*., **126,** 8336 (2004).
12. J. H. Jung, Y. Ono, S. Shinkai, *J. Chem. Soc., Perkin Trans. 2,* 1289 (1999).
13. Y. Ono, K. Nakashima, M. Sano, J. Hojo, S. Shinkai, *J. Mater. Chem.* **11,** 2412 (2001).
14. S. Kobayashi, N. Hamasaki, M. Suzuki, M. Kimura, H. Shirai, K. Hanabusa, *J. Am. Chem. Soc.* **124,** 6550 (2002).
15. M. Barboiu, S. Cerenaux, A. van der Lee, G. Vaughan, *J. Am. Chem. Soc.* **126,** 3545 (2004).
16. K. Yabuuchi, E. Marfo-Owusu, T. Kato, *Org. Biomol. Chem*., **1**, 3464 (2003).
17. S. Kawano, N. Fujita, K. J. C. van Bommel, S. Shinkai, *Chem. Lett.*, **32**, 12 (2003).
18. S. Tanaka, M. Shirakawa, K. Kaneko, M. Takeuchi. S. Shinkai, *Langmui*r, **21,** 2163 (2005).
19. D. S. Tsekova, B. Escuder, J. F. Miravet, *Cryst. Growth Des.*, **8**, 11 (2008).
20. J. F. Miravet, B. Escuder, *Chem. Commun*., 5796 (2005).
21. S. L. James, *Chem. Soc. Rev.*, **32**, 276 (2003).
22. M. J. Rosseinsky, *Microporous Mesoporous Mater.*, **73,** 15 (2004).
23. J. L. C. Rowsell, O. M. Yaghi, *Microporous Mesoporous Mater.*, **73**, 3 (2004).
24. B. Xing, M.-F. Choi, B. Xu, *Chem. Eur. J.*, **8**, 5028 (2002).
25. B. Xing,M.-F. Choi, B. Xu, *Chem. Commun*., 368 (2002).
26. J. B. Beck, S. J. Rowan, *J. Am. Chem. Soc*., **125**, 13922 (2003).
27. Q. Wei, S. L. James, *Chem. Commun*., 1555 (2005).
28. X. Bu, P. Feng, *Chem. Nanostructured Mater.,* 1 (2003).
29. D. S. Tsekova, E. Ts. Makakova, P. S Alov, G. A. Gorneva, I. K. Pajeva, L. P. Tancheva, V. V. Petkov, A. R. Surleva, B. Escuder, J. F. Miravet, E. Katz, *Bulg. Chem. Comm.,* **41**, 133 (2009).

МИКРОСТРУКТУРА НА НОВИ МЕТАЛО-ОРГАНИЧНИ ГЕЛОВЕ ПОЛУЧЕНИ ОТ ГЕЛООБРАЗУВАТЕЛИ С НИСКА МОЛЕКУЛНА МАСА

Д. С. Цекова[1]*, В. Б. Стоянова[2]

[1] Катедра „Органична химия“, Химикотехнологичен и металургичен университет, бул. „Климент Охридски“ № 8, 1756 София
[2] Институт по физикохимия „Ростислав Каишев“, Българска академия на науките, бул. „Акад. Г. Бончев“, бл. 11, 1113 София

Постъпила на 17 юли 2008 г., Преработена на 27 септември 2008. г.

(Резюме)

Изследвано е свойството самоорганизация на наскоро синтезирани нискомолекулни съединения съдържащи L-валин и пиридинови компоненти в молекулите си в присъствието на някои метални йони. Установено бе, че в етанолов разтвор те реагират с $CuCl_2$ до образуване на метало-органични полимери с гелова структура. Разгледани са също хидрогелове на същите органични съединения, включващи Na^+ и K^+ йони. Тук са представени някои топологични характеристики на такива продукти, включващи Na^+, K^+ и Cu^{2+} йони в структурата си.

Bulgarian Chemical Communications, Volume 41, Number 2 (pp. 153–159) 2009

Opioidergic system and second messengers affected the nociceptive effects of Tyr-MIF-1's after three models of stress

A. I. Bocheva*, E. B. Dzambazova

Department of Pathophysiology, Faculty of Medicine, Medical University, 2 Zdrave St., 1431 Sofia, Bulgaria

Received July 17, 2008; Revised September 25, 2008

The Tyr-MIF-1 family of neuropeptides (Tyr-MIF-1's) includes MIF-1, Tyr-MIF-1, Tyr-W-MIF-1 and Tyr-K-MIF-1. Nowadays it is certain that they can modulate pain and some forms of stress-induced analgesia (SIA) by antiopiate and μ-specific processes.

The objectives of the present study were twofold: 1) to determine the involvement of opioid system in analgesia induced by immobilization, cold and heat stress (IS, CS and HS); 2) to examine whether opioid system and second messengers are involved in the nociceptive effects of Tyr-MIF-1's after the three stress models mentioned above.

Male Wistar rats were used and nociception was measured by paw-pressure (PP) test. Tyr-MIF-1's (all in 1 mg/kg), naloxone (Nal, 1 mg/kg) and Methylene Blue (MB, 500 μg/paw) were dissolved in saline and were injected intraperitoneally (i.p.). In the first experimental series Nal was administered 20 min before or immediately after stress procedure. In the second experimental series Nal and MB were administered immediately after stress procedure, 20 min and 60 min, respectively, before the administration of the investigated peptides.

The results showed that: (i) opioid and non-opioid components are differently involved in each of stress models. The non-opioid system is mostly involved in CS, opioid – in HS, while both systems are equally presented in IS; (ii) different potency of Tyr-MIF-1's was observed on immobilization, cold or heat SIA, which may be due to their peptide structure, specific binding sites and different interaction with components of SIA; (iii) opioid system and second messengers are involved in the nociceptive effects of Tyr-MIF-1's after IS, CS and HS.

Key words: Tyr-MIF-1's, stress, nociception, opioid system, second messengers.

INTRODUCTION

The Tyr-MIF-1 family of peptides (Tyr-MIF-1's) includes MIF-1, Tyr-MIF-1, Tyr-W-MIF-1 and Tyr-K-MIF-1, which have been isolated from bovine hypothalamus and human brain cortex [1, 2]. Nowadays it is certain that these endogenous peptides are potent neuromodulators. They can modulate pain by antiopiate and μ-specific processes [3].

MIF-1 (Pro-Leu-Gly-NH_2) can antagonize opiate actions, and the first report of such activity also correctly predicted the discovery of other endogenous antiopiate peptides. MIF-1 has an effect similar to that of naloxone blocking the analgesic effects of enkephalins and morphine in the tail-flick test and blocking the non-analgesic thermal effects of morphine [4]. The tetrapeptide Tyr-MIF-1 (Tyr-Pro-Leu-Gly-NH_2) not only shows antiopiate activity, but also pronounced selectivity for the μ-opiate binding site. Tyr-MIF-1 and Tyr-W-MIF-1 (Tyr-Pro-Trp-Gly-NH_2) have antinociceptive effects by binding to μ-opioid receptors as well as to their specific non-opiate receptors in the brain [5]. Tyr-K-MIF-1 appears to bind to Tyr-MIF-1 specific sites and to its own specific sites [1, 3].

Stress is known to exert an influence on neuroendocrine, autonomic, hormonal, and immune functioning. It has debilitating effects on numerous body systems. Various stress models (immobilization, foot shock, hot and cold exposure) have been reported to induce analgesia referred to as stress-induced analgesia (SIA). It is an important phenomenon relevant to the perception and response to pain and to the modulation of behavioral responses, and it is partially due to release of endogenous opioid peptides. SIA has been categorized into one of two broad categories, opioid and non-opioid [6–8]. The opioid form of SIA is reversed by naloxone or naltrexone, whereas the nonopioid analgesia is insensitive to these opioid receptor antagonists [9].

Our and literature data showed that Tyr-MIF's are able to inhibit the expression of some forms of SIA in various species [8, 10].

Literature data about involvement of opioidergic system in SIA are rather contradictory. A potent blocker of opioids, naloxone (Nal), reduces the inhibition of the tail-flick and hot-plate responses induced by immobilization suggesting the involvement of opioid system [11–16]. SIA due to acute hot exposure is Nal-dependent [17]. There are also

* To whom all correspondence should be sent:
E-mail: adriana_bocheva@abv.bg

investigators who claim that the opioid system is not engaged in the nociceptive responses since Nal does not affect immobilization stress-induced antinociception in male mice [18, 19]. Also, Nal has no effect on cold SIA [17] or administered before the cold stress it blocks SIA [20].

The objectives of the present study were twofold: 1) to determine the involvement of opioid system in analgesia induced by immobilization, cold and heat stress (IS, CS and HS); 2) to examine whether opioid system and second messengers are involved in the nociceptive effects of Tyr-MIF-1's after the three stress models mentioned above.

EXPERIMENTAL

Chemistry. The synthesis of Tyr-MIF-1 peptides was based on well-established methods of peptides synthesis. For optimization purposes, three different activation procedures were used: mixed anhydride (MA), dicyclohexyl carbodimide (DCC/HOBt) or active ester (AE) methods. The strategy of the minimal side-chain protection was adopted [21]. After isolation and purification, the peptides were identified and characterized by optical rotation, TLC, analytical HPLC, mass-spectra and elemental analysis.

Animals. The experiments were carried out on male Wistar rats (180–200 g) housed at 12 h light/dark cycle. Food and water were available *ad libitum*. All experiments were carried out between 09.00 a.m./12.00 p.m. Each group included 8–10 rats.

Nociceptive test: *Paw-pressure (PP) test*. The changes in the mechanical nociceptive threshold of the rats were measured by analgesimeter (Ugo Basile). The pressure was applied to the hind-paw. The pressure (grams) required eliciting nociceptive responses such as squeak and struggle was taken as the mechanical nociceptive threshold. A cut-off value of 500 g was used to prevent damage of the paw.

Acute models of stress: Immobilization stress (IS). The animals were placed in a plastic tube with adjustable plaster tape on the outside so that the animals were unable to move. There were holes for breathing. The control group was not submitted to restraint. The immobilization procedure was carried out for 1 hour;

Cold stress (CS). The animals were placed in a refrigerating chamber at 4ºC. The cold stress procedure was carried out for 1 hour;

Heat stress (HS). Each rat of this group was subjected for a single exposure in the incubator at a temperature of 38 ± 1°C and relative humidity of 45–50% for one hour.

Drugs and treatment. MIF-1, Tyr-MIF-1, Tyr-W-MIF-1 and Tyr-K-MIF-1 (all at a dose of 1 mg/kg) were synthesized by the Group of Antimetabolites at the Institute of Molecular Biology, Bulgarian Academy of Sciences. Naloxone (Nal, 1 mg/kg) and Methylene Blue (MB, 500 μg/paw), an inhibitor of activation of guanylyl cyclase and NO-synthase, were obtained from Sigma. All drugs were dissolved in sterile saline (0.9% NaCl) solution. Peptides and Nal were injected intraperitoneally (i.p.). In the first experimental series Nal was administered 20 min before or immediately after stress procedure. In the second experimental series, Nal and MB were administered immediately after stress procedure, 20 min and 60 min, respectively, before the administration of the investigated peptides. The experiment began 15 min after injection of Tyr-MIF-1's. The control group was injected with saline 1ml/kg, i.p.

The experimental procedures were carried out in accordance with the institutional guidance and general recommendations on the use of animals for scientific purposes.

Data analysis. The results were statistically assessed by one-way analysis of variance (ANOVA). Values are mean ± S.E.M. Values of $P < 0.05$ were considered to indicate statistical significance.

RESULTS AND DISCUSSION

In the first experimental series we determined involvement of opioid system in analgesia induced by IS, CS and HS using a non-competitive antagonist of opiate receptors Nal (1 mg/kg, i.p.). It was administered 20 min before or immediately after stress procedure. In the first case the changes in analgesia were measured immediately after stress, while in the second case – 20 min later (Fig. 1).

Our results showed that IS, CS and HS have well-pronounced analgesic effects compared to the control (Figs. 1–4). Administration of Nal (1 mg/kg, i.p.) immediately after IS decreased significantly the pain threshold measured 20 min after injection of Nal ($P < 0.01$). Nal injected 20 min before IS did not show significant change in pain threshold compare to immobilization-SIA (ISIA) measured immediately after stress procedure. The obtained results for CS were similar. Nal injected immediately after CS decreased significantly cold-SIA (CSIA) when the pain threshold was measured 20 min later ($P < 0.05$). In contrast, Nal adminis- tered 20 min before HS or immediately after it strongly inhibited heat-SIA (HSIA) ($P < 0.001$) (Fig. 1).

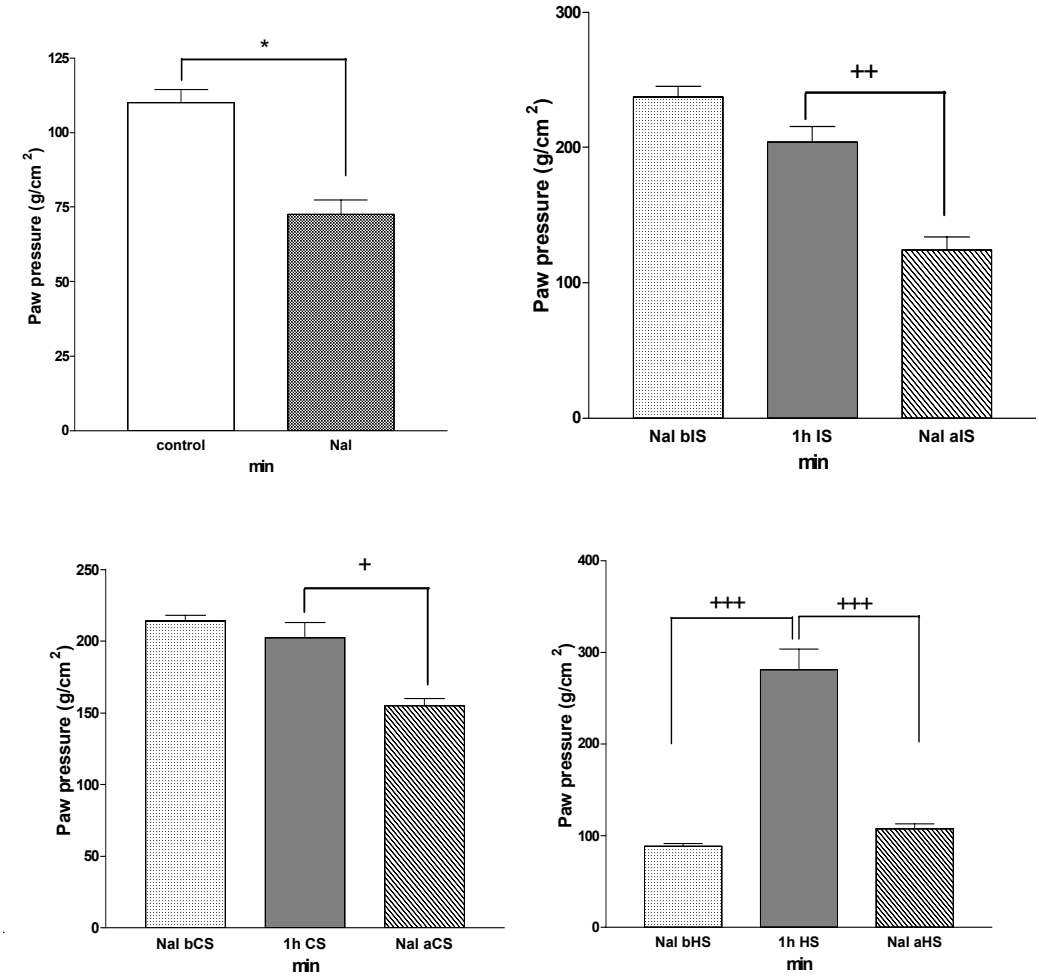

Fig. 1. Effects of naloxone (Nal), immobilization stress (IS), cold stress (CS) and heat stress (HS) on nociception measured with paw pressure (PP) test. Also administration of Nal (1 mg/kg, i.p.) before (Nal bIS, Nal bCS, Nal bHS) and after each of stress procedure (Nal aIS, Nal aCS, Nal aHS) in male Wistar rats (n = 5). Mean values ± S.E.M. are presented. *$P < 0.05$ vs. control; $^{+}P < 0.05$, $^{++}P < 0.01$, $^{+++}P < 0.001$ vs. respective stress.

In the second experimental series we examined the involvement of opioid system and second messengers in the nociceptive effects of Tyr-MIF-1's after the three stress models using Nal (applied immediately after stress procedure and 20 min before peptide) and MB (applied immediately after stress procedure and 60 min before peptide). The peptides applied alone were injected just after the stress procedure. The investigation started 15 min after peptides injection.

MIF-1 ($P < 0.01$), Tyr-MIF-1 ($P < 0.01$), and Tyr-K-MIF-1 ($P < 0.05$) (all at a dose of 1 mg/kg, i.p.) significantly decreased the pain threshold compared to the group of animals with ISIA (Fig. 2). Tyr-W-MIF-1 ($P < 0.05$) significantly decreased the pain threshold compared to IS 30 min after its injection (not shown in the figure). Combination of peptides with Nal or MB (with exception of MIF-1) after IS significantly decreased the pain threshold compared to respective peptide (Fig. 2).

Only two of the investigated peptides, Tyr-MIF-1 ($P < 0.05$) and Tyr-K-MIF-1 ($P < 0.05$) injected alone after CS, significantly inhibited CSIA (Fig. 3). Tyr-W-MIF-1 ($P < 0.05$) showed the same effect 30 min later (not shown in the figure).

Tyr-MIF-1 ($P < 0.01$), Tyr-W-MIF-1 ($P < 0.01$) and Tyr-K-MIF-1 ($P < 0.01$) significantly decreased the pain threshold compared to HSIA (Fig. 4).

MIF-1 ($P < 0.05$) did not show any effect on CSIA or HSIA. Co-administration of all peptides with Nal or MB after CS or HS significantly decreased the pain threshold compared to the respective peptide (Figs. 3 and 4).

The analgesia induced by stress is an adaptive response that occurs both in laboratory animals and humans. Opiod and non-opioid pain inhibitory pathways appear to be activated by such stimuli [6]. The SIA is classified as opioid when it is anta-

gonized by naloxone and non-opioid when different mediators such as dopamine, histamine, serotonin or excitatory amino acids seem to be mainly responsible for the analgesic effects observed after certain stress conditions [22]. A lot of literature documents demonstrated that the parameters of the laboratory stressor will determine the neurochemical identity of the resultant analgesia. In rats, low severity stressors produce opioid analgesia and higher severity stressors produce nonopioid analgesia [23].

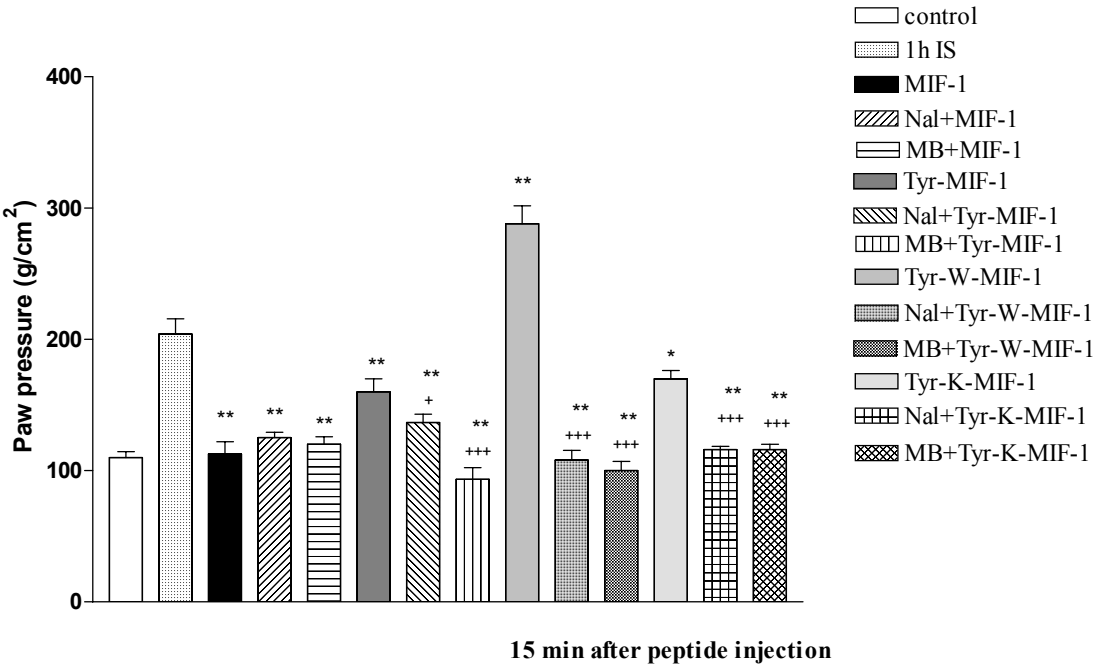

Fig. 2. Effects of MIF-1, Tyr-MIF-1, Tyr-W-MIF-1, Tyr-K-MIF-1 (all in 1 mg/kg, i.p.) and their combination with Nal (1 mg/kg, i.p.) and methylene blue (MB, 500 μg/paw) on nociception measured with paw pressure (PP) test after 1 hour immobilisation stress (IS) in male Wistar rats ($n = 5$). Mean values ± S.E.M. are presented. $^{*}P < 0.05$, $^{**}P < 0.01$ vs. IS; $^{+}P < 0.05$, $^{+++}P < 0.001$ vs. respective peptide.

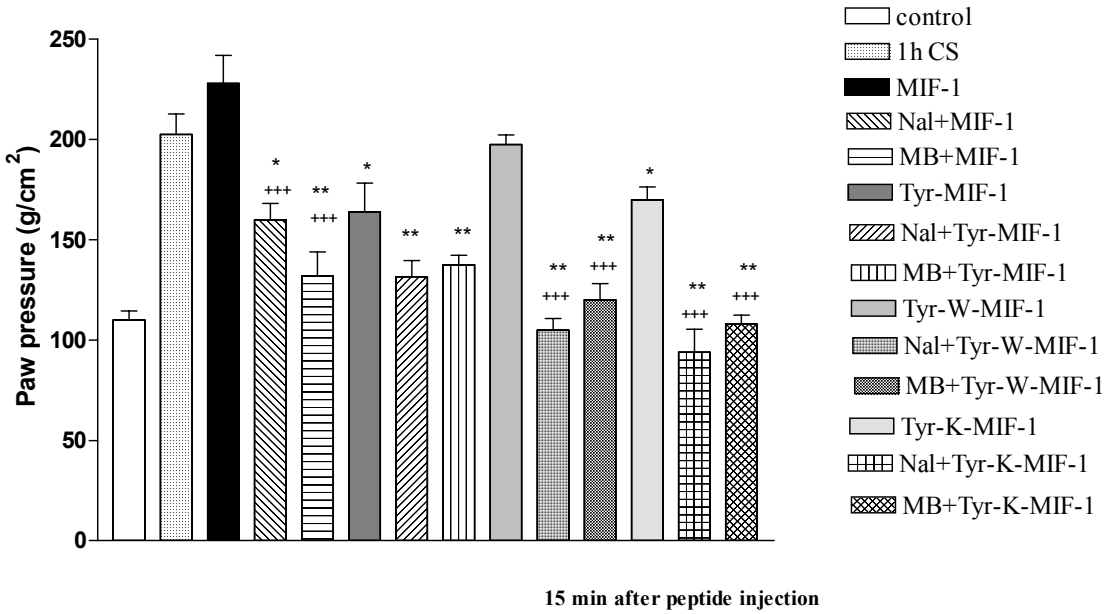

Fig. 3. Effects of MIF-1, Tyr-MIF-1, Tyr-W-MIF-1, Tyr-K-MIF-1 (all in 1 mg/kg, i.p.) and their combination with Nal (1 mg/kg, i.p.) and methylene blue (MB, 500 μg/paw) on nociception measured with paw pressure (PP) test after 1 hour cold stress (CS) in male Wistar rats ($n = 5$). Mean values ± S.E.M. are presented. $^{*}P < 0.05$, $^{**}P < 0.01$ vs. CS; $^{+++}P < 0.001$ vs. respective peptide.

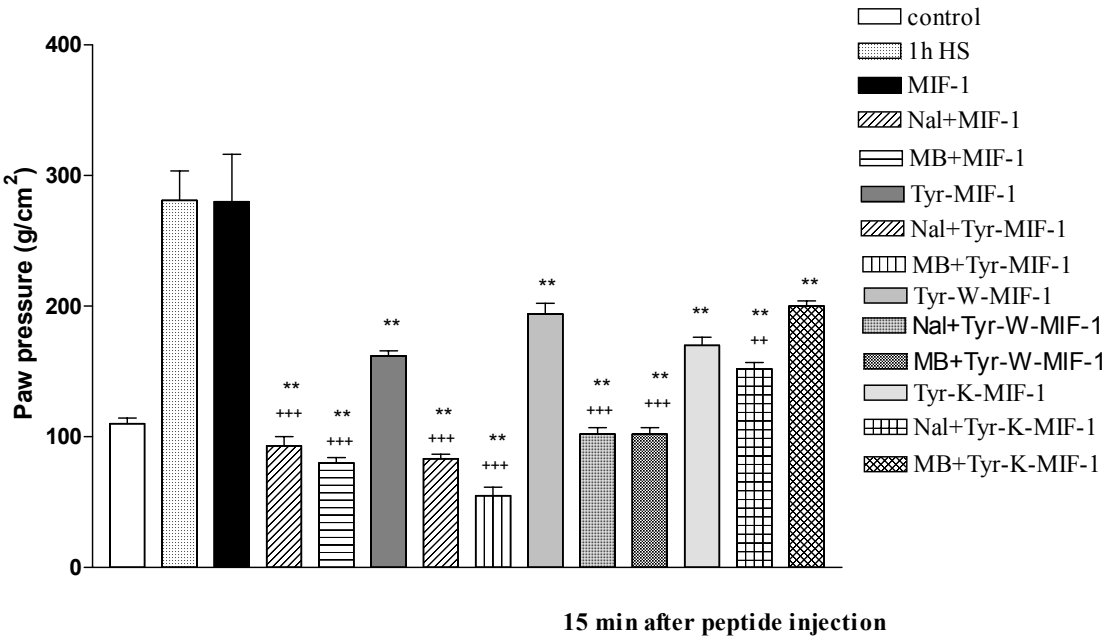

Fig. 4. Effects of MIF-1, Tyr-MIF-1, Tyr-W-MIF-1, Tyr-K-MIF-1 (all in 1 mg/kg, i.p.) and their combination with Nal (1 mg/kg, i.p.) and methylene blue (MB, 500 μg/paw) on nociception measured with paw pressure (PP) test after 1 hour heat stress (HS) in male Wistar rats (n = 5). Mean values ± S.E.M. are presented. $^{**}P < 0.01$ vs. HS; $^{++}P < 0.01$, $^{+++}P < 0.001$ vs. respective peptide.

According to the obtain results, the opioid system is involved in the three models of stress. Nal showed effect administered after each of stress exposures. The greatest influence was observed on HSIA. These results and literature data showed that opioid and non-opioid components are differently involved in each of stress models. The non-opioid system is mostly involved in CS, opioid – in HS, while both systems are equally presented in IS [24]. We confirm some findings that there is the so called mixed form of SIA, which possesses opioid and non-opioid components.

The observed different potency of Tyr-MIF-1 peptides may be due to their peptide structure, specific binding sites and different interaction with opioid or non-opioid components of the three stress models – IS, CS and HS. In particular, Tyr-MIF-1`s have anti-opioid properties, since they decreased the effect of morphine, L-NAME and some forms of SIA [2, 3, 10].

Our results are in accordance with some literature data that Tyr-MIF-1 modulates stress responses in mice. Authors suggest that the peptide regulates the endogenous biological alert system responding to stress exposure, perhaps, counter-acting the excessive response of the system [25].

It is known that different kinds of stress are known to alter the brain neurohormones and neuronal activities [26]. The endogenous peptide Tyr-MIF-1 has been shown to have modulating activity on the endogenous opiates released with SIA [1, 27]. In particular, Tyr-MIF-1 induces inhibitory effects on analgesia induced by shock, novel-environment and warm water-swim [28], defeat-induced analgesia and inhibition of aggression [29] and restraint induced analgesia in the mouse [30].

Opioid system and second messengers are involved in the nociceptive effects of Tyr-MIF-1's after IS, CS and HS since Nal and MB altered the pain thresholds of peptides.

CONCLUSIONS

i. Opioid and non-opioid components are differently involved in each of the stress models. The non-opioid system is mostly involved in CS, opioid – in HS, while both systems are equally presented in IS.

ii. Different potency of Tyr-MIF-1's was observed on immobilization, cold or heat SIA. This results may be due to their peptide structure, specific binding sites and different interaction with opioid or non-opioid components of SIA.

iii. Opioid system and second messengers are involved in the nociceptive effects of Tyr-MIF-1's after IS, CS and HS.

Acknowledgments: *This work was supported by grant of the Bulgarian National Scientific Research Foundation VU-L-04/05.*

REFERENCES

1. G. W. Reed, G. A. Olson, R. D. Olson, *Neurosci. Biobehav.*, **18**, 519 (1994).
2. F. Cesselin, *Fundam. Clin. Pharmacol.*, **9**, 409 (1995).
3. W. Pan, A. J. Kastin, *Peptides*, **28**, 2411 (2007).
4. J. E. Zadina, A. J. Kastin, L. J. Ge, V. Brantl, *Life Sci.*, **47**, 25 (1990).
5. J. E. Zadina, A. J. Kastin, L. J. Ge, L. Hackler, *Life Sci.*, **55**, 461 (1994).
6. L. R. Watkins, D. J. Mayer, *Ann. N Y Acad. Sci.*, **467**, 273 (1986).
7. A. Tsuda, Y. Ida, H. Satoh, S. Tsujimaru, M. Tanaka, *Parmacol. Biochem. Behav.*, **32**, 569 (1989).
8. M. Inoue, M. H. Rashid, T. Kawashima, M. Matsumoto, T. Maeda, S. Kishioka, H. Ueda, *Brain Res. Bull.*, **60**, 275 (2003).
9. I. B. Lapo, M. Konarzewski, B. Sadowski, *Physiol. Behav.*, **78**, 345 (2003).
10. A. Bocheva, E. Dzambazova-Maximova, *Meth. Find. Clin. Exp. Pharmacol*., **26**, 673 (2004).
11. S. Amir, Z. Amit, *Life Sci.*, **23**, 1143 (1978).
12. B. D. Appelbaum, S. G. Holtzman, *Life Sci.*, **36**, 1069 (1985).
13. D. B. Miller, *Brain Res.*, **473**, 327 (1988).
14. D. J. Calcagnetti, S. W. Fleetwood, S. G. Holtzman, *Pharmacol. Biochem. Behav.*, **37**, 193 (1990).
15. D. J. Calcagnetti, J. L. Stafinsky, T. Crisp, *Brain Res.*, **592**, 305 1992.
16. H. W, Suh, D. K. Song, S. O. Huh, Y. H. Kim, *Eur. Neuropsychopharmacol.*, **10**, 407 (2000).
17. M. Kavaliers, *Brain Res*., **410**, 111 (1987).
18. C. L. Wong, *Meth. Find. Exp. Clin. Pharmacol*., **16**, 309 (1994).
19. H. A. Jorgensen, O. B. Fasmer, O. G. Berge, L. Tveiten, K. Hole, *Pharmacol. Biochem. Behav*., **20**, 289 (1984).
20. K. K. Vaswani, C. W. Richard 3rd, G. A. Tejwani, *Pharmacol. Biochem. Behav*., **29**, 163 (1988).
21. T. Pajpanova, A. Bocheva, E. Golovinsky, *Meth. Find. Exp. Clin. Pharmacol.*, **21**, 591 (1999).
22. G. D. Gamaro, M. H. Xavier, J. D. Denardin, J. A. Pilger, D. R. Ely, M. B. Ferreira, C. Dalmaz, *Physiol. Behav.*, **63**, 693 (1998).
23. J. S. Mogil, W. F. Sternberg, H. Balian, J. C. Liebeskind, B. Sadowski, *Physiol. Behav.*, **59**, 123 (1996).
24. K. Pacák, M. Palkovits, *Endocr. Rev.,* **22**, 502 (2001).
25. H. Fukunaga, M. Takahashi, H. Kaneto, M. Yoshikawa, *Jpn. J. Pharmacol*., **79**, 231 (1999).
26. R. K. Sinha, *Iran. Biomed. J*., **11**, 101 (2007).
27. A. d'Amore, A. Loizzo, *Peptides*, **20**, 1425 (1999).
28. Z. H. Galina, A. J. Kastin, *Br. J. Pharmacol*., **90**, 669 (1987).
29. M. Kavaliers, M. Hirst, *Peptides*, **7**, 1007 (1986).
30. M. Kavaliers, D. G. Innes, *Peptides*, **13**, 1295 (1992).

ОПИОДЕРГИЧНАТА СИСТЕМА И ВТОРИЧНИТЕ ПОСРЕДНИЦИ ПОВЛИЯВАТ НОЦИЦЕПТИВНИТЕ ЕФЕКТИ НА TYR-MIF-1 ПЕПТИДИТЕ СЛЕД ТРИ МОДЕЛА НА СТРЕС

А. И. Бочева*, Е. Б. Джамбазова

Катедра „Патофизиология“, Медицински факултет, Медицински университет, ул. „Здраве“ № 2, 1431 София

Постъпила на 17 юли 2008 г.; Преработена на 25 септември 2008 г.

(Резюме)

Невропептидната група Tyr-MIF-1 (Tyr-MIF-1's) включва MIF-1, Tyr-MIF-1, Tyr-W-MIF-1 и Tyr-K-MIF-1. В наши дни е известно, че те могат да модулират болката и някои форми на стрес-индуцирана аналгезия (SIA) чрез антиопиоидни и μ-специфични действия.

Целта на настоящата работа бе: 1) да се определи участието на опиоидната система в аналгезията предизвикана от имобилизационен, студов и топлинен стрес (IS, CS и HS); 2) да се изследва дали опиоидната система и вторичните посредници са въвлечени в ноцицептивните ефекти на Tyr-MIF-1's след трите модела на стрес споменати по горе.

Мъжки плъхове линия Wistar бяха използвани и болковия праг бе измерван чрез paw pressure (PP) тест. Tyr-MIF-1's (всички в доза 1 mg/kg), налоксон (Nal, 1 mg/kg) и Метилен Блу (MB, 500 μg/лапа) бяха разтваряни във физиологичен разтвор и инжектирани интраперитонеално. В първата експериментална серия Nal бе въвеждан 20 min преди или веднага след стрес процедурата. Във втората серия експерименти Nal и MB бяха въвеждани веднага след стрес-процедурата, 20 min и 60 min респективно преди изследваните пептиди.

Резултатите показаха, че: i) опиоидната и неопиоидната компонента имат различно участие във всеки един от моделите на стрес. Неопиоидната система участва предимно при CS, опиоидната – при HS, докато двете системи са приблизително еднакво застъпени при IS; ii) Tyr-MIF-1's показаха различна потентност при имобилизационна, студова или топлинна SIA, което може би е свързано с тяхната пептидна структура, специфични места на свързване и различно взаимодействие с компонентите на SIA; iii) опиоидната система и вторичните посредници участват в ноцицептивните ефекти на Tyr-MIF-1's след IS, CS и HS.

Bulgarian Chemical Communications, Volume 41, Number 2 (pp. 160–164) 2009

Synthesis of two peptide mimetics as markers for chemical changes of wool's keratin during skin unhairing process and comparison of the wool quality obtained by ecological methods for skins unhairing

M. Koleva[1], D. Danalev[2]*, D. Ivanova[1], L. Vezenkov[2], N. Vassilev[3]

[1] *Department of Textile and Leather, University of Chemical Technology and Metallurgy, 8 Kliment Ohridski Blvd., 1756 Sofia, Bulgaria*
[2] *Department of Organic Chemistry, University of Chemical Technology and Metallurgy, 8 Kliment Ohridski Blvd., 1756 Sofia, Bulgaria*
[3] *Institute of Organic Chemistry with Centre of Phytochemistry, Bulgarian Academy of Sciences, Acad. G. Bonchev St., Block 9, 1113 Sofia, Bulgaria*

Received July 4, 2008; Revised September 18, 2008

During the last few years, a base attention is directed to improve the existing methods for unhairing of hides and skins. The major developments have been the rapid hair-saving with alkaline pretreatment and enzymatic. The sheep skins unhairing process with preliminary alkaline treatment of the wool leads to the obtaining of two unnatural dipeptide mimetics lysinoalanine (Lys*-Ala) and ornithinoalanine (Orn*-Ala). They are a result of the keratin hydrolysis process. The changes in wool keratin make it resistant to sulphide degradation. We synthesized and characterized these unnatural dipeptides under experimental conditions. The structures and mechanism of Lys*-Ala and Orn*-Ala obtaining were elucidated. The application of the newly synthesized products as markers for control of wool's keratin changes during skin unhairing process was demonstrated.

A comparison between the data on the three samples of wool and some recommendations for the ways this secondary solid waste can be considered as a raw material due to its physical and chemical properties were done.

Keywords: Peptides mimetics, unnatural amino acids, hides' and skins' unhairing.

INTRODUCTION

During the application of the classical methods (alkaline conditions) for wool's keratin unhairing two problems are raised:

- lost hair as additional material due to keratin hydrolysis;
- increasing of pollution problems related to waste water.

The highest polluted beam house liquid effluents in leather production are from unhairing and liming methods - high organic load, suspended solids, $Ca(OH)_2$ and Na_2S content, fats, hair wastes. There are two main directions for reducing the concentrations of these chemicals and wastes: unhairing with alkaline pretreatment of the hair keratin and its removal and /or recycling of waste waters.

Unhairing methods used in this work are hair-saving. The surface of the received wool was damaged, but the hair maintains the fiber structure. The waste waters have lower concentrations of total nitrogen, suspended solids, $Ca(OH)_2$ and Na_2S content, fats, hair wastes. The results show lower pollution to the environment. Depending on the quality of the wool, after the mechanical removal, it can find different industrial applications. The main is in agriculture as a source of compost and production of animal food [1]. Improvement of quality may enlarge its putting into practice, for example in textile and building industries.

Every new technological approach aiming the solvation of the mentioned problems needs of markers for monitoring the keratin hydrolysis process. The products of keratin hydrolysis process under alkaline conditions had been studied [2, 3]. In 1976 Feairheller *et al*. [2] and Money later [3] suggested the compounds, which are obtained as a result of unhairing by lime-sulphide method. They both reported that the treatment of leather by this method, except natural amino acid, leads to many products, which are modified amino acids and peptides like lantionin, lysinoalanine (Lys*-Ala), ornithino-alanine (Orn*-Ala), *etc*. (Fig. 1). Money published a possible mechanism for the obtaining of these products as a result of decomposition of cystin residues included in leather's hair. To characterize these products Feairheller *et al*. synthesized them by the methods described in [2].

* To whom all correspondence should be sent:
E-mail: dancho_danalev@yahoo.com

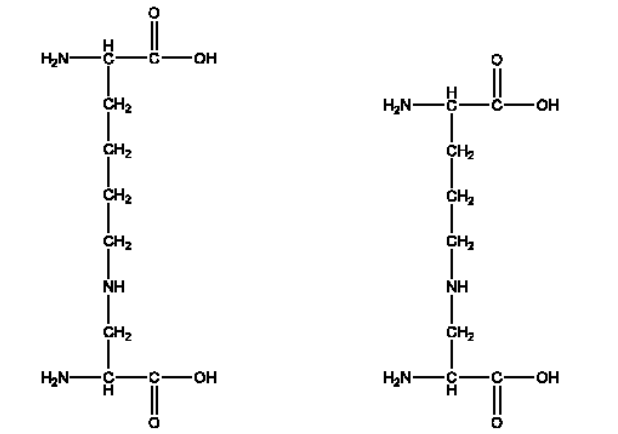

Fig. 1. Structures of published in [1] dipeptide mimetics Lys*-Ala and Orn*-Ala.

The aim of our work was the synthesis of markers to prove the above-mentioned dipeptide mimetics in wool keratin during the unhairing process by using the methods described in [2]. They are very important because their availability will allow process monitoring. On the second place, the goals are to make a comparison between the data of the three samples of wool and to give some recommendations for the ways this secondary solid waste can be considered as a raw material due to its physical and chemical properties.

EXPERIMENTAL

Procedure for preparing Lys-Ala and Orn*-Ala*

For preparation of Lys*-Ala and Orn*-Ala, methyl α-acetamidoacrylate was dissolved in 0.3 N NaOH solution with a three-fold molar excess of the appropriate protected amino acid (Zα-Lys-OH or Zα-Orn-OH) and allowed to stand at room temperature for about 6 h. The resulting solution was then evaporated to oil under vacuum. Excess 6 N HCl was then added to these residues and the resulting solution was heated at reflux for 24 h. The resulting mixture was evaporated under vacuum to dryness and until free of hydrogen chloride. The products were obtained from the residues as crystalline dihydrochlorides and were recrystralized from water-alcohol mixture [2].

The purity and synthesis of new the compounds were monitored by RP-HPLS through isocratic elution with 50% AcCN/50% K_2HPO_4:KH_2PO_4, pH = 7, C18 column, λ = 220 nm, rate 1 ml/min, diode array detector.

The obtained products were characterized by NMR spectra recorded on a Bruker DRX-250 spectrometer, operating at 250.13 MHz for 1H, using dual 1H/13C probe head, COSY, DEPT-135 and HMQC.

Lys-Ala*: ^{1}H NMR (D_2O) δ (ppm): 1.41–1.64 (m, 2H, H4), 1.601 (s, 3H, CH_3), 1.67–1.82 (m, 2H, H5), 1.90–2.15 (m, 2H, H3), 3.050 (t, J = 7.5 Hz, 2H, H6), 4.183 (t, J = 6.3 Hz, 1H, H2).

^{13}C NMR (D_2O) δ (ppm): 24.15 (C4), 28.06 (CH_3), 28.94 (C5), 31.85 (C3), 41.86 (C6), 55.42 (C2), 95.32 (C), 174.51 (C = O), 177.52 (C = O).

Orn-Ala*: ^{1}H NMR (D_2O) δ (ppm): 1.580 (s, 3H, CH_3), 1.67–1.82 (m, 2H, H4), 1.90–2.12 (m, 2H, H3), 3.072 (t, J = 7.5 Hz, 2H, H5), 4.100 (t, J = 6.3 Hz, 1H, H2).

^{13}C NMR (D_2O) δ (ppm): 24.43 (C4), 25.17 (C3), 28.06 (CH_3), 41.71 (C5), 55.46 (C2), 95.57 (C), 174.81 (C = O), 177.91 (C = O).

RESULTS AND DISCUSSION

Our investigation allows us to define more accurately the preliminary structures given in literature. It was interesting that by the method described in [2] we obtained two different major products (Fig. 2).

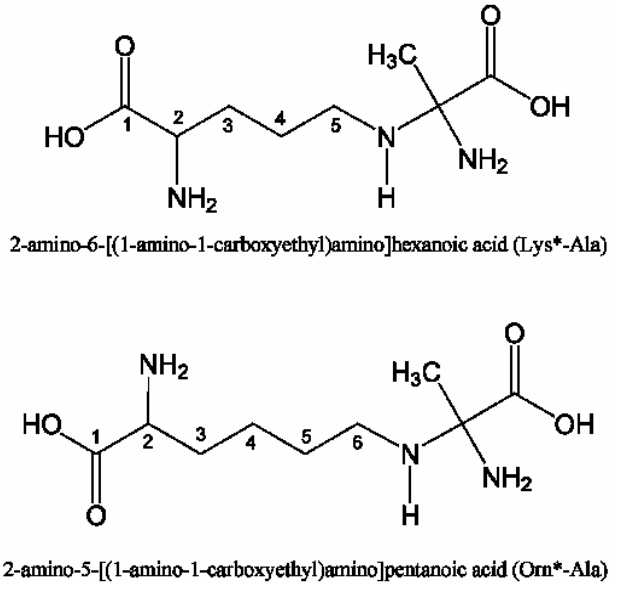

Fig. 2. Structures of dipeptide mimetics Lys*-Ala and Orn*-Ala obtained in the present study.

According to NMR data of the obtained products, the attack of the nucleofil N atom onto the quaternary C atom of methyl α-acetamidoacrylate was proven (Fig. 3).

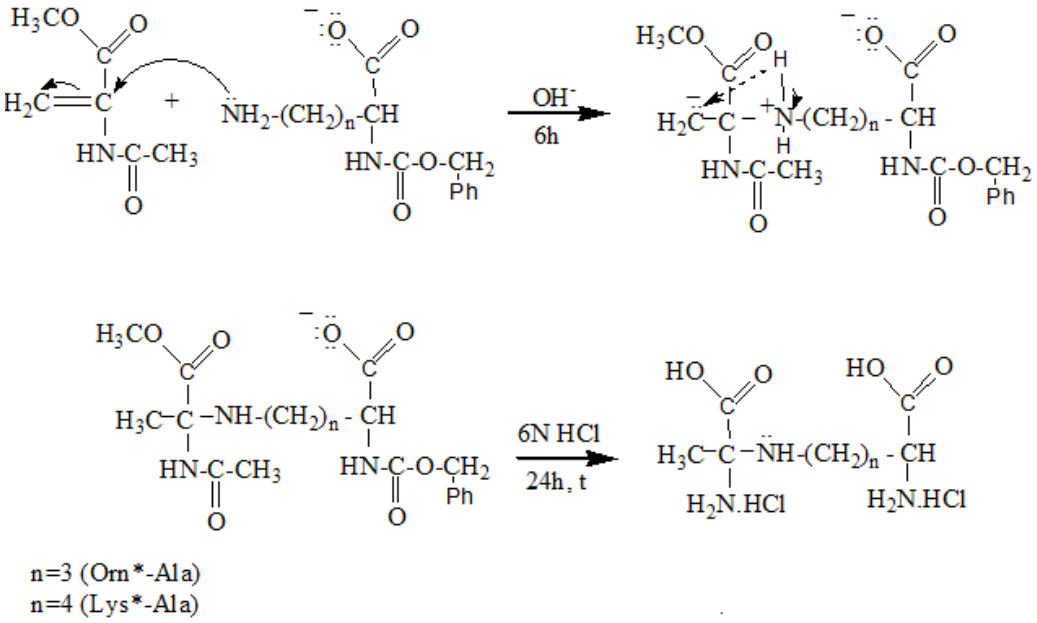

Fig. 3. Scheme of the reaction of Lys*-Ala and Orn*-Ala obtaining.

The immunization of keratin is the transformation by an alkaline pretreatment (or at alkaline conditions) of part of the existing –S–S– cross-links into more stable ones. Keratin has a high stability as a consequence of the disulphide bridges of cysteine amino acid between adjacent protein chains. The possible mechanism of the immunization reaction can be associated with the alkaline transformation of disulphide bonds of cystine into other, much more stable cross-links like amino acids lantionine, lysinoalanine and ornithinoalanine.

It is possible a direct transformation of cystine cross-links into two moles of α-amino acrylic residues and H_2S generation. Possibly, they react for example with lysine and ornithine, and lysinealanine and ornithinealanine, too.

Epidermal keratinized zones, root sheaths, and follicles chemically have low cystine content and do not contain cystine cross-links in comparison with the high amount of cystine in the hard keratin. The immunization of the mature keratin is easier than that of unmature in internal root sheath and external root sheath, as well as these in the epidermis. On the basis of all observations, the differences between the solubility of the hair and roots are increasing, as well as the saving of the wool during the unhairing process. The amino acid analysis of the wool, received by both the enzyme unhairing method and unhairing method with alkaline pretreatment of the wool, shows the availability of the obtained by us dipeptide mimetics. The wool, which was immunizated with alkaline pretreatment, has 261.46 nmol of both Lys*-Ala and Orn*-Ala. In the wool, obtained by the enzyme unhairing method, their amount is 79.46 nmol. The wool, received by the enzyme unhairing method, is with intact fibres, not met together, clean, undestructive, with good quality. Our results show that in these concentrations the peptide mimetics do not affect negatively the wool features and can be used for industrial purposes in different ways as a raw material.

Secondary electron micrographs (SEI) were produced using a JSM-6390 JEOL (Jeol Scanning Microscopy). Figure 4 shows the cuticle scales on a native wool fibre. There is no degradation of the scales, which can be getting in a drum unhairing process.

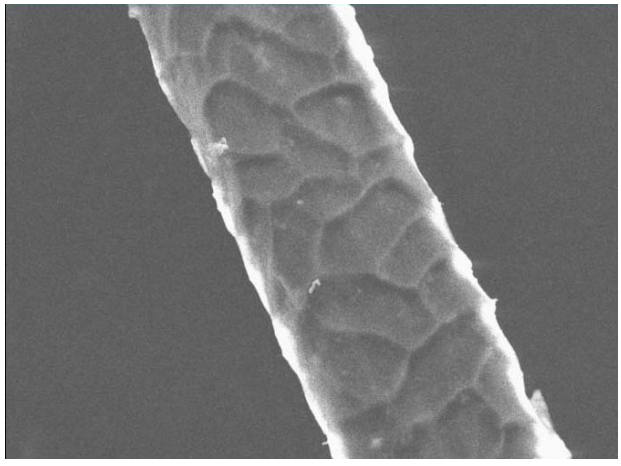

Fig. 4. The cuticle scales on a native wool fibre.

Figure 5 shows a wool fibre, obtained by the unhairing method with alkaline pretreatment of the

wool. Some $Ca(OH)_2$ can be seen upon the opened cuticle scales. It can be caused by the poor washing of the received wool. The prior immunization does not transform the existing –S–S– cross- links into amino acid lantionine in the keratin, but in modified unnatural amino acids lysinoalanine (Lys*-Ala) and ornithinoalanine (Orn*-Ala) [4]. Occasionally, this reaction does not cause the problems of remediation. The immunization reaction made the hair resistant to –S–S– bond reduction. The alkaline solubility data showed [5] a weak damage – 10–15%. This can be explained with the hydrolysis of part of the sulphur cross-links, as well as the bonds of the peptide chains.

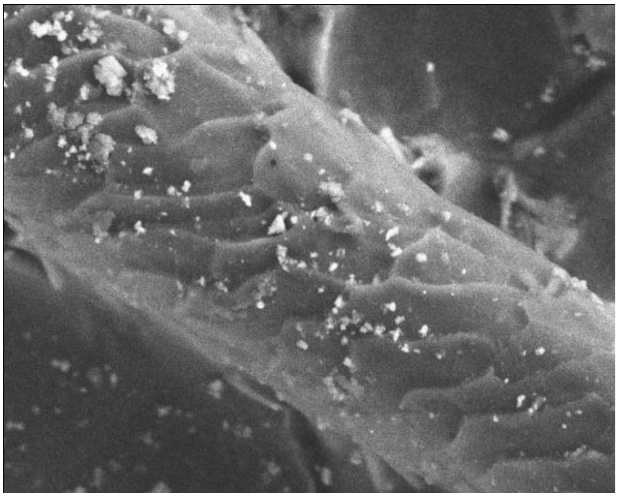

Fig. 5. Wool received after alkaline pretreatment.

The immunization reaction of wool fibres leads to little degrading intact cuticle. It can be caused by alkaline pretreatment. The wool is weakly damaged – with worsen alkaline solubility and mostly carbamid-disulfite solubility [5]. Quality by hand is for mat, weakly destructive material. The received hair is applicable in different productions, as it is whole, intact.

The wool received by the enzyme unhairing method is with little opened cuticle scales, but is still observed (Fig. 6). Probably, this is due to the alkaline pH of soaking and unhairing. This type of soak causes some immunization. The data of the amino acid analysis of wool show the availability of the obtained by us dipeptide mimetics [4]. Alkaline, acid and carbmide-disulphite solubility of the wool showed untouched peptide bonds and not damaged hair. The wool obtained by the enzyme unhairing method is with intact fibers, not met together, clean, undestructive, with good quality. It can be used for industrial purposes in different ways as a raw material.

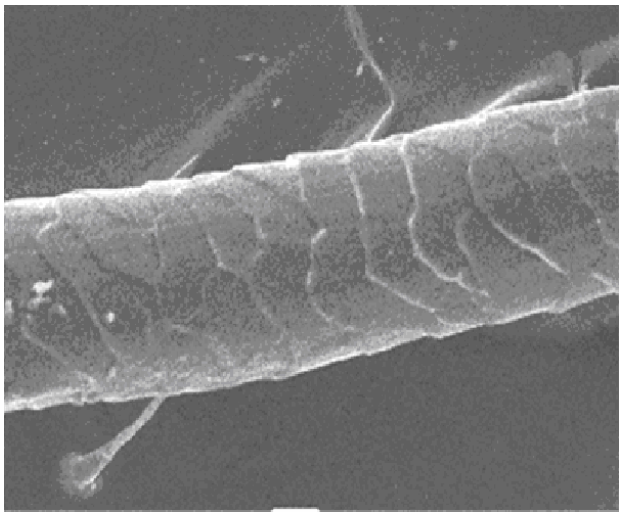

Fig. 6. Wool received from the enzyme unhairing method.

CONCLUSION

The synthesized by us markers could be used for keratin hydrolysis monitoring. For this aim some additional relationships between Lys*-Ala and Orn*-Ala concentrations and possibilities for later skins applications which will be used in practice have to be made.

Unhairing methods used in the work are hair-saving. The surface of the received wool was damaged, but the hair maintains the fibre structure. The results show lower pollution to the environment and possibilities of utilizing the received by-product (the wool of the unhairing methods) in other productions.

REFERENCES

1. C. S. Cantera, J. Burjan, *World Leather*, **10**, 51, (1997).
2. S. H. Feairheller, M. M. Taylor, D. G. Bailey, W. W. Windus, *J. Am. Lether Chem. Ass.*, **71**, 360 (1976).
3. C. A. Money, *JSLTC*, **80**, 175 (1996).
4. D. Danalev, M. Koleva, D. Ivanova, L. Vezenkov, N. Vassilev, *Protein Pept. Lett.*, **15**, 341 (2008)
5. M. Koleva, D. Ivanova, N. Pepeldjiska, L. Vezenkov, D. Danalev, *JUCTM*, **38**, 385 (2003).

СИНТЕЗ НА ДВА ПЕПТИДНИ МИМЕТИКА КАТО МАРКЕРИ ЗА ХИМИЧНИТЕ ПРОМЕНИ НА КЕРАТИНА НА ВЪЛНАТА ПО ВРЕМЕ НА ПРОЦЕСА НА ОБЕЗКОСМЯВАНЕ И СРАВНЯВАНЕ НА КАЧЕСТВОТО НА ПОЛУЧЕНАТА ВЪЛНА ПО ДВА ЕКОЛОГИЧНИ МЕТОДА НА ОБЕЗКОСМЯВАНЕ

М. Колева[1], Д. Даналев[2]*, Д. Иванова[1], Л. Везенков[2], Н. Василев[3]

[1] Катедра „Текстил и Кожи“, Химикотехнологичен и металургичен университет, бул. „Климент Охридски“ № 8, 1756 София
[2] Катедра Органична химия, Химикотехнологичен и металургичен университет, бул. „Климент Охридски“ № 8, 1756 София
[3] Институт по органична химия с център по фитохимия, Българска академия на науките, ул. „Акад. Г. Бончев“, бл. 9, 1113 София

Постъпила на 4 юли 2008 г.; Преработена на 18 септември 2008 г.

(Резюме)

През последните няколко години основно внимание се обръща на подобряване на съществуващите методи за обезкосмяване на кожи. Основните разработки са насочени към намиране на бързи и ефективни методи за обезкосмяване със запазване на свойствата на получените кожи чрез предварителна алкална обработка и чрез ензимни методи. Процесът на обезкосмяване на овчи кожи с предварителна алкална обработка на вълната води до получаването на два неприродни пептидни миметици лизиноаланин (Lys*-Ala) и орнитиноаланин (Orn*-Ala). Те се получават като резултат от процеса на хидролиза на кератина. Промените в кератина на вълната го правят резистентен към сулфидно разграждане. Ние синтезирахме и охарактеризирахме тези два пептидни миметика. Показана е възможността за използването им като маркери за контрол на промените в кератина на вълната по време на процеса на обезкосмяване. Сравнението, направено между данните на трите проби добита вълна и препоръките за нейното използване показва, че този отпадък може да се счита за суровина (суров материал) съобразно неговите химични и физични показатели.

8th International Symposium on

Electrochemical Impedance Analysis (EIA)

EDITORIAL

The present volume of Bulgarian Chemical Communications includes peer reviewed papers from the 6th issue of Impedance Contributions Online (Volume 6, 2008), the e-journal of the European Internet Centre for Impedance Spectroscopy (EICIS) published in the Centre's web site *http://accessimpedance.iusi.bas.bg*. The electronic issue comprises papers and presentations of key-note lectures, oral communications and posters from the 8th International Symposium on Electrochemical Impedance Analysis (EIA).

The Symposium was organized in combination with the 41st Heyrovsky Discussion, which united the traditions of the two events, ensuring a stimulating collegial atmosphere for creative discussions and exchange of fruitful ideas in the field of Electrochemical Impedance Analysis – the hot point of the impedance studies.

We would like to thank the authors of the papers for their contribution in the 6th issue of *Impedance Contributions Online* and in the present issue of Bulgarian Chemical Communications, our colleagues from the European Internet Centre for Impedance Spectroscopy for their alacrity in making quick and professional reviews of the manuscripts, as well as the editorial board of Bulgarian Chemical Communications for the print edition of the conference papers.

Lubomir Pospišil
J. Heyrovsky Institute of Physical Chemistry,
Academy of Sciences of the Czech Republic

Zdravko Stoynov
Institute of Electrochemistry and Energy Systems,
Bulgarian Academy of Sciences

Bulgarian Chemical Communications, Volume 41, Number 2 (pp. 167–175) 2009

Impedance spectroscopy measurements of phosphatidylcholine bilayers containing ether dibenzo-18-crown-6

M. Naumowicz[1]*, Z. A. Figaszewski[1,2]

[1] *Institute of Chemistry, University of Bialystok, Al. J. Pilsudskiego 11/4, 15-443 Bialystok, Poland*
[2] *Laboratory of Electrochemical Power Sources, Faculty of Chemistry, University of Warsaw, Pasteur St. 1, 02-093 Warsaw, Poland*

Received June 25, 2008; Revised July 15, 2008

The effect of ion carrier crown ether dibenzo-18-crown-6 on the electrochemical features of the phosphatidylcholine bilayer membrane was investigated by impedance spectroscopy. The experiments have been carried out with various forming solution compositions and at various potassium ion concentrations in the electrolyte solution. Potassium chloride was used as the electrolyte. A complex was formed between the dibenzo-18-crown-6 molecule and K^+ ion on the lipid bilayer/electrolyte solution interface. Based on derived mathematical equations, the heterogeneous equilibrium constant (K_h), association rate constant of the complex (k_R) and dissociation rate constant of the complex (k_D) were determined.

Key words: Bilayer lipid membrane, impedance spectroscopy, phosphatidylcholine, crown ether.

INTRODUCTION

Biological membranes show selectivity to penetration of different ions even if their physico-chemical parameters are very similar; selectivity to sodium or potassium ion is a classical example. The carrier theory is an attempt to explain the selectivity of the membranes: the ion is stated to form a transition complex with a membrane component, which enables their transport across the membrane. Some compounds are able to form complexes with mono- or divalent cations. This property makes it possible to use these compounds as artificial ion carriers to the cell or through mitochondrial membranes. Detailed studies on ion transport are facilitated by simple structure of artificial membranes in contrast to that of complex lipid and protein mixtures present in natural membranes. Several classes of macrocyclic compounds are frequently used in the studies on potassium ion penetration through lipid bilayers. Among them, there are depsipeptides like enniatin B or valinomycin and its analogues, polyesters-polyethers like monactin-dinactin and pure polyethers, e.g. crown ethers [1].

Crown ethers have been studied extensively since their discovery nearly four decades ago [2, 3]. Literally, thousands of crown ether derivatives [4] have been prepared and their ability to complex cations [5–7] under equilibrium conditions [8] has been evaluated. In addition, there are numerous reports of cation transport through bulk liquid membranes mediated by crowns of widely varying structures [9]. Sodium and potassium are the two most common cations in solutions *in vivo* and agents that complex and alter their natural balance are expected to exhibit biological effects. Indeed, the toxicity of certain crown ethers was established shortly after their discovery [10–13].

The first one discovered and most versatile of the aromatic crown compounds is dibenzo-18-crown-6 (Fig. 1) yielding 1:1 complex with the potassium ion. The aim of the authors was to utilize electrochemical impedance spectroscopy to study the formation of this complex at the membrane/electrolyte solution interface. The heterogeneous reaction was described by mathematical equations and was further verified experimentally. The following parameters, describing the complex, were determined: association rate constant of the complex, dissociation rate constant of the complex and heterogeneous equilibrium constant.

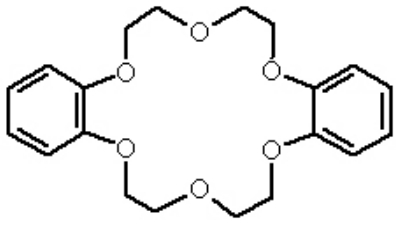

Fig. 1. The structure of 2,3,11,12-dibenzo-1,4,7,10,13,16-hexaoxacyclooctadeca-2,11-diene (dibenzo-18-crown-6).

* To whom all correspondence should be sent:
E-mail: monikan@uwb.edu.pl

THEORY

In the following we base the impedance analysis of the phosphatidylcholine membranes, modified with crown ether dibenzo-18-crown-6, on a model of carrier-mediated ion transport that has already been used for the treatment of phosphatidylcholine membranes containing valinomycin [14]. Specifically, this model assumes that a mobile, positively charged 1:1 complex MS+, is responsible for charge transport through the membrane. The formation of the complexes, which cross the membrane, preferentially occurs at the interfaces, where carrier molecules S from the membrane combine with cations M+ from the aqueous phases. This heterogeneous reaction can be described by rate constants k_R (association, recombination) and k_D (dissociation) and its mechanism can be formally written as:

$$M^+ + S \underset{k_D}{\overset{k_R}{\rightleftharpoons}} MS^+ \tag{1}$$

This reaction is at equilibrium:

$$K_h = \frac{k_R}{k_D} \tag{2}$$

where Kh is the heterogeneous equilibrium constant ($cm^3 \cdot mol^{-1}$).

If the volume concentrations of the complex MS+ and the free carrier S are denoted by c_{MS}^b and c_S^b (expressed in $mol \cdot cm^{-3}$) and the ion activity by a_M (expressed in $mol \cdot cm^{-3}$), the heterogeneous equilibrium constant has the form:

$$K_h = \frac{c_{MS}^b}{c_S^b \cdot a_M} \tag{3}$$

As membrane component concentrations can be related to its surface area by multiplying volume concentrations by the lipid bilayer thickness, the heterogeneous equilibrium constant is given also by the expression:

$$K_h = \frac{N_{MS}}{N_S \cdot a_M} \tag{4}$$

where: N_{MS} - surface concentration of the complex ($mol \cdot cm^{-2}$), N_S - surface concentration of the free carrier ($mol \cdot cm^{-2}$).

Introducing the total carrier surface concentration in the bilayer NT as the sum of complex and free carrier surface concentrations

$$N_T = N_{MS} + N_S \tag{5}$$

and combining Eqns. (4) and (5), the surface concentration of the complex is derived:

$$N_{MS} = \frac{K_h \cdot a_M \cdot N_T}{1 + K_h \cdot a_M} \tag{6}$$

The total quantity of the carrier, added to the solution forming the membrane, can be expressed as follows:

$$c_f V_f = c_m V_m + c_{aq} V_{aq} \tag{7}$$

here: c_f, c_m, c_{aq} – concentrations of the carrier in the membrane-forming solution, the membrane and the electrolyte solution ($mol \cdot cm^{-3}$), respectively; V_f, V_m, V_{aq} – volumes of the membrane-forming solution, the membrane and the electrolyte solution (cm^3), respectively.

The partition coefficient of the carrier γ_S can be represented in the form:

$$\gamma_S = \frac{c_m}{c_{aq}} \tag{8}$$

Therefore, from Eqns. (7) and (8), the total carrier surface concentration can be expressed by the equation:

$$N_T = \frac{\gamma_S \cdot c_f \cdot V_f \cdot d}{\gamma_S \cdot V_m + V_{aq}} \tag{9}$$

in which d is lipid bilayer thickness (cm).

Determination of membrane conductivity R_m^{-1} in terms of Ohm's Second Law yields:

$$R_m^{-1} = \frac{S}{d} \cdot \mu_{MS} \cdot \frac{N_{MS}}{d} \cdot F \tag{10}$$

here: S - membrane surface area (cm^2), μ_{MS} – mobility of the complex ($cm^2 \cdot V^{-1} \cdot s^{-1}$), F – Faraday's constant ($C \cdot mol^{-1}$).

If Eqn. (6) is inserted into Eqn. (10), the following expression for the membrane conductivity as a function of total carrier and/or electrolyte concentration is derived:

$$R_m^{-1} = \frac{S}{d^2} \cdot \mu_{MS} \cdot F \cdot \frac{K_h \cdot a_M \cdot N_T}{1 + K_h \cdot a_M} \tag{11}$$

The k_D value can be determined by the equations determining the real and imaginary parts of transfer across interface impedance [15]:

$$R_{it} = \frac{\nu^2 RT}{n^2 F^2} \cdot \frac{1}{N_{MS} \cdot k_D} \cdot \frac{1}{1 + (\omega / k_D)^2} \tag{12}$$

$$\frac{1}{\omega \cdot C_{\mathrm{it}}} = \frac{\nu^2 RT}{n^2 F^2} \cdot \frac{1}{N_{MS} \cdot k_{\mathrm{D}}} \cdot \frac{\omega / k_{\mathrm{D}}}{1 + (\omega / k_{\mathrm{D}})^2} \quad (13)$$

in which: R_{it} – resistance of the transfer across interface ($\Omega \cdot \mathrm{cm}^2$); C_{it} - capacity of the transfer across interface ($\mu\mathrm{F} \cdot \mathrm{cm}^{-2}$); ν – stoichiometric coefficient of the complex; ω – angular frequency (s^{-1}); R, T, n, F have their meaning.

At low frequencies, where ω is considerably smaller than k_{D}, the above formulae are reduced to:

$$R_{\mathrm{it}} = \frac{\nu^2 RT}{n^2 F^2} \cdot \frac{1}{N_{MS} \cdot k_{\mathrm{D}}} \quad (14)$$

$$\frac{1}{\omega \cdot C_{\mathrm{it}}} = \frac{\nu^2 RT}{n^2 F^2} \cdot \frac{1}{N_{MS} \cdot k_{\mathrm{D}}} \cdot \frac{\omega}{k_{\mathrm{D}}} \quad (15)$$

It results from Eqns. (14) and (15) that the resistance of the transfer across the interface is frequency independent for the frequencies approaching zero, whereas $1/\omega \cdot C_{\mathrm{it}}$ increases proportionally to ω .

At high frequencies, where ω is considerably greater than k_{D}, Eqns. (12) and (13) are simplified into:

$$R_{\mathrm{it}} = \frac{\nu^2 RT}{n^2 F^2} \cdot \frac{1}{N_{MS} \cdot k_{\mathrm{D}}} \cdot \left(\frac{k_{\mathrm{D}}}{\omega} \right)^2 \quad (16)$$

$$\frac{1}{\omega \cdot C_{\mathrm{it}}} = \frac{\nu^2 RT}{n^2 F} \cdot \frac{1}{N_{MS} \cdot k_{\mathrm{D}}} \cdot \frac{k_{\mathrm{D}}}{\omega} \quad (17)$$

It means that the resistance and the capacity of the transfer across the interface approach zero at high frequencies: both $1/\omega \cdot C_{\mathrm{it}}$ and R_{it} decrease with the increasing value of ω.

EXPERIMENTAL

Reagents and preparation of the forming solutions

99% pure egg phosphatidylcholine was purchased from Fluka (Neu-Ulm, Germany) and it had the following fatty acid composition: 16:0 ~ 33%, 18:0 ~ 4%, 18:1 ~ 30%, 18:2 ~ 14%, 20:4 ~ 4%. The 98% dibenzo-18-crown-6 was obtained also from Fluka (Neu-Ulm, Germany). Phosphatidylcholine was dissolved in chloroform to prevent oxidation and the solvent was evaporated in an atmosphere of argon. Dibenzo-18-crown-6 was added as a solution in chloroform (20 $\mathrm{mg \cdot ml^{-1}}$) and the solvent was again removed by argon. Dried residues (phosphatidylcholine or phosphatidylcholine and dibenzo-18-crown-6 mixture) were dissolved in a hexadecane-butanol mixture (10:1 by volume). The forming solutions contained phosphatidylcholine (20 $\mathrm{mg \cdot ml^{-1}}$ of solvent system) or a phosphatidylcholine-dibenzo-18-crown-6 mixture (weight ratios: 100:1, 90:1, 80:1, 70:1, 60:1, 50:1 and 40:1) and were stored at 4°C for less than a week. The method of preparation and storage gave reproducible electrochemical features of the membranes when samples prepared at different times were examined by impedance spectroscopy.

The solvents were of chromatographic purity standard grade: chloroform and butanol were from Aldrich (Milwaukee, WI, USA), hexadecane was from Fluka (Neu-Ulm, Germany).

1, 0.1, 0.01, 0.001 and 0.0001M potassium chloride solutions were used as electrolytes for the experiment. Potassium chloride produced by POCh Co. (Poland) was analytical grade of purity and was calcined prior to use at 400°C for 4 h to remove traces of organic material. Water purified by Milli-Qll (18.2 M, Millipore, USA) was used in all solutions and in all cleaning procedures.

All experiments were performed at room temperature 20 ± 1°C.

Preparation of the bilayer membranes

Bilayer membranes were obtained as bubbles at the Teflon cap, constituting a measuring vessel component. The use of hexadecane as the solvent allows one to obtain membranes of thickness and capacity values similar to those of membranes formed of monolayers [16, 17]; there is almost no solvent retained in the bilayer. Small quantity of butanol has a negligible effect on the impedance parameters of the bilayers created, but however it considerably accelerates the membranes formation. The thinning of the membranes was monitored visually by means of the microscope, which was being reached by reflected white light. The reflected light beam showed the grey colour initially, then, along with decreasing of thickness of the membrane, interference colours were appearing, until the image attained the black colour finally. After obtaining the black colour, the process of forming was ended - no further changes were being observed. The formation of the bilayers was also monitored electrically by measuring the membrane capacitance at low frequency. The capacity of the membranes increased with time after bilayers formation until a steady-state value was reached some 10–20 min later. The measurements started only after the low frequency capacitance became stable; increasing by less than 1% per hour. When the capacitance had stabilized it was assumed that diffusion of solvent out of the bilayer was complete, although some hexadecane molecules might remain “dissolved” in the membrane interior. The bilayers area was determined by a microscope with a micrometer scale built into the

lens and was between 4×10^{-2}–8×10^{-2} cm^2 (the values are given for the bilayers area with subtracted margin).

Impedance analysis

Electrochemical impedance spectroscopy was performed with an a.c. impedance system (EG&G, Princeton Applied Research, Model 388) that included a personal computer, a two-phase lock-in amplifier (Model 5208) and a potentiostat/galvanostat (Model 273), in which a four-electrode input was applied within the pre-amplifier. The electrochemical cell contained two identical reversible silver-silver chloride electrodes and two identical current platinum electrodes, and it was described in details in [18–20]. The use of the four-electrode system in the studies of electric phenomena occurring in membranes, makes it possible to considerably reduce the errors caused by electrode and electrolyte impedance [21, 22]. A 4-mV amplitude sine-wave signal perturbation was applied in the 0.1–10000 Hz frequency range. The PowerSuite 2.4 software package was used for acquisition of impedance data. These data were analyzed using complex nonlinear least squares (CNLS) fit to a model, represented by an equivalent electrical circuit. The CNLS program used in this work was ZSimpWin 3.21.

RESULTS AND DISCUSSION

Dependence of crown ether-modified phosphatidylcholine membranes in a potassium ion medium was measured as function of dibenzo-18-crown-6 concentration using electrochemical impedance spectroscopy. Impedance measurements of the lipid membranes were carried out with unmodified membranes and with membranes modified by seven different carrier concentrations and at five different KCl concentrations. The total carrier surface concentration in the individual forming solution was calculated using Eqn. (9), taking into account the partition coefficient of the carrier to be equal to 1.26×10^3 [23]. The following values NT were obtained: 2.54×10^{-14}, 2.82×10^{-14}, 3.17×10^{-14}, 3.62×10^{-14}, 4.21×10^{-14}, 5.03×10^{-14} and 6.26×10^{-14} mol·cm^{-2}. The arithmetic mean values of the impedance parameters were determined based on six independent measurements of the lipid bilayer.

Fig. 2 depicts typical impedance spectra of the phosphatidylcholine bilayers, both pure and containing dibenzo-18-crown-6. Very simple impedance diagrams were obtained in the absence of crown ether; they had the form of impedance semicircles in the entire analyzed frequency range; it was the evidence that the lipid bilayer was a dielectric layer with leakage (Fig. 2a). The semicircles were distorted because the lipid bilayer itself was not a simple and uniform dielectric layer. The dielectric layer was composed of substructures, which are difficult to extract unless the phase angle can be determined separately at each frequency and very accurately. Karolis *et al*. [17] demonstrated the presence of seven separate elements of lipid bilayer/electrolyte systems on the basis of low frequency impedance measurements of pure phosphatidylcholine bilayers. Four of these can be attributed to the acyl chain, carbonyl, glycerol bridge and phosphatidylcholine regions of the lecithin molecule. The equivalent circuit used for data analysis (Fig. 3a), consists of a parallel arrangement of the capacitor C_m and resistor R_m, attributed to the electrical properties of the bilayer, completed with a serial resistor R_0 for the conductivity of the bulk. The possibility of misinterpretation of the recorded data is reduced by the simplicity of the circuit. This electric circuit is characteristic for an artificial lipid membrane only, when ionophore systems, specific channels-pores and adsorption are absent [24]. Based on this equivalent circuit, the nonlinear least squares analysis was used to simulate the impedance plots; then the values of R_m and C_m were extracted from the fit. The CNLS fit is represented by the solid line in Fig. 2a and it is in good agreement with the data obtained.

The frequency response was drastically different, when ion carrier was added to the membrane (Fig. 2b). The impedance diagrams of the bilayers, modified with crown ether, exhibited capacitive contribution at high frequencies, with the indication of a second semicircle at low frequencies related to potassium ion transport in the area close to the membrane surface. The impedance experiments have been carried out with various forming solution compositions and at various potassium ion concentrations in electrolyte solution. Except for the Z values, all recorded impedance spectra are characterized by common general features and the same dynamic behaviour. For this reason, the data for one KCl concentration and for one ion carrier concentration are shown in Fig. 2b. Fig. 3b represents the equivalent circuit, used to describe the transport of ions through the bilayer. This circuit takes into account the impedance components of the membrane and the impedance representing the situation at the membrane interface. The membrane impedance is composed of the electric capacity of the membrane C_m, and of the electric resistance of the charged complex transport inside the membrane R_m.

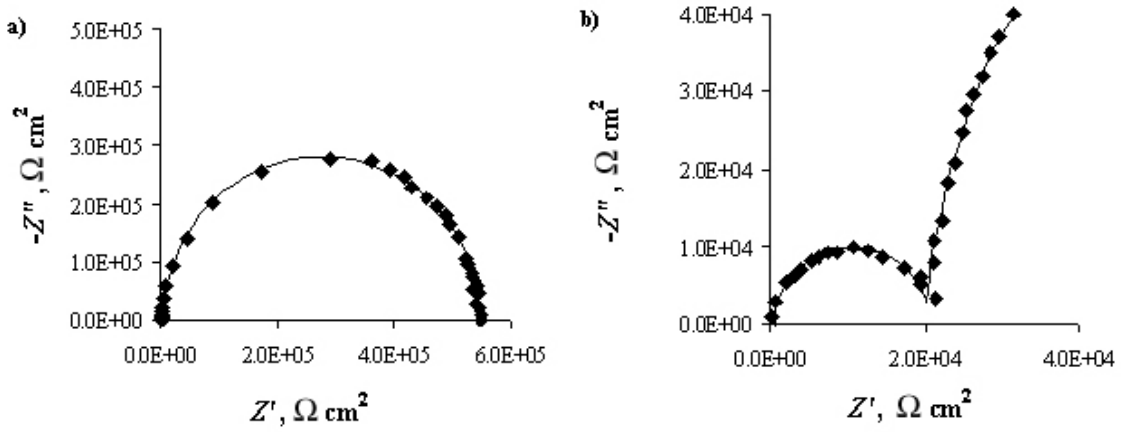

Fig. 2. Impedance diagrams obtained in a solution containing 0.0001 M KCl: a) a membrane made of phosphatidylcholine, b) a phosphatidylcholine bilayer, modified with dibenzo-18-crown-6 (total carrier surface concentration is equal 4.21×10^{-14} mol·cm^{-2}). The solid lines represent the results of the fitting procedure.

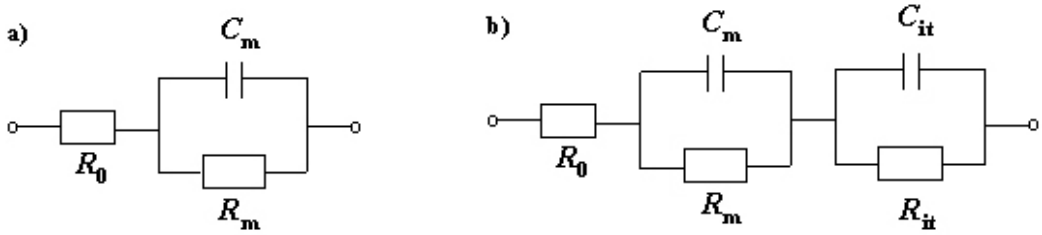

Fig. 3. Equivalent circuits representing the electrical properties of pure phosphatidylcholine membranes (a) and phosphatidylcholine membranes containing dibenzo-18-crown-6 (b). R_0 – electrolyte resistance; C_m and R_m – capacitance and resistance of the membrane, respectively; C_{it} and R_{it} capacitance and resistance of the transfer through interface membrane/electrolyte solution.

Capacity and resistance of the transfer through interface membrane/electrolyte solution are denoted by C_{it} and R_{it}, respectively (subscript it stands for transfer across interface). Based on this equivalent circuit, the nonlinear least squares analysis was used to simulate the plots; then the values of the impedance parameters were extracted from the fit (the CNLS fit is represented by the solid lines in Fig. 2b).

The Figs. 4 and 5 illustrate the experimental values of the R_m^{-1}, C_m, R_{it}, and C_{it} parameters as functions of potassium ion concentration in the solution and of total dibenzo-18-crown-6 surface concentration in the membrane. The presence of the crown ether in the membrane and of the K^+ ion in the solution has no significant effect on membrane capacity, which varies in the 0.6 μF·cm^{-2} < C_m < 0.8 μF·cm^{-2} range (Fig. 4b). This can be explained by the higher water content in the bilayer, which enhanced electric permittivity, and thus, the capacity of the membrane. No clear variation of the membrane capacity values with electrolyte concentration was also observed by other authors who studied the effect of carrier on potassium ion transport through lipid bilayers [25]. The standard deviations are not shown in Figs. 4a, 5a and 5b for the sake of clarity (otherwise, figures would be illegible by close super-imposed data due to too little difference in the impedance parameters values). Deviations amounted up to 5% of the mean capacity of the transfer across interface values and up to 15% of the mean resistance values.

The scatter of the results increased with increasing crown ether concentration as the membrane stability became then poorer. The capacity and resistance of the transfer through interface membrane/electrolyte solution values were not determined for 1 M KCl because the formation of a second semicircle was observed to start at a KCl concentration as high as 0.1 M KCl.

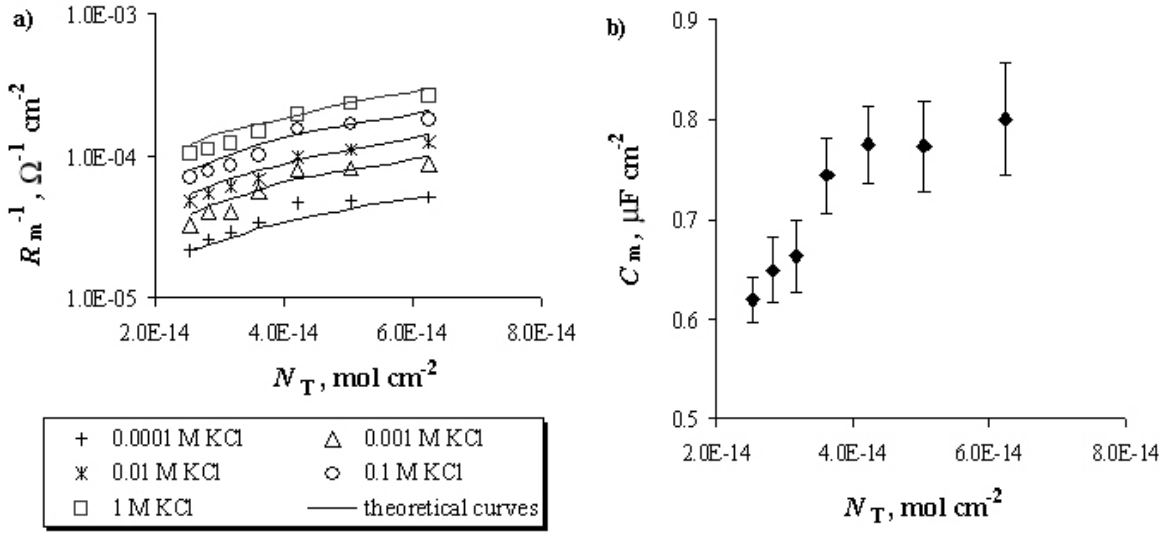

Fig. 4. The dependence of the conductance of the membrane (a) and the capacitance of the membrane (b) on the total dibenzo-18-crown-6 surface concentration at various electrolyte concentrations. The experimental values are marked by points and the theoretical values by solid lines.

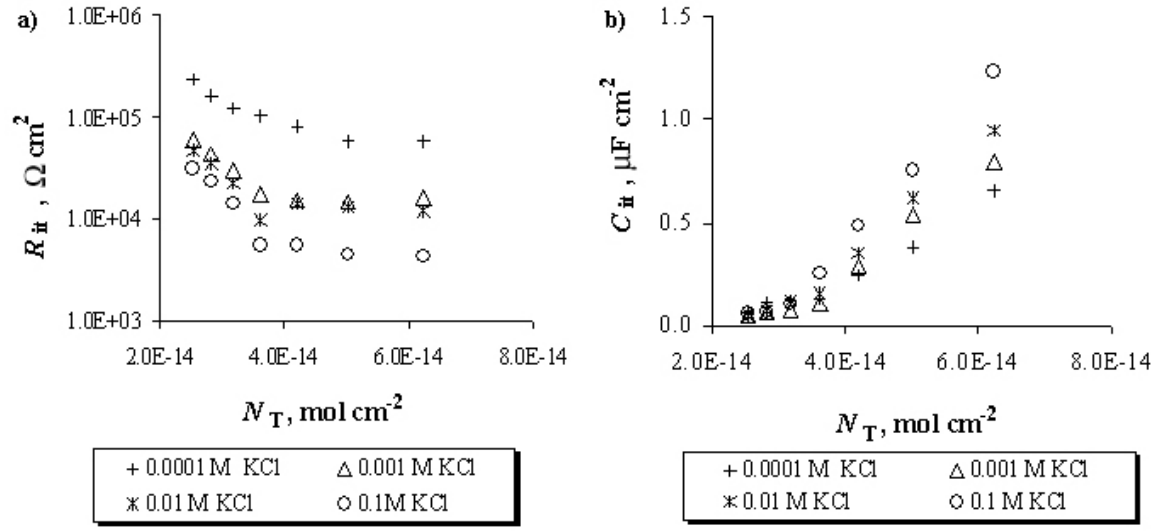

Fig. 5. The dependence of the resistance of the transfer across interface (a) and the capacitance of the transfer across interface (b) on the total dibenzo-18-crown-6 surface concentration at various electrolyte concentrations.

Analyzing the data represented in Figs. 4 and 5 it is possible to state, that an increase in potassium ion concentration at constant dibenzo-18-crown-6 surface concentration provokes a noticeable decrease in Rm (Fig. 4a) and in Rit (Fig. 5a) as well as a noticeable increase in Cit (Fig. 5b). Similarly, both resistances decrease and the capacity of transfer across interface increases with increasing carrier concentration at constant potassium ion concentration (increasing membrane conductivity). The increase in conductivity was due to the increasing amount of the dibenzo-18-crown-6-K^+ complex in the membrane, resulting from increasing potassium ion and crown ether concentration. The complex is more soluble in the hydrophobic phase than the hydrated potassium ion itself is. The conductivity increases in the presence of such a complex in the lipid phase, because the macrocyclic compound-potassium ion complex has a net positive charge. This point of view is supported by the results of the study of membrane non-isothermal potential and of kinetic studies on biphasic extraction [26 and literature cited there in].

There are several classes of macrocyclic compounds, which can yield observable changes in the selective K^+ permeability of the lipid membranes; the most important among them are depsipeptides and polyethers. The number of ring atoms in these active compounds varies from 18 in the case of enniatin B and dibenzo-18-crown-6 to 36 in valino-

mycin. Enniatin B and dibenzo-18-crown-6 affect the membrane resistance to much weaker extent than valinomycin and the polyene antibiotic, monactin-dinactin, with a 32-atom ring. Polyethers with less than 18 ring atoms cause a greater permeability increase through the lipid bilayer for the sodium ion than that for the potassium ion. Although the substituents on the rings vary in these different compounds, they are all aliphatic in character and lack functional groups. All these compounds, which are able to increase the permeability of the lipid bilayer to the potassium ion, are uncharged [1, 27].

According to Eqn. (11), the membrane conductivity can be expressed as a function of total carrier and/or electrolyte concentration. This Eqn. (11) is of the $y = ax$ type, where: $y = R_m^{-1}$, $x = N_T$ and $a = (S/d^2)\cdot\mu_{MS}\cdot F\cdot(K_h\cdot a_M)/(1 + K_h\cdot a_M)$. The a coefficient was determined using linear regression and it was applied to present the agreement of the Eqn. (11) data (solid lines) with the experimental data (points) in Fig. 4a. It can be seen from this figure that the agreement between the experimental and theoretical points is good, which verifies the correctness of equations presented in this article. From the linear dependence of the membrane conductance on the total crown ether surface concentration one can conclude that a single dibenzo-18-crown-6 molecule is the smallest transporting unit and that this molecule participates as a carrier but not as a channel [28]. The linear increase in the transport of cations together with the growing concentration of crown ether is in agreement with the classical carrier model for ion transport [29]; such a behaviour being observed also in case of polymer [30] and liquid [31] membranes, modified with dibenzo-18-crown-6. The conductance is also proportional to the potassium ion concentration logarithm; this dependence is illustrated graphically in Fig. 6. This fact, together with the Fig. 4a data, suggests that the 1:1 dibenzo-18-crown-6-K^+ complex is the carrier of charge in the membrane.

The above equation can be presented in another way, more suitable for calculation:

$$\frac{p}{a_M} = \frac{S}{d^2}\cdot\mu_{MS}\cdot F\cdot K_h - K_h\cdot p \qquad (19)$$

This equation is of the $y = ax + b$ type, where: $y = p/a_M$, $x = p$, $a = K_h$ and $b = (S/d^2)\cdot\mu_{MS}\cdot F\cdot K_h$.

The heterogeneous equilibrium constant of the 1:1 dibenzo-18-crown-6-K^+ ion complex formation calculated based on the parameter a amounts to about 3.43×10^3 $dm^3\cdot mol^{-1}$.

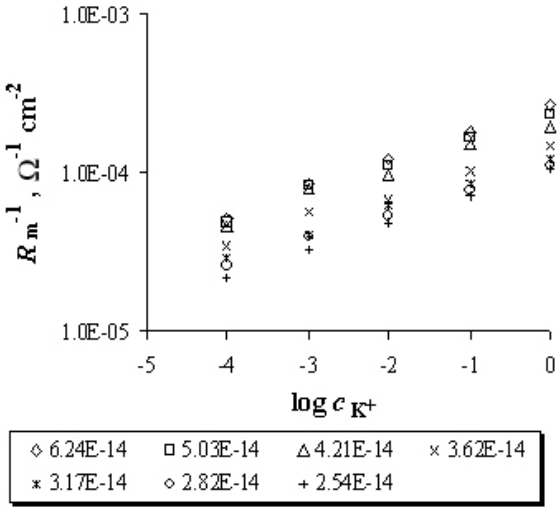

Fig. 6. The dependence of the conductance of the membrane on potassium ion concentration logarithm at various total dibenzo-18-crown-6 surface concentrations.

The values of the stability constants for the 1:1 complexes of the potassium ion with dibenzo-18-crown-6 in various solvents [32–40] are shown in Table 1. The nature of solvent plays the most important role in the complexation reaction because general and specific solvation effects differ in complexed and uncomplexed states [32]. The method of the measurement and the applied counter-ion has a smaller influence on the values of stability constant. The systems in which solvents are showing various solvating effects (from very solvating water to almost inert 1,2-dichloroethane) are represented in Table 1. The data collected in Table 1 reveal that the formation constants of the 1:1 dibenzo-18-crown-6-K^+ ion complexes in inert solvents (1,2-dichloroethane) are quite large compared with those in solvating solvents, for example, 10^8 times larger than those in water and 10^4 times larger than those in methanol. The desolvation process plays an important role in the complexation in solutions. Particularly, it was reported that the desolvation of metal ions has a large effect in solvating solvents [41].

Table 1. Selected values of stability constants of K^+ complexes with dibenzo-18-crown-6 in solvents differring in polarity at 25ºC.

Solvent	log$K$	References
water	1.74	[33, 34]
acetonitrile	4.80	[35]
metanol	5.00	[32, 36]
	5.08	[35]
nitromethane	5.94	[34]
	5.39	[37]
nitrobenzene	6.90	[38]
1,2-dichloroethane	9.36	[39]
	9.90	[40]

The value of heterogeneous equilibrium constant presented in this paper describing the chemical reaction at the interface between a carrier molecule from the membrane and a potassium ion from the aqueous phase ($\log K_h$ is equal to 3.54) shows how strong is cation solvation by water in the examined system.

In order to determine the value of dissociation rate constant of the complex and to propose a correct equivalent circuit to reproduce the electric properties of the phosphatidylcholine membrane, modified with crown ether, the experimental data were substituted both in Eqns. (14, 15) and (16, 17). The results were found to agree at low frequencies as it has been shown in Fig. 7 for the imaginary part of the impedance.

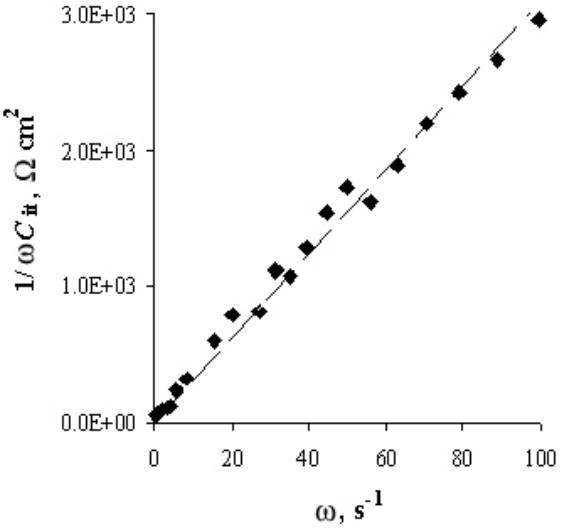

Fig. 7. Frequency dependence of the imaginary part of impedance (f < 15.85 Hz).

This fact was decisive in view that the transfer across interface parameters could be related to the semicircle occurring in the impedance spectrum at low frequencies. The mean k_D value determined from Eqns. (14) and (15) amounts to (133 ± 40) s^{-1}. With the dissociation rate constant of the complex being known, the association rate constant was thus calculated from the $k_R = K_h \cdot k_D$ relationship. The resulting value was $(4.56 \pm 1.37) \times 10^5$ $M^{-1} \cdot s^{-1}$. The dissociation and association rate constant values of the complex have not been reported in the available literature of the subject.

***Acknowledgements**: This work was supported by a grant from the Polish Committee of Scientific Research No 1 T09A 070 30.*

REFERENCES

1. D. C. Tosteson, *Fed. Proc.,* **27**, 1269 (1968).
2. C. J. Pedersen, *J. Am. Chem. Soc*., **89**, 2495 (1967).
3. C. J. Pedersen, *J. Am. Chem. Soc*., **89** 7017 (1967).
4. G. W. Gokel, W. M. Leevy, M. E. Weber, *Chem. Rev*., **104**, 2723 (2004).
5. R. M. Izatt, J. S. Bradshaw, S. A. Nielsen, J. D. Lamb, J. J. Christensen, D. Sen, *Chem. Rev*., **85**, 271 (1985).
6. R. M. Izatt, K. Pawlak, J. S. Bradshaw, R. L. Bruening, *Chem. Rev*., **91**, 1721 (1991).
7. R. M. Izatt, J. S. Bradshaw, K. Pawlak, R. L. Bruening, B. J. Tarbet, *Chem. Rev*., **92**, 1261 (1992}.
8. Cation Binding by Macrocycles, Y. Inoue, G. W. Gokel (eds.), Marcel Dekker, New York, 1990.
9. B. A. Moyer, in: Molecular Recognition: Receptors for Cationic Guests, G. W. Gokel (ed), vol. 1, Comprehensive Supramolecular Chemistry, J. L. Atwood, J. E. D. Davies, D. D. MacNicol, F. Vögtle, and J.-M. Lehn (eds.), Pergamon, Elsevier, Oxford, 1996, p. 377.
10. C. J. Pedersen, *Org. Synth*., **52**, 66 (1972).
11. R. R. Hendrixson, M. P. Mack, R. A. Palmer, A. Ottolenghi, R. G. Ghirardelli, *Toxicol. Appl. Pharmacol*., **44**, 263 (1978).
12. K. Takayama, S. Hasegawa, S. Sasagawa, N. Nambu, T. Nagai, *Chem. Pharm. Bull*., **25**, 3125 (1977).
13. S. C. Gad, W. J. Conroy, J. A. McKelvey, R. A. Turney, *Drug Chem. Toxicol*., **1**, 339 (1978).
14. M. Naumowicz, J. Kotyńska, A. D. Petelska, Z. A. Figaszewski, *Eur. Biophys*. J., **35**, 239 (2006).
15. K. J. Vetter, Elektrochemische Kinetik, Springer-Verlag, Berlin, 1961.
16. R. Benz, O. Fröhlich, O. Läuger, M. Montal, *Biochim. Biophys. Acta*, **374**, 323 (1975).
17. C. Karolis, H. G. L. Coster, T. C. Chilcott, K. D. Barrow, *Biochim. Biophys. Acta*, **1368**, 247 (1998).
18. M. Naumowicz, A. D. Petelska, Z. A. Figaszewski, *Cell. Mol. Biol. Lett*., **8**, 5 (2003).
19. M. Naumowicz, Z. A. Figaszewski, *Bioelectrochem.*, **61**, 21 (2003).
20. M. Naumowicz, A. D. Petelska, Z. A. Figaszewski, *Electrochim. Acta*, **50**, 2155 (2005).
21. S. Kalinowski, Z. A. Figaszewski, *Meas. Sci. Technol*., **6**, 1043 (1995).
22. S. Kalinowski, Z. A. Figaszewski, *Meas. Sci. Technol*., **6**, 1050 (1995).
23. W. F. Nijenhuis, E. G. Buitenhuis, F. de Jong, E. J. R. Sudhölter, D. N. Reinhoudt, *J. Am. Chem. Soc*., **113**, 7963 (1991).
24. P. Krysiński, *Post. Biochem*., **28**, 227 (1982).
25. R. Naumann, D. Waltz, S. M. Schiller, W. Knoll, *J. Electroanal. Chem*., **550-551**, 241 (2003).
26. G. Scibona, B. Scuppa, C. Fabiani, M. Pizzichini, *Biochim. Biophys. Acta*, **512**, 41 (1978).
27. W.-Y. Hwang, J.-S. Shih, *J. Chin. Chem. Soc*., **47**, 1215 (2000).
28. P. Läuger , *Science*, **178**, 24 (1972).
29. P. Läuger, *J. Membrane Biol*., **57**, 163 (1980).
30. A. J. Schow, R. T. Peterson, J. D. Lamb, *J. Membrane Sci*., **111**, 291 (1996).
31. D. W. Jr. McBride, R. M. Izatt, J. D. Lamb, J. J. Christensen, in: Inclusion Compounds III, J. L.

Atwood, J. E. D. Davies, D. D. Mac Nicol (eds.), Academic Press, London, 1984, p. 571.
32. E. Weber, F. Vőgtle, in: Host Guest Complex Chemistry I, F. L. Boschke (ed.), Akademie-Verlag, Berlin, 1982, p. 1.
33. R. M. Izatt, R. E. Terry, B. L. Haymore, L. D. Hansen, N. K. Dalley, A. G. Avondet, J. J. Christensen, *J. Am. Chem. Soc*., **98**, 7620 (1976).
34. S. Katsuta, Y. Ito, Y. Takeda, *Inorg. Chim. Acta*, **357**, 541 (2004).
35. Y. Takeda, *Bull. Chem. Soc. Jpn*., **56**, 866 (1983).
36. H. K. Frensdorff, *J. Am. Chem. Soc*., **93**, 600 (1971).
37. H. D. Inerowicz, J. Chojnacki, A. Merz, T. Futterer, *J. Inclusion Phenom. Mol. Recognit. Chem*., **38**, 123 (2000).
38. Y. Yoshida, M. Matsui, K. Maeda, S. Kihara, *Anal. Chim. Acta*, **374**, 269 (1998).
39. Y. Kikuchi, Y. Sakamoto, *Anal. Chim. Acta*, **370**, 173 (1998).
40. A. Sabela, V. Marecek, Z. Samec, R. Fuoco, *Electrochim. Acta*, **37**, 231 (1992).
41. V. P. Solov'ev, N. N. Strakhova, O. A. Raevsky, V. Rüdiger, H. J. Schneider, *J. Org. Chem*., **61**, 5221 (1996).

ИЗМЕРВАНИЯ НА ДВОЙНИ СЛОЕВЕ ОТ ФОСФАТИДИЛХОЛИН СЪДЪРЖАЩИ ДИБЕНЗО-18-КОРОНЕН-6 ЕТЕР ЧРЕЗ ИМПЕДАНСНА СПЕКТРОСКОПИЯ

М. Наумович[1]*, З. А. Фигашевски[1,2]

[1] *Химически институт, Университет на Бялисток, бул. „Й. Пилсудски" 11/4, Бялисток 15-443, Полша*
[2] *Лаборатория за електрохимични източници на ток, Химически факултет, Варшавски университет, ул. „Пастьор" № 1, Варшава 02-093, Полша*

Постъпила на 25 юни 2008 г., Преработена на15 юли 2008 г.

(Резюме)

Изследван е ефектът на йонно проводим дибензо-18-коронен-6 етер върху електрохимичните свойства на двуслойна мембрана от фосфатидилхолин чрез импедансна спектроскопия. Експериментите са проведени с различни композиции образуващи разтвор и при различни концентрации на калиевите йони в електролитния разтвор. Като електролит е използван калиев хлорид. На междуфазовата граница липиден двоен слой/електролит се образува комплекс между калиевия йон и молекулата на коронния етер. На основата на математически уравнения са определени константата на хетерогенно равновесие (K_h), константите на скоростта на образуване (k_R) и на скоростта на дисоциация на комплекса (k_D).

Bulgarian Chemical Communications, Volume 41, Number 2 (pp. 176–184) 2009

Experimental critical analysis of plate impedance

C. V. D´Alkaine[1]*, G. A. de Oliveira Brito[1], C. M. Garcia[2], P. R. Impinnisi[2]

[1] *Group of Electrochemistry and Polymers, Chemistry Department, Federal University of São Carlos, R. Washington Luiz Km 234, CEP 13560-905, São Carlos (SP), Brazil*
[2] *Batteries Laboratory, Institute of Technology for Development-LACTEC, UFPR Polytechnic Centre, POBox 19067, CEP 81531-980, Curitiba (PR), Brazil*

Received June 24, 2008: Revised September 12, 2008

Taking into account that there are no experimental proofs that Electrochemical Impedance Spectroscopy (EIS) four electrode plate cell measurements can be attributed only to the central plate, in the present work measurements with variable counter-electrode plate areas and one and the same central plate were made. This was done in a frequency range from 10^4 to 10^{-2} Hz and at different central plate states of charge. The results show that for positive-negative-positive plate ensembles, at all studied frequencies and state of discharge, the EIS data can be attributed to the central negative plate, except for the highest counter-electrode/central working electrode areas ratio, *r*, and higher discharge levels, at the lower studied frequencies. Instead of that, for negative-positive-negative ensembles, the EIS data can be attributed to the central positive plate only at the high and middle studied frequencies in all discharge levels and area ratios. Totally charged central positive plates must be excluded because their impedance depends on the counter-electrode area at all *r* ratios. All these results are discussed and suppositions are made for their interpretation.

Key words: electrochemical impedance spectroscopy, four electrode EIS method, single plate EIS, counter-electrode variable area, lead acid battery plate EIS.

1. INTRODUCTION

The Electrochemical Impedance Spectroscopy (EIS) of porous electrodes has been studied theoretically [1–7] and experimentally [6–12]. From theoretical point of view, most of the models have been based on one pore model EIS [1], sometimes not taking into account the surface in which the pore is present. From experimental point of view, there are results on many different pores structures, going from simple roughness surfaces [6] to the most varied real porous electrodes [6–12].

Theoretical work on a single pore has shown that EIS depends on the pore shape, if this is located on a conductive metal surface [2]. At low frequencies, the theoretical EIS tends to show a simple capacity behavior (a straight line perpendicular to real axis, in Nyquist's plot). This straight line gives at the real axis, by extrapolation, something near to an average resistance of the inner solution inside the pore. Nevertheless, the equations without extrapolation at middle and high frequencies, due to different inner solutions resistances for each pore surface region, give EIS values shifted to the left in Nyquist's plot. This is because there is a.c. current distribution, due to these resistance differences. They give rise to a lower real impedance component, which produces a shift to the left of simple capacity behavior at low frequencies. This fact can even give rise to a partial capacity loop, followed at low frequencies by the capacity behavior, when the pore has a geometrical drop shape [2].

The experimental data with flat metal electrodes [13] give results, which seem to indicate one constant phase angle component. In contrast to that, powder metal electrodes seem to give two different phase angles components, at two different frequency ranges [8].

Considering EIS experimental data from real porous systems, the simple capacity behavior has never been observed. In general, EIS plots of real porous systems [6–12, 14] present inductive loops at very high and low frequencies. In the middle frequency range, they can have one or more capacity loops. The observed structures are different in different frequency ranges because the current related to the perturbation will go deeply inside the porous structure when the frequency is reduced [9, 10]. This is valid only for electrode materials, which have reasonable electronic conductance.

In the specific case of lead acid batteries EIS measurements, several papers have been published on batteries "as received" from factory [14–18]. On the other hand, papers have been published on open batteries. This permits access to the plates and introducing a reference electrode [15, 19]. This procedure refers to battery configuration of succes-

* To whom all correspondence should be sent:
E-mail: dalkaine@dq.ufscar.br

sive plates: positive-separator-negative-separator-positive-etc., with positive and negative plate ensembles. For this kind of configuration, several papers attribute the measured impedance to one of the ensembles [14–17]. Nevertheless, it has not been demonstrated experimentally that the total impedance can be attributed only to one plate ensemble. This is true even having one of the ensembles one plate in excess. On the other hand, if in this configuration the system is discharged, the two ensembles of plates will be discharged, in general, under different conditions and the external plate working solution will be depleted during the discharge. This last problem is not solved by waiting for some time to come to the rest potential, before the EIS measurement.

To solve the problem of two ensembles of plates (positive and negative), there are papers that reduce the configurations only to negative-separator-positive(central)-separator-negative (NspsN) or positive-separator-negative(central)-separator-positive (PsnsP) ensembles [19–21]. These configurations, depending on the cell dimensions and waiting time before EIS measurements, can have or not variation of external solution concentration when the system is discharged or charged. Beside this, in these systems the problem of attributing the total impedance to central plate, as stated in references [19–21], has not been experimentally demonstrated. Is the introduction of two counter-electrode plates enough to disregard their impedance contributions? A more difficult problem is the case NspsN configurations, because the BET surface area of positive active mass can be 10 to 20 times higher than the negative one [22]. This problem also affects studies without separators, where the cell has negative-positive-negative (NpN) configuration, like in references [23, 24], or positive-negative-positive (PnP) configuration. Nevertheless, these kinds of configurations are nearer to the traditional form to do EIS measurements.

The EIS measurements in the literature, with the pointed out problems, have also been made at different states of charge or discharge, in general, considering they can be referred only to the central plate. These measurements have been made during charge or discharge [17], sometimes, after stopping charge or discharge and waiting [23].

Nevertheless, it is possible to point out for all these kinds of configurations that all literature results present common patterns. In general, for NspsN or PsnsP or NpN or PnP configurations or even batteries, EIS results can be presented in Nyquist plots: a) an inductive loop at high frequencies; b) at least, as a minimum, a capacity loop at middle and low frequencies and c) even a new inductive loop at very low frequencies. Some papers [21] have found this last very low frequency inductive loop during intermediate states of discharge. Sometimes, these components do not appear, depending on the kind of plates, measurement cell characteristics, ways to obtain EIS data, used frequencies range and state of discharge (or charge). Finally, total charged systems seem to have particular behaviour [24], at least for NpN configuration.

The problem to disregard the counter-electrode plate contributions in a four electrode plate cell (a central working plate electrode, two lateral counter-electrode plates of opposite polarity and a reference electrode) will be central objective in the present work. To do that, external solution concentration will be maintained constant and counter-electrode plate surface area will be varied, maintaining the central working plate electrode at the geometrical centre of the ensemble. The work results, if they really give the central working plate impedance, will permit us to state with certainty, which are the real EIS results for negative (in PnP configuration) and positive (in NpN configuration) plates, at constant external concentrations and different states of discharge.

EXPERIMENTAL

The used experimental set-up was a four-electrode configuration (a working central plate electrode, two lateral plate counter-electrode and a reference one) shown in Fig. 1a for the discharge cell of the central plate and in Fig. 1b, for the EIS measurement cell. These permit two configurations for the EIS measurement cell, the positive-negative-positive one (PnP) and the negative-positive-negative one (NpN), which will be referred to in all the discussions. In the measurement cell the counter-electrodes were of variable area with the central electrode always in the centre of them. The distances between the lateral counter-electrodes and the central one were 3 cm in both cells, to maintain the external solution concentration constant in the discharge cell and to be able to place and to remove the central electrode in both cells. The cell solutions were always 4.6 M H_2SO_4 and the reference electrodes always $Hg/Hg_2SO_4/4.6$ M H_2SO_4, in regard to which all potentials will be given. The reference electrodes in both cells were always located near the central working one (see Figures 1a and 1b).

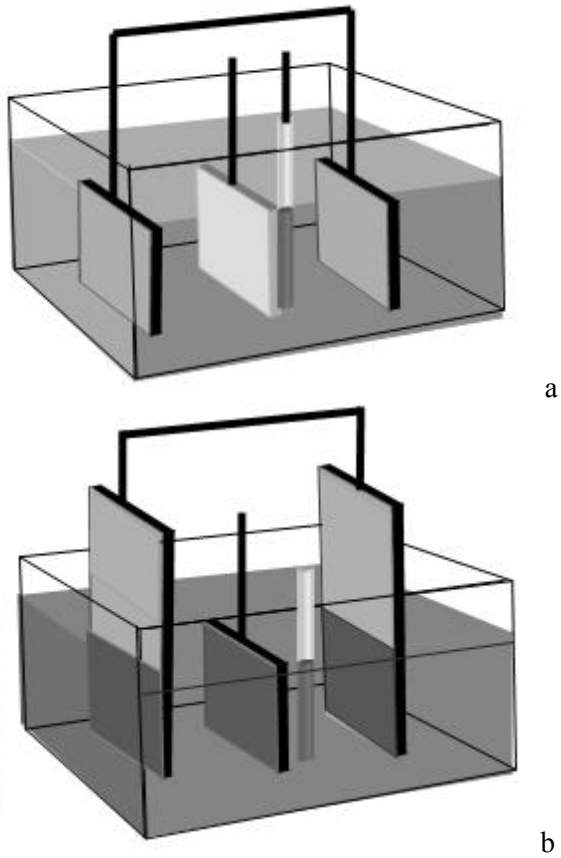

Fig. 1. Four electrode configuration with a central working plate, two lateral counter-electrode plates and a reference electrode. (a) Charge and discharge cell; (b) EIS measurement cell with variable counter-electrode area.

The electrode plates were real battery plates, removed from stationary batteries of two different sizes. The central electrodes were removed from a 12 Ah/6 Volts VRLA battery and the counter electrodes from a 600 Ah/2 Volts VRLA battery. All measurements, in the discharge and the EIS measurement cells, were made using the same central working electrode plate and counter-electrodes. The use of the same central plate was made because different plates can give slightly different data, which fact does not affect the results.

The central negative or positive working electrode plate dimensions were 4.4×6.6 cm (geometrical area about 60 cm^2 double face). Their real capacities, after stabilization, were 2.6 Ah for the negative plate electrode and 3.0 Ah for the positive one, in C_{20} discharge rates. These values will be used to calculate the state of discharge given in percentages, Q_d. The Q_d is in regard to the above real capacities. For the discharge cell, the counter-electrode plates had the same central working plate dimensions (see Fig. 1a) and they were always initially fully charged. On the other hand, counter-electrode dimensions for EIS measuring cell were 14.0×20.0 cm (total geometrical area 280 cm^2 single face), always with the same width (14.0 cm) and initially fully charged. To vary counter-electrode area in the EIS measurement cell, these counter-electrode plates were partially immersed at different depth (see Fig. 1b). This gives rise to counter-electrode geometrical immersed single face areas of: a) 45 cm^2 (14.0×3.2 cm), b) 110 cm^2 (14.0×7.9 cm) and c) 205 cm^2 (14.0×4.6 cm). The different area ratios between counter-electrodes and central plates (single areas), called *r*, will be expressed as 1.5/1.0, 3.7/1.0 and 6.8/1.0, respectively. For measurements and discussions, these last values will be used. The positive real counter-electrode capacity, totally immersed, was 25 Ah at a C_{20} rate and that of the negative one, 22 Ah. The central working plates were always fully immersed and located, as near as possible, in the centre of the two counter-electrode immersed areas.

In the discharge cell, the partial or total discharges of the central plate were performed galvanostatically. For central negative plates the current density was 2.5 $mA \cdot cm^{-2}$ (double face), at C_{17} discharge rate. For positive central plates this current density also was 2.5 $mA \cdot cm^{-2}$ (double face), at a C_{20} discharge rate. In cases of total state of discharge, the cutting potential was up to –0.70 V for central negative plates and 1.05 V for the central positive plates.

To perform the impedance measurements, the central electrode at a given state of discharge was removed, each time, from the discharge cell (Fig. 1a) and immersed into the EIS measurement cell (Fig. 1b) with a given *r*.

The EIS data were obtained in different states of discharge using a Gamry Impedance System. The EIS galvanostatic measurements were made at the rest reversible potential (zero continuous current) and only after two hours of immersion in the measurement cell, at open circuit potential. A sinusoidal perturbation of 1 mA rms amplitude was used, in the linear region, with a frequency range from 10^4 to 10^{-2} Hz and 10 points per decade.

RESULTS AND DISCUSSIONS

Taking into account that BET negative plate surface areas are about 0.5 $m^2 \cdot g^{-1}$, while those of positive plate can be from 5 to 10 $m^2 \cdot g^{-1}$, we shall be firstly analyzed data from PnP configuration. This configuration can be considered as having enough real area ratio *r*, between counter and working electrodes. On the other hand, data from NpN configuration could have area ratio problems.

This is why it will be discussed later. The problem is the geometrical counter-electrode area duplication (which does not mean real area duplication) that could be not enough, in NpN configuration. A high real area ratio *r* permits to disregard, in EIS measurements, counter-electrode impedance contribution. In both cases, PnP and NpN configurations, the analysis will begin with completely charged and discharged working electrode plates (central plates), discharged up to the cutting potential. Finally, changes on the polarization resistances of found capacity loops at different state of discharge of both configurations will be discussed.

The PnP configuration

In Fig. 2 EIS results are plotted of the PnP configuration with totally charged and discharged working plates, for different *r* values. For *r* 3.7/1.0, the working electrode was over discharged beyond the cutting potential, to show that for negative plate the impedance module in these states of discharge becomes very much larger. This must be related to the fact that new products are formed on electrode pore surface. This does not happen in the case of positive plate, showing that negative and positive plates have different behaviors even when, in general, it is considered that they give as discharge final product the same material: insoluble $PbSO_4$.

A second point observable in Fig. 2 is that, as expected for PnP configuration at the different *r* values, the charged or totally discharged plates, give the same Nyquist's plot. These results show that there is no *Z* dependence on *r*. The *Z* independence on *r* shows that the counter-electrode impedance can be disregarded. Nevertheless, there is an exception for highest *r* of charged plates. The explanation of 6.8/1.0 *r* value can be related to the existence of a non-uniform current distribution at the central plate, due to its specific geometrical configuration. To consider that the 6.8/1.0 result is the correct one is wrong. This is because it is incompatible with the other *r* values results.

A final point which arises from Fig. 2 is the fact that impedance imaginary components at the lowest measured frequency are equal inside the ensembles of charged or discharged negative plates. Nevertheless, the real component increases from charged to discharged plates, in agreement with the discharge growth. In connection with this fact, it must be taken into account that the impedances have been measured after 2 hours of stabilization in the measurement cell. In the charged cases, this implies auto-discharge reactions, producing very low discharge levels, which makes the charged and discharged electrodes not so different.

The EIS results for PnP configuration in intermediate states of discharge can be seen in Fig. 3 (Q_d 30%), Fig. 4 (Q_d 60%) and Fig. 5 (Q_d 90%). In all these figures, to compare the data for different *r* values, the serial resistance at high frequencies (R_s) for the highest *r* value was used as reference, shifting the other data. This was done at the respective inlets.

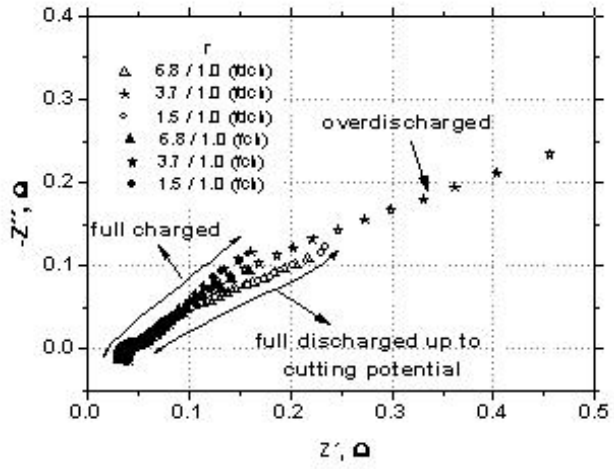

Fig. 2. PnP configuration EIS data under fully charged or fully discharged conditions, showing a case with central plate over discharge. Different *r* are pointed out in the figure. Fully charged: full symbols; fully discharged: open symbols.

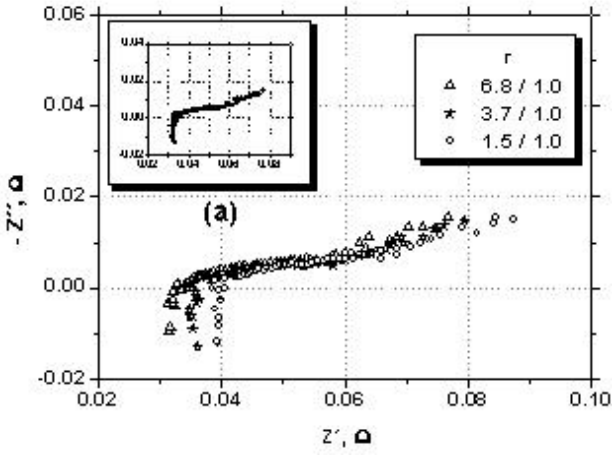

Fig. 3. PnP configuration EIS data for 30% state of discharge. Different *r* values pointed out in the figure. (a) Data shifting to coincide R_s at its lower value.

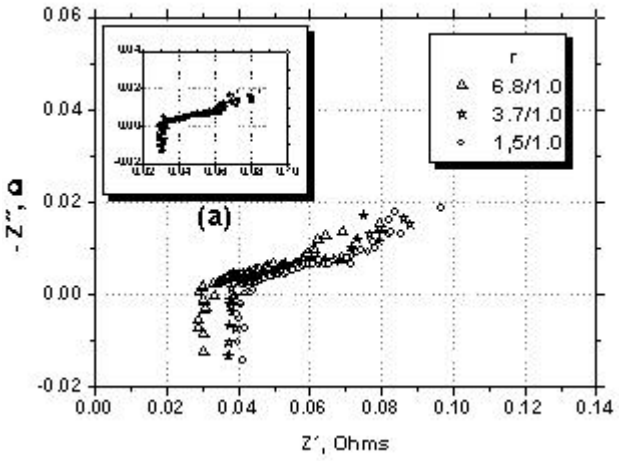

Fig. 4. PnP configuration EIS data for 60% state of discharge. Different *r* values pointed out in the figure. (a) Data shifting to coincide R_s at its lower value.

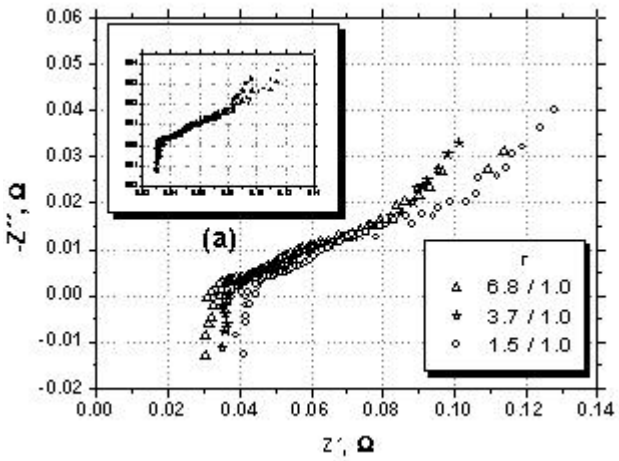

Fig. 5. PnP configuration EIS data for 90% state of discharge. Different *r* values pointed out in the figure. (a) Data shifting to coincide R_s at its lower value.

It is important to point out that R_s´s and, as a consequence, the differences between them are the same at each *r* in the three figures (the last ones giving approximately 0.032 Ω for 6.8/1.0, 0.035 Ω for 3.7/1.0 and 0.040 Ω for 1.5/1.0, with an error of ± 0.001 Ω). These differences agree quite well with theoretical calculations for different *r* values for the differences in solution resistances.

Figs. 3 and 4 show after shifting (see the inlets) that the data overlap for different *r*. This means that, in agreement with Fig. 2, the *Z* of the counter-electrode can correctly be disregarded. On the other hand, when discharge progresses, the real and imaginary *Z* components observed at the inlets, for the lowest frequency, practically do not grow (approximately, Z_{im} of 0.018 Ω and Z_{real} of 0.08 Ω). This fact is in agreement with the idea that the discharge reaction follows a zone reaction pattern [25].

When these data are compared with those at 90% of discharge, Fig. 5, a new aspect appears: the impedance differences for all the *r* ratios at low frequencies (see the inlet). It is like as if, with the reaction zone arriving to the end of plate pores a non-uniform current distribution appears influencing impedance measurements. The fact is interesting because in the evolution from Q_d 90% to 100% (total state of discharge), this situation disappears, as it is seen in Fig. 2. The supposition to accept as explanation of the above facts that the value of counter-electrode impedance cannot be disregarded, is incorrect. This is because the measured impedance has grown in view of Figs. 3 and 4 and the phenomenon occurs only at low frequencies. It is important to note that all these facts are totally reproducible with a given plate.

The NpN configuration

In Fig. 6, equivalent data to those in Fig. 2 are shown for NpN configurations. For this configuration, the two sets of data, for charged and discharged conditions, present problems in EIS measurements. This is because for both cases the impedance depends on *r*, for any value of this parameter. This is indicating that, in principle, counter-electrode impedance cannot be disregarded at least for *r* 1.5/1.0 and 3.7/1.0. The data for 6.8/1.0 must not be considered because it looks like presence of current distribution problems. All these are in agreement with the BET area ratios for negative and positive plates. Nevertheless, even considering that the central plate true impedance is not attainable, it is interesting to point out that in all these cases there is an important growth of the imaginary and real impedance components from charged to discharged central plates. This can be clearly seen at the lowest frequency. Here the impedance measurements under charged conditions were also made after sufficient waiting time during which some discharge can occur. These data are pointing out the differences in positive and negative plate behaviors in relation to discharge process, even when it is considered in the literature that both give the same final product: insoluble $PbSO_4$.

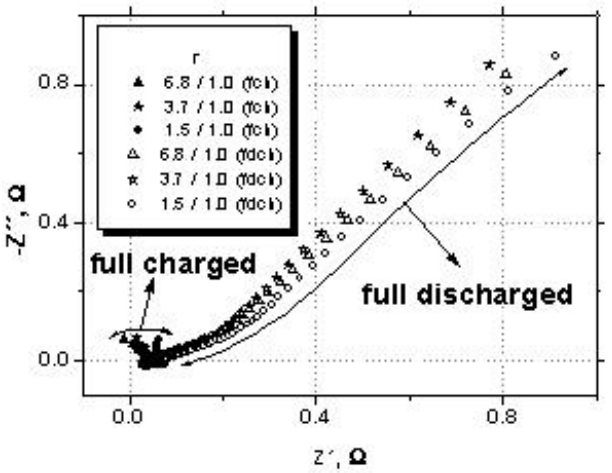

Fig. 6. NpN configuration EIS data under fully charged or fully discharged conditions. Different *r* values pointed out in the figure. Fully charged: full symbols; fully discharged: open symbols.

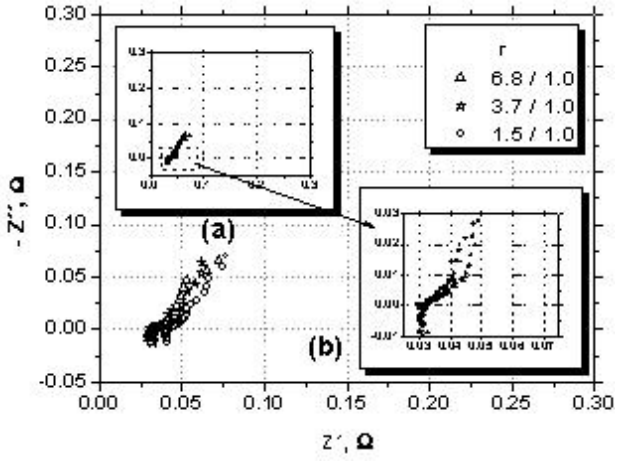

Fig. 7. NpN configuration EIS data for 20% state of discharge. Different *r* values pointed out in the figure. (a) Data shifting to coincide R_s at its lower value. (b) Magnification of inlet (a) region .

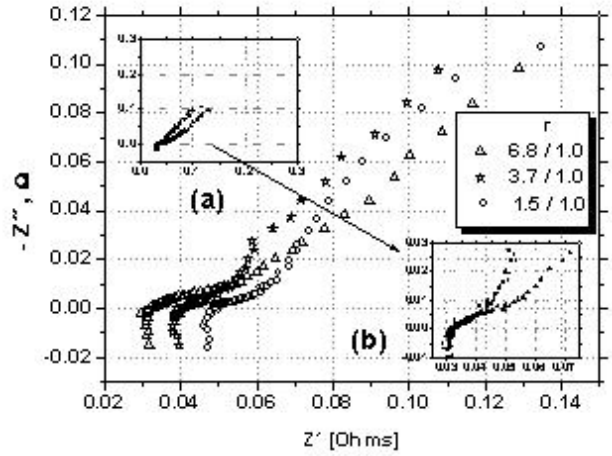

Fig. 8. NpN configuration EIS data for 40% state of discharge. Different *r* values pointed out in the figure. (a) Data shifting to coincide R_s at its lower value. (b) Magnification of inlet (a) region .

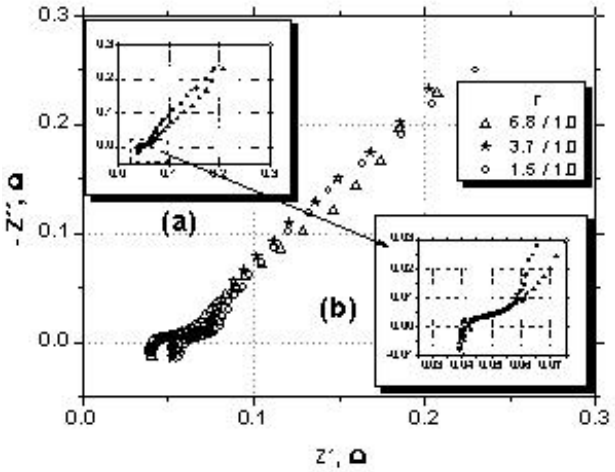

Fig. 9. NpN configuration EIS data for 80% state of discharged. Different *r* values pointed out in the figure. (a) Data shifting to coincide R_s at its lower value. (b) Magnification of inlet (a) region .

Another fact to be noted, because it is totally reproducible, is related to the discharge EIS plate data in Fig. 6 from 1.5/1.0 to 3.7/1.0, where there is a shift to the left in the figure. This is in agreement with the lower solution external resistance of the second case. Nevertheless, the data at *r* 6.8/1.0 seem to cross the others (this crossing is observable between 6.8/1.0 and 3.7/1.0, even without shifting the data). It is like the data from 1.5/1.0 to 3.7/1.0, which were "well" ordered (in some agreement with the external solution resistances). On the other hand, the data for 6.8/1.0 present "good" behaviour at high and middle frequencies, but problems at low frequencies. These problems can be interpreted in terms of a non-homogeneous current distribution, as it was previously supposed for other cases (Figs. 2 and 5).

The data with NpN configurations for partial discharged central positive plates are plotted in Figs. 7 (Q_d 20%), 8 (Q_d 40%) and 9 (Q_d 80%). In all these cases it is possible to see, looking at the respective inlets (which have the shifted data), that 1.5/1.0 and 3.7/1.0 ratios give always the same impedance behaviours. The *r* 6.8/1.0 presents for all cases and only at low frequencies a difference: a shifting to the right (see the inlets). At high and medium frequencies all the data coincide at the inlets. This means that the data under intermediate discharge conditions can be attributed to central positive plate impedance at high and middle frequencies. At low frequencies, increasing them with the discharge level, the data depend on *r*. This fact is in the sense that under these conditions (high discharge level and low

frequencies) there is a non-homogeneous current distribution interfering in the measurements. It is interesting that, under completely discharged conditions, the non-homogeneous current distribution becomes observable at all frequencies (see Fig. 6).

A last point in Figs 7, 8 and 9 is that, looking at observed impedance module for 1.5/1.0 and 3.7/1.0 ratios at the lowest frequency, they are practically constant from Fig 7 (Q_d 20%) to Fig. 8 (Q_d 40%). Nevertheless, there is an increase of module from Fig. 8 (Q_d 40%) to Fig. 9 (Q_d 80%). This gives another experimental basis to the idea that this last increase is related to the reaction zone reaching the bottom of the pores.

Analysis of polarization resistances versus discharge conditions

As it has been concluded in the two previous sections, it seems that the impedance measurements made in different states of discharge can be attributed only to the central plate impedance. Nevertheless, this statement is incorrect because of: a) the totally charged negative plates for *r* 6.8/1.0 (Fig. 2); b) the negative plate at high degree of discharge for r 6.8/1.0 and very low frequencies (Fig. 5); c) the positive plates at medium and high degree of discharge for *r* 6.8/1.0, at low frequencies (Figs. 8 and 9) and d) the totally charged or discharged positive plates at all the analyzed frequencies (Fig. 6). As a consequence, it can be stated that the data at *r* 1.5/1.0 are representative of the impedance of all central plates except for: i) totally charged or discharged NpN configurations; ii) positive partially charged plates, at low frequencies and iii) negative plates near to the end of the discharge, at low frequencies.

In all first three cases (a, b, and c), it seems that the phenomenon can be attributed not to an incorrect area ratio, but to a non-homogeneous current distribution at the central plate. Case d) (Fig. 6) seems to be related to PbO_2 electrode specific characteristics, together with its discharge product, both detected by the EIS method. These facts point out that the positive plate discharge product is different from that formed in negative plates [25].

The present EIS results on partially or totally discharged plates show an inductive loop at high frequencies and two capacities distributed loops, at middle and low frequencies. These ideas have been schematically represented in Fig. 10, together with some parameters used in the literature like R_s, Ω and R_{p2} [19]. In the present work it was possible to determine the polarization resistances $R_{p,1}$ and $R_{p,2}$ (see Fig. 10) in different states of discharge. They could be attributed to processes occurring on the surfaces of two different kinds of pores. The idea about two kinds of pores comes from the measurements of Hg porosimeter and BET surface areas, which give different results. The $R_{p,1}$ and $R_{p,2}$ results seem to be a polarization resistance of the processes on the surfaces of these two kind of pores. In this sense, it is interesting to plot the results of these two parameters ($R_{p,1}$ and $R_{p,2}$) for PnP and NpN configurations, against the plate state of discharge. To do that, the determination of $R_{p,1}$ and $R_{p,2}$ was made by non linear fitting of the points, considering only those from a single capacity loop.

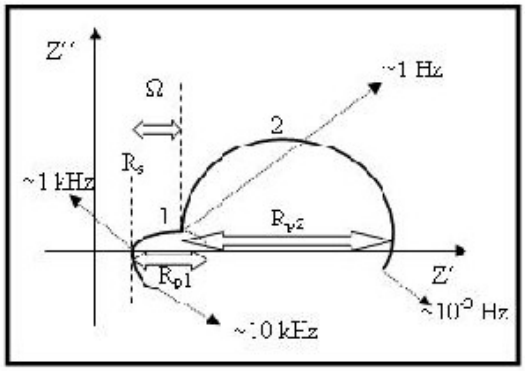

Fig. 10. Schematic representation of EIS lead acid battery plates results including all the observed phenomena in partial or totally discharged plates.

In Fig. 11 $R_{p,1}$ and $R_{p,2}$ are plotted results versus discharge levels for PnP configuration and, in Fig. 12, those for NpN configuration. The first important aspect is that both results are coherent in themselves, because they give rise to continuous curves for each case. A second point is that for both cases the $R_{p,1}$ seems to be independent of the state of discharge, except for the NpN configuration at high discharge level. In this region, there is a little increase of $R_{p,1}$. The average value of $R_{p,1}$ for the PnP configuration (related to negative central plate) was 46 ± 7 mΩ and that of NpN configuration, taking out the high discharge levels, was 24 ± 6 mΩ.

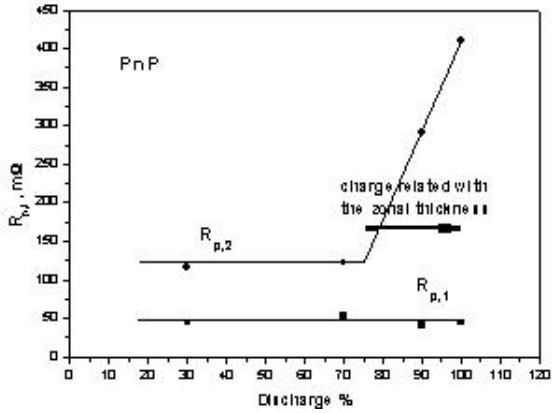

Fig. 11. $R_{p,1}$ and $R_{p,2}$ versus discharge percentage (state of discharge) plot for a PnP configuration.

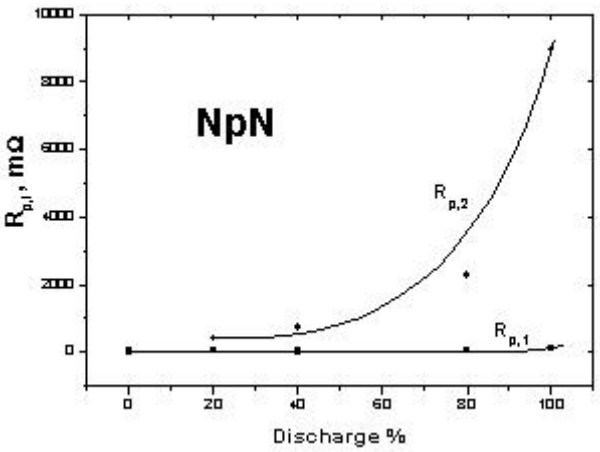

Fig. 12. $R_{p,1}$ and $R_{p,2}$ versus discharge percentage (state of discharge) plot for a NpN configuration.

On the other hand, the $R_{p,2}$ results are different for PnP and NpN configurations. In PnP configuration cases, considering the determined $R_{p,2}$ value as due only to negative central plate, there is a drastic change of behaviour of the related process in about 80% state of discharge. It can be attributed to the fact that this drastic change occurs, when the discharge reaction zone reaches the bottom of the pores measured, indirectly, through BET. For the NpN configuration results (considering now the $R_{p,2}$ related only to the positive central plate), they seem to have a more extended reaction zone, which makes impossible to detect clearly the reaching of the discharge reaction zone to the bottom of BET pores.

Pointing out that the determined $R_{p,1}$ and $R_{p,2}$ results are reproducible, these two concepts can give base to be used in understanding other systems, which have behaviour like those schematically represented in Fig. 10. In this sense, it is interesting to note that $R_{p,1}$ is higher in negative than positive plates, while $R_{p,2}$ has an opposite behavior for the same states of discharge. These last facts need to be more deeply studied in different lead acid battery systems.

CONCLUSIONS

On the basis of the fact that in the literature for EIS measurements in different kinds of four electrodes cells, there are no experimental proofs that the total measured impedance can be attributed only to the central plate studies were made in the present work, to clarify experimentally the problem. The four-electrode cells use lead acid battery plates as central electrode and lateral counter-electrodes with different polarity, plus a reference one. Literature sources consider the two counter-electrodes presence enough to resolve the counter-electrode impedance problem.

To perform these studies on plates a special four electrode EIS measurement cell was developed, to be able to vary the counter-electrode plate area at the same time when the central working plate area was maintained constant. The central plate was located geometrically at the centre of two counter-electrodes and at 3 cm distance from them. This last prerequisite was established to assure, so far as possible, that the increase in the counter-electrode areas does not introduce increasing currents at central plate borders. This cell was used under two configurations, PnP and NpN (see the text), with the central plate electrode in different states of discharge, and the reference electrode near to the central one. The used area ratios r between the counter-electrode and the central plate were 1.5/1.0, 3.7/1.0 and 6.8/1.0. For discharge cell an equivalent configuration but with r of 1.0 was used.

The results for the PnP configuration show that in these cases it was always possible to attribute the EIS measurements to the central negative plate, even for totally charged central plate. This does not occur only at lower used frequencies and higher degrees of discharge, where the EIS measurements become dependent on the r value. Nevertheless, in the present work there are arguments to attribute this fact to a current distribution problem at the central plate borders, and not to a specific counter-electrode contribution to the total impedances.

The results for NpN configuration are more complicated. In these cases (NpN) it can be stated that at high and middle frequencies the measured impedance can be attributed to the central plates, except for totally charged plates where it depends on r. On the other hand, at low frequencies, in all these cases (state of discharge, different r and even totally charged plates) there are dependences on the r values. Nevertheless, again, arguments are put forward in the sense that this dependence could not be related to counter-electrode impedance contributions, but to central plate current distribution problems. In this sense, it becomes an open problem, to which point non-homogeneous distribution of a.c. current densities. Perturbations can invalidate impedance measurements.

Acknowledgments: *All the authors thank Paraná State Energy Company (COPEL) for the financial support to the Program to which the present paper belongs. They also thank the undergraduate student Priscila Mengarda for her technical cooperation and to PIBITI Program of the CNPq for her scholarship.*

REFERENCES

1. R. de Levie, *Electrochim. Acta*, **8**, 751 (1963).
2. H. Keiser, K. D. Beccu, M. A. Gutjahr, *Electrochim. Acta*, **21**, 539 (1976).
3. W. H. Mulder, J. H. Sluyters, T. Pajkossy, L. Nyikos, *J. Electroanal. Chem*., **285**, 103 (1990).
4. A. Lasia, *J. Electroanal. Chem*., **397**, 103 (1995).
5. A. Lasia, *J. Electroanal. Chem*., **428**, 155 (1997.
6. R. de Levie, *Electrochim. Acta*, **10**, 113 (1965).
7. D. D. Macdonald, *Electrochim. Acta*, **51**, 1376 (2006).
8. J-P. Candt, P. Fouilloux, M. Keddam, H. Takenouti, *Electrochim. Acta*, **26**, 1029 (1981).
9. D. D. Macdonald, M. Uriquidi-Macdonald, S. D. Bhakta, B. G. Pound, *J. Electrochem. Soc*., **138**, 1359 (1991).
10. E. Karden, S. Buller, R. W. De Doncker, *Electrochim. Acta*, **47**, 2347 (2002).
11. S. Devan, V. R. Subramanian, R. E. White, *J. Electrochem. Soc*., **152**, A947 (2005).
12. F. La Mantia, J. Vetter, P. Novak, *Electrochim. Acta*, **53**, 4109 (2008).
13. A. L. Van Den Eeden, J. H. Sluyters, J. H. Van Lenthe, *J. Electroanal. Chem*., **171**, 195 (1984); A. L. Van Den Eeden, Thesis, Utrecht University, 1955, pp. 78-79.
14. F. Huet; *J. Power Sources*, **70**, 59 (1998}.
15. M. Keddam, Z. Stoynov, H. Takenouti, *J. Appl. Electrochem*., **7**, 539 (1977).
16. V. V. Viswanathan, A. J. Salkind, J. J. Kelleo, J. B. Ockerman, *J. Appl. Electrochem*., **25**, 729 (1995).
17. F. Huet, R. P. Nogueira, P. Lailler, L. Torcheux, *J. Power Sources,* **158**, 1012 (2006).
18. E. Karden, S. Uller, R. W. De Doncker, *J. Power Sources*, **85**, 72 (2000).
19. M. Keddam, C. Rakotomavo, H. Takenouti, in: Advances in Lead-Acid Batteries, K. R. Bullock, D. Pavlov (Eds.), The Electrochemical Society Inc., Pennington, N.J., USA, 1984, p. 277.
20. J. Jindra, M. Musilová, J. Mhra, A. A. Taganova*, J. Power Sources*, **37**, 403 (1992).
21. Z. Stoynov, B. Savova-Stoynov, T. Kossev, *J. Power Sources*, **30**, 275 (1990).
22. D. Berndt, Maintenance-Free Batteries, A Handbook of Battery Technology, Research Studies Press Ltd., Baldock, Hertfordshire, England, 2003, p. 262.
23. A. Kirchev, A. Delaille, M. Perrin, E. Lemaire, F. Mattera, *J. Power Sources*, **170**, 495 (2007).
24. A. Kirchev, A. Delaille, F. Karoui, M. Perrin, E. Lemaire, F. Mattera, *J. Power Sources*, **179**, 808 (2008).
25. C. V. D'Alkaine, A. Carubelli, M. C. Lopes, *J. Power Sources*, **64**, 111 (1997).

ЕКСПЕРИМЕНТАЛЕН КРИТИЧЕН АНАЛИЗ НА ИМПЕДАНС НА АКУМУЛАТОРНИ ПЛОЧИ

С. В. Д'Алкаине[1]*, Г. А. де Оливейра Брито[1], К. М. Гарсия[2], П. Р. Импиниси[2]

[1] Група по електрохимия и полимери, Химически департамент, Федерален университет на Соа Карлос, бул. „Вашингтон Луиз" 234, 13560-905 Сао Карлос, Бразилия

[2] Лаборатория по батерии, Институт по технологии за развитие, Политехнически център, ПК 19067, 81531-980 Куритиба, Бразилия

Постъпила на 24 юни 2008 г., Преработена на 12 септември 2008 г.

(Резюме)

Отчитайки отсъствието на експериментални доказателства за това, че измерванията на клетка с четири плочи чрез електрохимичната импедансна спектроскопия (ЕИС) се свързват само с централната плоча, в настоящата работа са проведени изследвания с различни по площ плочи на противоелектрода при една и съща централна плоча. Измерванията са проведени в честотната област от 10^4 до 10^{-2} Hz при различна степен на зареждане на централната плоча. Резултатите показват, че за комбинацията положителна-отрицателна-положителна плоча при всички изследвани честоти и състояние на разреденост данните от ЕИС могат да бъдат отнесени за централната отрицателна плоча, освен при най-голямо отношение на площите *r* сравнителен електрод/централен работен електрод и по-висока степен на разреждане в зоната на по-ниските работни честоти. За комбинацията отрицателен-положителен електрод резултатите от ЕИС могат да бъдат отнесени към централната положителна плоча само за високи и средни честоти при всички нива на разряд и отношения на площите. Напълно заредените централни положителни плочи трябва да бъдат изключени, защото техният импеданс зависи от площта на противоелектрода при всички съотношения *r*. Резултатите са обсъдени и са направени предположения за тяхното обяснение.

Bulgarian Chemical Communications, Volume 41, Number 2 (pp. 185–191) 2009

Impedance characteristics of the lipid membranes formed from a phospholipid-fatty acid mixture

M. Naumowicz[1], Z. A. Figaszewski[1,2,]*

[1] *Institute of Chemistry, University of Bialystok, Al. J. Pilsudskiego 11/4, 15-443 Bialystok, Poland*
[2] *Laboratory of Electrochemical Power Sources, Faculty of Chemistry, University of Warsaw, Pasteur St. 1, 02-093 Warsaw, Poland*

Received June 22, 2008; Revised July 26, 2008

Electrochemical impedance spectroscopy was used for the study of two-component lipid membranes. Phosphatidylcholine and stearic acid were to be investigated, since they play important biochemical role in cell membranes. The research on biolipid interaction was focused on quantitative description of processes that take part in a bilayer. Assumed models of interaction between amphiphilic molecules and the equilibria that take place there were described by mathematical equations for the studied system. The possibility of complex formation for this two-component system forming bilayers was assumed, that could explain the deviation from additivity rule. The molecular area and the equilibrium constant of the complex were determined.

Key words: Phosphatidylcholine, stearic acid, complex formation, equilibrium constant, bilayer lipid membrane, electrochemical impedance spectroscopy.

INTRODUCTION

The inspiration for lipid bilayer research work, without question, comes from the biological world. Although the first report on self-assembled bilayer lipid membranes in vitro appeared in 1961, experimental scientists including surface, colloid, and bioscientists have been dealing with these interfacial phenomena since Robert Hooke's time (1672). Bilayer lipid membranes have been used in a number of applications ranging from basic membrane biophysics studies to the conversion of solar energy via water photolysis, and to biosensor development using supported bilayer lipid membranes [1].

Bilayer lipid membranes are made predominantly of amphiphiles, a special class of surface-active molecules, which are characterized by having a hydrophilic and a hydrophobic group in the same molecule [2]. Usually, a zwitterionic or non-ionic lipid is used as the basic lipid for the preparation of bilayers. Phosphatidylcholines, whose construction is represented in Fig. 1a, are the most widely used bilayer-forming molecules because of their relevance to the behaviour of these components in cell membranes. They contain two fatty acids themselves, which are esterified to glycerol. The interaction between different acyl chains within a phospholipid molecule or among the different phospholipid molecules in the bilayer should determine the physical properties of biomembranes. The bilayer membranes mostly consist of either natural or synthetic phospholipids, but other double-tail surfactants such as dialkyl quaternary ammonium compounds in pharmaceutical applications are also used. In addition, minor amounts of single-tail surfactants, such as fatty acids (stearic acid depicted in Fig. 1b belongs to the class of fatty acids), may be added to affect specific characteristics such as the membrane permeability or electric charge density [3].

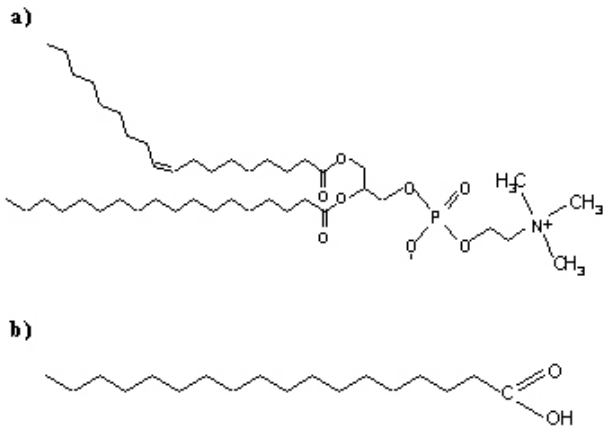

Fig. 1. Comparison of phosphatidylcholine and stearic acid molecular structures.

The physico-chemical studies of the phospholipid-fatty acid mixture may have an additional significance other than the interest to the alteration of membrane function caused by fatty acid. The study of the phase behaviour of the hydrated bilayer,

* To whom all correspondence should be sent:
E-mail: elchem@uwb.edu.pl

composed of a phospholipid-fatty acid mixture would be useful to understand the acyl-acyl interactions playing such an important role in phospholipid bilayers [4].

In this work, the electric capacity and the electric conductance of the phosphatidylcholine-stearic acid membranes were determined within the composition range, where the bilayer formation was possible. A 1:1 complex has been proposed to exist in the examined bilayers. The aims of these investigations were to study the mixed phosphatidylcholine-stearic acid bilayers, to characterize the molecular interaction between the phospholipid and fatty acid and to determine the values of parameters of the complex: the equilibrium constant and the molecular area.

The data presented in this work, mathematically obtained result and confirmed experimentally, are of great importance for the interpretation of the phenomena occurring in lipid membranes. The knowledge of equilibrium represented by the complexing reaction lets us understand the processes that take place on bilayer surface. The obtained results can be used in quantitative description of physical and chemical properties of biological membranes and, in our opinion, can help for a better understanding of biological membranes and in their biophysical studies.

THEORY

A two-component forming solution can be used to obtain a lipid membrane. The components may or may not form another compound.

The model, which has been represented in full detail previously [5–7] assumes that in the cases, where the membrane components do not form chemical compounds, any two-component system, regardless if it forms a monolayer or a bilayer, can be described by the equation expressing additivity of the capacitance:

$$C_{\mathrm{m}} = C_1 c_1^s S_1 + C_2 c_2^s S_2 \tag{1}$$

here:

$$x_1 = \frac{c_1^s}{c_1^s + c_2^s} \tag{2}$$

$$x_1 + x_2 = 1 \tag{3}$$

where: C_{m} [μF·m^{-2}] – the measured capacitance of the membrane; C_1, C_2 [μF·m^{-2}] – the capacitance of the mem-brane built by components 1 and 2, respectively; c_1^s, c_2^s [mol·m^{-2}] – the surface concentrations of components 1 and 2, respectively, in the membrane; S_1, S_2 [m^2·mol^{-1}] – the surface area, occupied by one mol of components 1 and 2, respectively; x_1, x_2 – the molar fractions of components 1 and 2, respectively.

Elimination of c_1^s and c_2^s yields the linear equation:

$$\left(C_{\mathrm{m}} - C_1\right) x_1 = -\frac{S_2}{S_1}\left(C_{\mathrm{m}} - C_2\right) x_2 \tag{4}$$

Since the first stability constant in complexes, as the most essential one, is usually the biggest and should be taken into consideration [8], the existence of 1:1 complex (compound 3) in lipid-fatty acid system was assumed. Then, the set of Eqs (1)–(3) is modified because the electric capacity is the sum of the contributions of all the compounds [9, 10]:

$$C_{\mathrm{m}} = C_1 c_1^s S_1 + C_2 c_2^s S_2 + C_3 c_3^s S_3 \tag{5}$$

here:

$$K_{\mathrm{R}} = \frac{c_3^s}{c_1^s \cdot c_2^s} \tag{6}$$

$$x_1 = \frac{c_1^s + c_3^s}{c_1^s + c_2^s + 2c_3^s} \tag{7}$$

$$c_{t1}^s = c_1^s + c_3^s \tag{8}$$

$$c_{t2}^s = c_2^s + c_3^s \tag{9}$$

$$x_1 + x_2 = 1 \tag{10}$$

where: C_3 [μF·m^{-2}] – the capacitance of the membrane built by compound 3; c_3^s [mol·m^{-2}] – the surface concentration of compound 3 in the membrane; c_{t1}^s, c_{t2}^s [mol·m^{-2}] – the total surface concentrations of components 1 and 2, respectively, in the membrane; S_3 [m^2·mol^{-1}] – the surface area, occupied by one mol of compound 3; K_{R} [m^2·mol^{-1}] – the stability constant of compound 3.

After solving equations system (5)–(10), the following basic equation is derived:

$$\left[\left(C_{\mathrm{m}} - C_1\right) B_2 x_1 + \left(C_{\mathrm{m}} - C_2\right) B_1 x_2\right]_{\times}$$

$$\left[\left(C_3 - C_1\right) B_2 x_1 + \left(C_3 - C_2\right) B_1 x_2 + \left(C_1 - C_2\right)\left(x_1 - x_2\right)\right] =$$

$$= K_{\mathrm{R}} S_3^{-1} B_1 B_2 \left[\left(C_{\mathrm{m}} - C_1\right)\left(x_2 - x_1\right) + \left(C_3 - C_{\mathrm{m}}\right) B_1 x_2\right]_{\times}$$

$$\left[\left(C_{\mathrm{m}} - C_2\right)\left(x_1 - x_2\right) + \left(C_3 - C_{\mathrm{m}}\right) B_2 x_1\right] \tag{11}$$

in which: $B_1 = \frac{S_3}{S_1}$ and $B_2 = \frac{S_3}{S_2}$.

The Eqn. (11) is an equation of second degree with respect to C_m, to the complex composition as well as with respect to the constants: C_1, C_2, C_3, B_1 and B_2. The opening of the parentheses results in a great complexity of the equation, and it is troublesome when directly applied to the determination of constants. The constants mentioned above can be determined in individual cases using simplified forms of this equation.

The Eqn. (11) may be simplified taking into account the sufficiently high value of the stability constant of the complex. With this assumption it represents a straight line for small x_2 values ($x_2 < x_1$):

$$\left(C_1 - C_m\right)\frac{x_1 - x_2}{x_2} = -B_1C_3 + B_1C_m \qquad (12)$$

while for the case of high x_2 values ($x_2 > x_1$) Eqn. (11) can be expressed by another straight line:

$$\left(C_2 - C_m\right)\frac{x_2 - x_1}{x_1} = -B_2C_3 + B_2C_m \qquad (13)$$

The Eqn. (11) can be simplified in some other way. In the case where $x_2 = x_1$, the following form is assumed:

$$\left[C_2S_1^{-1} + C_1S_2^{-1} - C_m\left(S_1^{-1} + S_2^{-1}\right)\right]\left(C_2S_1^{-1} + C_1S_2^{-1}\right) -$$
$$-\left[C_2S_1^{-1} + C_1S_2^{-1} - C_m\left(S_1^{-1} + S_2^{-1}\right)\right]\left(S_1^{-1} + S_2^{-1}\right)C_3 =$$
$$= K_R(S_1^{-1})^2(S_2^{-1})^2S_3\left(C_m - C_3\right)^2 \qquad (14)$$

The parameters describing the complex determined from equations (11) and (14) can be applied to represent the agreement of Eqn. (11) with the experimental data by using Eqn. (15):

$$K_RS_1^{-1}S_2^{-1}\left(a_1 + a_2\right)\left(a_3 - a_1\right)C_m^{\,2} +$$
$$+\left[K_RS_1^{-1}S_2^{-1}\left(C_1a_1 - C_3a_3\right)\left(a_1 + a_2\right) -\right.$$
$$\left. - K_RS_1^{-1}S_2^{-1}\left(C_2a_1 + C_3a_2\right)\left(a_3 - a_1\right) + a_4S_3^{-1}\left(a_3 + a_2\right)\right]C_m +$$
$$+K_RS_1^{-1}S_2^{-1}a_3C_3\left(C_3a_2 + C_1a_2\right) -$$
$$- K_RS_1^{-1}S_2^{-1}a_1C_1\left(a_1C_2 + a_2C_3\right) - a_4S_3^{-1}\left(C_2a_3 + C_1a_2\right) = 0 \qquad (15)$$

where:

$$a_1 = S_3^{-1}\left(x_2 - x_1\right);\ a_2 = S_2^{-1}x_1;\ a_3 = S_1^{-1}x_2;$$
$$a_4 = \left[S_3^{-1}\left(C_1 - C_2\right)\left(x_2 - x_1\right) +\right.$$
$$\left. + \left(C_1 - C_3\right)x_1S_2^{-1} + \left(C_2 - C_3\right)x_2S_1^{-1}\right].$$

MATERIALS AND EXPERIMENTAL DETAILS

Reagents and preparation of the forming solutions

The lipid bilayer was formed from the Fluka product of 99% egg lecithin (3-sn-phosphatidylcholine) and from stearic acid (97%) also produced by Fluka. Both substances were dissolved in chloroform to prevent oxidation and mixed in appropriate proportions to achieve the desired molar fractions. The solvent was evaporated under a stream of argon. The dried residues were dissolved in a hexadecane-butanol mixture (10:1 by volume). The resultant solution was used to form the model membrane containing 20 mg·ml^{-1} of substances in solution. This solution containing the membrane components was unsaturated; therefore, it contained any proportion of the components. During membrane formation, the solvent mixture was removed and the created membrane had the same proportion as that in the resultant solution.

The solvents were of chromatographic standard purity grade: chloroform and butanol were from Aldrich, hexadecane was from Fluka.

Potassium chloride solution of 0.1 mol·dm^{-3} was used as the electrolyte for experiments. KCl was analytical purity grade and was heated prior to use at 400°C for 4 h to remove traces of organic material. Water purified by Milli-Qll (18.2 M, Millipore, USA) was used to make the electrolyte and in all cleaning procedures.

Preparation of the bilayer membranes

Bilayer membranes were obtained as bubbles at the Teflon cap constituting a measuring vessel component. The use of hexadecane as a solvent allows one to obtain membranes of thickness and capacity values similar to those of membranes formed of monolayers. A small quantity of butanol has negligible effect on the impedance parameters of the bilayers created, whereas it accelerates considerably the formation of membranes. The process of membrane formation was monitored by visual observation in transmitted light and by measuring the membrane capacitance. The bilayer area was determined with a microscope employing a micrometer scale as $4\times10^{-2} - 8\times10^{-2}$ cm^2 (the values were given for the bilayer area without margin).

Impedance analysis

Electrochemical impedance spectroscopy was performed with an a.c. impedance system (EG&G, Princeton Applied Research, Model 388) that included a personal computer, a two-phase lock-in amplifier (Model 5208) and a potentiostat/galvanostat (Model 273), in which a four-electrode input

was fed to the pre-amplifier. The electrochemical cell contained two identical reversible silver-silver chloride electrodes and two identical platinum electrodes (described exactly in [11−13]). A 4-mV amplitude sine-wave signal perturbation was applied in the 0.1–10000 Hz frequency range. The PowerSuite 2.4 software package was used for acquisition of impedance data. These were analyzed by using the complex nonlinear least squares (CNLS) fitting to a model represented by an equivalent electrical circuit. The CNLS program used in this work was ZSimpWin 3.21. All the experiments were carried out at room temperature of 20 ± 1°C.

RESULTS AND DISCUSSION

The effect of stearic acid on capacitance and resistance of the phosphatidylcholine bilayer was examined in the presence of different amounts of the fatty acid by using electrochemical impedance spectroscopy. The stearic acid content was varied up to a 0.80 molar fraction, above this limit the acid induced disorder of the acyl chains of phosphatidylcholine and we were not able to form a bilayer stable enough to carry out measurements on it. The capacity of a bilayer membrane is well defined, when it is in the black state. The resistance may vary by at least one order of magnitude, possibly because of impurities in the bilayer, border leakage at the membrane support, the appearance of lipid "crystals" at the periphery of the bilayer, or way of introducing the lipid solution (if the forming solution is introduced with a micro-syringe, instead of a brush, the irreproducibility of the bilayer can be minimized). The resistance of a single membrane, however, is usually constant until a short time before the membrane ruptures. Therefore, any changes in the resistance due to addition of ions, proteins, drugs, etc., can be determined with a relatively high degree of accuracy [3]. The impedance technique was used in our study to characterize the membrane features as this method has been shown to measure the capacitance and resistance of bilayer lipid membranes accurately. The mean values of the determined parameters were obtained based on six independent measurements of the lipid bilayer. In view of numerous results given in the literature and our own experimental results, we assume that the membranes created by us do not contain solvent. If some solvents are contained in the membranes, then one should treat them as trace impurities. As it is impossible to determine their quantity and their nature, one cannot take them into account in quantitative considerations (except for a possible qualitative indication). In the opposite case, we would take into account the possible presence of any solvent in the derived equations.

Figs. 2a,b represent typical impedance spectra of the phosphatidylcholine membranes, pure and containing stearic acid. Very simple diagrams were obtained for all the examined membranes; they have the form of semicircles in the entire analyzed frequency range. The centres of the semicircles lie on the real axis, provided that the lipid bilayers are considered as dielectric layers with leakage and the apexes of the semicircles satisfy the equation $C_m R_m \omega = 1$. The CNLS fits (according to the equivalent circuit illustrated in Fig. 3) are represented by solid lines and are in good agreement with the data obtained.

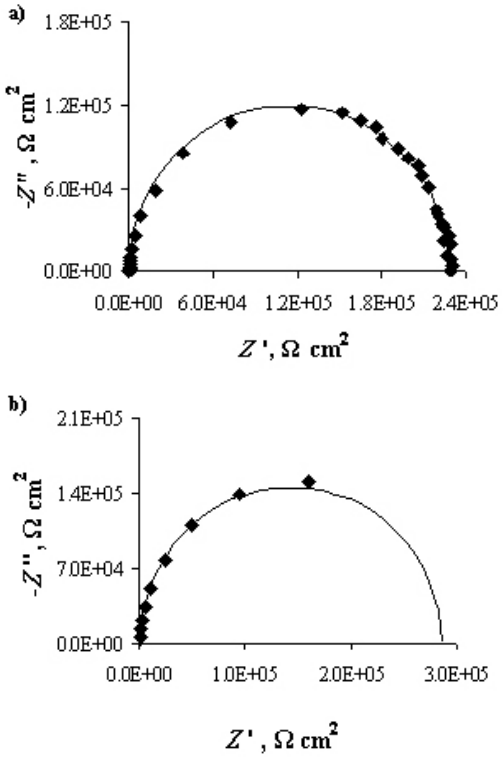

Fig. 2. Plots of the imaginary component of impedance – Z" versus the real component of impedance Z' over a frequency range of 0.1 Hz – 10 kHz for a phosphatidylcholine bilayer modified with stearic acid (x_2 = 0.80). (-) CNLS fit to the equivalent circuit shown in Fig. 3.

An equivalent circuit depicted in Fig. 3 describes the electric properties of the analyzed lipid membrane. The impedance of the phosphatidylcholine bilayers modified with stearic acid is represented by the electrolyte solution resistance R_0, which is in series with a paralleled circuit, composed of the resistance of the membrane R_m and of the membrane capacitance C_m. The possibility of misinterpretation of the recorded data is reduced by the simplicity of the circuit. This electric circuit is characteristic of an artificial lipid membrane only when ionophore

systems, specific channels, pores and adsorption are absent [14].

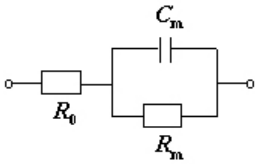

Fig. 3. An equivalent circuit representing electric properties of the phosphatidylcholine membrane modified with stearic acid: R_0 – resistance of the electrolyte, C_m – capacitance of the membrane, R_m – resistance of the membrane.

The dependence of the capacitance of phosphatidylcholine membranes containing stearic acid is illustrated in Fig. 4 as a function of the molar fraction of fatty acid. The resulting dependence deviates from linearity, indicating that some bonds are formed in the membrane. The capacitance value of pure phosphatidylcholine bilayer (component 1) C_1 was measured directly and represented earlier [7, 10, 12] as 0.62 ± 0.02 μF·cm^{-2}. There are no reliable literature data on capacitance values for the pure component 2 (stearic acid), because it does not form a bilayer membrane.

However, in order to characterize the course of the experimental curve, the C_2 value for the pure component is necessary, which will be used in the calculations. In this case, the hypothetical capacitance value for membrane built from stearic acid was estimated by fitting the experimental curve with a straight line for four different molar fractions of fatty acid and extrapolating $x_2 = 1$ value. The capacitance value obtained in this way for pure stearic acid is equal to 0.48 μF·cm^{-2}.

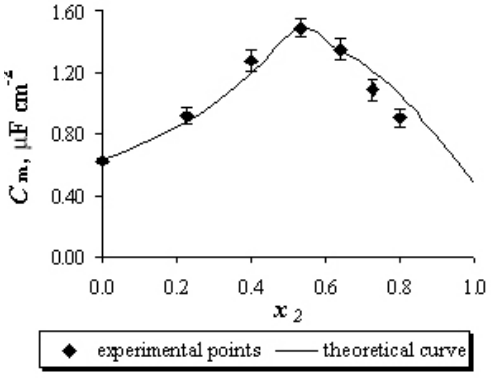

Fig. 4. Dependence of the capacitance C_m of the phosphatidylcholine-stearic acid membrane on the molar fraction of stearic acid x_2. Error bars indicate the experimental scatter. The solid line represents the theoretical values calculated from Eqn. (15).

The resistance value of pure phosphatidylcholine bilayer is equal to (2.30 ± 0.25)·10^5 Ω cm^2. The resistance value of phosphatidylcholine bilayer modified with the highest content of stearic acid (x_2 = 0.88) amounts to (2.99 ± 1.05)·10^5 Ω cm^2. The quantitative description of equilibrium in the phosphatidylcholine-stearic acid membrane, based on values of conductance, is not given here because of the very close values of resistances obtained for the analyzed bilayers and the irreproducibility of results.

Fig. 5 represents the dependence of $(C_m–C_1)x_1$ versus $–(C_m–C_2)x_2$ described by Eqn. (4). According to Eqn. (4), as it is in the case where the membrane components do not form chemical compounds, the values of this function should lie on a straight line. As one can see, this is not the case, which suggests that there is a complex or other chemical compound formation in the phosphatidylcholine bilayers containing stearic acid.

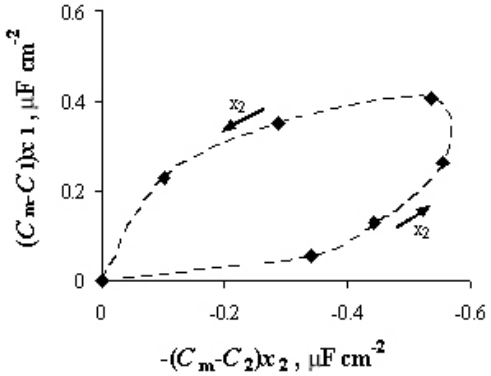

Fig. 5. Plot of $(C_m–C_1)x_1$ vs $(C_m–C_2)x_2$; C_m − capacitance of the membrane, C_1 − capacitance of the phosphatidylcholine membrane, C_2 − capacitance of the stearic acid membrane, x_1 – molar fraction of the phosphatidylcholine and the x_2 − molar fraction of stearic acid. The arrows denote the direction of the increasing x_2 values and the dashed line indicates the order of points.

Therefore, the formation of a complex in this system was assumed. Because the existence of a 1:1 complex is a typical case [8], the formation of a 1:1 phosphatidylcholine-stearic acid complex was accepted.

Thus, Eqn. (5) and the stability constant K_R, describing a third compound formed in this system, broaden the theoretical description. After a simple modification of Eqn. (5), one can obtain information represented by Eqn. (11). The capacitance values of C_1 and C_2 have been given above. The other constants B_1, B_2 and C_3 were obtained assuming that the value of the stability constant of the phosphatidylcholine-stearic acid complex was sufficient with respect to the simplified Eqns. (12) and (13). From the B_1 and B_2 constants, which were determined based on these equations it was possible to calculate the capacitance value of the complex C_3. The mean value is equal to 1.52 μF·cm^{-2}.

Eqns. (12) and (13) could also be applied to calculate the surface area per a single phosphatidylcholine-stearic acid molecule S_3. The values of the surface area, occupied by one mol of components 1 and 2, are necessary for this calculation. The surface area occupied by the phosphatidylcholine molecule, depends on the way the phospholipid is prepared, because this affects the length, conformation and degree of unsaturation of the fatty acids chains. Therefore, the values in the literature range between 54 and 99 Å^2 [15, 16]. In our case, we chose the S_1 value, determined in our laboratory as 85 Å^2 [17]. The surface area occupied by the stearic acid molecule, reported in the literature, is equal to 19 Å^2 [18]. The resulting S_3 value amounts to 122 Å^2 and it is bigger than the sum of areas occupied by each component of the complex (104 Å^2). It is probably connected with the arrangement of lecithin molecules in the complex and with its structure.

The only value to be determined was the stability constant of the phosphatidylcholine-stearic acid complex. It could be determined based on Eqn. (14) for $x_1 = x_2 = 0.5$ leading to 2.87×10^7 m^2·mol^{-1}. This value is relatively high, giving additional evidence for the prevailing of the 1:1 complex in mixed phosphatidylcholine-stearic acid bilayers. This value also confirmed that the assumptions, used to simplify Eqn. (11), were correct.

The parameters determined based on Eqns. (11) and (14) were applied to represent the agreement of the data, evaluated from Eqn. (11) (solid lines) with the experimental data (points) in Fig. 4 by using Eqn. (15). As Eqn. (15) is of second order, it can yield two solutions. The values yielding a better agreement of the experimental points with equation describing the complex formation between membrane components were chosen. Good agreement between experimental and theoretical points verifies the assumption about the formation of a 1:1 phosphatidylcholine-stearic acid complex in the lipid membrane as well as the assumption of the correct choice of the C_2 value for component of the membrane. The small variances between the experimental and the theoretical capacitance values indicate that complexes of different stoichiometries or associates are also possible in the phosphatidylcholine-stearic acid bilayer.

The phase behaviour of the phospholipid-fatty acid mixtures most extensively studied so far, is concerned with the mixture of diacylphosphatidylcholine and saturated fatty acids with C_{14}–C_{18} chain lengths, in which phase diagrams over the whole composition range have been reported for some mixture systems [19−23]. All the phase diagrams have exhibited the formation of a molecular compound (or phase compound) in the gel phase with the stoichiometry of diacylphosphatidylcholine:fatty acid = 1:2, which means that a strong attractive interaction acts between the two components in the gel phase bilayer. Although an agreement is documented for complex formation, there seems to be a discrepancy in the phase diagrams reported for the composition ranges of both low and high fatty acid concentrations [19, 20, 22].

In our previous paper [24], we represented the dependence of interfacial tension on the composition for the phosphatidylcholine-stearic acid membrane. A 1:1 complex has been assumed to exist in the bilayer, but the existence a fatty acid in the form a dimer was taken also into account. The value of stability constant of such complex is 2.18×10^9 m^2·mol^{-1}, whereas the experimental by determined area occupied by one phosphatidylcholine-stearic acid complex molecule is 187 Å^2 [24] (the only values available in the literature).

REFERENCES

1. H. T. Tien, A. L. Ottova, *J. Membrane Sci*., **189**, 83 (2001).
2. S. Przestalski, J. Sarapuk, H. Kleszczyńska, J. Gabrielska, J. Hładyszowski, Z. Trela, J. Kuczera, *Acta Biochim. Pol*., **47**, 627 (2000).
3. H. T. Tien, in: Bilayer Lipid Membranes (BLM): Theory and Practice, Marcell Dekker Inc., New York, 1974.
4. T. Inoue, S. Yanagihara, Y. Misono, M. Suzuki, *Chem. Phys. Lipids*, **109**, 117 (2001).
5. D. Petelska, M. Naumowicz, Z. A. Figaszewski, in: Advances in Planar Lipid Bilayers and Liposomes, H. T. Tien, A. Ottova (Eds.), vol. 3, Elsevier, Amsterdam, 2006, p. 125.
6. M. Naumowicz, Z. A. Figaszewski, *J. Membrane Biol*., **205**, 29 (2005).
7. M. Naumowicz, Z. A. Figaszewski, *Biophys. J*., **89**, 3173 (2005).
8. J. Inczendy, in: Analytical Applications of Complex Equlibria. Akademiai Kiado, Budapeszt, 1976.
9. M. Naumowicz, A. D. Petelska, Z. A. Figaszewski, *Electrochim. Acta*, 51, 5024 (2006).
10. M. Naumowicz, Z. A. Figaszewski, http://accessimpedance.iusi.bas.bg, Imp. Contribut. Online, 4 (2006) P1-1; *Bulg. Chem. Commun*., **39**, 175 (2007
11. M. Naumowicz, A. D. Petelska, Z. A. Figaszewski, *Cell. Mol. Biol. Lett*., **8**, 5 (2003).
12. M. Naumowicz, Z. A. Figaszewski, *Bioelectrochemistry*, **61**, 21 (2003).
13. M. Naumowicz, A. D. Petelska, Z. A. Figaszewski, *Electrochim. Acta*, **50**, 2155 (2005).
14. P. Krysiński, *Post Biochem*., **28**, 227 (1982).
15. P. Joos, R. A. Demel, *Biochim. Biophys. Acta*, **183**, 447 (1969).
16. M. K. Jain, The Bimolecular Lipid Membrane, Litton

Educational Publishing Inc., New York, 1972, p. 391.
17. A. D. Petelska, Z. A. Figaszewski, *Biophys. J.*, **78**, 812 (2000).
18. D. Vaknin, *J. Am. Chem. Soc*., **125**, 1313 (2003).
19. S. Mabrey, J. M. Stutevant, *Biochim. Biophys. Acta*, **486**, 444 (1977).
20. S. E. Schullery, T. A. Seder, D. A. Weinstein, D. A. Bryant, *Biochemistry*, **20**, 6818 (1981).
21. B. Kohn, S. E. Schullery, *Chem. Phys. Lipids*, **37**, 143 (1985).
22. R. D. Koynova, A. I. Boyanov, B. G. Tenchov, *Biochim. Biophys. Acta*, **903**, 186 (1987).
23. R. D. Koynova, B. G. Tenchov, P. J. Quinn, P. Laggner, *Chem. Phys. Lipids*, **48**, 205 (1988).
24. A. D. Petelska, M. Naumowicz, Z. A.Figaszewski, *Bioelectrochemistry*, **70**, 28 (2007).

ИМПЕДАНСНИ ХАРАКТЕРИСТИКИ НА ЛИПИДНИ МЕМБРАНИ ОБРАЗУВАНИ ОТ СМЕС НА ФОСФОЛИПИД И МАСТНА КИСЕЛИНА

М. Наумович[1], З. А. Фигашевски[1,2]*

[1] *Химически институт, Университет на Бялисток, бул. „Й. Пилсудски“ 11/4, 15-443 Бялисток, Полша*
[2] *Лаборатория за електрохимични източници на ток, Химически факултет, Варшавски университет, ул. „Пастьор“ № 1, 02-093 Варшава, Полша*

Постъпила на 22 юни 2008 г., Преработена на 26 юли 2008 г.

(Резюме)

Чрез електрохимична импедансна спектроскопия са изучени двукомпонентни липидни мембрани. Изследвани са фосфатидилхолин и стеаринова киселина, тъй като те играят важна биохимична роля в клетъчните мембрани. Изследването на биолипидните взаимодействия е фокусирано върху количественото описание на процесите, които протичат в двойния слой. Приетите модели на взаимодействие между амфифилните молекули и равновесието което се установява в изследваните системи са описани с математически уравнения. Допуска се възможността за образуване на комплекс в тази двукомпонентна система, която образува двойни слоеве, с което може да се обясни отклонението от правилото за адитивност. Определени са молекулната площ и равновесната константа на комплекса.

Bulgarian Chemical Communications, Volume 41, Number 2 (pp. 192–198) 2009

On-line error determination and processing for electrochemical impedance spectroscopy measurement data based on weighted harmonics autocorrelation

C. A. Schiller[1]*, R. Kaus[2]

[1] *Zahner Messsysteme, Kronach, Germany*
[2] *Fachhochschule Niederrhein, Krefeld, Germany*

Received July 12, 2008; Revised August 8, 2008

A procedure taking into account the inter-correlation of the harmonics, observed in experimental EIS, is shown to provide realistic error estimation useful for reliability considerations. The deduction of the algorithm of this "weighted harmonics autocorrelation" procedure as well as the results of EIS control experiments, performed on well known objects, are thoroughly discussed.

The influence of three different kinds of specific interference on the measurement results is shown: distortions by a nonlinear system characteristic, contamination of the response signal by pink noise and contamination of the response signal by single frequency disturbance. The uncertainty predicted by the weighted harmonics autocorrelation procedure is compared with the deviations observed in the practical measurements.

Key words: Electrochemical Impedance Spectroscopy, error determination, uncertainty, monochromatic oversampling, limited frequency selectivity, weighted harmonics autocorrelation.

INTRODUCTION

In Electrochemical Impedance Spectroscopy (EIS), measurement results are commonly used in conjunction with mathematical models to extract physical parameters or to identify physical phenomena. In the early years, the comparison between experiments and deterministic process models was mainly qualitative. With growing number of fields for EIS application and ongoing improvement of the measuring technique, the aim of EIS changed to more quantitative terms, i.e. finding out of precise numerical values of particular quantities of interest. Such values, representing physical and chemical system parameters, appear encoded in the spectral transfer function, which usually can be modeled by equivalent circuits (EC) or reaction mechanism analysis (RMA).

The parameters searched for are determining the model transfer function and express desired research information about (for instance losses/efficiencies of batteries) rate constants and diffusion parameters of electrochemical reactions and over potential shares in fuel cells. As for all experimentally determined quantities, the knowledge of their uncertainty is essential to judge their reliability. Many aspects of the principle error structure of EIS data have already been treated thoroughly in literature [1]. Also the error propagation through the typical simulation and fitting procedure can usually be determined reliably.

However, a complete error treatment can be performed only if a reasonable uncertainty estimation of the initial EIS measurement data is available, too.

It is necessary to enlighten the role of different possible error contributions to the deviations, observed experimentally in EIS. The popular assumption that deficient instrumentation is usually responsible for discrepancies between observed and expected impedance data does not usually hold true. In practice, a much more important class of error sources lies in the misinterpretation of the system under test: the less experienced scientist expects a certain frequency response by his object, which he assumes as ideal, but may overlook that the observed frequency response belongs to an imperfect real world object, often affected significantly by accompanying parasitic properties of the set-up around the sample. Parasitic reactance generated by stray capacitance, connection line inductance, bridge coupling [2] and mutual induction effect [3] represent an important class of error sources in the experimental practice. However, apart from mutual induction, errors caused by these effects can be taken into account without problems by extending the model accordingly and they are not subject of this work.

Instead, the topic here is the uncertainty due to the effect of Limited Frequency Selectivity (LFS): an experimental impedance spectrum assigns the course of certain measured impedance values to certain frequencies, but basically, this assignment can never be mathematically true. This can be

* To whom all correspondence should be sent:
E-mail: cas@zahner.de

understood considering the response to a monochromatic excitation: due to the very basic effect of limited measurement time, monochromatic excitation never exists in perfection [4]♦ and the response must be always the response to a mixture of different frequencies with – hopefully – the frequency of interest dominating. For the same reason, the best conceivable signal frequency filter in the data acquisition path of any impedance instrumentation has a LFS defined by the measurement time allocated, too.

Generally, the effect of the LFS appears as follows: apart from the wanted response signal, belonging to a certain frequency of interest, unwanted noise is recorded additionally. So the Signal to Noise ratio (S/N) can be considered as a measure of the uncertainty in principle.

As a strategy for error determination it has been suggested in the literature to measure the data at a certain frequency for more than few times or even for several complete spectra [5]. As a result, uncertainty can be calculated directly from the scattering. A severe disadvantage of this procedure is that the later error reduction by calculating the mean values scales only with the square root of the time interval, while continuous coherent data acquisition would have reduced the error proportionally with the time. Besides, coherent data acquisition often can suppress deviations perfectly, even if the individual time slot samples would exhibit large scattering – a too pessimistic error estimation is the consequence.

In the present work, an alternative approach, based on harmonic analysis, is described which avoids the drawbacks mentioned above. The reported procedure uses the fact that under monochromatic (sinusoidal) excitation of a system the harmonic distortion content of the response signal can be used as a measure of the uncertainty. This method requires two prerequisites: the EIS measurement procedure must provide the necessary information about the harmonics and the harmonic content must be unequivocally assigned to distortions.

EXPERIMENTAL

In order to determine the S/N ration of a single measurement, monochromatic over sampling (MOS) is applied. This means that in contrast to multi-spectral methods the harmonics are intentionally not excited, but they are detected in the response signal by Discrete Fourier Transformation (DFT) analysis, nevertheless. In an ideal case, single-sine excitation results in a response signal consisting of a single line in the frequency spectrum. Limited measurement time interval, non-linearity and noise in a real system however add additional lines to the response spectrum. The MOS method makes it possible to calculate the impedance solely from the fundamental, while the harmonic content can unambiguously be attributed to unwanted distortions. In contrast, when using multi-spectral excitation, the noise origin of harmonics in the response spectrum cannot be identified in general, because it is noise mixed with the intentionally excited frequency line response. As a work-around procedure it has been proposed [6, 7] to correlate sequential multi-spectral measurements with changing excitation content. It is obvious that this strategy should fail if the system under test is not strictly stable. Besides, a much higher time effort is necessary until the noise influence for a certain frequency sample becomes accessible.

However, also for MOS, the overall S/N ratio calculated from the harmonic content cannot simply be used as a reliable uncertainty measure. Instead the harmonic content has to be weighted in a certain manner because of reasons discussed in the following text.

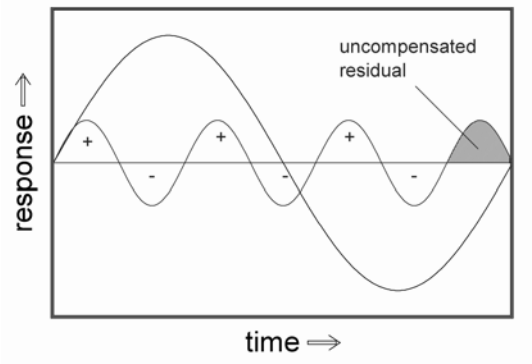

Fig. 1. Illustration of a signal and an interference at 3.5-fold frequency. The leakage due to the misfit in periodicity is larger than that in Fig. 2.

Fig. 1 shows schematically a measurement window time interval used for EIS with one period of sinusoidal excitation, together with an interference signal of 3.5 times the signal frequency. Fig. 2 sketches a similar situation, where the interference is 7.5 times the signal frequency. Comparing both figures one can suppose that the remaining interference due to the misfit between time window and periodicity decreases with increasing frequency. To be more precise, due to the limited measurement

♦ The correlation $\Delta\nu \propto 1/t$ between lifetime t and spectral purity respectively line width $\Delta\nu$ due to the quantum mechanical uncertainty principle is not only valid for photoemission but also determines measuring accuracy of EIS.

time interval (in the example it is the minimum time interval conforming to the systems theory), frequency components which are not exactly periodic with the time window are "rubbed off" on the results for the periodic signals, like for instance the fundamental wave. This "leakage" caused by the "aliasing" mechanism [8] declines with increasing frequency distance between interference and disturbed signal. It is maximal if the interference arises at (n + 0.5) times of the exci-tation frequency (n is an integer) and it vanishes, if the interference matches a harmonic (see Fig. 3).

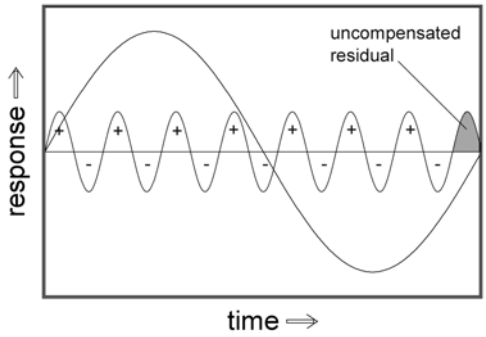

Fig. 2. Illustration of a signal and an interference at 7.5-fold frequency. The leakage due to the misfit in periodicity is smaller than that in Fig. 1 because of the shorter cycle time at higher frequency.

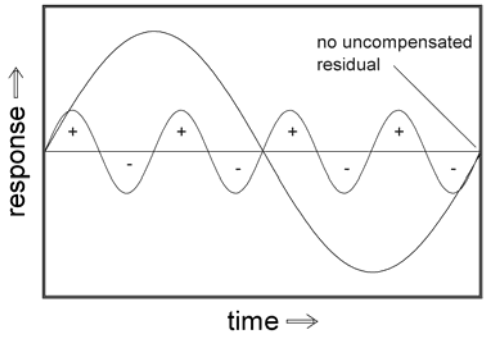

Fig. 3. Illustration of a signal and an interference at four-fold frequency. The leakage due to the misfit in periodicity vanishes at integer multiples of the signal frequency (harmonics).

If the interference frequency is an integer multiple of the signal frequency, i.e. a harmonic, a single line in the response spectrum results. As one can see in Fig. 3, in this case the distortion can be removed by the DFT filter perfectly. So, an additional single line in the Fourier spectrum does not indicate impaired accuracy automatically. In contrast, interfering signals with frequencies differing from the harmonics will generate several adjacent lines due to the leakage effect. They impair the accuracy and have to be taken into account in an uncertainty calculation. This can be accomplished using the autocorrelation algorithm described below.

The intensity of disturbing lines in relation to the fundamental ones must be considered, too. Apparently, a large signal is less affected by the same absolute amount of noise than a small signal.

If the excitation signal already contains distortions, e.g. due to imperfect functioning of the potentiostat, harmonics can be observed, which may not be mistaken for noise. The content of harmonics in the response, which are already present in the excitation signal, must be scaled down accordingly.

All these issues are considered in the "weighted harmonics autocorrelation" procedure, which is summarized in the following:

- Acquire the excitation and response signals with the MOS method application;
- Extract the fundamentals from the response spectrum. The quotient with the fundamental of the excitation spectrum is used to determine the impedance;
- Weight the harmonics of the response spectrum due to existing degrees of distortion in the excitation spectrum;
- Normalize each residual harmonic according to the intensity of the fundamental (division by the fundamental amplitude) and weight it according to its harmonic order (division by the frequency);
- Auto-correlate the weighted harmonic spectrum. The resulting amplitude of the first-order line distance yields the error indicator searched for.

The error indicator can be tested and calibrated in a way that the uncertainty prediction for white noise will match the error determined by a simulation. For the simulation purposes, a sine wave with an amplitude 'A' in a time window of 2^n is generated and superimposed by a defined distortion amplitude. This distortion can be generated either by white noise with a variable amplitude from 2 times 'A' to 0.1 times 'A', resulting in a S/N ratio of 0.5 to 10 respectively, or by a sinusoidal signal of comparable amplitude with an arbitrarily varying frequency. The resulting superimposed signal is treated by DFT (in particular the Fast Fourier Transform FFT) as a model for the MOS measurement procedure. Then, the amplitude of the fundamental is evaluated and the deviation between the known original and the evaluated amplitude affected by leakage in the disturbed case is recorded.

A linear correlation is found between the observed deviation and the output of the weighted harmonics autocorrelation procedure. Therefore, a single constant weighting factor can be determined to calibrate the weighted harmonics autocorrelation uncertainty forecast.

The result of a simulation done for an interfering sine-signal of varying frequency is depicted in Fig.

4. As it is expected, the deviation is minimal at integer multiples of signal frequency and it is locally maximal at (n + 0.5) times the signal frequency. Deviation also decreases with increasing frequency of the interfering signal, as it stated above.

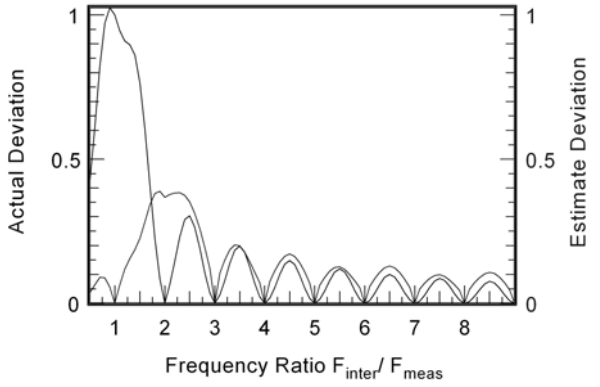

Fig. 4. Simulation of a sinusoidal interference of varying frequency.

The deviation observed from the simulation and the predicted uncertainty calculated by the weighted harmonics autocorrelation method are in good agreement except for interference frequencies close to the signal frequency

Obviously, the largest deviation appears for interference frequencies close to the signal frequency. This problem can be assigned to the fundamental relation between measurement time window and frequency uncertainty: if the frequency difference between a signal and a distortion tends to zero, the necessary measurement time for a successful separation tends to infinity.

The online error determination procedure was also tested in practical measurements. Three different kinds of specific interferences were used: superimposed pink noise, sine interference and inherent distortions due to a non-linearity of the object. The set-up used in case of external interference is sketched in Fig. 5: a signal generator FG for interference overlay produces either sine signal or noise with limited bandwidth, alternatively.

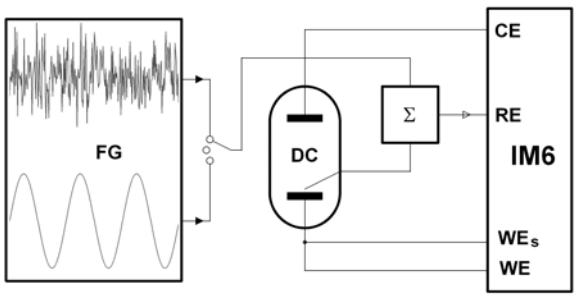

Fig. 5. Set-up for EIS control experiments consisting of a frequency generator FG, a dummy cell DC, a summing up circuit Σ, and an electrochemical workstation IM6.

The potentiostat terminals are WE for the working electrode current output, WE_s for the working electrode potential sense input, RE for the reference electrode potential sense input, and CE for the counter-electrode current output

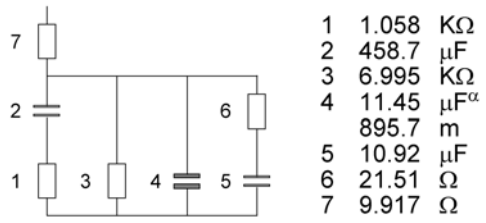

Fig. 6. Equivalent circuit of the dummy cell (DC in Fig. 5).

A dummy cell DC with well known properties is used as a reference object. EIS measurements were performed with the electrochemical workstation IM6, which uses the MOS principle. During measurements under interference overlay the generator signal is fed into the reference input RE of the IM6 via the summing up circuit Σ. The equivalent circuit of the dummy cell is depicted in Fig. 6.

RESULTS AND DISCUSSION

Injecting pink noise into the summing up circuit Σ (c.f. Fig. 5), results in an impedance spectrum of the dummy cell (Fig. 6) depicted in Fig. 7 as Bode plot.

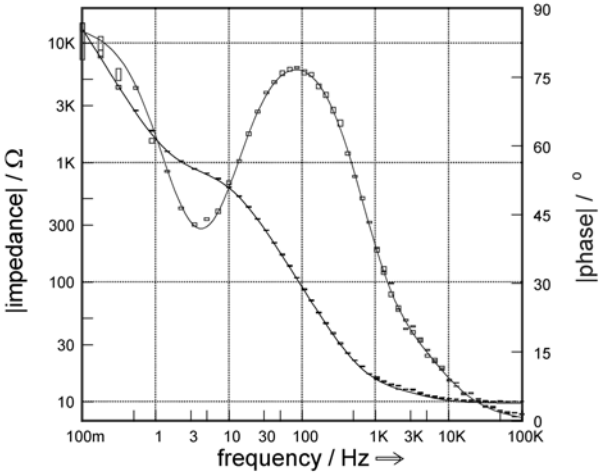

Fig. 7. Bode plot of a dummy cell (Fig. 6) measurement with the test set-up sketched in Fig. 5 with superimposed pink noise (error rectangles) and flawless measurement without noise (lines).

The rectangles characterize the measurement result under pink noise interference, whereas the lines represent the result of an undisturbed measurement. The size of the rectangles, indicating the standard deviation σ derived by the algorithm

discussed above, are in good agreement with the measurement error known from a comparison with the flawless measurement. This is more clearly visible in the complex plane representation (Fig. 8). Apparently the weighted harmonics autocorrelation algorithm leads to a useful prediction of the uncertainty caused by the presence of noise.

Measuring the dummy cell from 1 Hz to 1 kHz in the presence of a sinusoidal interference signal of 100 Hz leads to the result shown in Fig. 9 as complex plane plot.

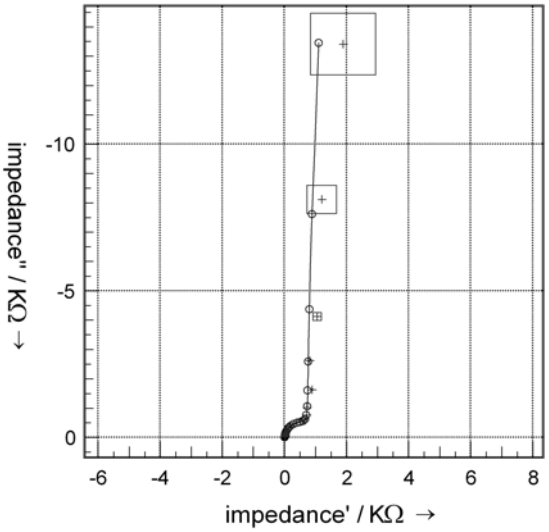

Fig. 8. Complex plane plot of a dummy cell (Fig. 6) measurement with the test set-up sketched in Fig. 5 with superimposed pink noise together with the result of a flawless measurement.

The straight line as well as the circles show the measurement without noise, the squares with centred crosses represent the predicted error with the measurement data under interfering noise.

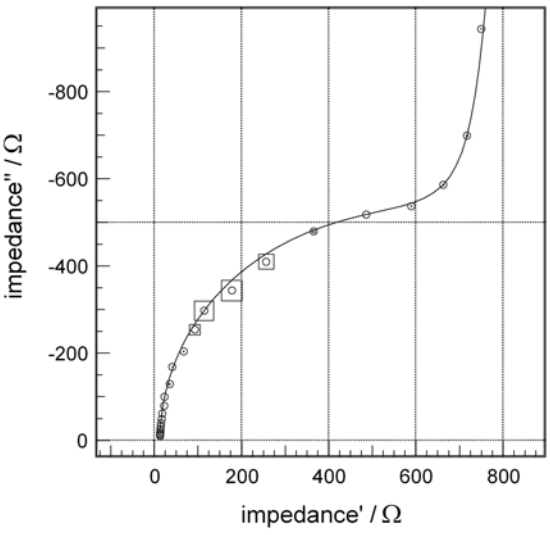

Fig.9. Complex plane plot of an EIS measurement of a dummy cell between 1 Hz and 1 kHz with a superimposed interfering sine wave of 100 Hz.

The squares with the centered circles indicate the uncertainty predicted by the weighted harmonics autocorrelation (one σ) and the measurement data with additional interference. The solid line characterizes the correct (undisturbed) result.

As it is stated above, the largest deviation between undisturbed (solid line in Fig. 9) and noisy measurement (circles in Fig. 9) is observed at signal frequencies around the interference frequency. The error predicted by the weighted harmonics autocorrelation algorithm is maximal in this frequency region, too. As it can be seen, the weighted harmonics autocorrelation algorithm leads to an acceptable uncertainty estimation for the case of a sine interference, too.

Further to external interference pick up, the non-linear behaviour of an investigated object can lead to errors in impedance measurements. As a representative example for this kind of error contribution, two power Schottky diodes connected in anti-parallel way were investigated by EIS under a bias current of 10 μA. In Figs. 10 and 11 a Bode and a complex plane plot respectively show the results. The straight lines represent a flawless measurement, using only amplitude of 1 mV.

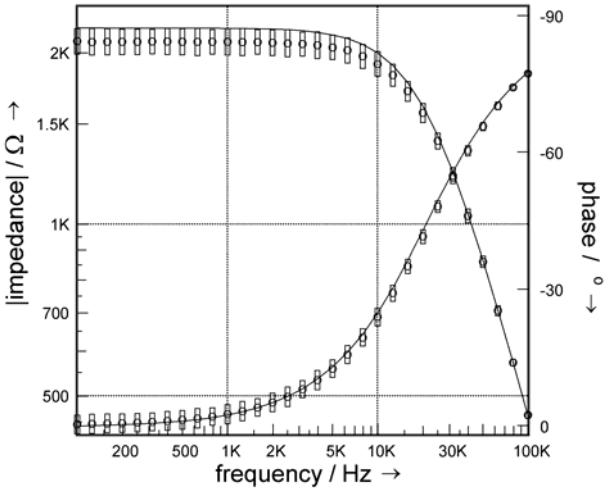

Fig. 10. Bode plot of impedance spectra of two anti-parallelly connected Schottky diodes.

The straight line was obtained with a 1 mV excitation amplitude, circles and rectangles represent the data points and the predicted uncertainty evaluated at 20 mV amplitude.

Under such small-signal conditions the Schottky diodes exhibit linear behaviour. An excitation amplitude of 20 mV, however, forces a non-linear response. Therefore, the spectrum must deviate from the former, i.e. the straight line. This can be clearly observed from a comparison of the measured data points (circles) and the straight line obtained with an amplitude of 1 mV.

Again, the uncertainty predicted by weighted harmonic autocorrelation is conform with the deviation between the high amplitude spectrum and the small signal control experiment: the larger the actual deviation, the larger the predicted error.

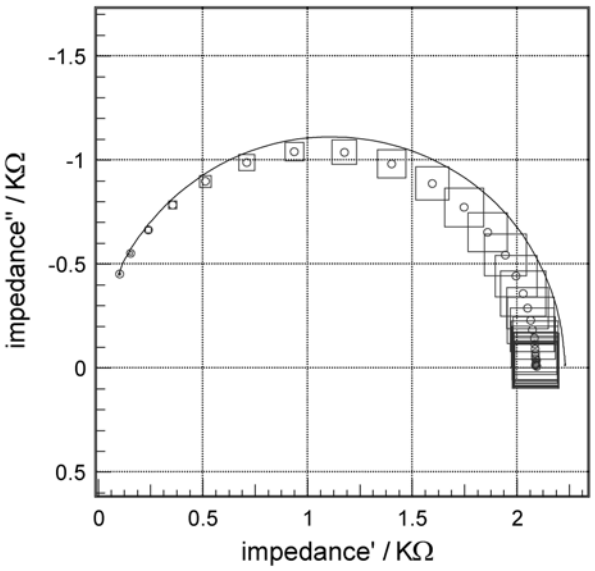

Fig. 11. Complex plane plot of the impedance spectra of the two anti-parallelly connected Schottky diodes. Further details as indicated in Fig. 10.

CONCLUSION

The weighted harmonics autocorrelation algorithm represented here is a valuable method to predict the uncertainty for most common kinds of distortions appearing in EIS. This has been demonstrated applying different kinds of artificial interference, which usually appear also in practical experiments. The uncertainty caused by superimposed noise was detected reliably, as well as the uncertainty appearing in the presence of a discrete frequency interference. Concerning the origin and the resulting effect, a totally different type of disturbance, assigned to inherent object non-linearity, can be detected by the algorithm as well. It is characteristic of this situation that well-shaped impedance spectra with no extensive visible scattering are observed. Nevertheless, the weighted harmonics autocorrelation algorithm can detect such a problematic situation and provide for a realistic error forecast in this case as well.

In contrast to the error analysis of multi-spectral excitation measurements, the represented algorithm provides a straight forward, instant way of error estimation even for a single sample. It is therefore applicable not only to impedance spectra, but also to single-frequency measurements versus time, potential, temperature etc. No time consuming, barely transparent procedure relying on the reproducibility of repetitive excitations is necessary, so even the time drift of objects that are not perfectly in steady state, does not affect the reliability of the uncertainty determination.

REFERENCES

1. M. E. Orazem, *J. Electroanal. Chem*., **572**, 317 (2004).
2. H. Göhr, M. Mirnik, C.-A. Schiller, *J. Electroanal. Chem.,* **180**, 273 (1984).
3. F. Richter, C.-A. Schiller, W. Strunz, N. Wagner, http://accessimpedance.iusi.bas.bg, Imp. Contribut. Online, 4 (2006) P5-1; *Bulg. Chem. Commun.*, **39**, 211 (2007).
4. G. Nicolay, F. Reinert, S. Schmidt, D. Ehm, P. Steiner, S. Hüfner, *Phys. Rev*., **B 62**, 1631 (2000).
5. J. R. Dygas, M. W. Breiter, *Electrochim. Acta*, **44**, 4163 (1999).
6. G. S. Popkirov, R. N. Schindler, *Electrochim. Acta*, **40**, 2517 (1995).
7. E. Van Gheem, R. Pintelon, J. Vereecken, J. Schoukens, A. Hubin, P. Verboven, O. Blajiev, *Electrochim. Acta*, **49**, 4753 (2004).
8. E. O. Brigham, The Fast Fourier Transform, Prentice Hall, Inc., Englewood Cliffs, N.J., 1974.

ОН-ЛАЙН ОПРЕДЕЛЯНЕ И ОБРАБОТКА НА ГРЕШКИ ПРИ ДАННИ ПОЛУЧЕНИ С ЕЛЕКТРОХИМИЧНА ИМПЕДАНСНА СПЕКТРОСКОПИЯ НА ОСНОВАТА НА АВТОКОРЕЛАЦИЯ НА ПРЕТЕГЛЕНИ ХАРМОНИЦИ

К. А. Шилер[1]*, Р. Каус[2]

[1] *Цанер Мессистем, Кронах, Германия*
[2] *Университет Долен Рейн, Крефелд, Германия*

Постъпила на 12 юли 2008 г., Преработена на 8 август 2008 г.

(Резюме)

Представена е процедура, отчитаща вътрешната корелация на хармониците наблюдавана при експерименти с електрохимична импедансна спектроскопия (ЕИС), която дава реалистична оценка на грешката и осигурява необходимата надежност на данните. Подробно е дискутирано извеждането на алгоритъма на процедурата за „автокорелация на претеглените хармоници“, както и резултатите от контролни експерименти с ЕИС, проведени върху добре познати обекти.

Показано е влиянието на три различни вида специфични взаимодействия върху експерименталните резултати: деформации от нелинейни системни характеристики, замърсяване на изходящия сигнал с розов шум, замърсяване на изходящия сигнал с единична честотна пертурбация. Неточността предсказана от автокорелационната процедура на претеглените хармоници е сравнена с отклоненията наблюдавани при обикновените измервания.

Bulgarian Chemical Communications, Volume 41, Number 2 (pp. 199–206) 2009

Inductance correction in impedance studies of solid oxide fuel cells

G. Raikova[1]*, P. Carpanese[2], Z. Stoynov[1], D. Vladikova[1], M. Viviani[3], A. Barbucci[2]

[1] *Institute of Electrochemistry and Energy Systems, Bulgarian Academy of Sciences, Acad. G. Bonchev St., Block 10, 1113 Sofia, Bulgaria*
[2] *DICheP, Universita Di Genova, P. Le Kenedi 1, 16129 Genova, Italy*
[3] *CNR, IENI, V. De Marini 6, 16149, Genova, Italy*

Received October 16, 2008; Revised December 10, 2008

A procedure for evaluation and elimination of errors, caused by parasitic inductance and resistance in EIS studies of two solid oxide fuel cells (SOFC) materials: yttria stabilized zirconia (YSZ) electrolyte and lanthanum strontium manganite (LSM)/YSZ composite cathode is presented in this paper. It is shown that for these low impedance systems the parasitic inductance can affect not only the high frequencies but also the middle and low ones. The parasitic errors correction procedure increases significantly the reliability of the electrochemical impedance spectroscopy (EIS) results.

Key words: electrochemical impedance spectroscopy (EIS), parasitic inductance error correction, yttria stabilized zirconia (YZS), composite lanthanum strontium manganite\yttria stabilized zirconia (LSM\YSZ) cathode.

INTRODUCTION

The complexity of the cathode and anode reactions processes at the triple phase boundary (gas/solid/solid), as well as the ionic-conductivity of the electrolyte in solid oxide, require new approaches for optimization of their performance. The Electrochemical Impedance Spectroscopy is emerging as one of the most powerful, informative and promising techniques, which combines the advantages of the methods, elucidating the knowledge about the electrochemical kinetics of the processes based on assessment of the general cell's behaviour.

The new generation high frequency response analyzers work in a wide frequency range (1 mHz – 50 MHz), which ensures simultaneous study of phenomena with big differences in the rates and in the time-constants. However, for low impedance systems, such as SOFCs, the direct application of EIS encounters the problem of the errors caused by the parasitic inductance. It originates basically from the nature of the objects under study, from the configuration of the measurement cell, including the cables connected with the electrochemical interface, which introduce also a parasitic resistance error. The parasitic inductance can influence not only the high frequencies but also the middle and low ones.

The theoretical analysis and topology simulation show that the errors caused by the parasitic inductance: (i) limit the measurement frequency; (ii) lead to inaccurate parametric identification; (iii) deform the impedance diagram [1–5]. Thus, the correct model recognition requires an accurate estimation of the parasitic inductance influence on the measured impedance.

It has been found [1, 4, 6–8] (Eqn. 1) that the inductance error ε_L is proportional to the square of the frequency (ω) and it depends on the values of the object's inductance (L) and of the capacitance (C_m), which are specific properties of the object:

$$\varepsilon_L = \frac{Z_{im}^L - Z_{im}}{Z_{im}} = -\omega^2 L C_m \quad , \qquad (1)$$

where Z_{im}^L is the imaginary component of the system's impedance and Z_{im} is the imaginary component of an ideal system with zero inductance.

For large systems with high impedance the error is dominated by the capacitance [1, 4, 9]. For low impedance systems, such as SOFCs, the error is dominated by the inductance [1, 2, 9, 10].

Figures 1 and 2 represent structural deformations of some simple models, caused by the inductance influence. At low inductance values the complex plan impedance diagram of a Faradaic reaction is similar to that of an inductance free model (Fig. 1). With the increase of the inductance the capacitive semicircle, typical for this model, changes its size and shape drastically. The capacitive loop disappears and only the imaginary component of the main semi-circle remains, indicating that the Faradaic process is entirely hidden by the influence of the inductance.

* To whom all correspondence should be sent:
E-mail: graikova@bas.bg

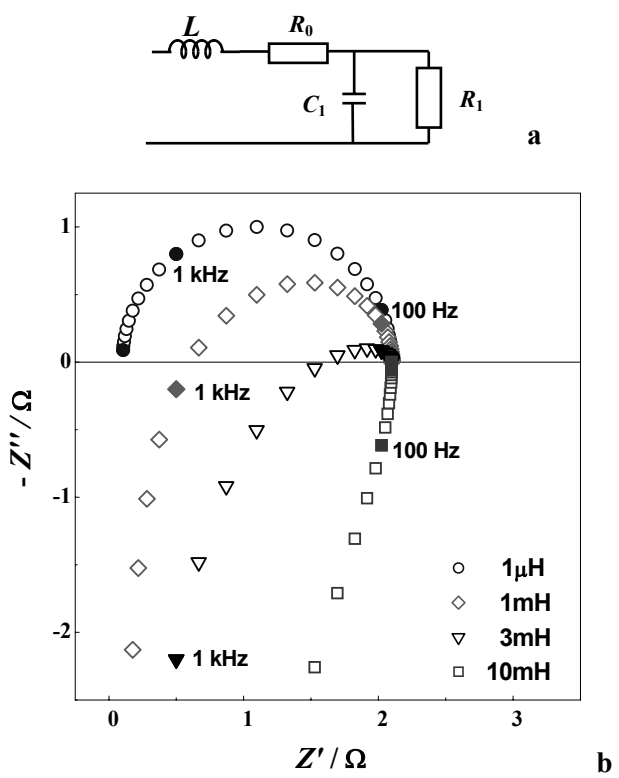

Fig. 1. A model of simple Faradaic reaction (R_0 = 0.1 Ω; $C_1 = 10^{-3}$ F; R_1 = 2 Ω): a) Equivalent circuit; b) Complex plane impedance diagrams at different values of L.

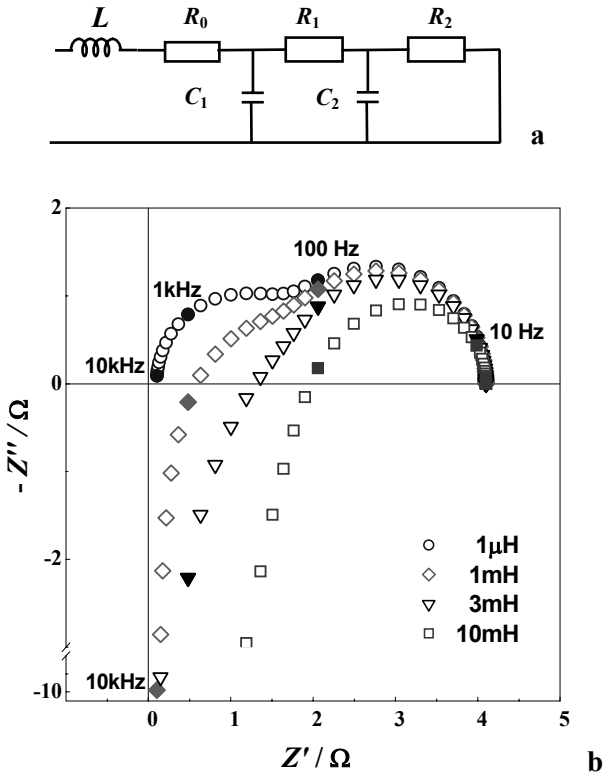

Fig. 2. A model of two-step Faradaic reaction involving one adsorbed spesies (R_0 = 0.1 Ω; $C_1 = 10^{-3}$ F; R_1 = 2 Ω; C_2 = 0.01 F; R_2 = 2 Ω): a) Equivalent circuit; b) Complex plane impedance diagrams at different values of L.

The results for a more complicated model of a two-step reaction are similar (Fig. 2). At lower inductance values, the deformation influences the high frequency semicircle. With the increase of L the first loop disappears and the deformation of the impedance shape resembles that of one step reaction (Fig. 2b).

The theoretical analysis of the errors shows that the influence of the parasitic inductance can be reduced by optimization of the cell's configuration and the sample's shape and size. Thus, when it is possible, the impedance measurements of objects with very low resistance, such as SOFCs, have to be carried out with small experimental cells, ensuring small electrode's surface area and thus smaller C_m (Eqn. (1)).

The deformed zones of the impedance diagrams, caused by parasitic inductance, often include significant information about the investigated object or phenomenon, which cannot be analyzed properly. The simple elimination of the inductive tail or the performance of measurements at lower initial frequencies [12] cannot solve the problem.

There are two main approaches for elimination of the parasitic inductance and resistance errors. The first one is to perform the identification procedure including terms for the cell's inductance and resistance in the hypothetical model (this approach cannot eliminate the difficulty to predict the correct model in the presence of strongly deformed diagram). The second approach is to perform calibration procedures in the same frequency range, followed by extraction of the parasitic components for every frequency. Since the first approach can be applied only for lumped elements, the second one could be regarded as a more general solution [1, 4, 5]. This paper presents a method for correction of the parasitic inductance, based on calibration measurements and its application to impedance characterization of materials for SOFCs.

EXPERIMENTAL

Impedance measurements

The impedance measurements of YSZ electrolyte were performed on single crystal samples produced by ESCETF Single Crystal Technology B.V, containing 8.5 mol% Y_2O_3. They had a square form with side length 10 mm and thickness 0.5 mm. Platinum electrodes were first painted onto both faces of the sample and then sintered in air at 900°C for 120 min [4, 8, 12–14]. The impedance measure-

ments were carried out on Solartron 1260 FRA in the frequency range 13 MHz – 0.1 Hz with density 9 points per decade. The amplitude of the a.c. signal was 50 mV. The measurements were performed in the temperature range from 200 to 950°C, in air atmosphere, at 50°C intervals. Before each measurement the sample was allowed to equilibrate thermally for 1 hour. For reduction of the cabling self-inductance, the components of the measuring system were connected externally by coaxial cables and the connecting leads were as short as possible.

The measurements of the composite cathode material (LSM/YSZ) were performed on three-electrode half-cells with an apparent cathode surface area of 0.23 cm^2 and thickness of 50 μm. More information about the cell's construction is given in [15–17]. The impedance measurements were carried out in air in the temperature interval between 400 and 900°C using an alumina-based rig with shielded Pt wires. A frequency response analyzer Solartron 1260 and an electrochemical interface (Solartron 1186) were used. The measurements were performed within the frequency range 0.1 Hz–50 kHz with amplitude of the a.c. signal 10 mV.

Calibration and inductance errors correction procedure

The performed calibration and correction procedure includes the following steps:

- Short circuit measurement. It serves for evaluation of the cell's inductance and resistance, including that of the cabling. The cathode and anode contacts of the cell are connected in a short circuit. This measurement is performed at the experimental frequency and in the temperature range.

- Measurement of a dummy object. This measurement, serves for evaluation of the sample's self-inductance and resistance. It is carried out using a highly conducting (metal) dummy object with shape and dimensions identical to those of the real one. In the case of fuel cells, which are working at high temperatures (700–1000°C), the melting point of the metal has to be taken into consideration.

- Measurement of the investigated object (in the cell).

- Correction of the impedance measured at every frequency. This procedure is performed under the assumption that the impedance of the object and of the parasitic components are additive quantities.

RESULTS AND DISCUSSION

Calibration studies

In comparison with the impedance diagram of a simulated inductance model (Fig. 3a), the Nyquist's plot of the short circuit measurements obtained with the cell for YSZ studies (Fig. 3b) exhibit a "pipe" shaped form [4, 8, 14]. Its shift from the zero point determines the internal resistance of the cabling. This result shows that (i) the inductance of the cell and of the cabling is frequency dependent and (ii) the calibration determines both the parasitic inductance and resistance of the experimental configuration.

It is important to note that changes in the cables' length and configuration (for instance presence of a single loop) strongly influence the impedance and consequently the short circuit calibration measurement (Fig. 4.)

The comparison of a short circuit measurement of the experimental cell and of the external cable is given in Figure 5. The impedance of the cell at short circuit is shifted to the right with respect to that of the cable, due to the cell's parasitic resistance.

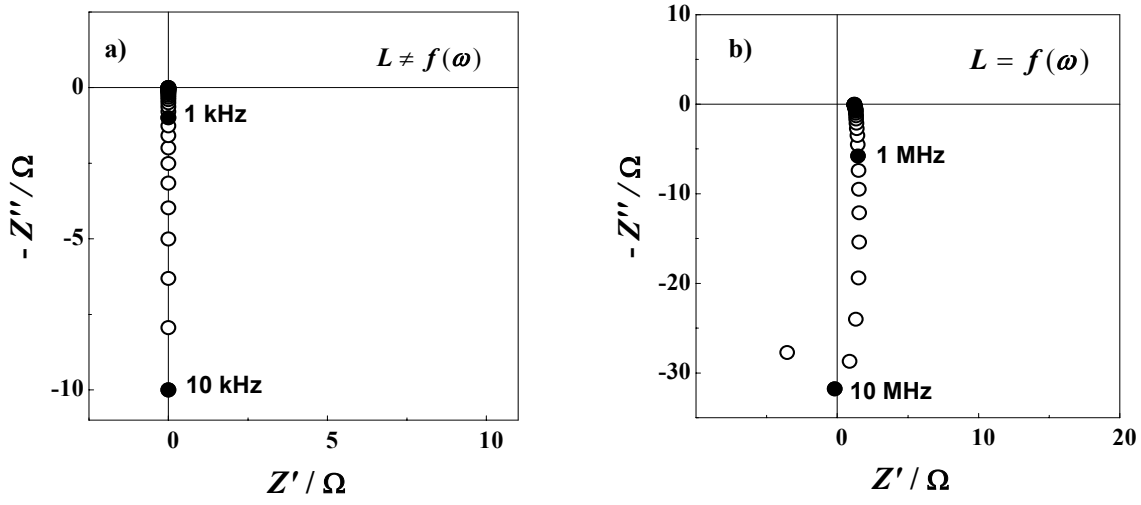

Fig. 3. Complex plane impedance diagram of: a) simulated inductance model (L=10H); b) calibration short circuit measurement of YSZ experimental cell.

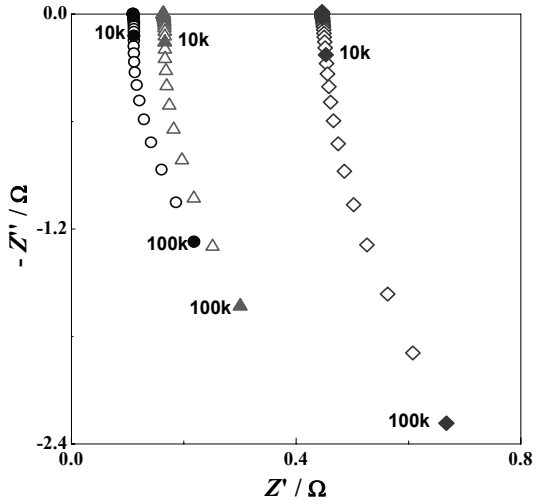

Fig. 4. Complex plane impedance diagram of the cabling: (○) cable with 80 cm length; (△) cable with the same length in the presence of a loop; (◇) cable with 130 cm length.

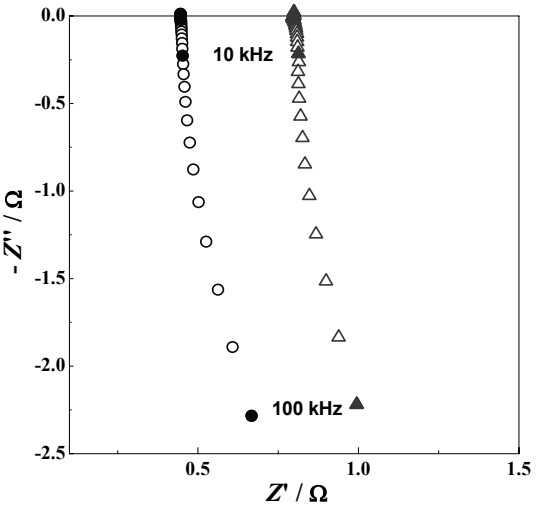

Fig. 5. Complex plane impedance diagram of the cabling (○) and of short circuit calibration measurement (△) of LSM/YSZ experimental cell.

Figure 6 represents the calibration measurements of a dummy object - brass disk with dimensions of the YSZ sample. Obviously, the difference between the cell's and the objects' inductance is negligible and its influence can be neglected.

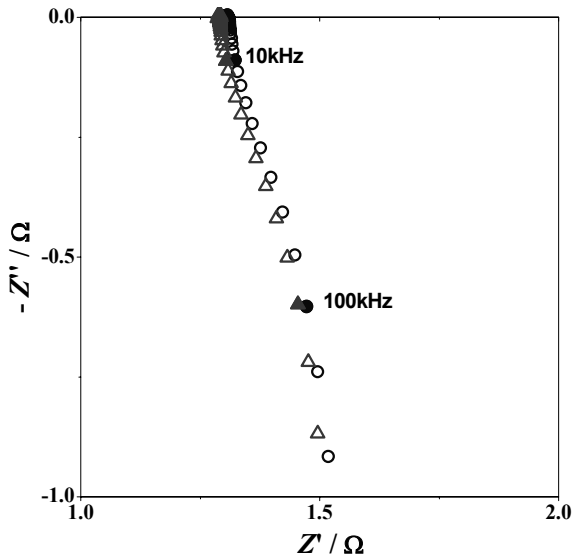

Fig. 6. Zoomed high frequency part of impedance diagrams of short circuit measurements (△) and of a dummy object (○).

Since the short circuit impedance is temperature dependent (Fig. 7), the performance of calibration measurements at each working temperature improves additionally the accuracy of the inductance errors' correction procedure.

The analysis of the calibration measurements shows that they have to be carried out with fixed configuration of the measurement cell and cables, which should remain unchanged in the course of the experiment.

Inductance errors correction in impedance studies of YSZ electrolyte

The high frequency inductance pipe-shaped "tail" in the impedance diagrams of YSZ appears at temperatures above 450°C (Fig. 8).

The characteristic frequency ω_L, at which the inductive and capacitive parts of the imaginary component becomes equal [4], determines the high frequency intercept with the real axis:

$$\omega_L L - \frac{\omega_L^2 R\tau}{1+\omega_L^2\tau^2} = 0\,, \qquad (2)$$

where $\tau = RC$ is the time-constant.

In this example ω_L does not change with the temperature T:

$$\omega_L \approx \sqrt{1/LC_{\text{eff}}} \neq \text{f}(T)\,, \qquad (3)$$

where C_{eff} is the effective capacitance of the system.

The procedure for correction of the inductance and resistance errors was performed on the basis of the assumption that the impedance of the object and of the parasitic components are additive. It has been applied to every working temperature.

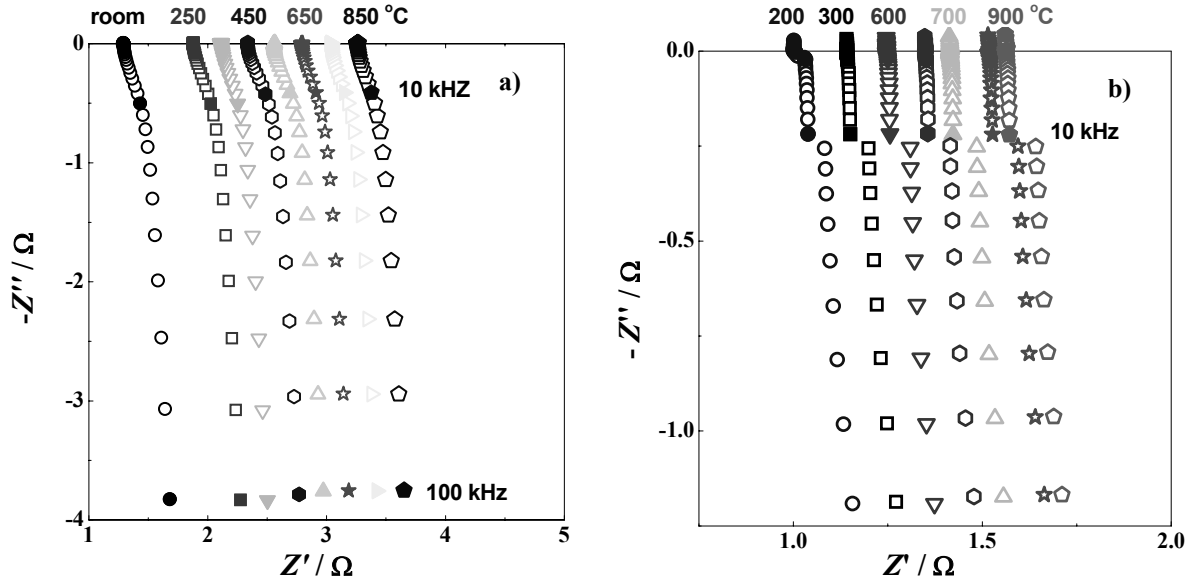

Fig. 7. Complex plane impedance diagrams of short circuit calibration measurements at different temperatures of: (a) cell for YSZ studies; (b) cell for LSM/YSZ studies.

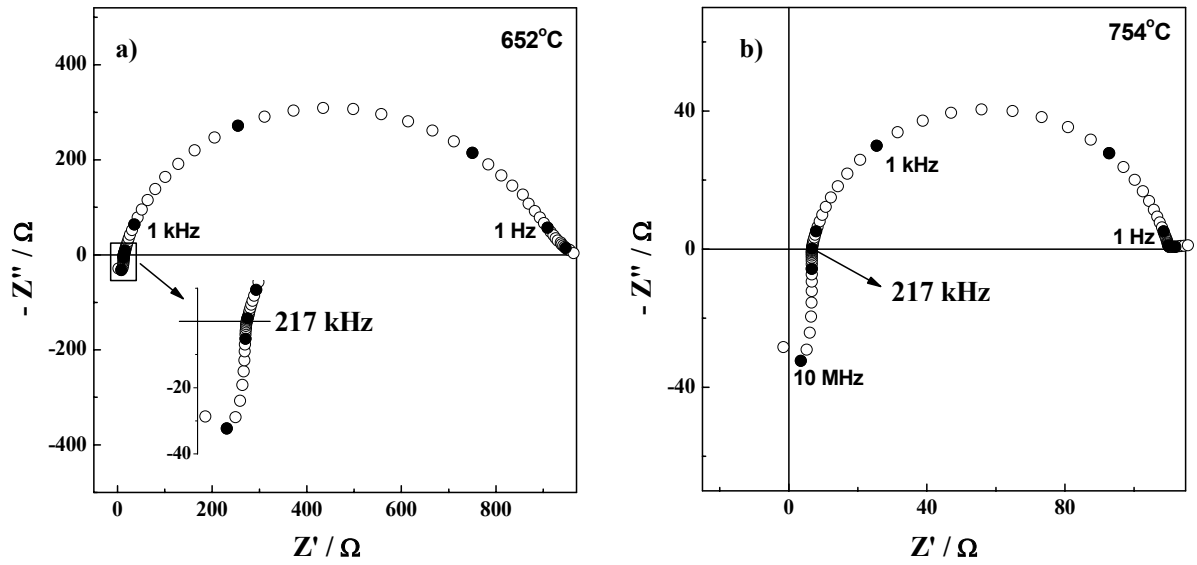

Fig. 8. Complex plane impedance diagrams of YSZ electrolyte measured at different temperatures (data before *L*-correction).

Figure 9 illustrates the correction procedure for YSZ single crystal sample at 838°C: calibration measurement at short circuit (Fig. 9a), measurement of the cell with the sample (Fig. 9b), correction of the sample's impedance for the cell's parasitic inductance and resistance at each working frequency (Fig. 9c, d).

The comparison of the impedance data obtained at higher temperatures before and after the parasitic errors correction shows (Fig. 10) that the deformations affect not only the high, but also the lower frequency range. Part of the first semicircle, which represents the resistance of the bulk material, is well visible even at the highest temperatures due to the correction.

The high frequency intercept with the real axis shifts toward smaller values after the correction (Figs. 9d, 10). The procedure increases the accuracy of determination of the electrolyte resistances. The inductance influences also the electrode reaction behaviour, which is revealed in the low frequency region. After the correction the estimated polarization resistance decreases (Fig. 10).

The estimated parasitic inductance of the investigated YSZ sample is about 7 nH.

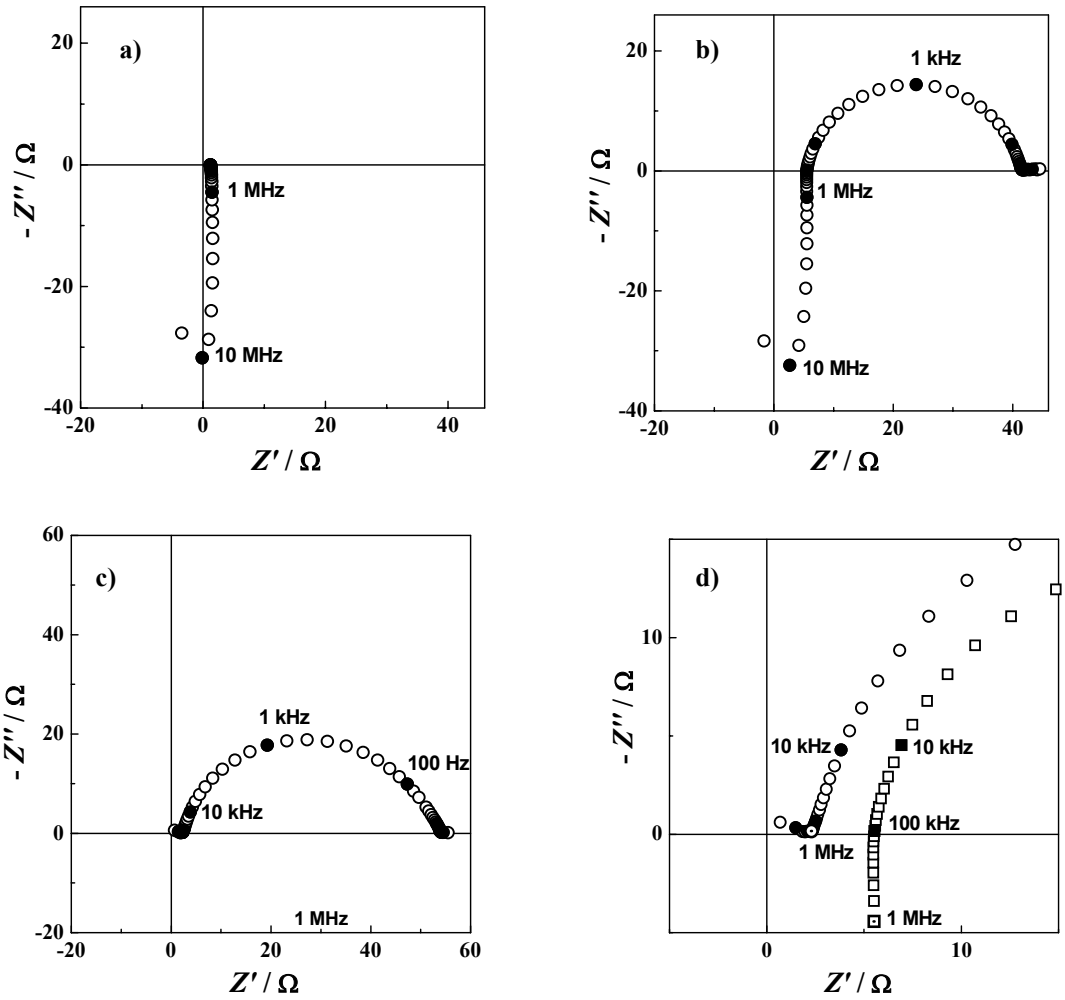

Fig. 9. Correction procedure for impedance of YSZ single crystal sample measured at 838°C. Complex plane impedance diagrams of: a) short circuit measurement; b) sample's measurement; c) sample's impedance after the correction; d) zoomed high frequency part of b) and c).

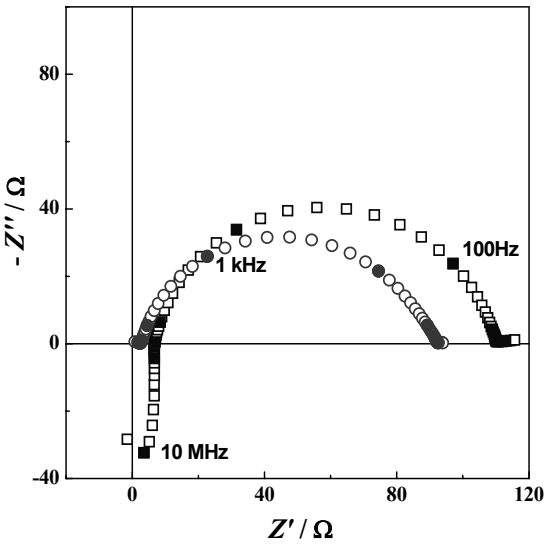

Fig. 10. Complex plane impedance diagrams for YSZ at 793ºC: (□) raw impedance data; (○) data after the errors correction

Inductance errors correction in impedance studies of LSM/YSZ cathode material

The inductive "tail" in the impedance diagrams of LSM/YSZ composite cathode appears at 690°C (Fig. 11). In this object ω_L is temperature dependent, which could be attributed to C_{eff} (Eqn. (3)).

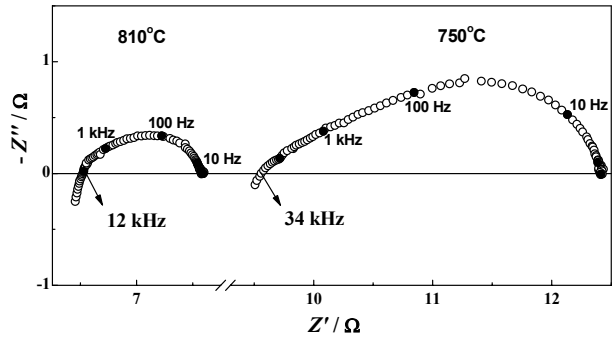

Fig. 11. Complex plane impedance diagram of composite LSM/YSZ cathode material at different temperatures.

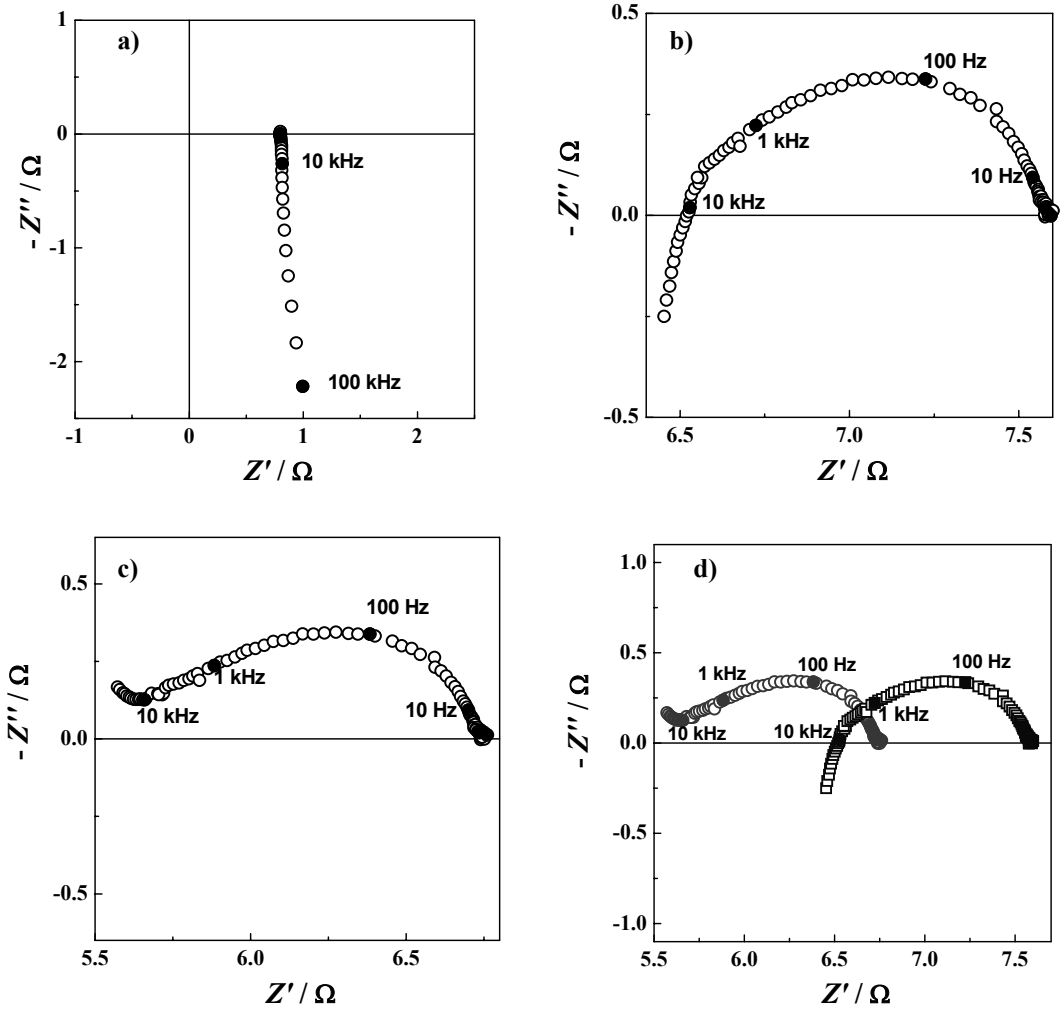

Fig. 12. Correction procedure for the LSM/YSZ sample measured at 840°C. Complex plane impedance diagrams of: a) short circuit measurement; b) sample's impedance raw data; c) sample's impedance after the correction; d) comparison of impedance data before (□) and after (○) the errors correction.

The procedure of the parasitic inductance (and resistance) correction is represented in Figure 12. The comparison of the impedance diagrams before and after the correction (Figs. 12d, 13) indicates that for this system the errors influence mainly the higher frequencies (50–1 kHz). After the correction, the high-frequency inductance "tail" is replaced by a section of a semicircle, which represents the response of the electrolyte (Fig. 13).

The errors influence also the high-frequency region of the response related to the cathode reaction behaviour (10–1 kHz), i.e. the "left" part of the lower frequency arc (Fig. 13). While the raw data describe a depressed semicircle at this segment, the corrected ones follow a more linear shape. This difference can affect an eventual modeling procedure.

The evaluated parasitic inductance for the investigated LSM/YSZ sample is about 4 nH.

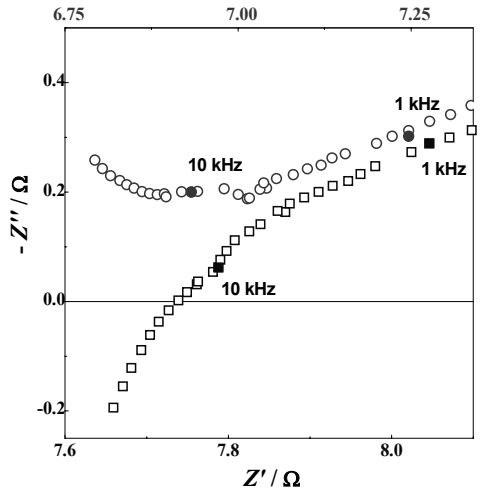

Fig. 13. Comparison of the zoomed high-frequency parts of the complex plain impedance diagrams of LSM/YSZ sample measured at 780°C before (□) and after (○) the errors correction.

CONCLUSIONS

The correction of the parasitic inductance and resistance increases the informational capability of the impedance experimental data. The herein presented impedance studies of yttria stabilized zirconia solid electrolyte and LSM/YSZ composite cathode materials show the importance of the calibration measurements. The fixed configuration of the cell, cables and whole set-up during the experiments ensure reproducible impedance data. The results demonstrate the high accuracy, obtained by applying the parasitic errors correction procedure, which can be used for impendance studies of low resistance systems.

***Acknowledgements**: The authors gratefully acknowledge the financial support by the European Commission (Programme Energy-2007-1-RTD) under contract № 213389 "Innovative Dual mEmbrAne fueL Cell" (IDEAL-Cell) and the project Alternative Energy Sources (ALENES, contract No BG 051PO 001/07/3.3-02/17.06) that made possible the presentation and edition of this paper.*

REFERENCES

1. B. Savova-Stoynov, Z. Stoynov, *J. Appl. Electrochem*., **17**, 1150 (1987).
2. Z. Stoynov in: Materials for Lithium-Ion Batteries, C. Julien, Z. Stoynov (Eds.), Kluwer Academic Publishers, 2000, p. 349.
3. Z. Stoynov, B. Grafov, B. Savova-Stoynova, V. Elkin, Electrochemical Impedance, Nauka, Moscow, 1991 (in Russian).
4. D. Vladikova, Z. Stoynov, G. Raikova, in: Portable and Emergency Energy Sources, Z. Stoynov, D. Vladikova (Eds.), Marin Drinov Academic Publishing House, Sofia, 2006, p. 383.
5. Z. Stoynov, D. Vladikova, Differential Impedance Analysis, Marin Drinov Academic Publishing House, Sofia, 2005.
6. Z. Stoynov, B. Savova-Stoynova, T. Kossev, *J. Power Sources*, **30**, 275 (1990).
7. D. Vladikova, http://accessimpedance.iusi.bas.bg, Impedance Contributions Online, 1 (2003) L3-1; *Bulg. Chem. Commun*., **36**, 29 (2004).
8. D. Vladikova, Z. Stoynov, G. Raikova, http://accessimpedance.iusi.bas.bg, Impedance Contributions Online, 3 (2005) P8-1; *Bulg. Chem. Commun*., **38**, 226 (2006).
9. M. Keddam, Z. Stoynov, H. Takenouti, *J. Appl. Electrochem*., **7**, 539 (1977).
10. Z. Stoynov, B. Savova-Stoynova, T. Kossev, *J. Power Sources*, **30**, 301 (1990).
11. S. B. Adler, *Solid State Ionics*, **135**, 603 (2000).
12. G. Raikova, D. Vladikova, J. A. Kilner, S. J. Skinner, Z. Stoynov, http://accessimpedance.iusi.bas.bg, Impedance Contributions Online, 2 (2004) P8–1; *Bulg. Chem. Commun*., **37**, 46 (2005).
13. D. Vladikova, G. Raikova, Z. Stoynov, H. Takenouti, J. Kilner, S. J. Skinner, *Solid State Ionics*, **176**, 2005 (2005).
14. D. Vladikova, J. Kilner, S. J. Skinner, G. Raikova, Z. Stoynov, *Electrochim. Acta*, **51**, 1611 (2006).
15. A. Barbucci, M. Viviani, P. Carpanese, D. Vladikova, Z. Stoynov, *Electrochim. Acta*, **51**, 1641 (2006).
16. A. Barbucci, M. Viviani, P. Carpanese, D. Vladikova, Z. Stoynov, http://accessimpedance.iusi.bas.bg, Impedance Contributions Online, 4 (2006) P4-1; *Bulg. Chem. Commun*., **39**, 203 (2007).
17. D. Vladikova, Z. Stoynov, A. Barbucci, M. Viviani, P. Carpanese, G. Raikova, in: New Developments in Advanced Functional Ceramics 2007, L. Mitoseriu (Ed.), Transworld Research Network, Kerala, India, 2007, p. 457.

КОРЕКЦИЯ НА ИНДУКТИВНИ ГРЕШКИ В ИМПЕДАНСНИ ИЗСЛЕДВАНИЯ НА ТВЪРДООКИСНИ ГОРИВНИ КЛЕТКИ

Г. Райкова[1]*, П. Карпанезе[2], З. Стойнов[1], Д. Владикова[1], М. Вивиани[3], А. Барбучи[2]

[1] *Институт по електрохимия и енергийни системи, Българска академия на науките, ул. „Акад. Г. Бончев", бл. 10, 1113 София*
[2] *Факултет по инженерна химия, Университет Генуа, пл. „Кенеди" № 1, 16129 Генуа, Италия*
[3] *Институт за енергетика, Национален изследователски център, ул. „Де Марини" № 6, 16149, Генуа, Италия*

Постъпила на 16 октомври 2008 г., Преработена на 10 декември 2008 г.

(Резюме)

Предложена е процедура за оценка и отстраняване на грешки, причинени от паразитни индуктивност и съпротивление, при импедансни изследвания на два материала за твърдоокисни горивни клетки (SOFC): итриево-стабилизиран циркониев оксид електролит (YSZ) и композитен катод на базата на лантан-стронциев манганит/итриево-стабилизиран циркониев оксид (LSM/YSZ). Показано е, че при такива ниско-импедансни системи паразитната индуктивност може да повлияе не само на високочестотната, но също така на средно- и нискочестотната зона. Процедурата за корекция и отстраняване на грешки от паразитна индуктивност повишава значително надеждността на резултатите получени с електрохимичната импедансна спектроскопия (ЕИС).

CONTENTS

СЪДЪРЖАНИЕ